Functionality tailored porous materials toward detection and sequestration of toxic pollutants

A Thesis

Submitted in Partial Fulfillment of the Requirements for the

Degree of

Doctor of Philosophy

by

Debanjan Mahato

Reg. ID: 20162020

Indian Institute of Science Education and Research (IISER), Pune

2023

Dedicated to

Maa, Baba

Indian Institute of Science Education and Research (IISER), Pune

Certificate

It is hereby certified that the work described in this thesis entitled *"Functionality tailored porous materials toward detection and sequestration of toxic pollutants"* submitted by *Mr. Debanjan Mahato* was carried out by the candidate, under my supervision. The work presented here or any part of it has not been included in any other thesis submitted previously for the award of any degree or diploma from any other university or institution.

Date: 05/04/2023

Dr. Sujit K. Ghosh
Research Supervisor
Email: sghosh@iiserpune.ac.in
Contact No.:+91(20)25908076

Declaration

I declare that this written submission represents my ideas in my own words and wherever other's ideas have been included; I have adequately cited and referenced the original sources. I also declare that I have adhered to all principles of academic honesty and integrity and have not misrepresented or fabricated or falsified any idea/ data/ fact/ source in my submission. I understand that violation of the above will cause for disciplinary action by the Institute and can also evoke penal action from the sources which have thus not been properly cited or from whom proper permission has not been taken when needed.

Debanjan Mahato

Date: 04/04/2023

Debanjan Mahato

Reg. Id: 20162020

Acknowledgement

First and foremost, I would like to take this opportunity to express my sincere gratitude to my research supervisor Dr. Sujit K. Ghosh for his unwavering encouragement and support throughout my PhD tenure. As an Int-PhD student of the institute, I joined his team as a master's student and despite different ups and downs in the process, his guidance in all aspect helped me a lot with accumulation of various skills. I would like to take the opportunity to convey my deepest gratitude to my research supervisor Dr. Sujit K. Ghosh for his continuous support and motivation throughout my PhD tenure. I feel his illimitable encouragement has propelled my research in proper direction. I believe that his inspiring guidance, expertise, insightful feedback, and unwavering dedication has helped me to design and execute different research projects successfully. Thank you very much Sir for all your diligent efforts, trust in me and most importantly for being such a wonderful guide.

I earnestly acknowledge the former director of Indian Institute of Science Education and Research (IISER) Pune Prof. K. N. Ganesh and the current director Prof. J. B. Udgaonkar for providing state of the art facilities and having a vibrant research environment. I am also extremely thankful to my research advisory committee (RAC) members, Dr. Sakya Sen (NCL, Pune) and Dr. Partha Hazra (IISER, Pune) for their valuable inputs, advices and support during the annual RAC meetings. I am also grateful to Prof. M. Jayakannan (former Chair, Chemistry department), Prof. H, N. Gopi (former Chair, Chemistry department), Prof. Nirmalya Ballav (Present Chair, Chemistry department) and all other faculty members of the department of chemistry for nurturing such healthy research friendly environment and being reachable for any assistance. I sincerely thank my collaborator Dr. Mandar M. Shirolkar (Symbiosis international (Deemed University), whose assistance was helpful for theoretical insights in projects.

It has been a great pleasure for me to be a part of the 'Microporous Materials Lab' and I am extremely grateful to all the past and present members of the team. I would like to thank all of them (Dr. A, V, Desai, Dr. Partha Samanta, Dr. Tarak Nath Mandal, Dr. Sreenu Bhanoth, Dr. Shivani Sharma, Dr. Samraj Mollick, Dr. Yogeshwar More, Dr. Arunabha Sen, Dr. Subhajit Dutta, Sumanta Let, Writakshi Mandal, Sahel Fajal, Gourab

Kumar Dam, Dipanjan Majumdar, Arkendu Roy, Priyanshu Chandra, Dibyaranjan Sahoo, Kishalay Biswas, Dipayan Ghosh and Anirban Roy) who have contributed at different phases in their capacities. My sincere thanks to Dr. Subhajit Dutta with whom I have worked during my master's project and learned a lot of things. I would like to thank my seniors Dr. Partha Samanta, Dr. A. V. Desai, Dr. Samraj Mollick and Dr. Arunabha Sen for guidance and valuable suggestions. I would specially mention Sahelda and Writakshidi for their unconditional help and inputs that guided me in proper direction in this journey. I wish to acknowledge prompt guidance and assistance from Sumantada, Gourab and Dipanjan to achieve the desired target. I would like to express my special appreciation to all my current lab members, because without them this journey would not have been as exciting and memorable as it has been. I am thankful to all of you for being helpful and cooperative and helping me improving my scientific knowledge.

I would like to convey my regards to my school and university teachers who have encouraged me throughout different stages of life. I am especially grateful to late Shibuda jethu (first teacher of my life) for guiding me since my childhood days. I would like to thank all of my school teachers for their education and guidance which paved the way to move forward. I am very much thankful to Saktida and swapanda two of my school teachers who were not only excellent teachers but also helped me to be a better person. I am also very grateful to Dr. Arogyavaram Saha, Dr. Hrisikesh Chatterjee, Dr. Prasanta Ghosh, Dr. Pulak Ganguly, Dr. Bikashbaran Ghosh, Dr. Bimal Kumar Sadhukhan, Dr. Amit Saharoy, and Dr. Rathindranath Ghosh of Ramkrishna Mission Residential College, Narendrapur (University of Calcutta) for guiding me and generating the love inside me for Chemistry. I am also thankful to Prof. R. Bhoomishankar (IISER Pune), Prof. S. G. Srivatsan (IISER Pune) for providing me the opportunity to carry out my lab rotation work in his lab.

I acknowledge Council of Scientific & Industrial Research (CSIR), India and IISER, Pune for providing me fellowship. I would also like to thank American Chemical Society (ACS), Royal Society of Chemistry (RSC), John Wiley & Sons (Wiley-VCH), Elsevier for the various research articles that I managed to publish in my PhD tenure. For smooth progress in such a long academic program, the support of technical and administrative staff is crucial. I thank Dr. Umeshareddy Kacherki and Shiva Shankar Mahato for library support,

technical staff of the institute - Parveen Nasa, Archana, Mahesh Jadhav, Nilesh Dumbre, Swati, Anil, Yatish, Ganesh Dimbar, Suresh Prajapat, Sandeep, Nitin, Megha, Deepali and administrative staff - Mayuresh, Nayana, Tushar, Vrushali, Suresh, Prabhas, Priyadarshani for their prompt assistance at multiple occasions. During my PhD tenure, I had the opportunity to attend national (MTIC-2017) conference for which I thank IISER-Pune for funding.

I wish to thank all my friends for their support and help at different stages of my life. I thank all my batch-mates (Integrated PhD batch 2016) specially pulak and saikat. I would heartily thank my childhood friends Badgu, Dola and my school friends Snehasish, Subhadip, Sanchayan and my college friends Protik, krishnendu, Rahul, Abhishek. I apologize in advance for not being able to take all of your names, but am sure, it would not offend you to a great extent. I would like to mention about my friends in campus Akash, Ankur, Aditya and Arkendu for sharing innumerable rejoicing moments. I also thank my seniors Dr. Supratik, Dr. Saptarshwa and my friends in the campus Indra, Abhishek, Panda, Pratim, Pooja and Sumit and wish them for a prosperous future. I wish to thank all my seniors, mates and juniors whom I played table tennis with in this long time in campus. Lastly, I am really grateful to all my family members (my parents, Maman, kaku, kakima, dida). I don't have enough words to express my gratitude towards my parents but without their constant sacrifices and support, I wouldn't have reached to this point.

- Debanjan Mahato

Contents

Synopsis

The main motivation of all the works included in this thesis is to design and synthesize of functional porous materials for different sustainable applications. In the domain of porous materials, metal-organic frameworks (MOFs) are made of metal-ligand coordination bond and porous organic materials linked in covalent linkages between functional moieties. The primary benefits of these materials are their synthetic tuneability, which results in the development of pores within and enables the materials to function as host matrix. The pores can be designed with required functional groups, which can produce an exceptional host-guest interaction. In the case of neutral framework material, the pores are inhabited by guest molecules and in the case of ionic frameworks there are counter ions. Because of these characteristics, porous materials have become one of the frontrunners in the domain of material science having application in gas separation, heterogeneous catalysis, drug delivery etc. However, using MOFs and porous organic materials for recognition and sequestration of toxic and harmful species from water has been rarely investigated. In this context functionalized metal organic framework was developed for selective recognition of cyanide ion in water medium. Furthermore, based on principles of ion exchange and host guest interaction functionalized porous organic materials were developed for capture of hazardous water pollutants.

Chapter 1. Introduction

This section includes a brief discussion on porous materials (MOFs and porous organic compounds) and their uses. Classification of different porous materials and target specific synthesis of such porous materials have been discussed further. The vast range of applicability of porous materials have been illustrated. One of the main uses for porous materials is as a tool for the identification and removal of various hazardous and toxic chemicals from water. In this context increase in various types of water pollution with increase in industrialization was also discussed. Also, scope of designing various functionalized MOFs and porous organic materials for the sequestration of pollutants from water has been discussed in the later part of the section.

Chapter 2. Selective and Sensitive Fluorescence Turn-on Detection of Cyanide Ions in Water by Post Metallization of a MOF

In this chapter, a post metallized metal-organic framework (MOF) has been synthesized for "turn on" detection of toxic CN^- ion. To sense cyanide ion in water medium first water stable $CuCl_2$@MOF-867 MOF has been synthesized and subsequently characterized. Post metalized copper center strategically incorporated into the MOF as cyanide is quite reactive towards Cu^{2+} generating stable $Cu(CN)_2$ species. Post metallization results in luminescence quenching, whereas upon addition of cyanide, leaching of copper results in regeneration of luminescence intensity as pristine MOF-867. In order to check selectivity of the probe, $CuCl_2$@MOF-867 has been treated with other interfering anions such as Br^-, NO_3^-, I^-, SO_4^{2-}, OAc^-, SCN^-, NO_2^-, etc. The probe has been found to be selective for CN^- ion with a very low limit of detection (0.19 µM), which is significantly lower than WHO standardized limit that is 1.9 µM.

Reference: Debanjan Mahato, Sahel Fajal, Partha Samanta, Writakshi Mandal and Sujit K. Ghosh ChemPlusChem , 2022, 87, e202100426

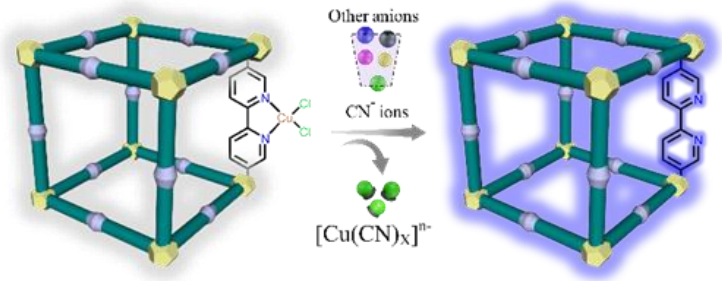

Chapter 3. Efficient Removal of Mercury from Aqueous Medium by Ionic Functionalized Porous Organic Polymer

Mercury pollution is a global concern as these toxic heavy meatal cycles through water, soil and atmosphere to spread across different regions of the world and it is the reason for several harmful effects

on the nervous, digestive and immune systems, lungs and kidneys, and may be fatal. So, sequestration of mercury is a significant issue, and the search for the perfect adsorbent is ongoing. In this chapter, two chemically stable anionic microporous organic polymers have been synthesized. Two anionic polymers have different functionality which plays vital role in capture studies. Hard soft acid base (HSAB) principle does a crucial role in capture efficiency and recyclability. Both the compound showed efficient mercury removal from aqueous medium and kinetics data fits with the pseudo second order model. Also capture studies have been performed in presence of other contaminated cations (e.g., Pb^{2+}, Cd^{2+}, K^{+} etc.). Thus, polymeric materials can be used for sequestration of mercury from aqueous medium.
(*Manuscript under preparation*)

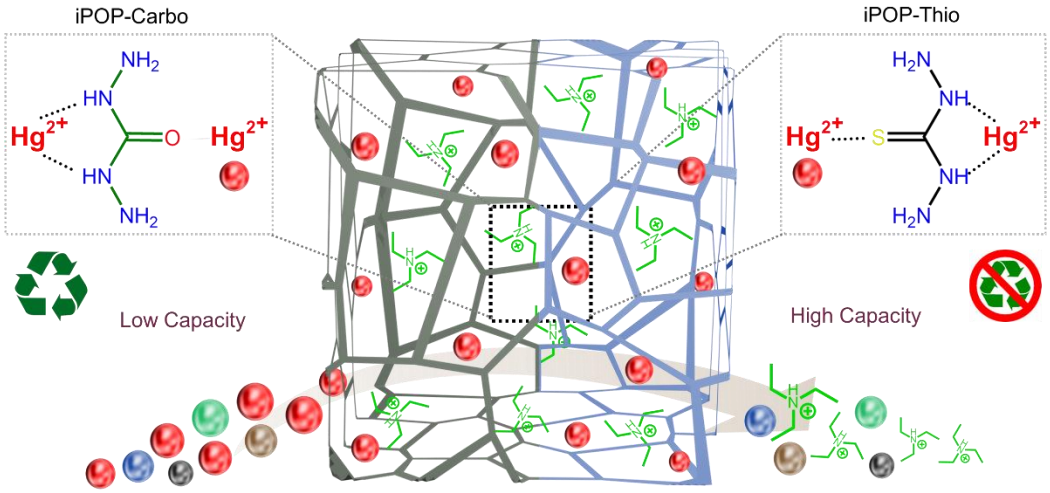

Tuning of Hg^{2+} Metal Ion Removal Kinetics and Exchange Capacity by iPOPs

Chapter 4. Role of Framework Integrated Template Anions in Troger Base Polymer for Selective Ultrafast Removal of Toxic Pollutant from Water

Porous materials further utilized for anionic pollutant (heavy metal oxo-anion) capture apart from cationic pollutants (heavy metals). Due to toxic, carcinogenic, mutagenic nature of chromium, removal of Cr(VI)-based oxo-anions (e.g., chromate and dichromate anions) has gained significant attention. On the other hand, technetium (^{99}Tc), a radioactive waste, exists in nature in its most favorable oxo-anion form. The capture investigation was done using the surrogate ReO_4^- ion because it is not possible to handle radioactive species in a lab setting. In this regard two post synthetically modified cationic organic polymer was synthesized having different counter anion. These are utilized for removal of the targeted analytes in aqueous medium even in existence of concurrent anions such as Cl^-, NO_3^- and ClO_4^- ions. The

role of template anion for removal of oxo-anions has been demonstrated.

(Manuscript under preparation)

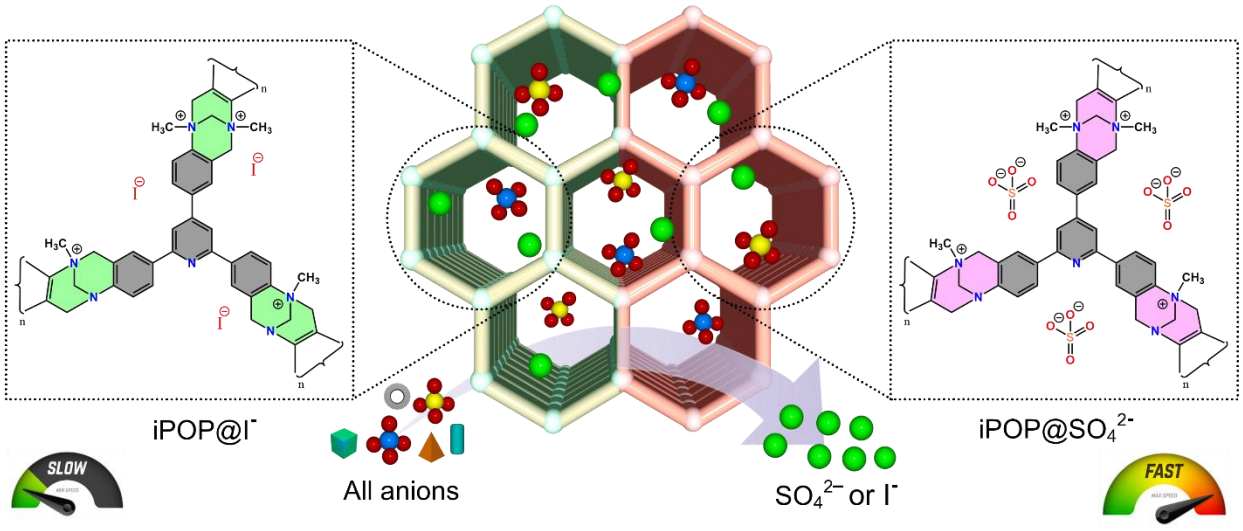

Modulating of Oxyanions Sequestration Kinetics by Tuning of Framework Integrated Free Anions

Chapter 5. Post Synthetically Modified Troger Base Polymer for Anionic Organic Pollutant Removal from water

In this chapter, a chemically stable post synthetically modified troger base polymer has been synthesized. Further the cationic polymer was employed for removal of anionic dyes (Indigo carmine (IC), methyl orange (MO)) via anion exchange. It is found that the polymer is selective towards anionic dyes over cationic dyes. In this regard, methylene blue a cationic dye was utilized, however the polymer shows negligible uptake. Moreover, the polymer demonstrated that it could selectively sequestrate of anionic dyes from a binary combination of cationic and anionic dye (methylene blue and methyl orange) in aqueous medium.

(Manuscript under preparation)

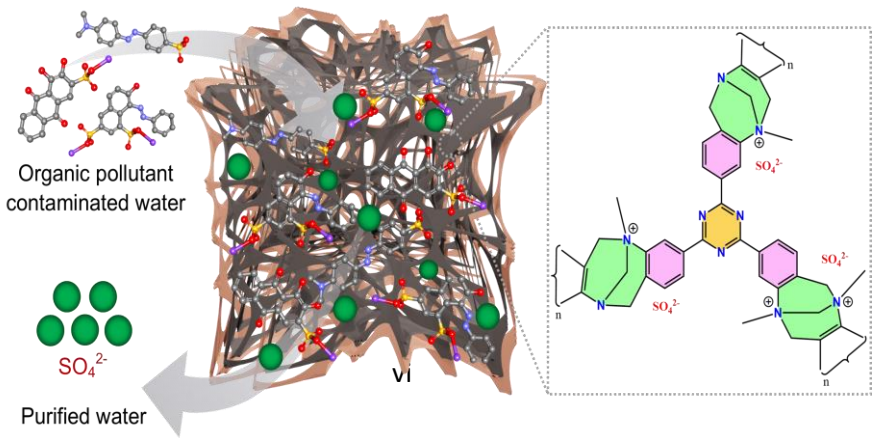

Efficient Removal of Toxic Organic Dyes from Water by Chemically Stable Ionic POP

Abbreviations

Anal.	Analysis
Calc.	Calculated
DMF	N,N'-dimethylformamide
DCM	Dichloromethane
EtOH	Ethanol
FT-IR	Fourier transform infra-red spectroscopy
g	Gram
HCP	Hyper-cross-linked polymer
MeOH	Methanol
mg	Milligram
min	Minutes
mL	Milliliter
mM	Millimolar
mmol	Milli moles
MOF	Metal-Organic Framework
PCP	Porous Coordination Polymer
PXRD	Powder X-Ray Diffraction
RT	Room Temperature
TGA	Thermo-gravimetric Analysis
UV	Ultraviolet
FE-SEM	Field Emission Scanning Electron Microscopy
MeCN	Acetonitrile
NMR	Nuclear Magnetic Resonance
EDX	Energy Dispersive X-ray Analysis
ICP-AES	Inductively Coupled Plasma Atomic Emission Spectroscopy

Rights and Permissions

Chapter 2:

Research Publications

(† - indicates equal contribution)

Included in Thesis:

1. Selective and Sensitive Fluorescence Turn-on Detection of Cyanide Ions in Water by Post Metallization of a MOF.
   Debanjan Mahato, Sahel Fajal, Partha Samanta, Writakshi Mandal and Sujit K. Ghosh.
   ChemPlusChem, 2022, **87**, e202100426
2. Efficient Removal of Mercury from Aqueous Medium by Ionic Functionalized Porous Organic Polymer.
   Debanjan Mahato, Sahel Fajal and Sujit K. Ghosh.
   (Manuscript Under Preparation)
3. Role of Framework Integrated Template Anions in Troger Base Polymer for Selective Ultrafast Removal of Toxic Pollutant from Water.
   Debanjan Mahato, Sahel Fajal, Writakshi Mandal and Sujit K. Ghosh.
   (Manuscript Under Preparation)
4. Post Synthetically Modified Troger Base Polymer for Anionic Organic Pollutant Removal from water.
   Debanjan Mahato, Sahel Fajal and Sujit K. Ghosh.
   (Manuscript Under Preparation)

Not Included in Thesis:

5. Recognition and Sequestration of Toxic Inorganic Water Pollutants with Hydrolytically Stable Metal-Organic Frameworks.
   Subhajit Dutta, Sumanta Let, Shivani Sharma, **Debanjan Mahato** and Sujit K. Ghosh.
   The Chemical Record, 2021, **21**, 1666-1680
6. Nanotrap Grafted Anion Exchangeable Hybrid Materials for Efficient Removal of Toxic Oxoanions from

Water.

Samraj Mollick, Sahel Fajal, Satyam Saurabh, **Debanjan Mahato** and Sujit K. Ghosh

ACS Cent. Sci.,2020, **6**, 9, 1534–1541.

7. A Water Stable Cationic MOF with Hydrophobic Pore Surface as Efficient Scavenger of Oxo-anion Pollutants from Water.

   Subhajit Dutta, Partha Samanta, Biplab Joarder, Sumanta Let, **Debanjan Mahato**, Ravichandar Babarao and Sujit K. Ghosh

   ACS Appl. Mater. Interfaces, 2020, **12**, 37, 41810–41818.

8. Three-in-One C2H2-Selectivity-Guided Adsorptive Separation across an Isoreticular Family of Cationic Square-Lattice MOFs.

   Subhajit Dutta, Soumya Mukherjee, Omid T. Qazvini, Arvind K. Gupta, Shivani Sharma, **Debanjan Mahato**, Ravichandar Babarao and Sujit K. Ghosh.

   Angew. Chem. Int. Ed., 2022, **61**, e202114132.

9. Unveiling the Impact of Diverse Morphology of Ionic Porous Organic Polymers with Mechanistic Insight on the Ultrafast and Selective Removal of Toxic Pollutants from Water.

   Writakshi Mandal, Sahel Fajal, Samraj Mollick, Mandar M. Shirolkar, Yogeshwar D. More, Satyam Saurabh, **Debanjan Mahato** and Sujit K. Ghosh.

   ACS Appl. Mater. Interfaces, 2022, **14**, 20042−20052.

Chapter 1

Introduction

1.1 Porous Materials

Porosity is the measurement of vacant space or voids within a substance. It has a significant impact on physical chemical and mechanical behavior of a wide range of materials found in nature. So, it has been an important domain for researchers to design and develop various porous architectures by mimicking the nature.[1] Naturally occurring porous materials are materials that have small cavities or pores in their structure, which can allow fluids, gases, and other substances to pass through them. These materials can be found in various forms in nature, such as rocks, soils, and biological tissues. Examples of naturally occurring porous materials include pumice, zeolites, sandstone, and coral reefs etc. These materials can have significant applications in different fields, for instance in construction work, water purification and geology. Understanding the properties and characteristics of naturally occurring porous materials is essential in developing innovative solutions for many practical problems. With this idea in mind variety of materials with intrinsic porosity have emerged during past few decades. Due to its several applicability varying its porosity, it has attracted a lot of attention (Fig. 1.1).[2] Substances with pore aperture smaller than 2 nanometers (nm) are referred to as microporous materials, while those with pores between 2 and 50 nm are referred to as mesoporous materials. Macro porous materials are those that have pores larger than 50 nm.[3] Zeolites, activated carbons, porous silica belongs to the early domain of porous substances whereas from the past two decades there has been an advancement in strategy for the synthesis of new class of materials utilizing functional building blocks.[4] There are two methods used to synthesize these materials, a) construction of inorganic organic porous hybrid structures by utilizing organic inkers and inorganic nodes, such as metal organic gels (MOGs), Metal organic polyhedras (MOPs), metal-organic frameworks (MOFs) b) Another is metal free porous material build by various organic building block through covalent and noncovalent interaction called as porous organic materials (POMs).[5] POMs are made up of both amorphous materials, which include various types of porous polymers, and crystalline porous architectures, such as hydrogen bonded organic frameworks (HOFs), covalent-organic frameworks (COFs), and porous organic cages (POCs). [6] Metal organic polyhedra, or MOPs, are complex molecular structures composed of metal centers and organic building units arranged in a highly ordered fashion. These structures are typically polyhedral in shape and feature an intricate network of metal-ligand interactions that give rise to their unique physical and chemical properties. MOPs have garnered significant interest in recent past due to their significant utilization in a variety of domains, including catalysis, sensing, and drug delivery.

Figure 1.1: Schematic depiction for classification of porous materials.

Moreover, because of tunable structure and properties these has become fascinating stage for noble composite porous materials development.[7] MOGs are typically three-dimensional porous network structure composed of metal ions or clusters and organic linkers attached via coordination bond. Unlike other coordination polymers, MOGs exhibit a gel-like consistency and are able to retain their shape even in the absence of a solid support. This is because of in the gel matrix where there are large amount of solvent or water molecules present, providing a high degree of flexibility and tunability to the material's properties. MOGs also exhibit unique mechanical properties that make them attractive for utilization in flexible electronics and devices for energy storage. These materials have been shown to possess high elasticity and toughness, making them ideal candidates for stretchable or bendable electronic device. [8c,d]

Covalent organic framework (COFs), are a relatively new branch of porous materials that have gained huge attraction among the researchers in the field of materials science due to their three-dimensional network of covalently bonded organic molecules, resulting in a highly ordered and crystalline structure. COFs are typically synthesized through a process called reticular chemistry, which involves the self-assembly of organic building blocks through covalent bonding. [6f] This process allows for the creation of highly ordered structures with a range of different topologies, including two-dimensional sheets, one-dimensional rods, and three-dimensional frameworks. Major benefits of COF materials over other porous materials, including activated carbons and zeolites, is because of their capability to be designed and synthesized with specific functional groups. Which leads to the creation of materials with tailored properties, such as enhanced

selectivity for certain gases or improved catalytic activity. In addition, COFs can be easily modified post-synthesis, allowing for the incorporation of new functional moieties or the tuning of existing ones. [6e,g] Hydrogen bonded organic framework (HOFs) are unique class of material distinct from other conventional porous materials like MOFs and COFs as in their structure is clutched concurrently by hydrogen bonds. When a hydrogen atom is covalently bound to a highly electronegative atom (such nitrogen, oxygen, or fluorine) and is pulled to another electronegative atom in its vicinity, the intramolecular force between the hydrogen atom and the electronegative atom is termed as hydrogen bond. The organic building blocks used in HOFs can vary widely and include a range of functional groups such as carboxylic acids, amines, and pyridines. These building blocks are typically linked together through hydrogen bonds to form extended, three-dimensional networks that possess a high degree of order and periodicity. The resulting structures can have a range of pore sizes and shapes, making them suitable for similar applications like other porous materials. The high porosity of HOFs makes them attractive for storing and separating gases like hydrogen, methane, and carbon dioxide. [6h,I,j] A bottom up approach is used to synthesize Porous organic cages (POCs), where metal center and organic linkers are assembled through covalent bonding to create a cage-like structure. Tuning of length, shape, and connectivity of the building blocks can determine the size and shape of the cage molecule. POCs can also be modified with different functional groups to enhance applicability, such as increasing their hydrophobicity, enhancing their catalytic activity, or improving their selectivity in gas separation. The unique cage-like structure of POCs allows them to selectively adsorb and store gases like hydrogen, methane, and carbon dioxide. In addition, POCs can be designed to have high stability and selectivity towards specific gases, making them ideal for use in gas separation processes. POCs have also shown promise in catalysis applications. The empty cavities within the cage structure provide a confined environment for chemical reactions to occur, which can enhance the selectivity and activity of the catalyst. Another promising application of POCs is in molecular sensing. The cage-like structure of POCs can be designed to selectively recognize and bind to specific molecules, making them ideal candidates for use in sensors and detectors. [6k,l,m]

Intrinsic and extrinsic these two types of porosity are the results of fabrication of porous materials. While intrinsic porosity refers to the development of pores because of the shape and geometry of the building units, extrinsic porosity refers to the porosity formed in molecular architectures as a result of packing between the molecules. [8] Based on all these synthetic strategies different class of porous materials were synthesized and used as a host matrix for various application. In this regard, there are two ways to introduce functionality or charge throughout the extended networks of MOFs or porous organic materials: pre-synthetic alteration and post-synthetic modification. The proper selection of the molecular building blocks has been crucial in the pre-synthetic route for functionalization inside the network. However, as pre-

synthetic functionalization of porous materials is not always simple and straightforward, post-synthetic modification have shown its importance in synthetic chemistry.[9] As desired functionality can be inserted into the pores for specific purposes, post-synthetic modification has attracted tremendous interest.

1.1.1 Advance Porous Materials (APMs):

Advanced porous materials refer to materials with intricate porous structures, engineered at the nano- or micro-scale to exhibit specific and desirable properties. Utilizing materials porous architecture has helped in various applications. Materials can be systematically designed and synthesized for selective applications due to excellent command over the order and functionality. The ability to force certain local and expanded order in these materials is made more flexible by the growing use of molecular building pieces that cipher structure. To generate task specific materials in other words, advance porous materials (APMs) careful selection of functional moieties and use of targeted methodologies are required. The primary building blocks are designed with application specific functionality which were further incorporated to the framework backbone to create a porous scaffold, that is interactive and useful for the specific application.

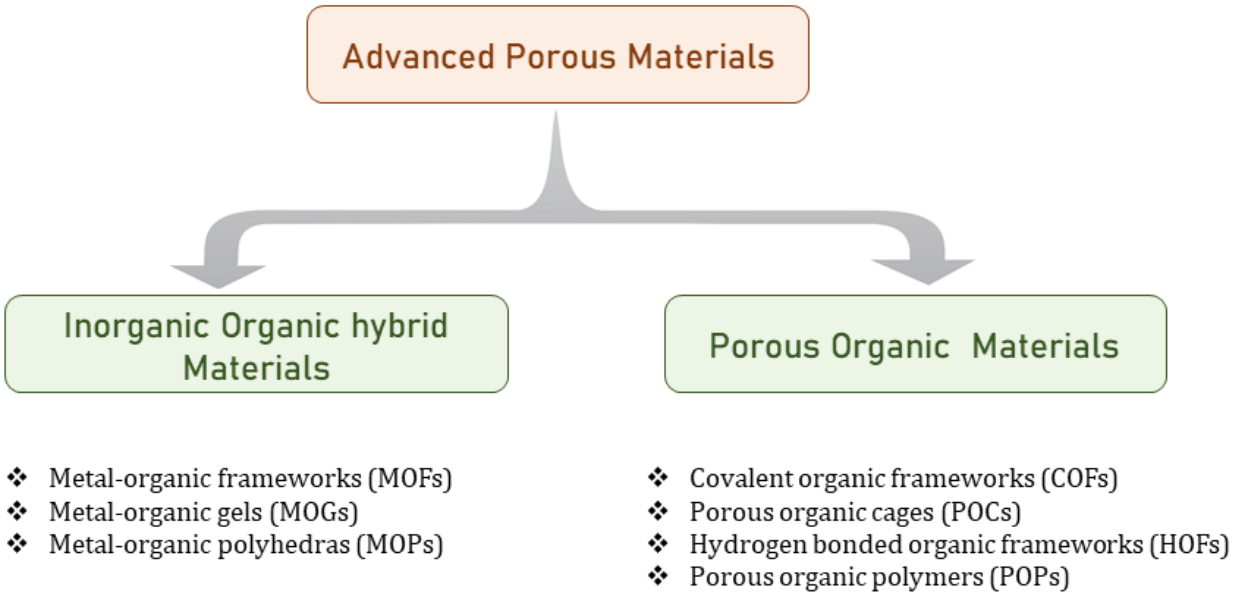

Figure 1.2: Schematic representation for classification of various types of advanced functional porous materials.

1.2 Metal-organic frameworks (MOFs)

Advance porous materials (APMs) have a sub-class metal-organic framework (MOFs) which has drawn special recognition for their distinct advantage over traditional porous materials such as mesoporous silica, activated carbon and zeolites (Fig. 1.2). MOFs are porous crystalline solid constructed due to coordination bond connecting inorganic metal nodes/clusters and organic ligands.[10] In the course the formation of MOFs solvent molecules in the reaction medium generally occupies the void space created by framework. In order to access the void for various applications of the framework, these guest solvents must be removed from MOF pores via de-solvation by vacuum treatment or heating.[11] These MOFs are divided into three generations based on these. After de-solvation, the 1st generation frameworks lose their structural integrity. While 2nd generation framework remains stable and rigid after solvent removal. 3rd generation framework is also known as 'Dynamic framework' shows flexible behavior upon guest removal. Another key characteristic of these materials is their reversible dynamicity.[12] Another technique for synthesizing functional MOFs is called "post synthetic modification" (PSM), in which a porous MOF that was created using the pre-synthetic strategy described above and contains a functional subunit is used to undergo chemical modification to create porous MOFs that are structurally identical but have different functions. The primary benefit of PSM is that it facilitates the production of those functional MOFs that are challenging to make using standard synthetic methods. [9d]

Further, MOFs can be classified depending upon ionic nature of the framework, forming neutral MOFs and ionic MOFs (*i*-MOFs).[13] The framework's nature can be strategically modified depending on the type of organic counterpart used in MOF synthesis. Neutral MOFs form via binding of anionic carboxylate ligand and cationic metal nodes whereas *i*-MOFs are branched into two types anionic and cationic frameworks depending upon their electrostatic nature. Ionic MOFs are formed when framework backbone charge is neutralized by additional counter ion to retain charge neutrality. Cationic MOFs formed by neural N-donor based ligand and positive metal center where excess positive charge of the framework is neutralized by additional counter anion. On the other hand, anionic framework was created where positive metal nodes fail to satisfy charge neutrality after coordination with ligand containing multiple anionic sites and excess counter cations are required for charge balance.

Because of their structural characteristics and huge surface area, MOFs are used in a vast array of applications. The distinct pore aperture of the material and the attached functionalities in the framework's backbone provide a stage for host-guest chemistry. Most relevant applications are gas storage and separation from mixture of gases, as it includes separation of greenhouse gas like carbon dioxide, methane etc. Due to high energy requirement in conventional way of separating hydrocarbons, MOFs can be useful having narrow pore window and long-range order. The porous cavity inside MOF also been utilized for guest recognition via fluorescence turn-on or turn-off response. Functional nodes of framework help in

heterogenous catalysis, electrochemical applications like batteries and supercapacitors. MOFs have shown biocompatible application like drug delivery encapsulating analytes in the void space. Extra ions in ionic framework helps in on exchange-based applications. Also, development of composite material via encapsulation of nano particles or functional moiety has shown its application in clean energy and environment.[14]

1.3 Porous organic materials (POMs)

Porous organic materials (POMs) are a type of organic materials those are composed of organic molecules attached together by covalent bonds to form a three-dimensional network of heterocycles and fused aromatic systems. Although MOFs have several benefits over its congener materials, but poor physiochemical stability and poor scalability hinders its application.[15] In this context various porous materials like porous aromatic frameworks (PAFs), covalent triazine frameworks (CTFs), conjugated microporous polymers (CMPs), hyper crosslinked polymers (HCPs) and covalent organic frameworks (COFs) have attracted attentions of the researchers. Various organic reaction like Friedel crafts reactions and Suzuki coupling are used to develop porous architecture which includes formation of HCP via Friedel craft reaction, CTF trimerization via acid catalyzed and ionothermal reaction, along with Suzuki coupling, Yamamoto coupling for polymers with intrinsic microporosity and conjugation.[16] The purposeful choice of functional moieties as well as reaction sites yields in infinite network structures. The fundamental benefit offered by Porous organic polymers (POPs) is that it has characteristics of both porous materials and organic polymers. While polymeric backbones result in rigid structural topologies, the existence of porous gaps generates enough room for host-guest interaction. Variation of different parameters such as synthetic route, monomer size and shape and component reactivity can be utilized to optimize and tune the porosity of the material. [16c,16d] The reaction condition including initial concentration along with reaction temperature and amount of solvent and catalyst used can have a slight impact in the porous nature of the generated porous solids. POPs are widely recognized for having a large surface area, which produces great porosity, and a robust structure, which produces high stability in a variety of chemical environments. POPs' lack of metals makes them useful as low-density materials, and in some situations, the short-range order in their structures, which is brought about by the nature of molecular packing, makes POPs more solution processibility. Since these materials can be used in both the solution and solid states along with thin films, which is significant for real-time applications.[17] As these compounds are constructed from elements which are light weight in nature, (such as C, N, O etc.) they have advantages for real time application. Both covalent and non-covalent interaction can be used to synthesize these compounds but covalently connected POPs have higher stability.

Materials can be two dimensional or three dimensional depending upon the free rotation of the chemical bond and structure of the building block. [17a] Among all types of materials COFs and few CTFs are crystalline in nature whereas most of other porous materials are found to be amorphous.

Due to their ease of functionalization and adjustable pore surfaces, porous organic materials have also shown their applicability in various domains alike MOFs. The large pores can be applied as molecular recognition, heterogeneous catalysis, gas separation as well as biomedical applications. [18,26] Target specific interaction and incorporation of guest molecules can be tuned by the choice of incorporation of hydrophobic along with hydrophilic functional groups. Applications in the field of molecular identification result from this, including the molecular separation, sensing, and selective capture of a specific molecule from both water and organic media.[18] Extended conjugation within the POPs' backbones aids in the attainment of various photophysical and light-harvesting applications, and the subtle addition of the appropriate functional moieties encourages the usage of these materials for various electrochemical uses.[27]

1.1.2 Characterization of porous materials:

Void spaces inside porous materials can be of different sizes, shapes and distribution which can alter the behavior and property of the material. Characterization of porous material involves analysis of the void spaces as well as other properties such as thermal, water, physiochemical stability and structural rigidity and robustness. Some commonly used methods are

Gas adsorption: This method involves exposing the porous material to a gas and measuring the amount of gas adsorbed at various pressures. Which is further utilized to determine the surface area and pore size distribution of the material.

X-ray diffraction (XRD): This method involves analyzing the crystal structure of the material to determine its composition and crystal structure. In the domain of porous materials crystalline polymers with single crystal can only be characterized by XRD.

Scanning electron microscopy (SEM): This method involves imaging the surface of the material at high magnification to visualize the pore structure and morphology.

Thermo-gravimetric analysis (TGA): TGA analysis talks about the thermal stability of the material as well as the presence of solvents molecules inside the pore network.

Fourier transform infrared spectroscopy (FT-IR): To know about the various functionality and structural bonding FT-IR analysis is been carried out.

Solid state NMR: This method involves using a magnetic field to measure the structural properties of the material which tells about the formation of network.

X-ray Photoelectron Spectroscopy (XPS): XPS is a surface analysis technique. It is a spectroscopic technique based on the photoelectric effect. It analyses the elemental composition, chemical state, and electronic state of the elements within a material.

Overall, the characterization of porous materials is important for understanding their properties and behavior, and for designing and optimizing their use in various applications.

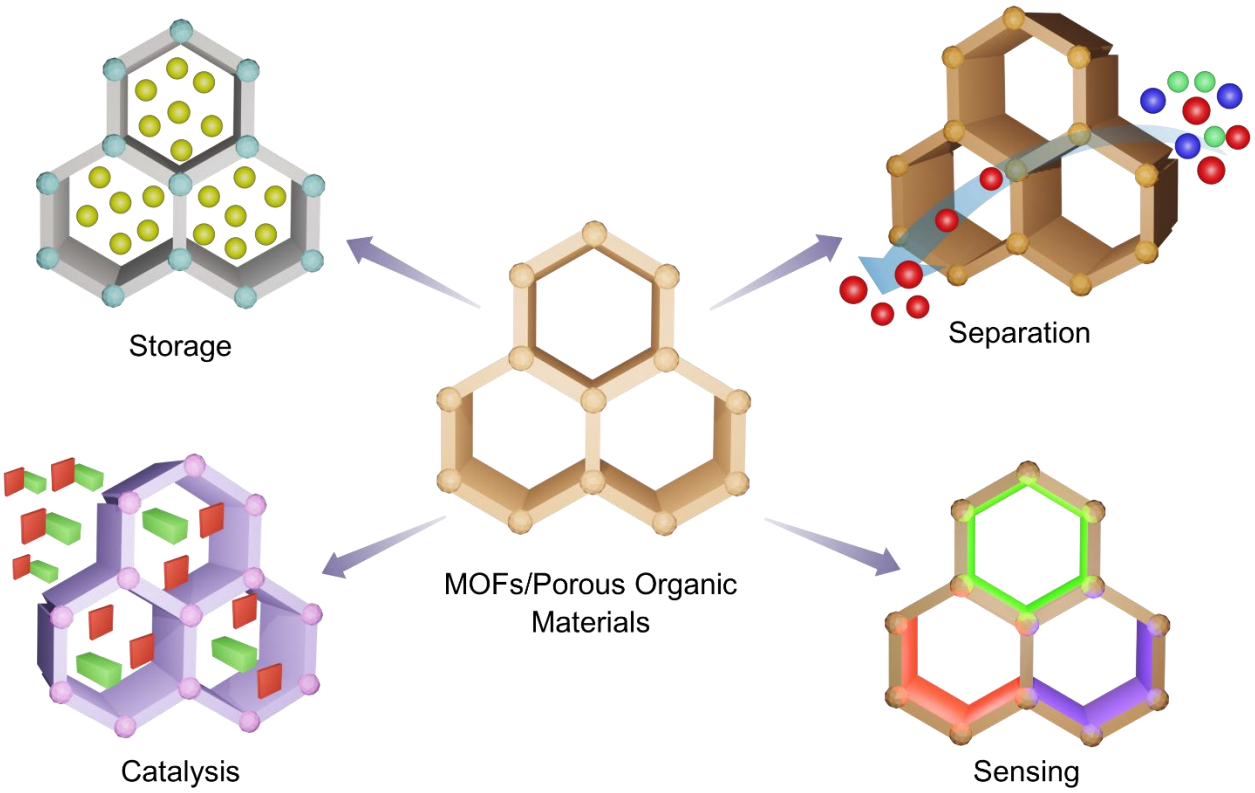

Figure 1.3: Schematic representation of different types of application of MOFs and porous organic materials.

1.4 Applications of MOFs and Porous Organic Materials:

Both metal-organic frameworks and porous organic materials have shown tremendous potential in various fields like, gas storage, separation, drug delivery, and energy storage. Catalysis, sensing of various

hazardous and toxic species, fuel cell applications, electrochemical applications. [14,16] Some of the recent advances and applications of MOFs and porous materials are discussed briefly.

Gas storage: One of the significant applications of MOFs and other porous materials are gas storage and separation. These materials have high surface areas and tunable pore sizes, which make them ideal for storing and separating gases. For example, they have been used to store hydrogen for fuel cells, methane for natural gas vehicles, and carbon dioxide for carbon capture and storage.[24]

Catalysis: Another important application of MOFs and porous materials is catalysis. Having high surface areas, tunable pore sizes, and metal centers these materials can be used as active sites for catalytic reactions. Different metalloporphyrin based polymer have been used as heterogeneous catalysts for various reactions like oxidation, hydrogenation, and carbon-carbon Suzuki coupling using different metal chelated to the porphyrin ring.[25]

Sensing: Luminescent MOFs and porous materials have also shown its potential as sensing materials. These materials can be designed to selectively interact with certain molecules, which can be detected through various techniques such as fluorescence, colorimetry, and electrochemistry. In past few years various MOFs have been used as sensors for explosive, volatile organic compound (VOCs) detection, toxic metal ion detection, and detection of herbicides, pesticides and antibiotics. [14b]

Drug delivery: The domain of porous materials have also been explored for drug delivery applications. These materials can be designed to have high drug loading capacity and controlled release properties. For example, several MOFs and porous materials like mesoporous silica have been used for targeted and controlled drug delivery, where the drug is released at the site of the disease.[26]

Energy storage: Crystalline porous materials have also shown potential for electrochemical energy storage and conversion applications. These materials can be architected to have high porosity, high surface areas, and large pore volumes. which make them ideal for energy storage applications such as supercapacitors and batteries. Similarly, porous materials like carbon nanotubes have been used for energy storage applications.[27]

Gas separation: MOFs have been used for crucial gas separation applications because of their selective adsorption properties. Due to their narrow pore window, long range order and structural integrity and prominent chemical features the cab be used to separate different gas molecules which are very hard to separate in a conventional way.[28]

Although these materials have been utilized widely in the aforementioned applications, they have rarely been investigated for the capture of toxic and hazardous contaminants from waste water. Both MOFs and porous organic materials have been discovered to be qualified participants for these environmental applications in this regard. On the other hand, LMOFs, or luminescent metal-organic frameworks, hold great potential for the recognition of poisonous and environmentally dangerous species. But often poor hydrolytic stability of MOFs limits their application in aqueous medium. As previously mentioned, in this context porous organic materials can be suitable candidate of sequestration of toxic pollutants in aqueous medium.

1.5 Water Pollutions and Remediation

The presence of harmful substance or pollutants in the environment causes adverse effect on living organism, ecosystem and natural environment. Pollution can occur in various forms typically generated by human activities, industrial process, agriculture and urbanization. Polluted environment poses serious threat to biodiversity, sustainability of ecosystems and to human health. This can also adversely affect wildlife and their habitat, leading to a declining species population and a disruption of natural ecosystem. One of the prime origins of environmental pollution is water pollution. In this section a brief discussion about water pollution and role of porous materials for remediation application will be carried out.

Water pollution takes place when contaminants pollute water sources and makes the water unusable in cooking, drinking, swimming, cleaning, and other activities. There are some primary and secondary reasons for water pollution which affects directly or indirectly. One of the primary reasons are industrial waste water, whereas use of modern technique in farms are a major source of secondary water pollution. Besides that, domestic sewage water mostly carries nitrates and phosphates. If large number of these material accumulates it allows algae to develop in the surface of water bodies, which consequently reduces oxygen level of water bodies and thus leads to early death of water system. The runoff of oil in deep sea from the oil tankers, leads to significant increase in sea water pollution. Other than that sediment (result of soil erosion) imbalances river water and harmful for aquatic animals.

In our country ground water contamination is still a major threat, as there is lack of general awareness among peoples for heavy metal contamination in the ground water. According to Composite Water Management Index (CWMI) 2018 study by NITI Aayog, two lakh people die each year due to inadequate access to drinkable clean water and it is expected to rise in upcoming years. The government has taken

steps like “Swachh Bharat Mission” to reduce ground water contamination. Further under the “Namami Ganga” program, the government has taken several initiations in major projects to clean Ganga by proper waste water treatment of the industrial effluents. Other than that, since Aug 2019 central government is working with states to carry out “Jal Jeevan Mission (JJM)”, which aim goals to supply drinkable tab water in every rural household in India by 2024. Involvements of common citizens and general awareness are the necessary behavioral change that can fast track the process for a cleaner environment.

Although the rapid industrialization of past few decades has improved the standard of living and economic prosperity but it has also resulted in terrible environmental degradation effects. Global attention is being paid to the remediation of the pollutants as a result of the gradual rise in environmental contamination. Among others, major global concern of the twenty-first century is water pollution, which has serious negative effects on both the marine ecosystem and human life. Industrial waste, radioactive waste and various human activities are the major sources of water pollution. Large-scale freshwater consumption and rising water pollution have been seen to have a consequential impact on the planet's water eco system (Fig. 1.4).[19] According to a recent study, even though the world's population has grown four times in the past ten years, the number of individuals who face a severe water shortage has increased sixteen times. Of these 1.1 billion people, the majority live in East and South Asia, North Africa, and the Middle East. In upcoming future, the situation is expected to be worsen. In a fresh report, the United Nations (UN) predicted that there will be a 40% shortage of clean water within the next 15 years.[20] Further waterborne diseases like diarrhea, poor hygiene causes death of almost 2 million people each year. There are several types of water pollution, mainly chemical water pollution, physical water pollution and pollution by different pathogens. Microorganisms that cause disease are called pathogens. Fever, diarrhea, abdominal discomfort, and other health issues can arise from pathogen-caused water contamination. Such pathogen-related water contamination might result from untreated sewage discharges into water effluents or on-site sanitation systems. In addition, the release of various physical compounds into sewage or other water effluents can result in physical water pollution. Toxic and hazardous chemical wastes from industries are the main source of chemical water pollution which is life threatening for the living organisms. Chemical pollutants can be introduced into the environment in various ways, including industrial activities, agricultural practices, sewage and wastewater discharges, and accidental spills. These chemicals can have serious and long-lasting consequences on aquatic life, human health, and the surroundings. Chemical water pollution can take many forms, including heavy metals, pesticides, fertilizers, pharmaceuticals, and industrial chemicals. Heavy metals such as lead, mercury, and cadmium are toxic to aquatic organisms, and can accumulate in the food chain, posing risks to human health. Pesticides and fertilizers are commonly used in agriculture to increase crop yield and control pests, but they can also leach into water bodies and cause harmful algal blooms, fish

kills, and other ecological damage. Pharmaceutical compounds, including antibiotics and hormones, can enter waterways through sewage treatment plants, and can have negative impacts on aquatic life and human health. Industrial chemicals such as PCBs, dioxins, and polycyclic aromatic hydrocarbons (PAHs) can be released into waterways through industrial processes, spills, and runoff, and can have serious long-term health effects on both humans and wildlife. One of the biggest challenges of chemical water pollution is its persistence in the environment. Unlike other types of pollution such as sedimentation or organic matter, chemical pollutants are often resistant to degradation and can persist in the environment for years or even decades. Chemical water pollution can also have serious impacts on human health. Subjection to contaminated water can lead to a range of health problems, including cancer, neurological disorders, developmental delays, and reproductive issues. This is particularly concerning for vulnerable populations such as children, pregnant women, and low-income communities who may be more likely to rely on contaminated water sources. In addition, chemical pollutants can enter the food chain through fish and other aquatic organisms, posing additional risks to human health. Chemical water pollutants has been divided into two types, organic and inorganic pollutants (Fig 1.5).[19c,21]

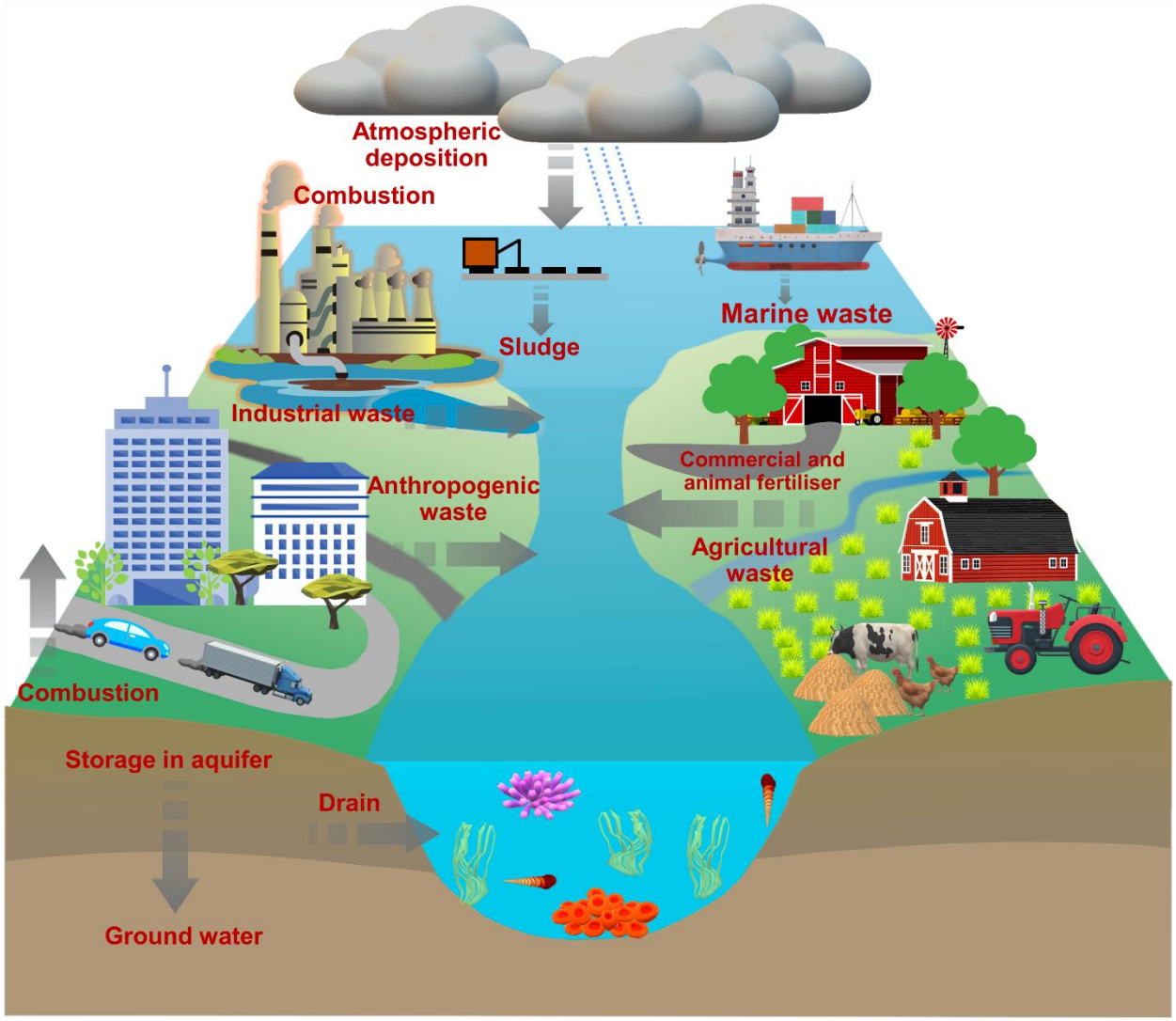

Figure 1.4: Schematic representation of sources of water pollution.

Several types of dye molecules, herbicides/pesticides, oils, pharmaceutical goods, personal care products, polyaromatic hydrocarbons, detergents, etc. are among the most popular and well-known organic pollutants. It has been discovered that organic pollutants are released by a variety of residential activities, industries, agricultural fields, etc. [22] Whereas its inorganic counterpart includes different types of heavy metal (e.g., Hg^{2+}, Pb^{2+}, Cd^{2+} etc.), oxo-anion (e.g., CrO_4^{2-}, $Cr_2O_7^{2-}$, AsO_4^{3-}, SeO_3^{2-}, SeO_4^{2-} etc.), radionuclides (e.g., ^{99}Tc, ^{131}I, ^{129}I, ^{137}Cs, ^{89}Sr, ^{235}U etc.).[23] Inorganic contaminants are less prevalent and have a smaller diversity than organic pollutants. Yet, compared to organic pollutants, inorganic pollutants stay in the environment for a considerably longer duration and are very difficult to degrade or convert into some lesser toxic species. Organic pollutants, on the other hand, tend to be less persistent in the environment

and easier to decompose. But the huge discharge of organic pollutants in water levels organic pollutant as pseudo-persistent pollutant. Most of these organic and inorganic contaminants are poisonous, dangerous, and cancer-causing in nature and leads to several lethal diseases.

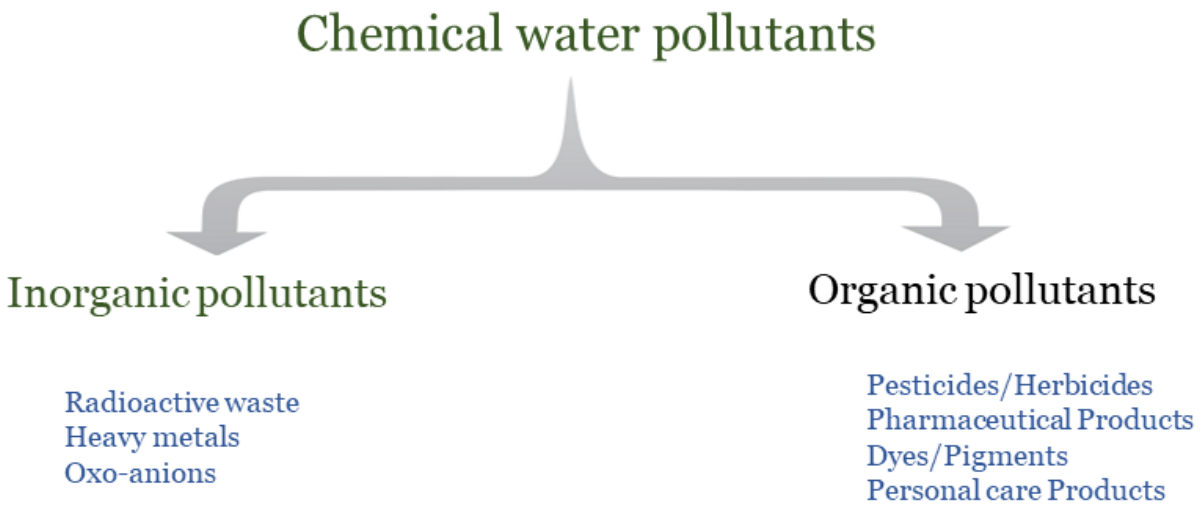

Figure 1.5: Schematic representation of various types of the water pollutants.

In order to ensure that everyone has access to clean water, the United Nations adopted the Sustainable Development Agenda. Desalination of saltwater for freshwater or clean water extraction from groundwater has emerged as one of the top options in this regard. However, in order to be used in real time, these strategies must be effective and cost-effective globally. Furthermore, widespread application of such methods may cause groundwater crises, and desalination facilities used to treat seawater may contaminate coastal areas. [19c,22d] Reusing water has emerged as most effective and most promising solutions, outside of the purification of groundwater and seawater and several technologies have been employed for it. Those are flocculation/coagulation, precipitation, filtration, membrane technology, sedimentation, advanced oxidation process etc. Although these methods are effective, researchers are looking for alternate solutions because of complicated operation, high operation cost, generation of secondary low efficiency of these standard materials. In this regard, an adsorption-based technique has emerged as substitutes due to their efficiency, low operating costs, ease of use, recyclability, relative lack of secondary pollution formation

etc. Many materials, including polymer resins, zeolites, activated carbons, mesoporous silica, mesoporous clay materials, etc., have been tested so far for the removal of toxic and hazardous chemical waste using adsorption method. However, it has been found that slow kinetics, low capacity, comparatively difficult adsorbate production, poor selectivity of those materials frequently poses threats for real-time applications.

MOF-based materials have recently begun to be investigated for use in environmental applications. The detection and containment of environmentally dangerous species using MOFs has attracted enormous interest. However, due of their weak chemical stability, MOFs frequently fall short of meeting all the requirements for capture studies. Furthermore, porous organic materials have come out as one of the best materials for the purification of water pollution due to their high physiochemical stability, ease of design and synthesis, and tunable architecture. Such applicability of porous polymers has rarely been explored; therefore, it has tremendous potential for the required application. The robust nature of the porous organic material helps for scavenging various pollutants in harsher chemical environment. These materials can be easily synthesizable and large pores of these materials can help for larger amount of absorbance of pollutants. These arguments make it clear that covalently bonded porous organic materials may be a strong contender for addressing chemical water contamination.

1.6 Toxic pollutants sensing:

Selective and sensitive detection of harmful species in aqueous medium has become a leading research area for monitoring and maintaining balance in environmental ecosystem. Although in past years several methods have been established such as mass spectroscopy, Raman spectroscopy, electro-chemical methods and photoluminescence-based technics. Having said that, from all the techniques photoluminescence-based techniques have earned prominent attention over others due to their several benefits like cost effectiveness, low detection limit with high precision. In this context luminescent MOFs (LMOFs) have exhibited suitability for sensing application.[14] However literature report suggests, most of the LMOF based sensors exhibits “turn-off” response, by fluorescence quenching. This process often struggles with the problem of sensitivity and selectivity. Considering the real time application, molecular “turn on” technique is a favorable technique for detection.

1.7 Thesis Overview

Here the work carried out in the thesis has targeted on design and synthesis of functional MOFs and porous organic materials for detection and sequestration of toxic pollutants (Fig 1.6). In this context, functionalized MOFs have been used to detect toxic pollutants, but the use of MOFs for pollutant capture has not yet been investigated because most MOFs lack the desirable and necessary chemical stability. Further use has been made of functionalized porous organic materials for the sequestration of hazardous water contaminants. Both pre and post synthetic route has been employed for developing the required material. Each piece of work featured in this thesis has applied task-specific porous materials for the remediation of water contaminants.

In the second chapter (chapter 2) a post metalized MOF was utilized as potential sensory material to detect hazardous cyanide ion, i.e., CN^- ion. To conduct the sensing experiment in aqueous medium a water stable MOF (MOF-867) was chosen. Further, copper chloride was loaded in the MOF via post synthetic modification for selectively loading copper in the bipyridyl moiety. The copper loaded MOF shows decrease in luminescence intensity, which in presence of CN^- ion regains it luminosity as previous. This can be attributed to the formation of more stable $Cu(CN)_2$ species. Thus, reaction-based cleavage of pyridyl copper bond and formation of $Cu(CN)_2$ leads to a luminescence response. The probe material illustrates highly sensitive and selective aqueous phase "turn-on" detection of potential hazardous cyanide ions from waste water.

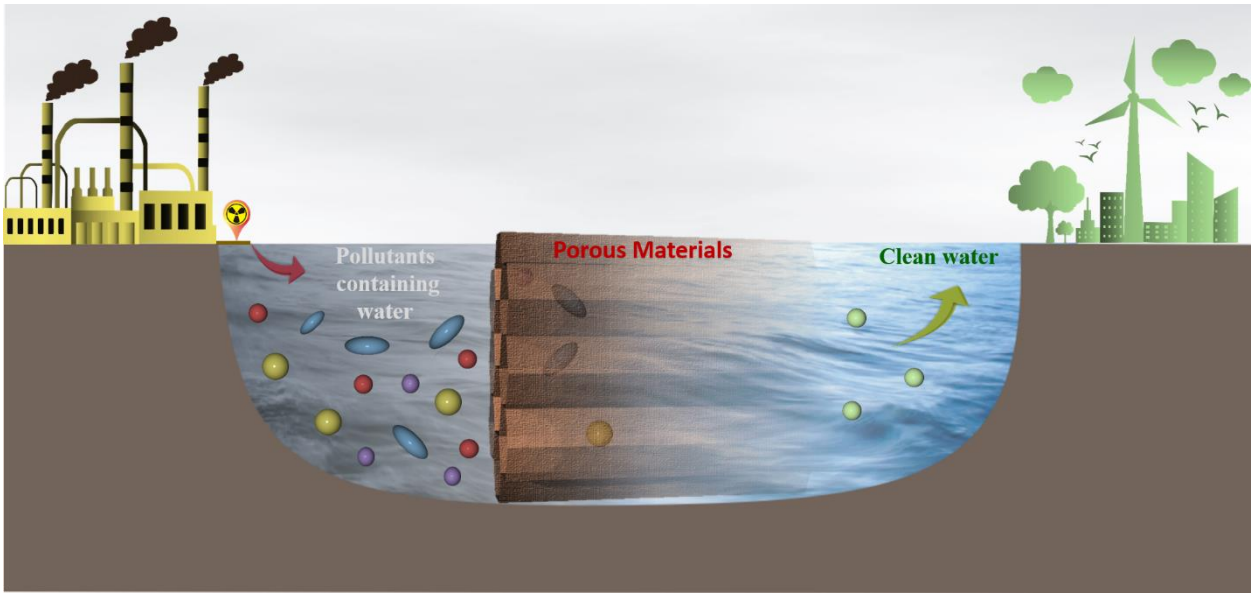

Figure 1.6: Schematic depiction of remediation of the water pollutants using porous materials.

Even if MOF-based sensing was used in the chapter before, only sensing contaminants wasn't sufficient for clean and pure water. Covalently linked porous organic materials were used further due to their excellent chemical stability to conduct out the capture research of hazardous pollutants from water. Based on that in the third chapter (chapter 3), two chemically stable ionic porous organic polymer (*i*POP) was utilized for capture of lethal and toxic heavy metal, Hg^{2+} ion. For these, two rare anionic polymer was designed and synthesized having carbohydrazide (POP-1) and thio-carbohydrazide (POP-5) functional moiety playing different roles in capture studies. Both the compound showed efficient mercury removal from aqueous medium and kinetics data fits with the pseudo second order model. Also capture studies have been performed in presence of other contaminated cations (eg. Pb^{2+}, Cd^{2+}, K^{+} etc.). Overall capacity and recyclable efficiency of the two *i*POPs are directly dependent of the functionality of the polymer. POP-5 having thio carbohydrazide functionality shows higher capacity value whereas POP-1 was found to be reusable and recyclable up to three cycles.

Apart from cationic heavy metal pollutant, oxo-anions of different radioactive metals or heavy metals are also hazardous. Cr(VI)-based oxoanion have attracted a lot of recognition because of carcinogenic and mutagenic nature of the chromium. On the other hand, technetium (^{99}Tc) a radioactive waste, remains in it its favorable oxo-anion form in nature. Because handling radioactive species in a laboratory environment is not practical, capture study was carried out using surrogate ReO_4^- ion. In this chapter (chapter 4) a new troger base polymer have been synthesized and further post synthetic modification was carried out to convert the neutral polymer into two cationic polymers having SO_4^{2-} ion and I^- as a counter ion respectively. The role of template anion for removal of targeted analytes has been demonstrated. The cationic polymers show efficient removal of both the targeted analyte in aqueous medium even when the concurrent anions like Cl^-, NO_3^- and ClO_4^- are present. Further the compound was reused for several cycles with tertbutyl ammonium sulfate. The ultrafast removal efficiency of the polymer opens new door for real time application.

Apart from inorganic pollutants, organic pollutants like dyes, pesticides, herbicides are also recognized as major pollutants. The following work (chapter 5) involved post synthetically modified, chemically stable polymer for anionic dye removal. For this a new troger base polymer was synthesized and post synthetically modified using similar synthetic route as the previous chapter. Further the polymer was used to capture dyes like Indigo carmine (IC), methyl orange (MO) etc. via anion exchange. This process followed the size of dye molecules, larger the size lower is the adsorption capacity. Methylene blue, a cationic dye, was used to further demonstrate selectivity, where polymer shows negligible uptake of methylene blue. Moreover, the polymer demonstrated particular removal of anionic dyes from a binary mixture of anionic and cationic dye (methylene blue and methyl orange) in aqueous medium.

In conclusion various porous materials have been employed for detection and sequestration of harmful pollutants from water.

1.8 References

1. (a) A. I. Cooper, *ACS Cent. Sci*., 2017, **3**, 544-553. (b) D. Zhao, P. K. Thallapally, C. Petit and J. Gascon, *ACS Sustainable Chem. Eng.,* 2019, **7**, 7997-7998.

2. (a) D. Wu, F. Xu, B. Sun, R. Fu, H. He, and K. Matyjaszewski, *Chem. Rev.*, 2012, **112**, 3959−4015.

3. (a) M. E. Davis, *Nature*., 2002, **417**, 813-821.

4. (a) A. G. Slater, A. I. Cooper, *Science*, 2015, **348**, 8075, (b) M. E. Davis and R. F. Lobo, *Chem. Mater*., 1992, **4**, 756-768, (c) A. Corma, *Chem. Rev.*, 1997, **97**, 2373-2419. (d) A. J. Howarth, M. J. Katz, T. C. Wang, A. E. Platero-Prats, K. W. Chapman, J. T. Hupp and O. K. Farha, *J. Am. Chem. Soc*., 2015, **137**, 7488−7494. (e) T. Kitao, Y. Zhang, S. Kitagawa, B. Wang and T. Uemura, *Chem. Soc. Rev*., 2017, **46**, 3108–3133. (f) Z. Hu, B. J. Deibert and J. Li, *Chem. Soc. Rev.*, 2014, **43**, 5815–5840. (g) Z. Chang , D. -H. Yang , J. Xu , T. -L. Hu and X. -H. Bu, *Adv. Mater*., 2015, **27**, 5432–5441. (h) W. Xia, A. Mahmood, R. Zou and Q. Xu, *Energy Environ. Sci*., 2015, DOI: 10.1039/C5EE00762C. (i) M. Sindoro, N. Yanai, A. -Y. Jee and S. Granick, *Acc. Chem. Res*., 2014, **47**, 459-469. (j) J. Aguilera-Sigalat and D. Bradshaw, *Coord. Chem. Rev*., 2016, **307**, 267-291. (k) L. Zhu, X. -Q. Liu, H. -L. Jiang and L. -B. Sun, *Chem. Rev*., 2017, **117**, 8129−8176. (l) C. R. Kim, T. Uemura and S. Kitagawa, *Chem. Soc. Rev.*, 2016,**45**, 3828-3845. (m) J. Canivet, A. Fateeva, Y. Guo, B. Coasne and D. Farrusseng, *Chem. Soc. Rev.*, 2014, **43**, 5594-5617. (n) J. -P. Zhang, Y. -B. Zhang, J. -B. Lin, and X. -M. Chen, *Chem. Rev*., 2012, **112**, 1001–1033. (o) J. Rocha, L. D. Carlos, F. A. A. Paza and D. Ananias, *Chem. Soc. Rev.*, 2011, **40**, 926–940. (p) O. Shekhah, J. Liu, R. A. Fischer and C. Wöll, *Chem. Soc. Rev.*, 2011, **40**, 1081–1106. (q) R. E. Morris and J. Čejka, *Nat. Chem.*, 2015, DOI: 10.1038/NCHEM.2222. (r) H. M. El-Kaderi, J. R. Hunt, J. L. Mendoza-Cortés, A. P. Côté, R. E. Taylor, M. O'Keeffe and O. M. Yaghi, *Science*, 2007, **316**, 268–272. (s) S. Furukawa, J. Reboul, S. Diring, K. Sumida and S. Kitagawa, *Chem. Soc. Rev.*, 2014, **43**, 5700–5734.

5. (a) J. Jhiang, Y. Zhao and O.M. Yaghi, *J. Am. Chem. Soc.*, 2016, **138**, 3255-3265, (b) H.-C. Zhou and S. Kitagawa, *Chem. Soc. Rev.*, 2014, **43**, 5415-5418, (c) D. J. Tranchemontagne, Z. Ni, M. O'Keeffe and Omar M. Yaghi, *Angew. Chem., Int. Ed*., 2008, **47**, 5136-5147, (d) J. H. Jung, J. H. Lee, J. R. Silverman and G. John, *Chem. Soc. Rev.*, 2013, **42**, 924-936, (e) R. Dawson, A. I. Cooper and D. J. Adams, *Prog. Polym. Sci.*, 2012, **37**, 530-563.

6. (a) S. Yuan, X. Li, J.Zhu, G. Zhang, P. V. Puyvelde and B. V. Bruggen, , *Chem. Soc. Rev.*, 2019, **48**, 2665-2681, (b) J. Luo, J.-W.Wang, J.-H. Zhang, S. Laia and D.-C. Zhong, *CrystEngComm.*, 2018, **20**, 5884–5898, (c) M.A. Little and A. I. Cooper, *Adv. Funct. Mater.*, 2020, **30**, 1909842, (d) D. Wu, F. Xu, B. Sun, R. Fu, H. He and K. Matyjaszewski, *Chem. Rev.*, 2012, **112**, 3959-4015. (e) K. Geng, T. He, R. Liu, S. Dalapati, K. T. Tan, Z. Li, S. Tao, Y. Gong, Q. Jiang and D. Jiang, *Chem. Rev*. 2020, **120**, 16, 8814–8933. (f) O. M. Yaghi, *ACS Cent. Sci.*, 2019, 5, **8**, 1295–1300. (g) I. Ahmed and S. H. Jhung, *Coordination Chemistry Reviews*, 2021, **441**, 213989. (h) B. Wang, R.-B. Lin, Z. Zhang, S. Xiang and B. Chen, *Journal of the American Chemical Society*, 2020, **142**, 14399-14416. (i) R.-B. Lin, Y. He, P. Li, H. Wang, W. Zhou and B. Chen, *Chem. Soc. Rev.*, 2019, **48**, 1362-1389. (j) R.-B. Linand B. Chen, *Chem*, 2022, **8**, 2114-2135. (k) D. Hu, J. Zhang and M. Liu, *Chem. Commun*., 2022, **58**, 11333-11346. (l) A. G. Slater, P. S. Reiss, A. Pulido, M. A. Little, D. L. Holden, L. Chen, S. Y. Chong, B. M. Alston, R. Clowes, M. Haranczyk, M. E. Briggs, T. Hasell, G. M. Day and A. I. Cooper, *ACS Cent. Sci.*, 2017, **3**, 734−742. (m) H. Wang, Y. Jin, N. Sun, W. Zhang and J. Jiang, *Chem. Soc. Rev.*, 2021, **50**, 8874-8886.

7. (a) S. Lee, H. Jeong, D. Nam, M. S. Lah and W. Choe, *Chem. Soc. Rev.*, 2021, **50**, 528-555. (b) M. Jung, H. Kim, K. Baek and K. Kim, *Angew Chem.*, 2008, **120**, 5839-5841. (c) N. Ahmad, H. A. Younus, A. H. Chughtai and F. Verpoort, *Chem. Soc. Rev.*, 2015, **44**, 9-25. (d) N. Chaoui, M. Trunk, R. Dawson, J. Schmidt and A. Thomas, *Chem. Soc. Rev.*, **2017**, 46, 3302-3321. (e) K. Geng, T. He, R. Liu, S. Dalapati, K. T. Tan, Z. Li, S. Tao, Y. Gong, Q. Jiang and D. Jiang, *Chem. Rev.*, **2020**, 120,8814–8933. (f) X. Guan, F. Chen, Q. Fang and S. Qiu, *Chem. Soc. Rev.*, **2020**, 49, 1357–1384. (g) X. Zhao, P. Pachfule and A. Thomas, *Chem. Soc. Rev.*, **2021**, 50, 6871. (h) X.-Y. Guan, F.-Q. Chen, S.-L. Qiu, Q.-R. Fang, *Angew. Chem., Int. Ed.*, **2023**, 62, e202213203. (i) T. Zhang, G. Xing, W. Chen and L. Chen, *Mater. Chem. Front.*, **2020**, 4, 332-353.

8. (a) M. J. Bojdys, M.l E. Briggs, J. T. A. Jones, D. J. Adams, S. Y. Chong, M. Schmidtmann and A. I. Cooper, *J. Am. Chem. Soc.*, 2011, **133**, 16566-16571, (b) J. R. Holst, A. Trewin and A. I. Cooper, *Nat. Chem.*, 2010, **2**, 915-920. (c) L. Wang, H. Xu, J. Gao, J. Yao and Q. Zhang, *Coordination Chemistry Reviews*., 2019, **398**, 213016. (d) J. K. Wychowaniec, H. Saini, B. Scheibe, D. P. Dubal, A. Schneemann and K. Jayaramulu, *Chem. Soc. Rev*., 2022, **51**, 9068-9126.

9. (a) Z. Wang and S. M. Cohen, *Chem. Soc. Rev*., 2009, **38**, 1315–1329, (b) Z. Yin, S. Wan, J. Yang, M. Kurmoo and M. -H. Zeng, *Coord. Chem. Rev.*, 2019, 378, 500-512, (c) T. Islamoglu, S. Goswami, Z. Li, A. J. Howarth, O. K. Farha and J. T. Hupp, *Acc. Chem. Res.*, 2017, **50**, 805−813. (d) S. M. Cohen, *J. Am. Chem. Soc.*, 2017, **139**, 2855-2863.

10. (a) 18] H. Furukawa, K. E. Cordova, M. O'Keeffe and O. M. Yaghi, *Science.*, 2013, **341**, 6149, (b) S. Kitagawa, R. Kitaura, , S.-i. Noro, *Angew. Chem. Int. Ed.* 2004, **43**, 2334-2375. (c) J. An, C. M. Shade, D. A. Chengelis-Czegan, S. Petoud, N. L. Rosi, *J. Am. Chem. Soc.* 2011, **133**, 1220-1223. (d) L. Li, X. Wang, J. Liang, Y. Huang, H. Li, Z. Lin, R. Cao, *ACS Appl. Mater. Interfaces* 2016, **8**, 9777-9781. (e) P. Li, N. A. Vermeulen, X. Gong, C. D. Malliakas, J. F. Stoddart, J. T. Hupp, O. K. Farha, *Angew. Chem. Int. Ed.* 2016, **55**, 10358-10362.

11. (a) D. Wu, P.-F. Zhang, G.-P. Yang, L. Hou, W.-Y. Zhang, Y.-F. Han, P.Liu abd Y.-Y.Wang, *Coord. Chem. Rev*., 2021, **434**, 213709. (b) H.-F. Ma, Q.-Y. Liu, Y.-L. Wang, S.-G. Yin, *Inorg. Chem.* 2017, **56**, 2919-2925. (c) H. Fei, L. Paw U, D. L. Rogow, M. R. Bresler, Y. A. Abdollahian, S. R. J. Oliver, *Chem. Mater*. 2010, **22**, 2027-2032. (d) I. R. Colinas, K. K. Inglis, F. Blanc, S. R. J. Oliver, *Dalton Trans.* 2017, **46**, 5320-5325.

12. (a) S. Horike, S. Shimomura and S. Kitagawa, *Nat. Chem.*, 2009, **1**, 695-704. (b) S. Horike, S.Shimomura and S. Kitagawa, *Nat.Chem.*, 2009, **1**, 695-704. (c) X. Li, H. Xu, F. Kong, R. Wang, *Angew. Chem. Int. Ed.* 2013, **52**, 13769-13773. (d) M. Guo, H. Guo, S. Liu, Y. Sun, X. Guo, *RSC Adv*. 2017, **7**, 51021-51026.

13. (a) A. Karmakar, A. V. Desai and S. K. Ghosh, *Coord. Chem. Rev.*, 2016, **307**, 313–341. (b) Y. He, B. Li, M. O'Keeffe and B. Chen, *Chem. Soc. Rev*., 2014, **43**, 5618-5656. (c) J. -P. Zhang, Y. -B. Zhang, J. -B. Lin and X.-M. Chen, *Chem. Rev*., 2012, **112**, 1012-1033.

14. (a) B. Seoane, J. Coronas, I. Gascon, M. E. Benavides, O. Karvan, J. Caro, F. Kapteijna and J. Gascon, *Chem. Soc. Rev*., 2015, **44**, 2421-2454, (b) S. Mukherjee, A. V. Desai and S. K. Ghosh, *Coord. Chem. Rev.*, 2018, **367**, 82-126, (c) M. D. Allendorf, C. A. Bauer, R. K. Bhaktaa and R. J. T. Houka, *Chem. Soc. Rev*., 2009, **38**, 1330-1352, (d) B. Li, M. Chrzanowski, Y.Zhang and S. Ma, *Coord. Chem. Rev*., 2016, **307**, 106-129, (e) X.Cao, C. Tan, M. Sindorob and H. Zhang, *Chem. Soc. Rev*., 2017, **46**, 2660-2677, (f) L. Wang, M. Zheng and Zhigang Xie, *J. Mater. Chem. B*., 2018, **6**,

707-717, (g) T. Yamada, K.Otsubo, R. Makiurac and H. Kitagawa, *Chem. Soc. Rev*., 2013, **42**, 6655-6669, (h) Q. –L. Zhu and Q. Xu, *Chem. Soc. Rev*., 2014, **43**, 5468-5512. (i) S. Mukherjee, D. Sensharma, O.T. Qazvini, S. Dutta, L. K. Macreadie, S. K. Ghosh, R. Babarao, *Coord. Chem. Rev*., 2021, **437**, 213852.

15. (a) W. Lu, D. Yuan, J. Sculley, D. Zhao, R. Krishna and H. –C. Zhou, *J. Am. Chem. Soc*., 2011, **133**, 18126–18129. (b) S. Keskin, T. M. van Heest and D. S. Sholl, *ChemSusChem*, 2010, **3**, 879–891. (c) X. Feng, X. Ding and D. Jiang, *Chem. Soc. Rev*., 2012, **41**, 6010–6022. (d) S. Das, P. Heasman, T. Ben and S. Qiu, *Chem. Rev*., 2017, **117**, 1515−1563. (e) P. J. Waller, F. Gándara and O. M. Yaghi, *Acc. Chem. Res.*, 2015, **48**, 3053−3063. (f) L. Zou, Y. Sun, S. Che, X. Yang, X. Wang, M. Bosch, Q. Wang, H. Li, M. Smith, S. Yuan, Z. Perry and H. -C. Zhou, *Adv. Mater*., 2017, **29**, 1700229. (g) Y. Xu, S. Jin, H. Xu, A. Nagai and D. Jiang, *Chem. Soc. Rev*., 2013, **42**, 8012–8031. (h) R. P. Bisbey and W. R. Dichtel, *ACS Cent. Sci*., 2017, **3**, 533−543. (i) B. Aguila, Q. Sun, J. A. Perman, L. D. Earl, C. W. Abney, R. Elzein, R. Schlaf and S. Ma, *Adv. Mater*., 2017, **29**, DOI: 10.1002/adma.201700665. () U. Diaza and A. Corma, *Coord. Chem. Rev.*, 2016, **311**, 85–124. (i) D. D. Medina, T. Sick and T. Bein, *Adv. Energy Mater*., 2017, DOI: 10.1002/aenm.201700387. (j) J. Wu, F. Xu, S. Li, P. Ma, X. Zhang, Q. Liu, R. Fu and D. Wu, *Adv. Mater.*, 2018, DOI: 10.1002/adma.201802922. (k) F. Beuerle and B. Gole, *Angew. Chem. Int. Ed.*, 2018, **57**, 4850–4878. (l) M. S. Lohse and T. Bein, *Adv. Funct. Mater.*, 2018, **28**, DOI: 10.1002/adfm.201705553. (l) S. M. J. Rogge, A. Bavykina, J. Hajek, H. Garcia, A. I. Olivos-Suarez, A. Sepúlveda-Escribano, A. Vimont, G. Clet, P. Bazin, F. Kapteijn, M. Daturi, E. V. Ramos-Fernandez, F. X. Llabrés i Xamena, V. Van Speybroeck and J. Gascon, *Chem. Soc. Rev*., 2017,**46**, 3134-3184.

16. (a) S. Das, P. Heasman, T. Ben and S. Qiu, *Chem. Rev*., 2017, **117**, 1515-1563, (b) D.Wu, F.Xu, B. Sun, R. Fu, H. He and K.Matyjaszewski, *Chem. Rev.*, 2012, **112**, 3959-4015. (c) S. Das, P. Heasman, T. Ben and S. Qiu, *Chem. Rev*., 2017, **117**, 1515-1563. (d) X. Zou, H. Rena and G. Zhu, *Chem. Commun.*, 2013, **49**, 3925—3936.

17. (a) Y. Yuan and G. Zhu, *ACS Cent. Sci.*, 2019, **5**, 509-518. (b) Y. Yuan and G. Zhu, *ACS Cent. Sci.*, 2019, **5**, 509-518. (c) D.Wu, F.Xu, B. Sun, R. Fu, H. He and K.Matyjaszewski, *Chem. Rev.*, 2012, **112**, 3959-4015.

18. (a) N. Chaoui, M. Trunk, R. Dawson, J. Schmidt and A. Thomas, *Chem. Soc. Rev.*, 2017, **46**, 3302-3321, (b) L. Tan and B. Tan, *Chem. Soc. Rev.*, 2017, **46**, 3322-3356 , (c) N. Fontanals, R. M. Marcé, F. Borrulla and P. A. G. Cormack, *Polym. Chem*., 2015, **6**, 7231–7244. (d) N. Fontanals, R. M. Marcé, F. Borrulla and P. A. G. Cormack, *Polym. Chem*., 2015, **6**, 7231–7244. (e) L. Tan and B. Tan, *Chem. Soc. Rev.*, 2017, **46**, 3322-3356. (f) N. Chaoui, M. Trunk, R. Dawson, J. Schmidt and A. Thomas, *Chem. Soc. Rev.*, 2017, **46**, 3302-3321.

19. (a) A. J. Howarth, Y. Liu, J. T. Hupp and O. K. Farha, *CrystEngComm*, 2015, **17**, 7245–7253, (b) J.B. Derraik, *Mar. Pollut. Bull.*, 2002, **44**, 842–852, (c) M. Mon, R. Bruno, J. Ferrando-Soria, D. Armentano and E. Pardo, *J. Mater. Chem. A*, 2018, **6**, 4912–4947. (d) J. Murria, *Nat. Hazards Rev.*, 2003, **4**, 166. (e) R.P. Schwarzenbach, B.I. Escher, K. Fenner, T.B. Hofstetter, C.A. Johnson, U. Gunten and B. Wehri, *Science.*,2006**, 313**, 1072–1077.

20. (a) M. Kummu, J. H. A. Guillaume, H. de Moel, S. Eisner, M. Flörke, M. Porkka, S. Siebert, T. I. E. Veldkamp & P. J. Ward Scientific Reports. 2016, 6, 38495, (b) D. T. Sun, L. Peng, W. S. Reeder, S. M. Moosavi, D. Tiana, D. K. Britt, E. Oveisi and W. L. Queen, *ACS Central Science*, **2018**, *4*, 349-356, (c) WWAP (United Nations World Water Assessment Programme). Water for a Sustainable World; The United Nations World Water Development Report: UNESCO:Paris, 2015; pp 1−67.

21. https://www.epa.gov/dwstandardsregulations., (b) P. Samanta, P. Chandra, S. Dutta, A. V. Desai, S. K. Ghosh, *Chem. Sci*. **2018**, *9*, 7874–7881. (c) Organic Pollutants in Water, ed. I. H. Suffet and M. Malaiyandi, *American Chemical Society*, Washington, DC, 1986, vol. **214**. (d) A. Waheed , N. Baig, N. Ullah and W. Falath, *Journal of Environmental Management*., 2021, **287**, 112360. (e) E. M. Dias and C. Petit, *J. Mater. Chem. A*, 2015, **3**, 22484–22506.

22. (a) Organic Pollutants in Water, ed. I. H. Suffet and M. Malaiyandi, American Chemical Society, Washington, DC, 1986, vol. 214. (b) I. Ali, M. Asim and T. A. Khan, *J. Environ. Manage.*, 2012, **113**, 170–183. (c) M. Yang, *J. Environ. Sci. Health, Part C: Environ. Carcinog. Ecotoxicol. Rev.*, 2011, **29**, 223–249. (d) E. M. Dias and C. Petit, *J. Mater. Chem. A*, 2015, **3**, 22484–22506.

23. (a) P. B. Tchounwou, C. G. Yedjou, A. K. Patlolla and D. J. Sutton, *EXS*, 2012, 133–164. (b) J. Li, X. Wang, G. Zhao, C. Chen, Z. Chai, A. Alsaedi, T. Hayat and X. Wang, *Chem. Soc. Rev.*, 2018, **47**, 2322-2356. (c) S. N. Groudev, S. G. Bratcova and K. Komnitsas, *Miner. Eng.*, 1999, **12**, 261–270. (d) Q. Gao, J. Xu and X. -H. Bu, *Coord. Chem. Rev.*, 2019, DOI:10.1016/j.ccr.2018.03.015.

24. (a) Z. Chen, K. O. Kirlikovali, K. B. Idrees, M. C. Wasson and O. K. Farha, *Chem*.,2022, 8, **3**, 693-716. (b) T. A. Makal, J.-R. Li, W. Lu and H.-C. Zhou, *Chem. Soc. Rev*., 2012, **41**, 7761-7779. (c) Y. He, W. Zhou, G. Qian and B. Chen, *Chem. Soc. Rev.*, 2014, **43**, 5657-5678. (d) G. Singh, J. Lee, A. Karakoti, R. Bahadur, J. Yi, D. Zhao, K. AlBahilyc and A. Vinu, *Chem. Soc. Rev.*, 2020, **49**, 4360—4404.

25. (a) Y. Zhang and S. N. Riduan, *Chem. Soc. Rev.*, 2012, **41**, 2083-2094. (b) Y.-Z. Chen, R. Zhang, L. Jiao, H.-L. Jiang, *Coordination Chemistry Reviews.*, 2018, **362**, 1–23.

26. (a) H. D. Lawson, S. P, Walton and C. Chan, *ACS Appl. Mater. Interfaces.*, 2021, 13, **6**, 7004–7020. (b) Y. Zhu, P. Xu, X. Zhang and D. Wu, *Chem. Soc. Rev.*, 2022, **51**, 1377-1414.

27. (a) L. Kong, M. Zhong, W. Shuang, Y. Xu and X.-H. Bu, *Chem. Soc. Rev.*, 2020, **49**, 2378-2407. (b) J. Zhou and B. Wang, *Chem. Soc. Rev.*, 2017, **46**, 6927-6945. (c) T. Liu and G. Liu, *Nat.Commun*., 2020, **11**, 1-3. (d) T. Zhang, G. Xing, W. Chen and L. Chen, *Mater. Chem. Front*., 2020, **4**, 332-353.

28. (a) Q. Qian, P. A. Asinger, M. J. Lee, G. Han, K. M. Rodriguez, S. Lin, F. M. Benedetti, A. X. Wu, W. S. Chi, and Z. P. Smith, *Chem. Rev.*, 2020, 120, **16**, 8161–8266. (b) R.-B. Lin, S. Xiang, W. Zhou and B. Chen, *Chem*, 2020, **6**, 337–363.

Chapter 2

Selective and Sensitive Fluorescence Turn-on Detection of Cyanide Ions in Water by Post Metallization of a MOF

2.1 Introduction

Among the commonly found anions in biological system, cyanide (CN^-) is considered as one of the most harmful and potentially deadly anion, which poses a serious threat to the environment and mainly to the living organisms by consumption in the gastrointestinal tract or through lungs and rapidly distributed throughout the body.[1] The toxic effect of cyanide is exerted by combining with ferric ion in cytochrome oxidase, which inhibits cellular oxygen utilization, leading to potentially dangerous hypoxia.[2] As mentioned by WHO, the maximum tolerable limit of cyanide in drinkable water is 1.9×10^{-6} M.[3] Beyond this level, higher concentration of CN^- ions in water causes serious environmental hazard and can be fatal to living organisms. Despite of this, cyanide-based compounds are routinely used as a critical reagent in different industries like plastic production, electropainting, gold mining, petrochemical industries etc., which raises the potential contamination of cyanide ion in the environment.[4] Therefore, systematic identification and management of such toxic species in aquatic medium has become a priority research topic with the aim of monitor and maintain the balance in the environmental ecosystem. Several methods have been established in recent years for the recognition of cyanide ions such as mass spectrometry, electro-chemical methods, chromatographic techniques, Raman spectroscopy, photoluminescence-based techniques etc.[5] However, among all of those aforementioned methods, photoluminescence (PL)- based techniques have tempted more attention over others, because of their benefits like low detection limit, rapid analysis, cost effectiveness and simplicity in the handling procedures with high precision.[6] Although examples of diverse chemosensors previously been reported for recognition of CN^- ions, but their inherent limitations such as low sensitivity, limited selectivity and applicability in non-aqueous medium, restricted their application in real time.[7] Consequently, in recent years, scientific community render for new materials, which can offer efficient and excellent aqueous phase recognition of CN^- ions with superior selectivity and very low limit of detection.

Constituted from organic ligands and metal ions or cluster, metal-organic frameworks (MOFs) have gained paramount research interests in the domain of solid crystalline materials over the past twenty years.[8] Due to the intrinsic characteristics for instance structure property correlation, high surface area, modifiable functionality, selective host guest interactivity etc. Metal organic frameworks have acquired tremendous attention towards a broad spectrum of applications, which includes catalysis, gas storage, hydrocarbon separation, remediation of pollutants etc.[9] In addition, use of suitable metal clusters (or ions) and/or π-rich conjugated organic linkers can lead to the formation of intense fluorescent MOF. This kind of fluorescent MOFs can be classified as luminescent MOFs (LMOFs) which have demonstrated excellent suitability for sensing applications.[10] By virtue of predesigning ability and confinement effect in the nano-space, MOFs can actuate suitable host-guest interaction with specific analytes.[11] Rational

incorporation of functional moieties into the framework (LMOFs) can be executed either by pre-synthetic approach, where the pristine MOFs are constructed with desired functional sites, or by post-synthetic modification (PSM), where the targeted functional moieties are subjected to be incorporated in the pristine MOFs. Post-synthetic modification-based approach offers a promising platform for versatile and facile development of LMOFs based sensory probes, for the detection of various toxic pollutants in water.[12] In addition, most of the LMOF based sensors in the literature have exhibited 'turn-off' sensing mechanism, following the typical energy or electron transfer process from the lowest unoccupied molecular orbital (LUMO) of LMOF to the LUMO of analytes. Such transfer of electron or energy can lead to the fluorescence quenching of LMOFs.[13] However, this turn-off mechanism has been found to be struggled often with low sensitivity and relatively less selectivity towards a particular analyte when there is more than one analyte with, identical electronic nature.[14] Therefore, considering the real time application, in order to achieve high sensitivity along with superior selectivity, turn-on sensing approach is highly desirable.

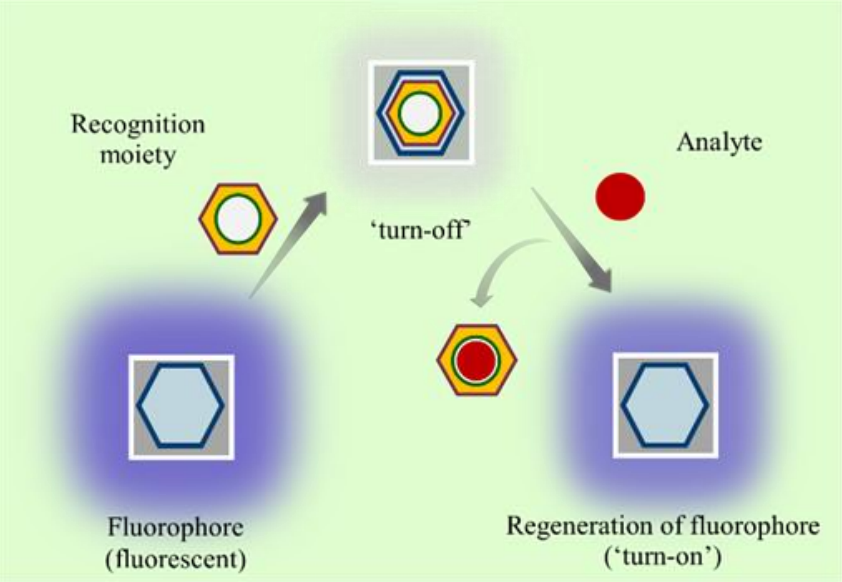

Scheme 2.1: Schematic representation of generation of turn-on response by combining recognition sites with fluorophore, up on addition of external analyte.

Again, it has been well understood that in case of fluorescence-based recognition, molecular "turn-on" technique is a promising way of detection. Owing to its high signal to noise ratio, along with the minimization of flash response as the recognition process occurs against a relative dark background, this technique has gained a lot of attention.[15] This desired turn-on signal can easily be achieved by designing

the LMOFs with target specific recognition moiety embedded with a fluorophore.[16] The electronic energy transfer between the recognition sites and the fluorophore results into the quenching of luminescence of the probe. Furthermore, the molecular energy-transfer changes upon addition of external analytes, which generates a conformational or electronic modification of the recognition site, further generating a turn-on florescence response (Scheme 2.1). Among various cyanide ions detection approaches reported till date, sensors exploiting copper-cyanide affinity have drawn-out special attention.[7a, 17] Owing to the electronic energy transfer (EET) or photoinduced electron transfer (PET) process amidst the Cu-center and the fluorophores, the fluorescence intensity got quenched.[18] On the other hand, it is also well established that Cu^{2+} reacts with cyanide in a very facile way to generate a stable $Cu(CN)_2$ species.[19] Therefore, it can be envisaged that complexation of negatively charged CN^- ions with the fluorescence quencher Cu^{2+} would alter the energy levels and subsequently meddle with the EET or PET quenching process amidst the Cu^{2+} chelated moiety and the fluorophore. This process can contribute to fluorescence emission intensity enhancement of the sensory material (Scheme 2.1).[20] In that case, this would act as a suitable turn-on fluorescence sensing beacon for cyanide anions. Despite the fact that, few MOF based CN^- sensing materials have been documented earlier [13, 21] turn-off sensing mechanism and chemosensor-based detection approach limits their practical applicability in terms of both sensitivity and good selectivity.[14] In this scenario, chemodosimeter-based sensing offer a promising platform for the molecular recognition, owing to its high sensitivity and selectivity.[22] In addition, considering the real time application (such as bioimaging), water stability of the probe is another critical parameter for recognition of cyanide ions in water medium.

Taking this into account, we chose a water stable MOF, namely MOF-867, which is isostructural with UiO-67. Being constructed from π-conjugated 2,2′-bipyridine-5,5 - dicarboxylic acid ($BPYDCH_2$) linker and high-valent metal ion (Zr^{4+}), MOF-867 has been found to have luminescent property with bipyridyl functionality.[23] The selection of the bipyridyl functionality can be justified by the easy chelation with the metal cations to facilitate the installation of Cu-center inside the porous network.[24] Also, MOFs constructed from Zr^{4+} metal cation are well explored for their high hydrothermal as well as good chemical stability.[25] Post metalation of MOF-867 has been performed using $CuCl_2$ as a suitable recognition site, which results in fluorescence quenching of the pristine MOF-867 (Figure 2.1). Further, thus synthesized $CuCl_2$@MOF-867 was employed to recognize CN^- ions in aqueous medium, which demonstrates a very sensitive and selective turn-on sensing for cyanide ions in company of other co-existing anions in aqueous system. Further we investigated the reason behind the emission intensity enhancement, which might be attributed to the easy liberation of the recognition moiety (Cu^{2+}) from the $CuCl_2$ loaded MOF by selective

interaction of CN^- anions with the copper unit to form a relatively more stable complex, following the chemodosimeter-based approach.

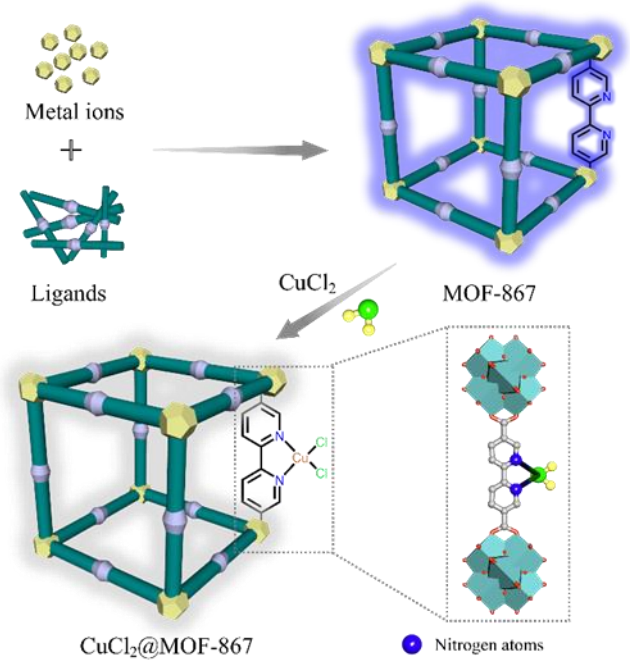

Figure 2.1: Schematic representation of synthesis of MOF-867 and post metalation of fluorophore MOF-867 with $CuCl_2$ as recognition sites, which result quenching in fluorescence intensity of MOF-867.

2.2 Experimental

2.2.1 Materials:

The compounds 2,2′-bipyridine-5,5′-dicarboxylic acid (H_2bpydc), Tetrabutylammonium cyanide, triethylamine, $ZrCl_4$ and metal salts were purchased from sigma-Aldrich and Merck respectively. $CuCl_2$ was purchased from TCI. All other chemicals were purchased locally and used directly beyond any further purification. Stock solutions of $HCO3^-$, I^-, OAc^-, Br^-, Cl^-, SCN^-, F^-, NO_2^-, SO_4^- and NO_3^- were prepared from $NaCO_3$, KI, NaOAc, KBr, NaCl, KSCN, KF, $NaNO_2$, Na_2SO_4 and $NaNO_3$ respectively.

2.2.2 Physical Measurements:

The powder X-ray diffraction (PXRD) pattern was measured on a Bruker D8 Advance X-ray diffractometer at ambient temperature (rt) using Cu Kα radiation (λ = 1.5406Å). Thermogravimetric analysis (TGA) was recorded by using a PerkinElmer STA 6000 analyzer under a nitrogen atmosphere

where temperature was increased from 30°C to 800°C at a heating rate of 10°C/min. Fourier Transform Infrared Spectroscopy (FT-IR) spectrum was collected on a Nicolet 6700 FT-IR spectrophotometer using KBr pellets method in the range 400-4000 cm-1. The SEM images were obtained using FEI Quanta 3D dual beam FESEM at 30KV. Energy dispersive X-ray (EDX) analyses carried out with a Hitachi S3400 N EDX instrument. Solid-state UV-Vis absorption and reflectance spectra were collected on Shimadzu UV-3600 UV VIS-NIR spectrophotometer over the range of 200-800 nm. All fluorescence measurements data were recorded on Jobin Yvon Fluoromax-4 spectrofluorometer. 1H NMR spectra were recorded on a 400 MHz Jeol ECS-400 spectrometer.

2.2.3 Synthesis:

Synthesis of MOF-867: The synthesis of MOF-867 was carried out under solvothermal process according to previously reported protocol.[23] Briefly a mixture of H2bpydc(19.5 mg), ZrCl4(18.64 mg), triethylamine(30µL) and acetic acid(1.38ml) were dissolved in 10 ml of N,N-dimethylformamide (DMF) and transferred into a 20 ml vial and put in 85 ºC oven for 24 hours. After slow cooling to ambient temperature the resulting MOF-867 was isolated by centrifuging (4,400 rpm for 20 min) and followed by washing with DMF three times. Obtained MOF was dipped in methanol for 4 days and solvent was exchanged with fresh MeOH in every 12 hours. The methanol exchanged was separated and subjected to vacuum activation at 60 °C for 12 hours to obtain guest free MOF-867.

Synthesis of $CuCl_2$@MOF-867: Post synthetic metalation was performed by reported protocol with slide modification where microcrystalline MOF-867 (80mg), $CuCl_2$ (0.5 equiv. per H2bpydc), and acetonitrile (3ml) were mixed in a 20ml Teflon-capped vial.[26] The vial is then placed on a hot plate at 85 °C and heated for a week. This resulted in a green colored powder. Then the aforementioned powder was immersed in fresh acetonitrile at 85 °C to get rid of any unreacted metal source. Finally, the powder was filtered and dried for further use.

Analyte preparation: First, stock solutions of cyanide was prepared from Tetrabutylammonium cyanide in water of concentration 1mM. Solutions of other anions were made ready from respective metal salts in water of concentration 1mM.

Titration with Cyanide ion and competing analyte studies with $CuCl_2$@MOF-867: 2 mg $CuCl_2$@MOF-867 has been dispersed in a cuvette having 2 mL water. Initial luminescence spectra of $CuCl_2$@MOF-867 in water has been recorded by exciting at 310 nm. The emission spectra was analyzed in between 330-600 nm. Then 1mM stock solution of cyanide ion in aqueous medium (20 µL to 240 µL) was added gradually in the dispersed MOF in water and with each addition the spectra were recorded. With each addition of cyanide ion, we found enhancement in the fluorescence emission of $CuCl_2$@MOF-

867. For competing studies, we have taken HCO_3^-, I^-, OAc^-, Br^-, Cl^-, SCN^-, F^-, NO_2^-, SO_4^- and NO_3^- ions in water. In a typical way, for initial study we have taken 2 mg of $CuCl_2$@MOF-867 in 2 mL of water. To the dispersed MOF we have added 200 μL of the conflicting ions from the prepared 1mM solution and recorded the fluorescence spectra to check the reaction of $CuCl_2$@MOF-867 towards other analytes. Later, in a similar way to the prementioned MOF (2 mg) in aqueous medium (2 mL) we have added 200 μL of competing anion and followed by 200 μL cyanide ion solution addition. We have recorded both responses of MOF in presence of competing anions and in presence of both competing anion and cyanide ion. By combining two responses we got the sensitivity of $CuCl_2$@MOF-867 towards cyanide ion in presence of other competing ions.

2.3 Results and discussion

MOF-867 was synthesized by using a previously described protocol (Figure 2.1) (see experimental section for details).[23]

Thus, synthesized MOF was thoroughly characterized with thermogravimetric analysis (TGA), powder X-ray diffraction (PXRD), Fourier transform infra-red (FTIR) spectroscopy, field emission scanning electron microscopy (FESEM) etc. The sharp diffraction peaks in the background subtracted powder XRD pattern of the as-synthesized phase indicated high crystalline nature of the MOF-867 (Appendix 2.1). Additionally, the well corroboration in the background free powder XRD patterns of the as-made phase with the calculated MOF-867 patterns revealed bulk phase purity as well as similar structure integrity of MOF-867 (Figure 2.2a, Appendix 2.1). The initial weight loss in TGA curve of as-synthesized phase of MOF-867 up to~125 ^oC exhibited the occupancy of guest solvent molecules within the internal pores of the MOF (Appendix 2.2). After that a negligible change was observed up to ~450 ^oC in the TGA profile of MOF-867 (Appendix 2.2). The FTIR spectra of the MOF indicated towards the formation of metal-ligand (carboxylate oxygen) bonds (Appendix 2.3). The absence as well as appearance of peaks at 3250 cm-1 and 1360 cm-1, respectively, in the as-synthesized phase of the MOF demonstrated the formation of carboxylate from carboxylic acid ligand (Appendix 2.3). Moreover, the morphology of MOF-867 was evaluated by FESEM analysis which manifested the cubic microcrystalline nature of the respective MOF (Appendix 2.4). From the elemental mapping and EDX analysis of the synthesized MOF, homogeneous distribution of all the relevant elements (C, N, O, Zr) was observed (Appendix 2.5).

After the characterization, microcrystalline powder of MOF-867 was soaked with low boiling solvent (methanol), prior to de-solvation, by heating at ~60 ^oC under vacuum (see experimental section for details). In order to check the structural robustness as well as crystallinity of the de-solvated phase of the MOF, we performed PXRD experiment. No certain change in the powder XRD pattern of the de-solvated

phase of the MOF revealed the retention of the original framework with high crystalline nature (Appendix 2.1). The completion of de-solvation was also confirmed from the TGA pattern which showed no considerable weight loss up to ~450 ^{o}C (Appendix 2.2). Moreover, unaltered peaks in the FTIR spectra of the de-solvated MOF compared to pristine, indicated no change in metal-ligand bond (Appendix 2.3). Similar FESEM images of de-solvated phase of the MOF indicated identical morphology with pristine MOF-867 (Appendix 2.6). Thereafter, the porous nature of the de-solvated MOF was investigated by performing the low temperature (77K) nitrogen gas adsorption measurement, which revealed type-I uptake of N2 gas, further, indicated the microporous nature of the MOF (Appendix 2.28).

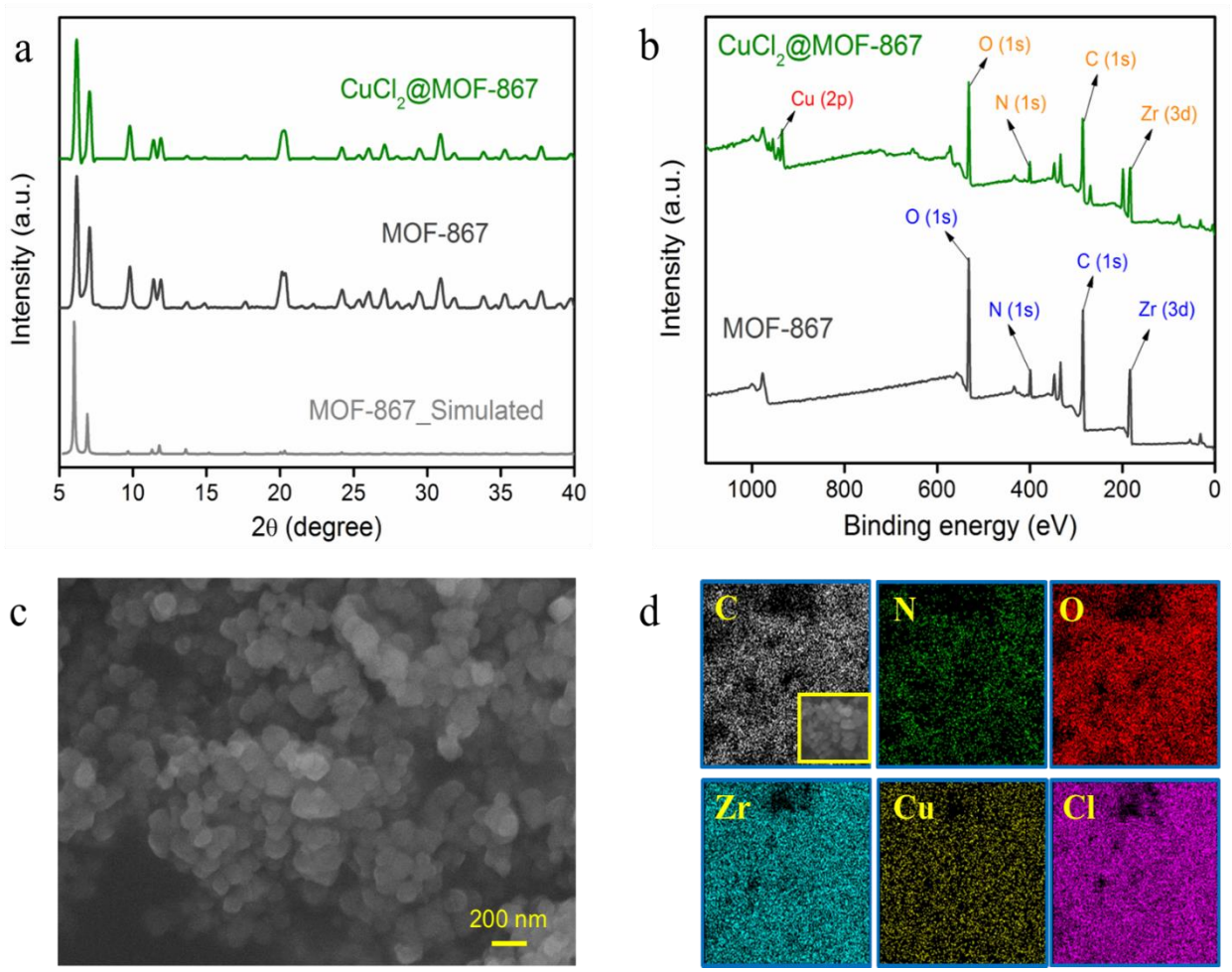

Figure 2.2: a) PXRD profile of simulated MOF-867, MOF-867 and CuCl2@MOF-867; b) XPS profile of MOF-867 and CuCl2@MOF-867; c) FESEM image of CuCl2@MOF-867; d) Elemental mapping of CuCl2@MOF-867.

Following that, infiltration of CuCl2 in MOF-867, to obtain CuCl2@MOF-867, was carried out following the previously reported protocol with slight modification (See experimental section for details).[26] The phase purity of the bulk sample along with isostructural nature of the CuCl2@MOF-867 with MOF-867

was confirmed from the identical PXRD pattern (Figure 2.2a). The TGA profile of $CuCl_2$ loaded MOF showed loss of guest molecule initially in low temperature range up to 100 ^oC, which can be attributed to the loss of acetonitrile solvent (Appendix 2.7). Again, the post synthetically metal loaded MOF showed similar thermal stability with MOF-867 (Appendix 2.7). Further, in order to understand the effective grafting of $CuCl_2$ metal salt into the bipyridine chelating sites of the MOF, X-ray photoelectron spectroscopy (XPS) analysis has been conducted. The XPS survey analysis of pristine MOF along with post metal integrated MOF-867 revealed the appearance of both Cu and Cl elements, which indicated binding of $CuCl_2$ with the MOF-867 (Figure 2.2b). Now, to gain more insights, the XPS spectra of N 1s orbital of MOF-867 was plotted against the N 1s orbital of $CuCl_2$@MOF-867. The XPS peak at 398.88 eV corresponding to the N 1s of MOF-867 was found to shifted to 399.98 eV for $CuCl_2$@MOF-867, which validated the strong coordination between pyridine N atoms of MOF with copper atoms Appendix 2.8).[27] Moreover, the characteristic shakeup satellite peaks at 942 eV and 962 eV related to Cu 2p3/2 and Cu 2p1/2, respectively in the XPS spectra of $CuCl_2$@MOF-867 indicated the +2 oxidation state of copper metal ions (Appendix 2.9).[28] In addition, the microcrystalline surface morphology of $CuCl_2$@MOF-867 composite was also found to be identical with the pristine one as revealed from the FESEM analysis (Figure 2.2c). The existence of both copper metal and chloride element in the EDX spectra as well in elemental mapping of $CuCl_2$@MOF-867 indicated the successful incorporation of $CuCl_2$ into the bipyridine moiety of the ligand present in the MOF which is in accordance with earlier reports (Figure 2.2d, Appendix 2.10).[24] Thus, synthesized and thoroughly characterized MOF was again de-solvated with vacuum treatment before performing the sensing experiment.

To understand the optical properties of $CuCl_2$@MOF-867 we initially recorded solid state UV-vis spectral profile, which showed maximum absorbance wavelength (λ_{max}) near 310 nm (Figure 2.3a). After that, the photoluminescence emission spectrum was obtained in between 330-600 nm upon exciting the material at 310 nm(λex). The compound displayed a smooth emission profile having maximum intensity at wavelength 430 nm (Figure 2.3b). Thereafter, to examine the initial response of the post synthetically modified MOF towards cyanide ions, 2 ml aqueous dispersion of the compound was taken in a cuvette. Interestingly, a turn-on response (from non-fluorescent to strong blue emission) was observed under UV light when an aqueous cyanide solution was added into the MOF suspension (Figure 2.3c). A similar observation was found in case of solid samples, as the color of the compound was changed from dark green to off-white, in day light and non-fluorescent to fluorescent under UV light (Figure 2.3d). Again, upon inclusion of cyanide solution to the aqueous dispersion of pristine MOF-867, no apparent color change was observed under UV light. This observation demonstrated that the emission of pristine MOF-867 was independent towards CN^- ions (Figure 2.3e).

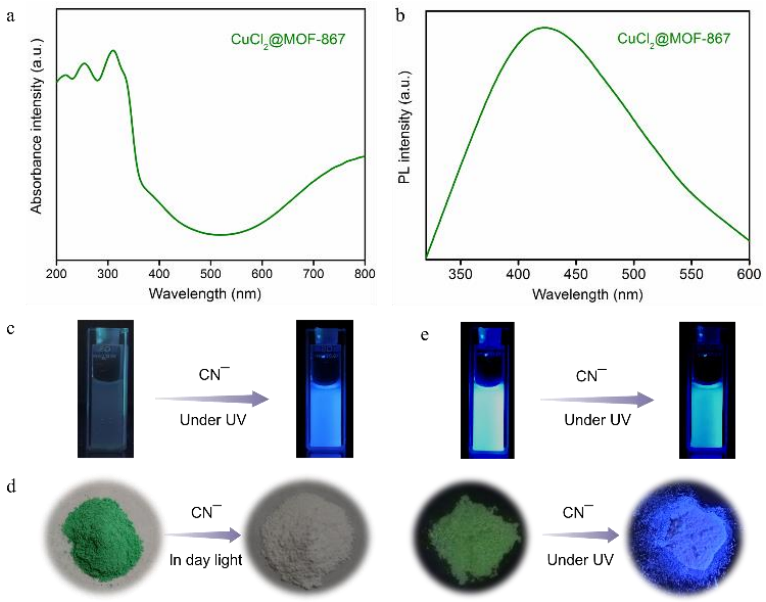

Figure 2.3: (a) Solid-state UV-vis spectra of $CuCl_2$@MOF-867; (b) Photoluminescence emission spectra of $CuCl_2$@MOF-867; (c) Images of enhancement of fluorescence intensity of aqueous suspension upon CN^- addition. (d) Solid-state digital images of $CuCl_2$@MOF-867 upon addition of cyanide solution, under day light and UV. (e) No change in the fluorescence intensity of MOF-867 upon addition of cyanide solution, under UV.

Inspired from this exciting inspection we further explored the sensing study of $CuCl_2$@MOF-867 towards CN^- ions in water. The typical sensing titration experiment was performed with aqueous solution of tetrabutylammonium cyanide salt (see experimental section for details). At first, fluorescence emission spectra, of the dispersed de-solvated $CuCl_2$@MOF-867 powder was recorded in water. The fluorescence emission spectra were found to be enhanced upon gradual addition of CN^- ion solution in aqueous medium (Figure 2.4a). The emission profile of the compound was observed to be enhanced by three-fold, up to a total of 240 µL of CN^- ion solution was attained with an interval of 20 µL of 1 mM CN^- ion solution (Figure 2.4a). Such potent enhancement with high sensitivity of $CuCl_2$@MOF-867 towards CN^- ions was ascribed to the strong probe analyte interaction, which is equipotential to the current MOF based fluorescence sensors for CN^- ions detection. It should be pointed out that there was a blue-shift observed in the PL spectra of the probe upon cyanide treatment, which can be ascribed to the increase in the π-electron density or conjugation in the bipyridyl units because of removal of the chelated Cu-ions from the bipyridyl units of the MOF. Moreover, a potential sensory probe must recognize the targeted species at a very low concentration for its real time applicability. The materials efficiency to detect a particular analyte at a low concentration is calculated by limit of detection (LOD) of any sensors. The limit of detection of $CuCl_2$@MOF-867 towards CN^- ions was calculated to check the sensitivity using the equation LOD = 3σ/m, (where m and σ stands for slope of the concentration vs intensity plot and standard

deviation, respectively) (Figure 4b, Appendix 2.11).[29] The LOD of $CuCl_2$@MOF-867 was found to be 0.19 µL (see supporting information for details), which was further found to be well fitted for sensing applications as it was well below the WHO permissible limit (1.9 µL).[30]

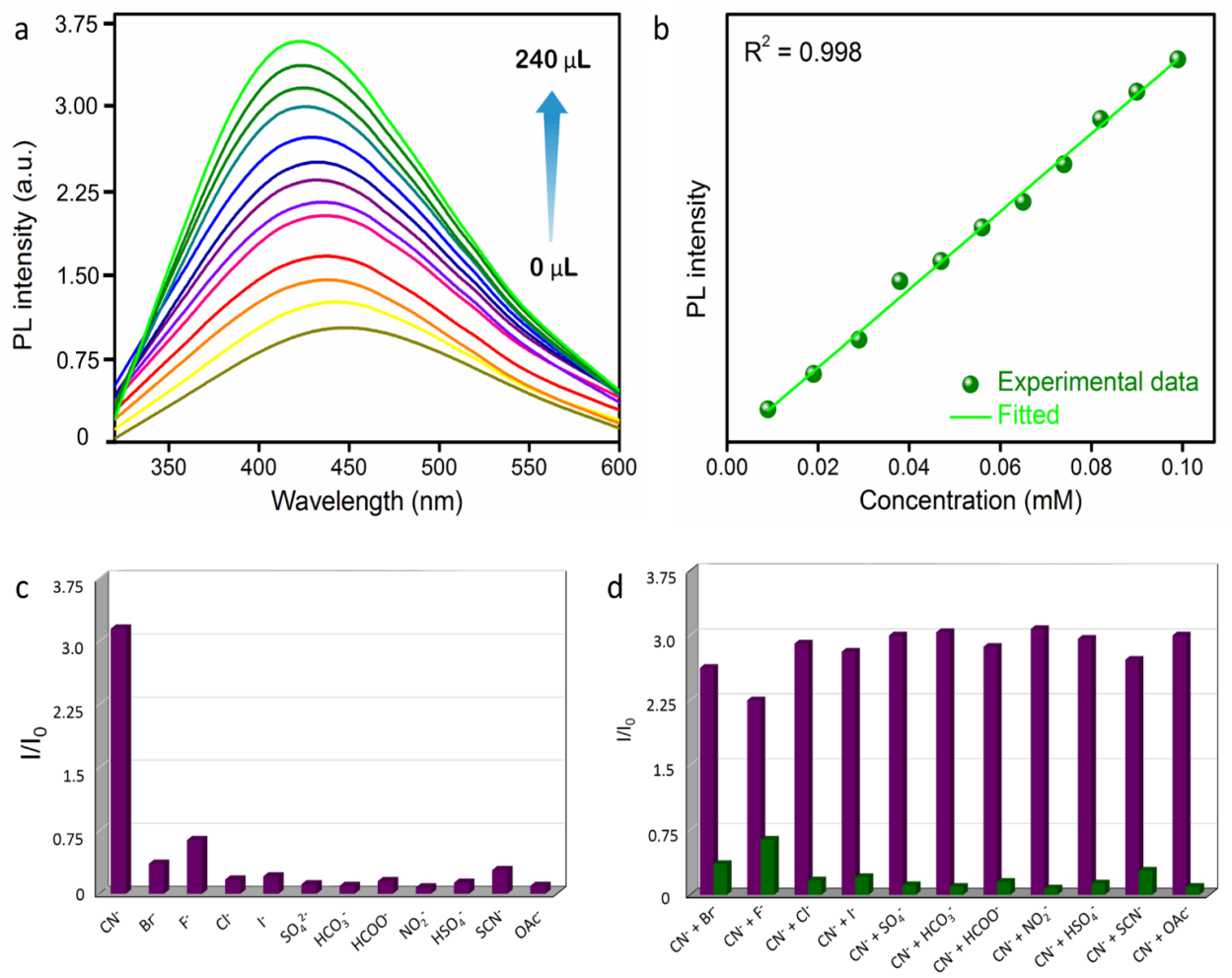

Figure 2.4: a) Photoluminescence turn-on response of $CuCl_2$@MOF-867 towards cyanide ions upon incremental addition of 20 µL. b) Correlation between photoluminescence intensity and CN^- concentration. c) Relative turn-on response of the probe towards different anions. d) Relative enhancement of the emission intensity of $CuCl_2$@MOF-867 in addition of different interfering anions before addition of CN^- anions.

Considering both the crucial factors, one being CN^- ion exists in real water samples along with other interfering anions and other is of selective recognition by a probe towards a particular anion is a critical factor for practical utilization of any sensory probe. Hence $CuCl_2$@MOF-867 was employed to carry out the selective CN^- sensing study in the company of other co-existing anions in water. For this a typical experiment was performed where 2 mg compound was dispersed in 2 ml water accompanied by addition

of 240 µL of 1 mM aqueous solution of $HCO3^-$, I^-, OAc^-, Br^-, Cl^-, SCN^-, F^-, NO_2^-, SO_4^{2-} and NO_3^-. After recording the respective fluorescence spectra, no considerable enhancement was detected in the emission spectra of different aforementioned anions treated MOF (Figure 4c, Appendix 2.12-2.22). This result indicated the selectivity of $CuCl_2$@MOF-867 towards CN^- ions. Again, to examine the observation a binary competitive sensing experiment was conducted for cyanide anions along with other interfering anions. Following the similar experimental protocol, at first, we recorded the emission profile of compound in company of respective competitive anions prior to the cyanide anions addition. Initially the emission intensity of the MOF exhibited negligible enhancement with addition of 200 µL interfering anions, while, after the equivalent amount of cyanide anions addition, the fluorescent intensity was enhanced considerably (Figure 4d). This result exhibited the high selectivity of the probe towards CN^- ions in water.

Thereafter, we tried to understand the probable reason behind such high selective fluorescence intensity enhancement of the compound after cyanide addition. The post sensing stability of the compound was carried out by performing the PXRD and digested NMR of MOF-system analysis. PXRD revealed that the cyanide treated sample showed similar structural integrity with no significant loss in the crystallinity with the pristine sample (Appendix 2.23). Moreover, to identify the linker chemical configuration after cyanide solution treatment, we performed 1H NMR study of the digested sample. Which exhibited retention of the identical chemical structure of the ligand with the linker of MOF-867 (Appendix 2.24).

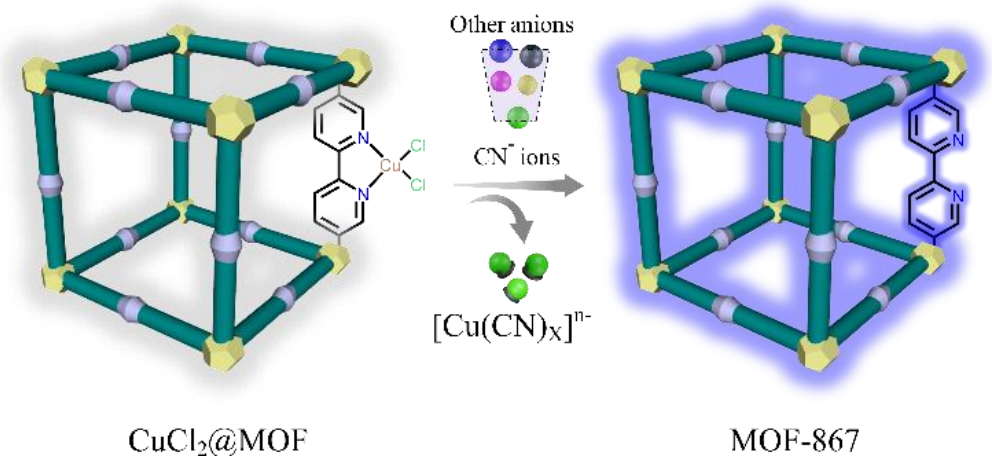

Figure 2.5: Schematic representation of generation of fluorescence turn-on response by CuCl2@MOF-867 up on addition of CN^- aqueous solution.

Identical cubic microcrystalline morphology of cyanide treated sample indicated retention of surface morphology (Appendix 2.25). In addition, from the XPS analysis of post CN^- ions treated MOF sample, it was observed that the corresponding peaks of both Cu and Cl species were absence, which demonstrated liberation of $CuCl_2$ up on treatment of aqueous cyanide solution (Appendix 2.26). Similar result has been observed from the EDX and elemental mapping analysis of CN^- ions treated MOF system (Appendix 2.27). All this result exhibited that the selective enhancement in the intensity of fluorescence spectra might be ascribed to the presence of predesigned rational functionalized moiety, i.e. $CuCl_2$ loaded MOF, complexation of negatively charged CN^- ions with the fluorophore chelated Cu^{2+} forming a stable $Cu(CN)_2$ species has led to such selective and sensitive detection of CN^- ions.[17] Therefore, MOF-867 was regenerated, which cause the turn-on response in the PL intensity (Figure 5, Appendix 2.29). Thereafter, in order to check the response of other metal cations (such as Ni^{2+}, Co^{2+}, Fe^{3+}) loaded MOF-867, towards cyanide ions detection, similar sensing experiment was performed. It was found that, a turn-on response was observed in each case upon CN^- ions treatment. However, the PL intensity enhancement efficiency was found to be relatively less as compared to Cu^{2+} chelated MOF-867, towards selective CN^- ions recognition (Appendix 2.30, Appendix 2.1). Moreover, so far turn-off-based detection of various targeted analytes by MOFs has been well explored, whereas in this study we demonstrated a simple yet versatile effective way for turn-on recognition of cyanide ions in water with such admirable LOD values.

2.4 Conclusions

In conclusion, a stable post metallization of a MOF ($CuCl_2$@MOF-867) has been employed as a potential sensor to recognize toxic cyanide ion in water. The MOF exhibited selective and sensitive turn-on signal particularly to cyanide ions from a mixture of co-existing ions in water. Recognition of CN^- ions in aqueous medium with a very low limit of detection value (0.19 μM) as well as good selectivity over commonly interfering anions promote this material promising sensory probe for monitoring CN^- ions in water sample. This work highlights the smart designing of LMOF based potential scaffold for efficient sensing of toxic pollutants. We believe that this present finding, utilizing post synthetically metal incorporation strategy to impart selective moiety for recognizing target specific anions paves the way for the advancement of novel probe for detecting other species also.

2.5 Appendix Section

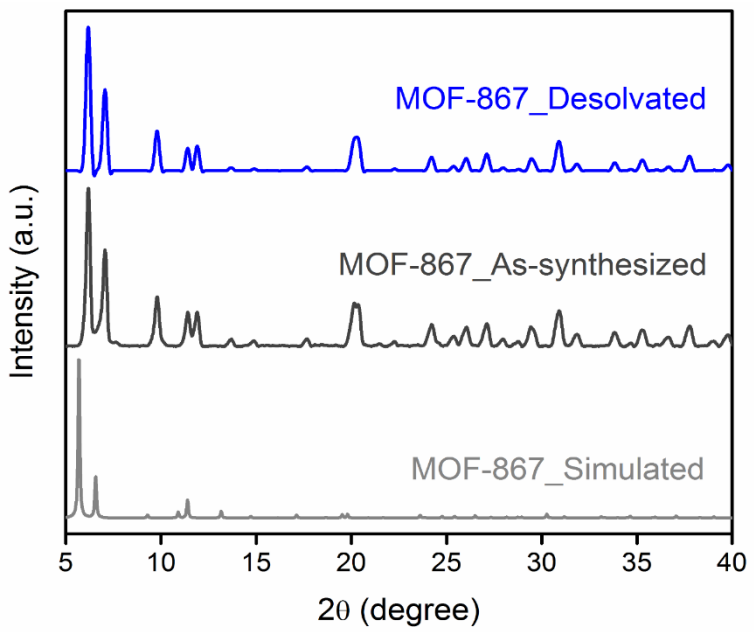

Appendix 2.1: Powder X-ray patterns of simulated UiO-67 (gray), as-synthesized phase of MOF-867 (dark gray) and de-solvated phase of MOF-867 (blue).

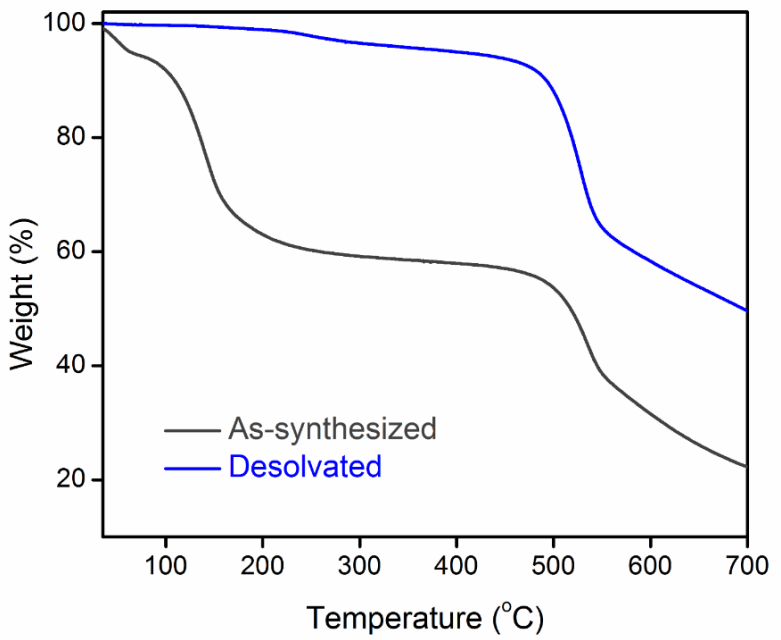

Appendix 2.2: Thermo-gravimetric analysis (TGA) profiles of as-synthesized MOF-867 (dark gray) and de-solvated MOF-867 (blue).

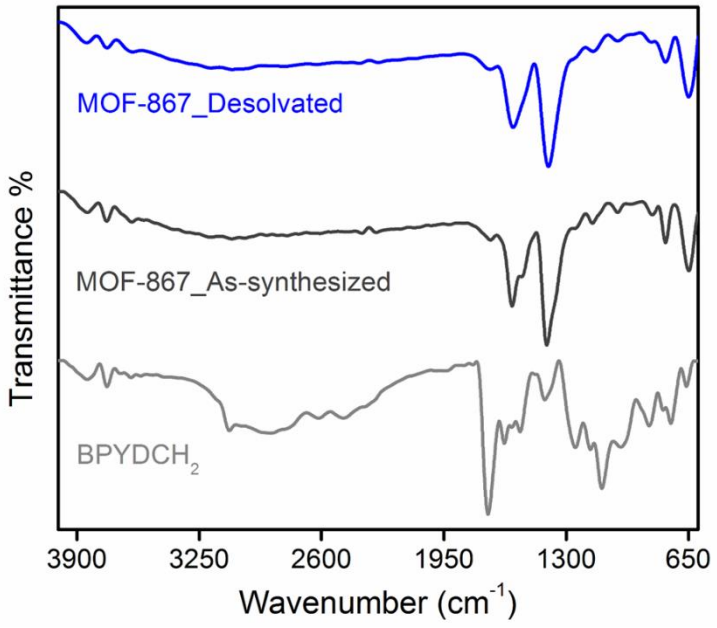

Appendix 2.3: IR spectra of Ligand ($BPYDCH_2$) (gray), as-synthesized MOF-867 (dark gray) and de-solvated MOF-867 (blue).

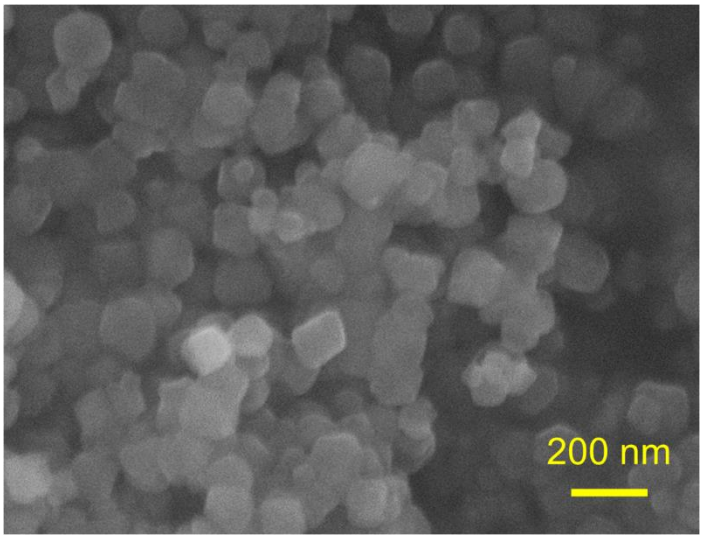

Appendix 2.4: FESEM image of as-synthesized MOF-867.

a)

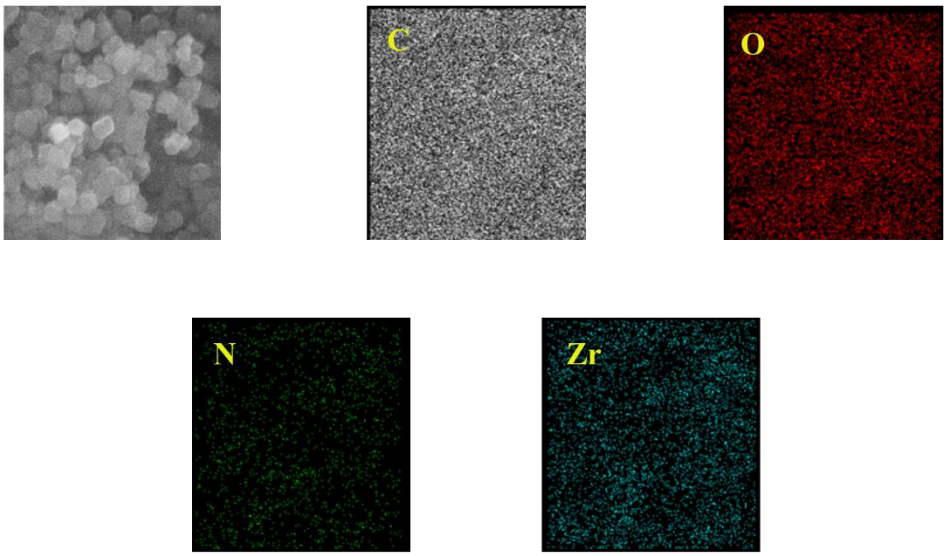

b)

Element	Weight %
Carbon	81.50
Oxygen	14.43
Nitrogen	1.58
Zirconium	2.49

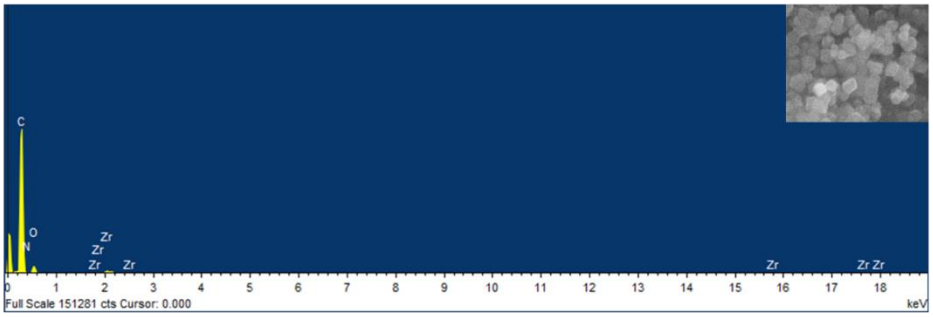

Appendix 2.5: a) Elemental mapping of MOF-867, b) EDX analysis of MOF-867 (shows the presence of Carbon, Oxygen, Nitrogen and Zirconium).

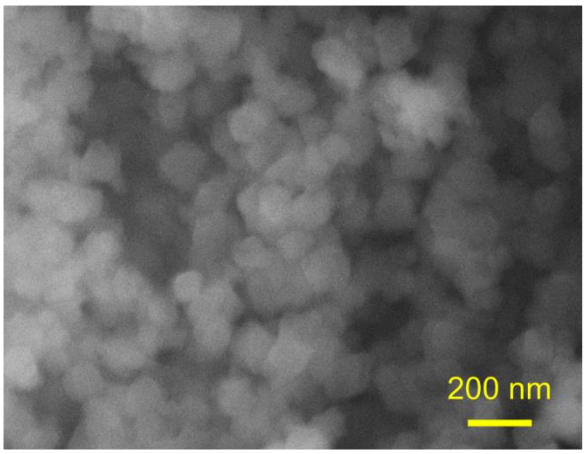

Appendix 2.6: FESEM image of de-solvated MOF-867.

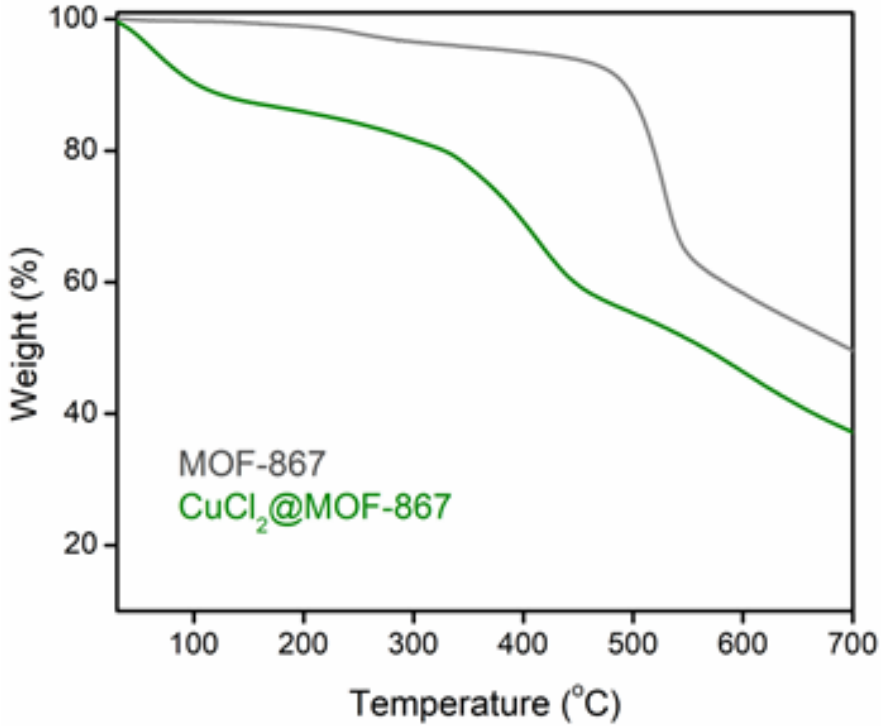

Appendix 2.7: TGA profile of MOF-867 and $CuCl_2$@MOF-867.

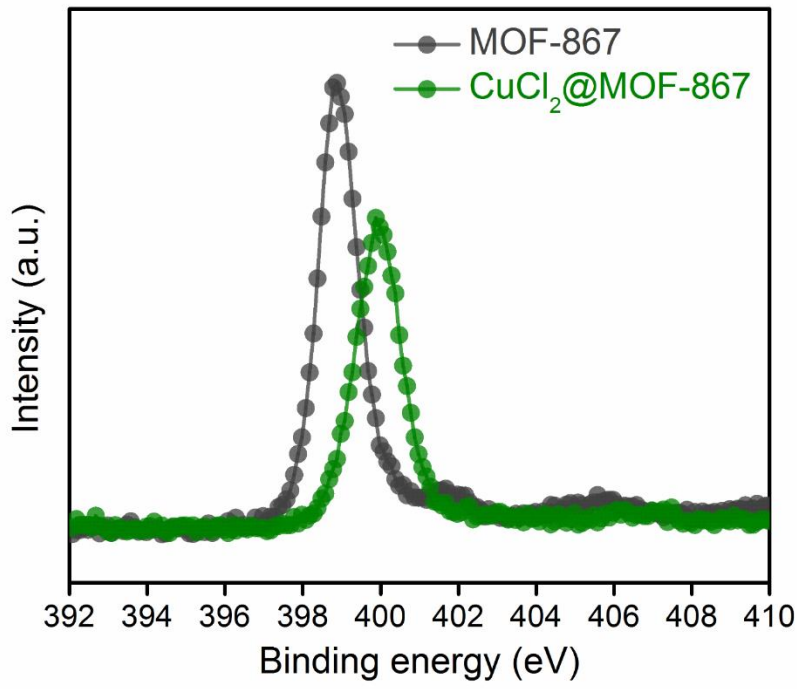

Appendix 2.8: XPS spectra of N 1s orbital of MOF-867 and $CuCl_2$@MOF-867.

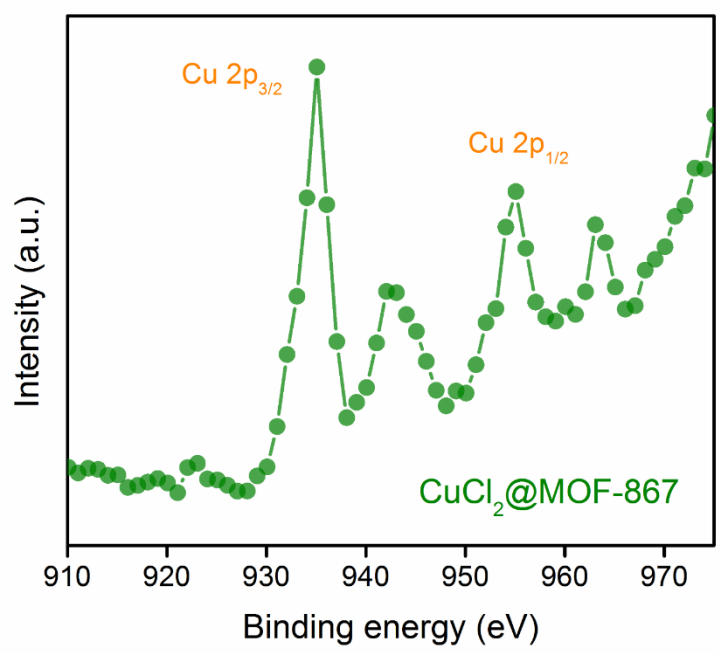

Appendix 2.9: XPS spectra of $CuCl_2$@MOF-867.

Element	Weight%	Atomic%
Carbon	47.95	67.19
Nitrogen	3.84	4.62
Oxygen	18.49	19.45
Chlorine	8.65	4.11
Copper	9.42	2.49
Zirconium	11.64	2.15
Totals	100.00	

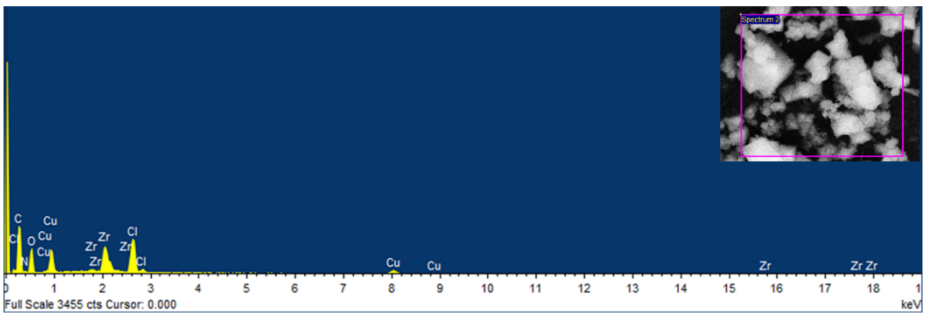

Appendix 2.10: EDX spectra of $CuCl_2$@MOF-867.

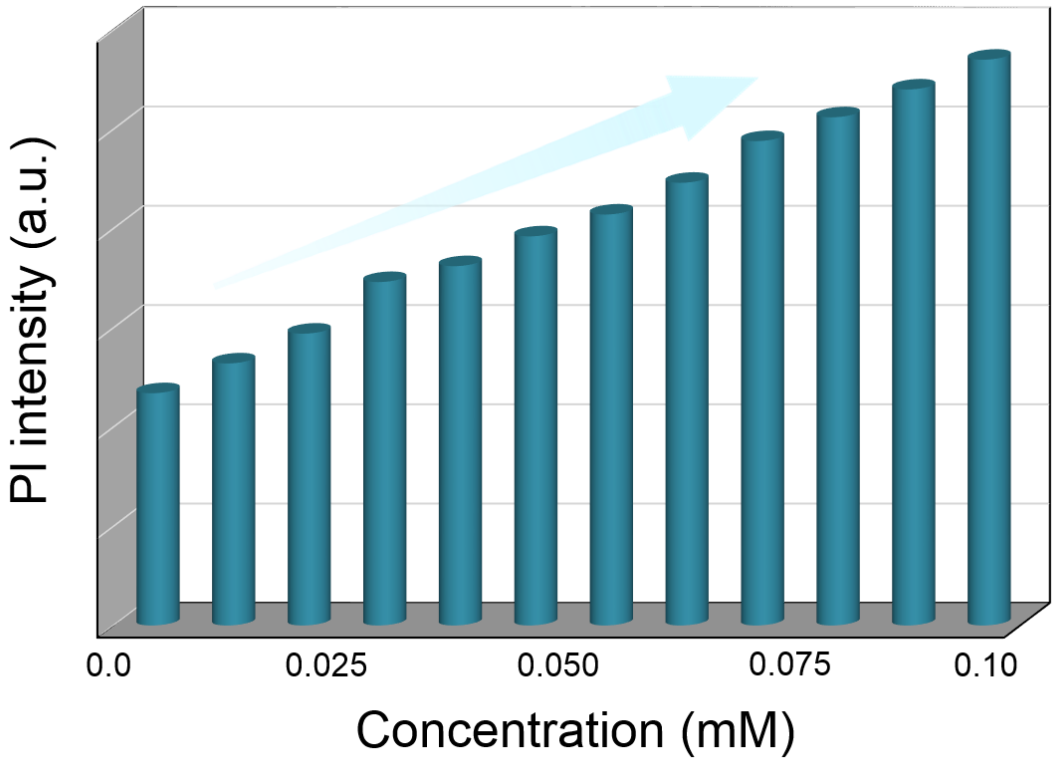

Appendix 2.11: Turn-on response upon gradual addition of cyanide ions in aqueous phase to $CuCl_2$@MOF-867.

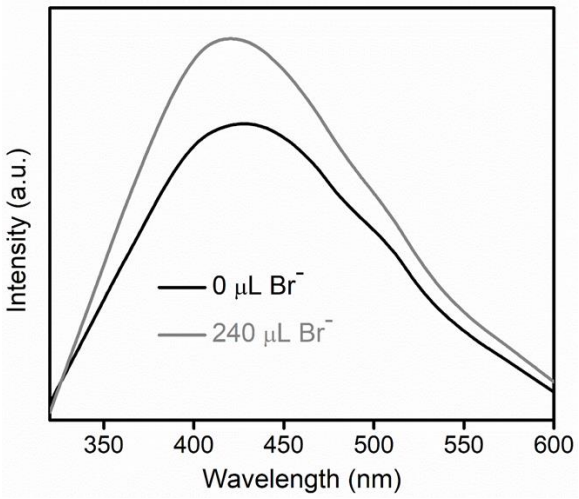
Intensity (a.u.)
0 μL Br⁻
240 μL Br⁻
350 400 450 500 550 600
Wavelength (nm)

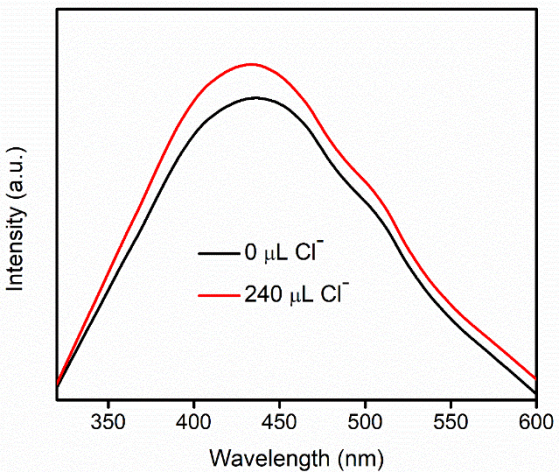
Intensity (a.u.)
0 μL Cl⁻
240 μL Cl⁻
350 400 450 500 550 600
Wavelength (nm)

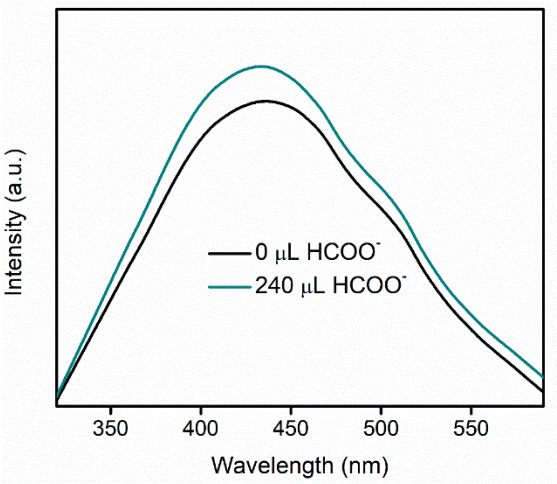
Intensity (a.u.)
0 μL HCOO⁻
240 μL HCOO⁻
350 400 450 500 550
Wavelength (nm)

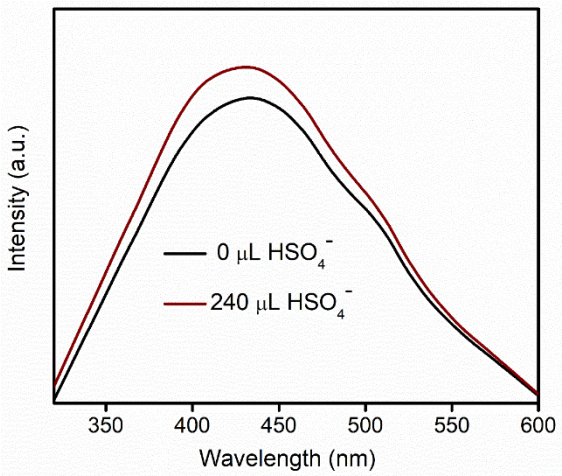
Intensity (a.u.)
0 μL HSO4⁻
240 μL HSO4⁻
350 400 450 500 550 600
Wavelength (nm)

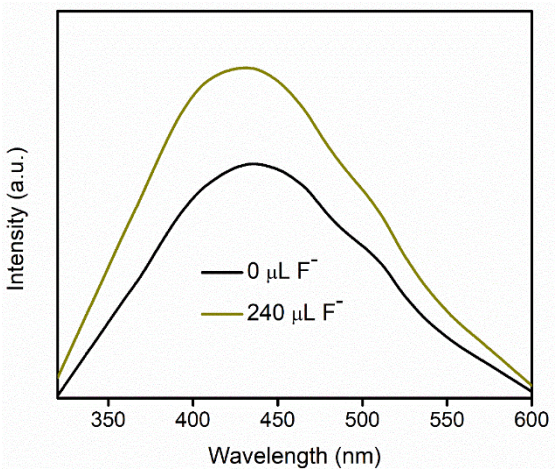
Intensity (a.u.)
0 μL F⁻
240 μL F⁻
350 400 450 500 550 600
Wavelength (nm)

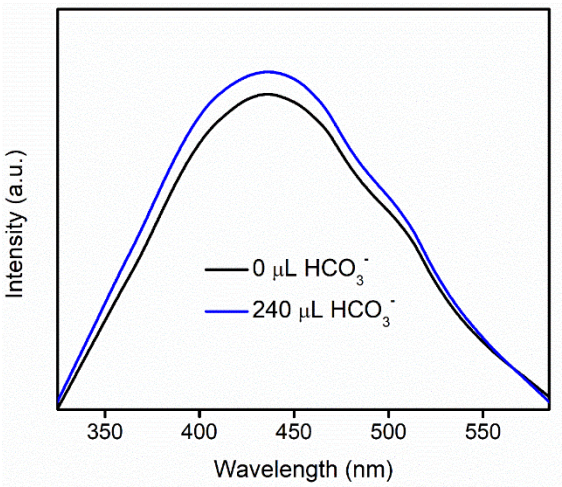
Intensity (a.u.)
0 μL HCO3⁻
240 μL HCO3⁻
350 400 450 500 550
Wavelength (nm)

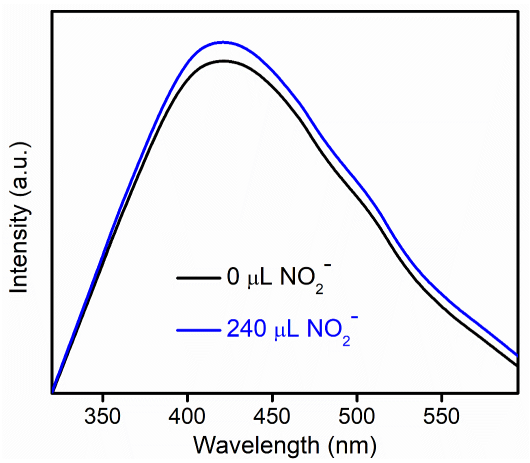

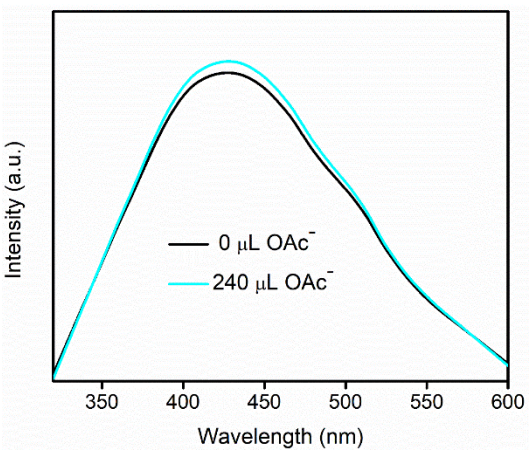

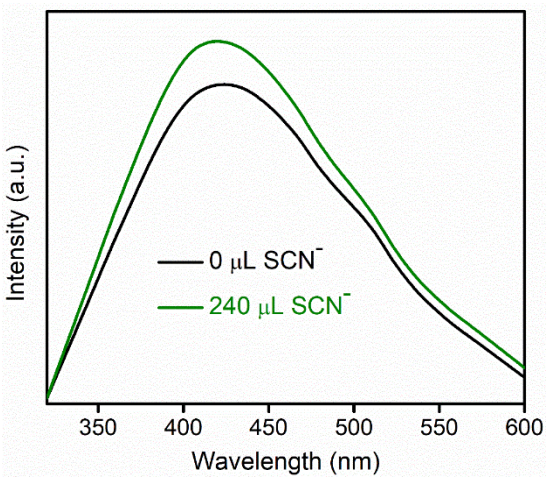

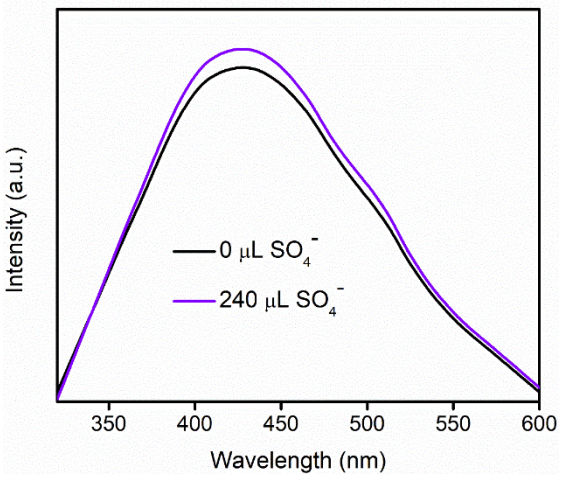

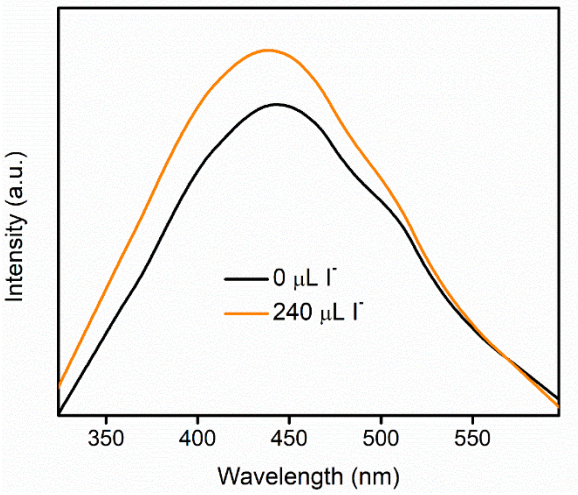

Appendix 2.12-2.22: Change in the fluorescence intensity of $CuCl_2$@MOF-867 after treating with various anionic solution.

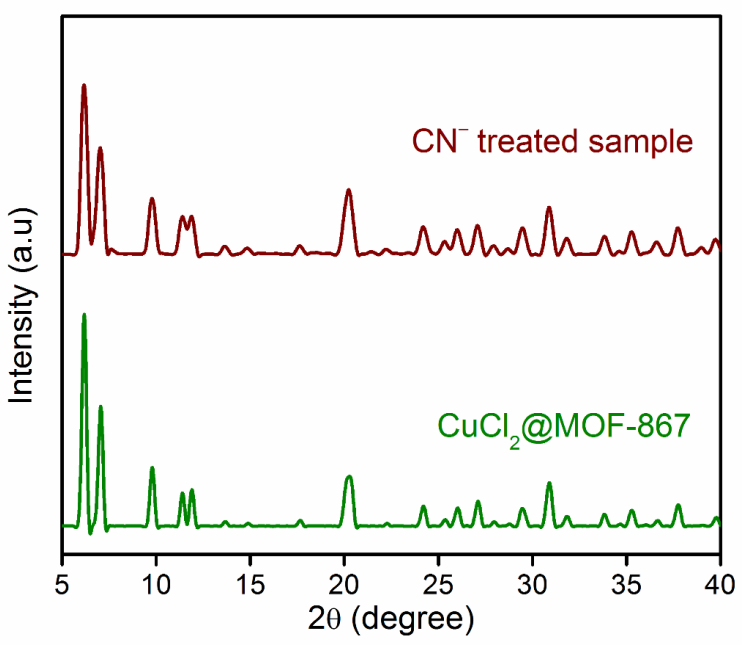

Appendix 2.23: PXRD profile of $CuCl_2$@MOF-867 and cyanide treated sample.

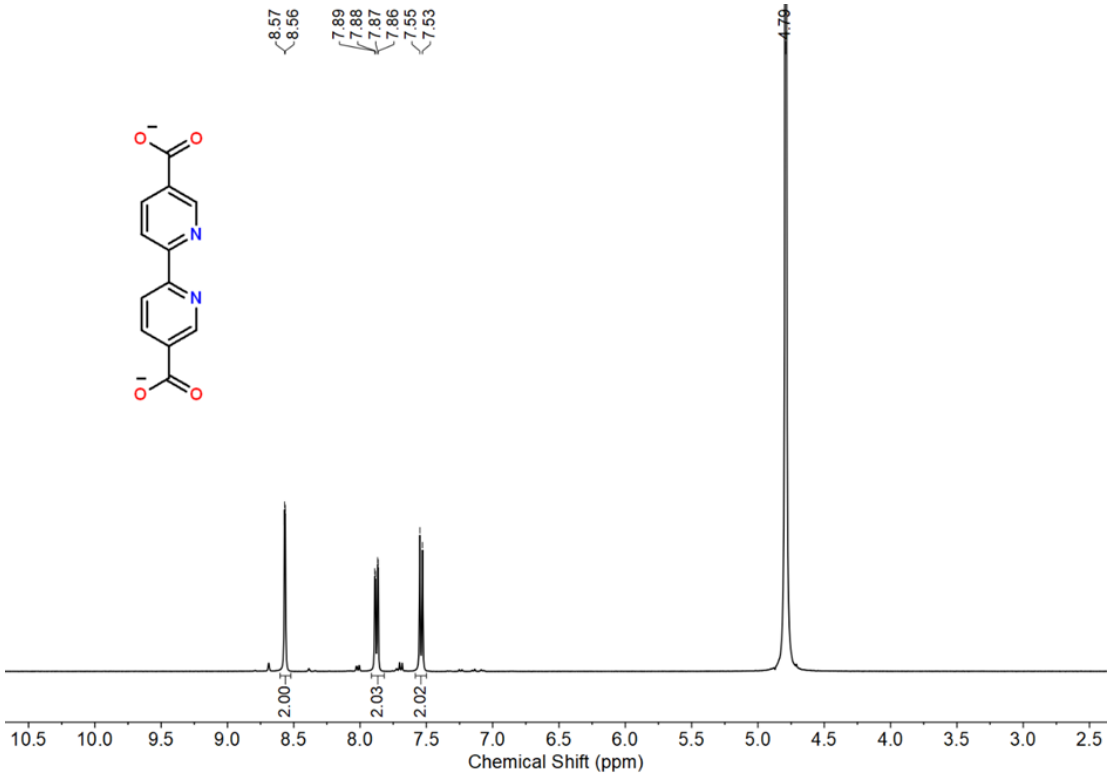

Appendix 2.24: Digested ^1H NMR spectra of $CuCl_2$@MOF-867 after cyanide treatment.

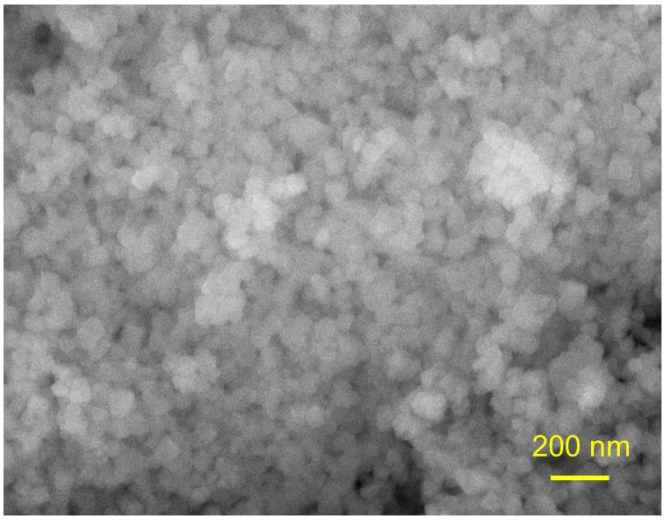

Appendix 2.25: FESEM image of $CuCl_2$@MOF-867 after cyanide treatment.

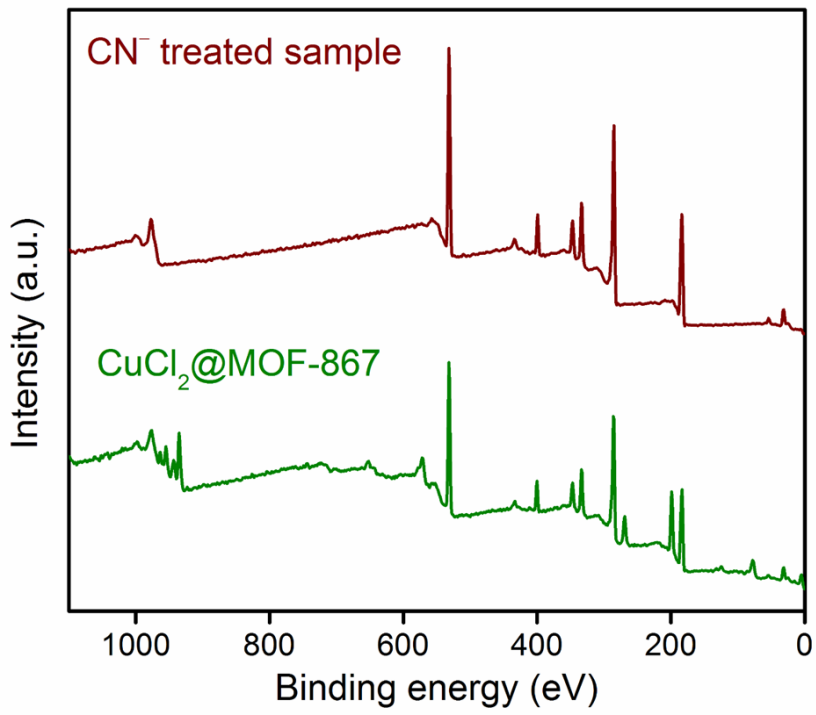

Appendix 2.26: XPS survey profile of $CuCl_2$@MOF-867 and after cyanide treatment.

a)

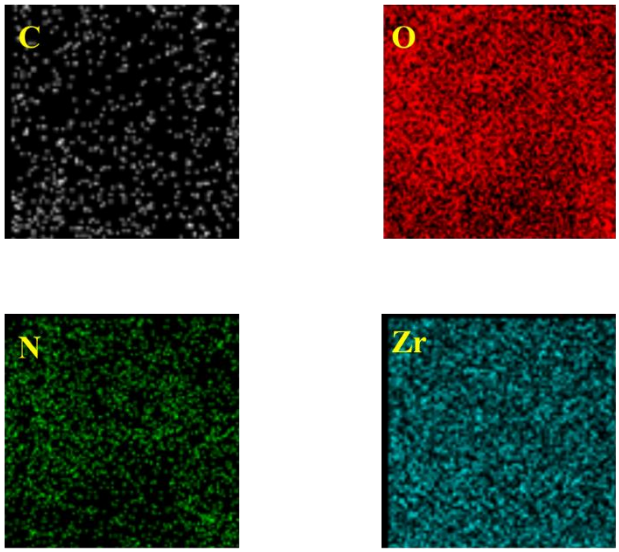

b)

Element	Weight %
Carbon	75.50
Oxygen	18.43
Nitrogen	1.87
Zirconium	3.76

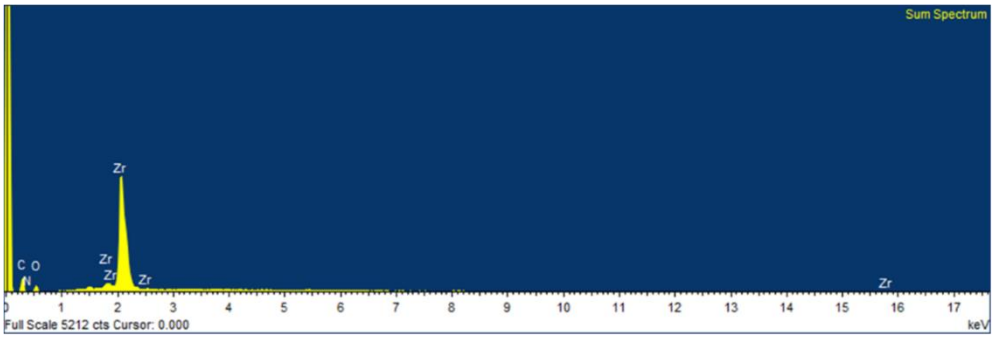

Appendix 2.27: a) Elemental mapping, b) EDX analysis of $CuCl_2$@MOF-867 and after cyanide treatment.

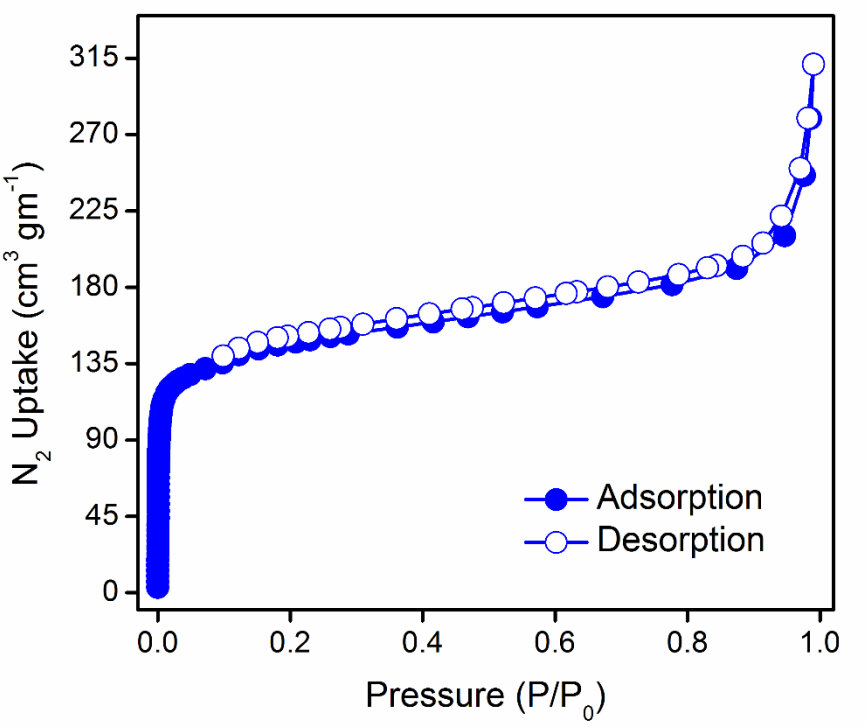

Appendix 2.28: Low temperature (77K) nitrogen gas adsorption-desorption measurement of MOF-867.

2.6 References

[1] a) Guidelines for Drinking-Water Quality, World Health Organization,Geneva, Switzerland, 1996; b) K.W. Kulig, Cyanide Toxicity, U. S. Department of Health and Human Services, Atlanta, 1991; c) A. Helal, S. Kim, H-S. Kim, *Bull. Korean Chem. Soc.* 2011, **32**, 3123-3126.

[2] a) Cyanide in Biology, ed. B. Vennesland, E. F. Comm, J. Knownles, J. Westly and F. Wissing, Academic, London, 1981; b) A. E. Lindsay, A. R. Greenbaum, D. O'Hare, *Analytica Chimica Acta*. 2014, 511,185–195.

[3] a) Guidelines for Drinking-Water Quality, 3rd edn, vol. 1. WHO Libr. Cat., 2004.

[4] a) G. C. Miller and C. A. Pritsos, Cyanide: Soc., Ind. Econ. Aspects, Proc. Symp. Annu. Meet. TMS, 2001, p. 73; b) C. A. Johnson, R. W. Leinz, D. J. Grimes, R. O. Rye, *Environ. Sci. Technol*. 2002, **36**, 840-845.

[5] a) K. Kaur, S. K. Mittal, A. Kumar, S. K. Kumar, S. Kumar, *Anal. Methods* 2013, **5**, 5565 –5571. b) T. T. Christison, J. S. Rohrer, *J. Chromatogr. A* 2007, **1155**, 31–39 c) (c) V. K. Rao, S. R. Suresh, N. B.

S. N. Rao and P. Rajaram, Bull. *Electrochem.* 1997, **13**, 327; d) D.-G. Cho, J. L. Sessler, *Chem. Soc. Rev.* 2009, **38**, 1647-1662. e) J. Chan, S. C. Dodani, C. J. Chang. *Nat. Chem*. 2012, **4**, 973-984.

[6] a) L. E. Kreno, K. Leong, O. K. Farha, M. Allendorf, R. P. V. Duyne, J. T. Hupp, *Chem. Rev*. 2012, **112**, 1105–1125.

[7] a) Z. Xu, X. Chen, H. N. Kim, J. Yoon, *Chem. Soc. Rev*. 2010, **39**, 127–137. b) F. Wang, L. Wang, X. Chen, J. Yoon, *Chem. Soc. Rev*. 2014, **43**, 4312-4324.

[8] a) H.-C. Zhou, S. Kitagawa, *Chem. Soc. Rev*. 2014, **43**, 5415-5418; b) Z. Chang, D-H Yang, J. Xu, T.-L. Hu, X.-H. Bu, *Adv. Mater*. 2015, **27**, 5432–5441; c) H.-C. Zhou, J. R. Long, O. M. Yaghi, *Chem. Rev.* 2012, 112, 673–674 ; d) Y. Bai, Y. Dou, L.-H. Xie, W. Rutledge, J.-R. Li, H.-C. Zhou, *Chem. Soc. Rev.* 2016, **45**, 2327; e) T. He, X.-J. Kong, J.-R. Li, Acc. *Chem. Res*. 2021, **54**, 3083-3094; f) H.-X. Wu, X.-M. Lu, J.-Y. Chen, X.-G. Yang, W.-J. Qin, L.-F. Ma, *Inorg. Chem*. 2021, **60**, 846−851.

[9] a) H. Furukawa, K. E. Cordova, M. O'Keeffe, O. M. Yaghi, *Science* 2013, **341**, 1230444; b) S. Horike, S. Shimomura, S. Kitagawa, *Nat. Chem*. 2009, **1**, 695-704; c) J. E. Mondloch, M. J. Katz, W. C. Isley III, P. Ghosh, P. Liao, W. Bury, G. W. Wanger, M. G. Hall, J. B. DeCoste, G. W. Peterson, R. Q. Snurr, C. J. Cramer, J. T. Hupp, O. K. Farha, *Nat. Mater*. 2015, **14**, 512-516; d) S.-Y. Moon, Y. Liu, J. T. Hupp, O. K. Farha, *Angew. Chem.* 2015, **127**, 6899 –6903; e) S. Mollick, S. Fajal, S. Saurabh, D Mahato, S. K. Ghosh, *ACS Cent. Sci.* 2020, **6**, 1534-1541, f) J.-O. Kim, J.-Y. Kim, J.-C. Lee, S. Park, H.-R. Moon, D.-P. Kim, *ACS Appl. Mater. Interfaces* 2019, **11**, 4385−4392.

[10] a) W. P. Lustig, S. Mukherjee, N. D. Rudd, A. V. Desai, J. Li, S. K. Ghosh, *Chem. Soc. Rev*. 2017, 46, 3242-3285; b) A. A. Barkhordarian, C. J. Kepert, J. Mater. Chem. A 2017, 5, 5612–5618; c) Z. Wang, Y. Huang, J. Yang, Y. Li, Q. Zhuang, J. Gu, *Dalton Trans.* 2017, 46, 7412–7420; d) S. Dutta, S. Let, S. Sharma, D. Mahato, S. K. Ghosh, *The Chemical Record*, 2021, 21, 1666-1680; e) P. Samanta, S. Let, W. Mandal, S. Dutta, S. K. Ghosh, *Inorg. Chem. Front*. 2020, 7, 1801.

[11] a) L. Zhu, X.-Q. Liu, H.-L. Jiang, L.-B. Sun, *Chem. Rev*. 2017, 117, 8129−8176; b) W. Lu, Z. Wei, Z.-Y. Gu, T.-F. Liu, J. Park, J. Park, J. Tian, M. Zhang, Q. Zhang, T. Gentle III, M. Bosch, H.-C. Zhou, *Chem. Soc. Rev*. 2014, 43, 5561—5593; c) S. Shimomura, M. Higuchi, R. Matsuda, K. Yoneda, Y. Hijikata, Y. Kubota, Y. Mita, J. Kim, M. Takata, S. Kitagawa, *Nat. Chem*. 2010, 2, 633-637.

[12] a) J. G. Nguyen, S. M. Cohen, *J. Am. Chem. Soc*. 2010, 132, 4560–4561; b) S. M. Cohen, *J. Am. Chem. Soc*. 2017, 139, 2855–2863; c) Z. Wang, S. M. Cohen, *Chem. Soc. Rev*. 2009, 38, 1315–1329; d) H.-R. Fu, X.-X. Wu, L.-F. Ma, F. wang, J. Zhang, *ACS Appl. Mater. Interfaces* 2018, 10, 18012−18020;

e) Y.-N. Zeng, H.-Q. Zheng, J.-F. Gu, G.-J. Cao, W.-E. Zhuang, J.-D. Lin, R. Cao, Z.-J. Lin, *Inorg. Chem*. 2019, 58, 13360−13369.

[13] A. Karmakar, N. Kumar, P. Samanta, A. V. Desai, S. K. Ghosh, *Chem. Eur.J*. 2016, 22, 864 –868.

[14] J. Li, S. Yuan, J.-S. Qin, J. Pang, P. Zhang, Y. Zhang, Y. Huang, H. F. Drake, W. R. Liu and H.-C. Zhou, *Angew. Chem*. 2020, 132, 1 – 6.

[15] A. Sen, A. V. Desai, P. Samanta, S. Dutta, S. Let, S. K. Ghosh, *Polyhedron* 2018, 156, 1-5.

[16] J. A. Cotruvo Jr., A. T. Aron, K. M. Rammos-Torres, C. J. Chang, *Chem. Soc. Rev*. 2015, 44, 4400—4414.

[17] a) Q. Zeng, P. Cai, Z. Li, J. Qin, B. Z. Tang, *Chem. Commun*. 2008, 1094–1096; b) U. G. Reddy, P. Das, S. Saha, M. Baidya, S. K. Ghosh, A. Das, *Chem. Commun*. 2013, 49, 255—257; c) M. Wang, J. Xu, X. Liu, H. Wang, *New J. Chem*. 2013, 37, 3869—3872; d) C. R. Maldonado, A. Touceda-Varela, A. C. Jones, J. C. Mareque-Rivas, *Chem. Commun*, 2011, 47, 11700-11702.

[18] a) A. P. d. Silva, H. Q. N. Gunaratne, T. Gunnlaugsson, A. J. M. Huxley, C. P. McCoy, J. T. Rademacher, T. E. Rice, *Chem. Rev*. 1997, 97, 1515−1566; b) B. Valeur, I. Leray, *Coord. Chem. Rev*. 2000, 205, 3-40; c) Rosenthal, S. J. Lippard, *J. Am. Chem. Soc*. 2010, 132, 5536–5537; d) Y. Zhou, K. Liu, J.-Y. Li, Y. Fang, T.-C. Zhao, C. Yao, *Org. Lett*. 2011, 13, 1290–1293; e) A. W. Varnes, R. B. Dodson, E. L. Wehry, *J. Am. Chem. Soc*. 1972, 94, 946–950; f) J. A. Kemlo and T. M. Shepherd, *Chem. Phys. Lett*. 1977, 47, 158.

[19] a) K. Kurnia, D. E. Giles, P. M. May, P. Singh, G. T. Hefter, *Talanta* 1996, 43, 2045-2051; b) X. Lou, L. Zhang, J. Qin, Z. Li, *Chem. Commun*. 2008, 5848–5850; c) X. Lou, J. Qin, Z. Li, *Analyst* 2009, 134, 2071–2075; d) X. Lou, Li. Qiang, J. Qin, Z. Li, ACS *Appl. Mater. Interfaces* 2009, 1, 2529–2535.

[20] a) Y. Liu, X. Lv, Y. Zhao, J. Liu, Y-Q Sun, P. Wang, W. Guo, *J. Mater. Chem*. 2012, 22, 1747–1750. b) A. Sebastian, E. Prasad, *Langmuir* 2020, 36, 10537–10547.

[21] a) L. D. Rosales-Vazquez, J. Valdes-Garcia, I. J. Bazany-Rodriguez, J. M. German-Acacio, D. Martinez-Otero, Alfredo R. Vilchis-Nestor, A. Dorazco-Gonzalez, Dalton Trans. 2019, 48, 12407–12420; b) R. Dalapati, S. Nandi, H. Reinsch, B. K. Bhunia, B. B. Mandal, N. Stock, S. Biswas, CrystEngComm 2018, 20, 4194–4201; c) C. Gogoi, N. Nagarjun, S. Roy, SK. Mostakim, D. Volkmer, A. Dhakshinamoorthy and S. Biswas, Inorg. Chem. 2021, 60, 4539-4550.

[22] P. Samanta, A. V. Desai, S. Sharma, P. Chandra, S. K. Ghosh, Inorg. Chem. 2018, 57, 2360 −2364.

[23] K. M. Choi, H. M. Jeong, J. H. Park, Y.-B. Zhang, J. K. Kang, O. M. Yaghi, ACS Nano 2014, 8, 7451–7457.

[24] a) C. Wang, J.-L. Wang, W. Lin, J. Am. Chem. Soc. 2012, 134, 19895−19908; b) R. J. Marshall, R. S. Forgan, Eur. J. Inorg. Chem. 2016, 27, 4310–4331; c) Z. Gao, Y. Lai, Y. Tao, L. Xiao, L. Zhang, F. Luo, ACS Cent. Sci. 2021, 7, 1066–1072.

[25] a) Y.-Z. Zhang, T. He, X.-J. Kong, X.-L. Lv, X.-Q. Wu, J.-R. Li, ACS Appl. Mater. Interfaces 2018, 10, 27868–27874; b) Z. Chen, S. L. Hanna, L. R. Redfern, D. Alezi, T. Islamoglu, O. K. Farha, Coord. Chem. Rev. 2019, 386, 32–49; c) J. Hou, H. Wang, H. Zhang, Ind. Eng. Chem. Res. 2020, 59, 12907–12923.

[26] M. I. Gonzalez, E. D. Bloch, J. A. Mason, S. J. Teat, J. R. Long, Inorg. Chem. 2015, 54, 2995–3005.

[27] J. Marsh, L. Minel, M. G. Barth´es-Labrousse and D. Gorse, *Appl. Surf. Sci*. 1998, **133**, 270 – 286.

[28] a) M. Gopiraman, S. G. Babu, Z. Khatri, W. Kai, Y. A. Kim, M. Endo, R. Karvembu and I. S. Kim, *Carbon* 2013, **62**, 135 – 148; (b) M. Gopiraman, D. Deng, S. G. Babu, T. Hayashi, R. Karvembu and I. S. Kim, *ACS Sustainable Chem. Eng.* 2015, **3** , 2478 –2488.

[29] a) S. Fajal, P. Samanta, S. Dutta, S. K. Ghosh, *Inorganica Chimica Acta*. 2020, **502**, 1193592

[30] A. Karmakar, B. Joarder, A. Mallick, P. Samanta, A. V. Desai, S. Basu, S. K. Ghosh, *Chem. Commun*. 2017, **53**, 1253-1256

Chapter 3

Efficient Removal of Mercury from Aqueous Medium by Ionic Functionalized Porous Organic Polymer

3.1 Introduction

With the booming of industrial sector and standard of living, environmental pollution is increasing day by day. Huge quantity of toxic and precarious waste has been developed and discharged in the water system eventually contaminating ground water.[1] Heavy metals (Hg^{2+} ,Li^{+} ,Cd^{2+}) possess serious threat to the environment and living beings due to their high toxicity and carcinogenetic nature. Evaluating biological toxicity order of the top five toxic metal ions are as follows Hg^{2+}>Pb^{2+}>Cr^{6+}>As^{5+}>Cd^{2+}.[2] Divalent mercury (Hg^{2+}) having high water solubility poses a threat to living species by accumulating in living organs via binding with the thiol groups of proteins, leading to irreparable damage of kidneys, central nervous system and other organs. The infamous Minamata disease caused by methylmercury (CH_3Hg^{+}) which is metabolized by bacteria from discharged industrial divalent mercury (Hg^{2+}).[3] Thus United States Environment Protection Agency (USEPA) and world health organization (WHO) listed Mercury as one of the priority pollutants and recommended permissible limit for drinking water to be 2 ppb.[4] In the past, several techniques have been developed to sequestrate heavy metals like reduction, adsorption and precipitation.[5] Among them adsorption based technique has drawn prominent attention because of their simplicity and efficiency. Traditional adsorbents such as zeolites, activated carbon and grapheme has already been utilized for water treatment. However, those adsorbents are limited by their low surface area, moderate porosity and poor affinity due to absence of selective adsorption sites. [6] In this context advance porous materials namely covalent organic frameworks (COFs), metal-organic frameworks (MOFs) have shown their potential in mercury removal by modification with various thiol or thio-ether functional groups. However strong binding affinity between mercury and sulphur limits the recyclability of the material.[7] Although a variety of materials have been utilized to remove mercury, more has to be done in terms of chemical stability, high efficiency, and cost-effectiveness.

In past several thiourea derivatives-based materials have been well explored for heavy metal adsorption. These materials contain lots of sulphur and nitrogen which causes heteroatomic effect which has an affinity for chelation with mercury ion.[8] Other than that carbohydrazide functional group consisting of oxygen and nitrogen has shown reversable bindings with mercury ion. [8c] In the domain of new adsorbate materials charged adsorbents boasts the adsorption capacity as well as selectivity because of their host-guest electrostatic interaction and guest-guest ion exchange. As a result, charged adsorbents surpass their neutral forms. Literature reports suggests ion exchange-based adsorption technique have been vastly used for mercury ions removal by MOF, though that is not the case for anionic polymer.[9] Most of the anionic polymers are prepared post synthetically but they lack of modifications in all cites, so pre-synthetic anionic polymer is the need of the hour. To address the real time challenge of sequestration of heavy metal pollutant i.e., mercury this work aimed to design and synthesize two anionic porous organic polymers for effective

mercury removal from aqueous system. In process after synthesizing hexacoordinated silicon-based aldehyde and reacted with carbohydrazide and thio-carbohydrazide, two polymers POP-1 and POP-5 was synthesized respectively. Both of the anionic polymers have exchangeable triethyl amine cation. This work highlights the role of carbohydrazide and thio-carbohydrazide functionality for mercury capture performance in various aspect. Further this work also exhibits fast kinetics and selective capture performance.

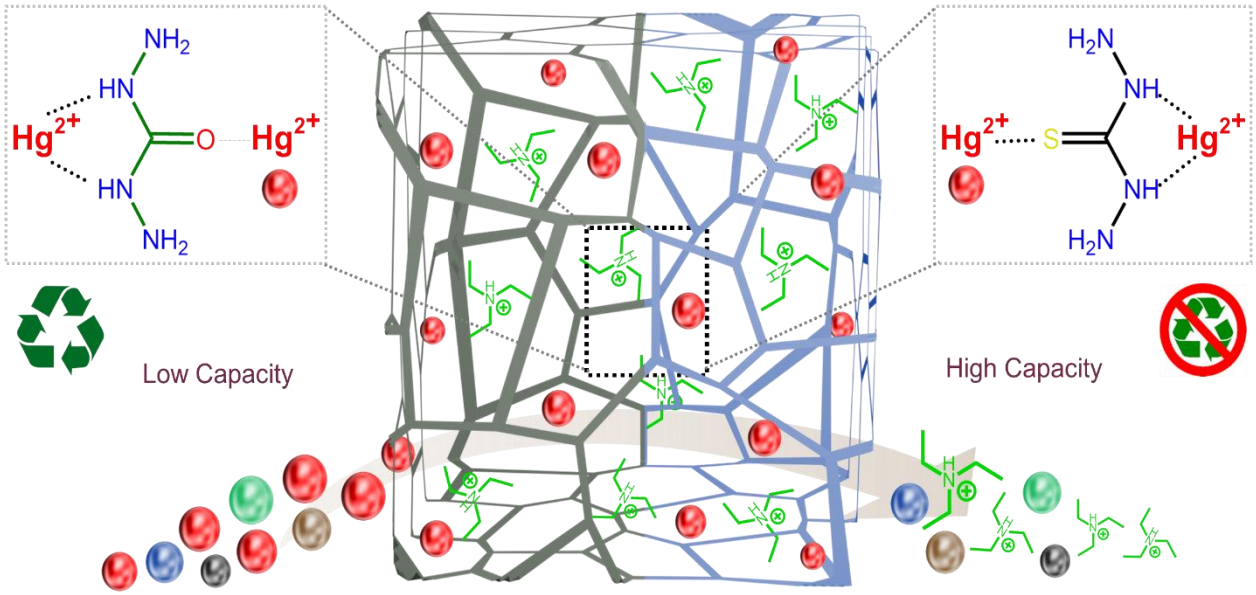

Scheme 3.1: Schematic representation of mercury capture by two functionalized porous organic polymers (POPs).

3.2 Experimental

3.2.1 Materials:

3,4-Dihydroxybenzaldehyde, carbohydrazide, thio-carbohydrazide, mercury (II) chloride were purchased from Merck. Further, tetra ethyl orthosilicate (TEOS), triethyl amine, solvents (acetonitrile, ethanol) were obtained locally. These chemicals weren't further purified before usage.

3.2.2 Physical measurements

Thermogravimetric analysis (TGA) was performed by using a PerkinElmer STA 6000 analyser under a nitrogen atmosphere where temperature was gradually increased from 30°C to 800°C at a heating rate of 10°C/min. All Infra-red (IR) Spectra were measured by using NICOLET 6700 FT-IR spectrophotometer in the range of 400-4000 cm^{-1} using KBr pellet. Low temperature nitrogen adsorption measurements were performed by using Bel Sorp-max instrument from Bel Japan. The SEM images were acquired using FEI Quanta 3D dual beam FESEM at 30KV. Energy dispersive X-ray (EDX) analyses was performed with a Hitachi S3400 N EDX instrument. TEM imaging were obtained on the HRTEM (JEM-2200FS, JEOL) operating at acceleration voltage of 200 kV. UV spectra were acquired on Shimadzu UV 2600 Spectrophotometer. Solid state NMR spectra were performed on Bruker 400 MHz NMR spectrometer. Carbon chemical shifts are expressed in parts per million (δ scale).

3.2.3 Synthesis:

Synthesis of Si-precursor: Si-precursor $(Et_3NH)_2\{[(CHO)C_6H_3O_2]_3Si\}$ was synthesized following a reported protocol [10] where 3,4-Dihydroxybenzaldehyde (10 g, 72.5 mmol) and triethyl amine (4.5g, 48.5 mmol) were mixed in acetonitrile (125 ml) and stirred at room temperature followed by slowly dropwise addition of tetra ethyl orthosilicate (TEOS) (5.05g, 24 mmol) solution in acetonitrile (50ml). Continuing the stirring for 24 hours the mixture solution was dried with rotary evaporation and further washed with ether and dried to give the Si-precursor.

Synthesis of POP-5: In a 25 mL Teflon-lined autoclave thio-carbohydrazide (0.15 mmol, 0.0016 g), Si-precursor (0.10 mmol, 0.0641 g) and anhydrous ethanol (9 mL) was mixed together and stirred for 10 min. Followed by the autoclave heated for 4 days at 135 °C. Further it is cooled down to normal temperature and the solid polymer (POP-5) was filtered off and followed by Soxhlet extraction for 72 hours using methanol as a solvent. The polymer POP-5 then air dried and kept under vacuum 100 °C (12 hours) to get de-solvated phase of the compound. CHNS study found C, 49.25%; H, 5.46%; N, 11.91%; S, 3.86%. POP-5 was further characterized by solid state ^{13}C NMR.

Synthesis of POP-1: In a 25 mL Teflon-lined autoclave carbohydrazide (0.15 mmol, 0.0014 g), Si-precursor (0.10 mmol, 0.0641 g) and anhydrous ethanol (9 mL) was mixed together and stirred for 10 min. Followed by the autoclave heated for 4 days at 135 °C. Further it is cooled down to normal temperature and the solid polymer (POP-1) was filtered off and followed by Soxhlet extraction for 72 hours using methanol

as a solvent. The polymer POP-1 then air dried and kept under vacuum 100 °C(12 hours) to get de-solvated phase of the compound. CHNS study found C, 49.61%; H, 7.46%; N, 11.91%. POP-1 was further characterized by solid state ^{13}C NMR.

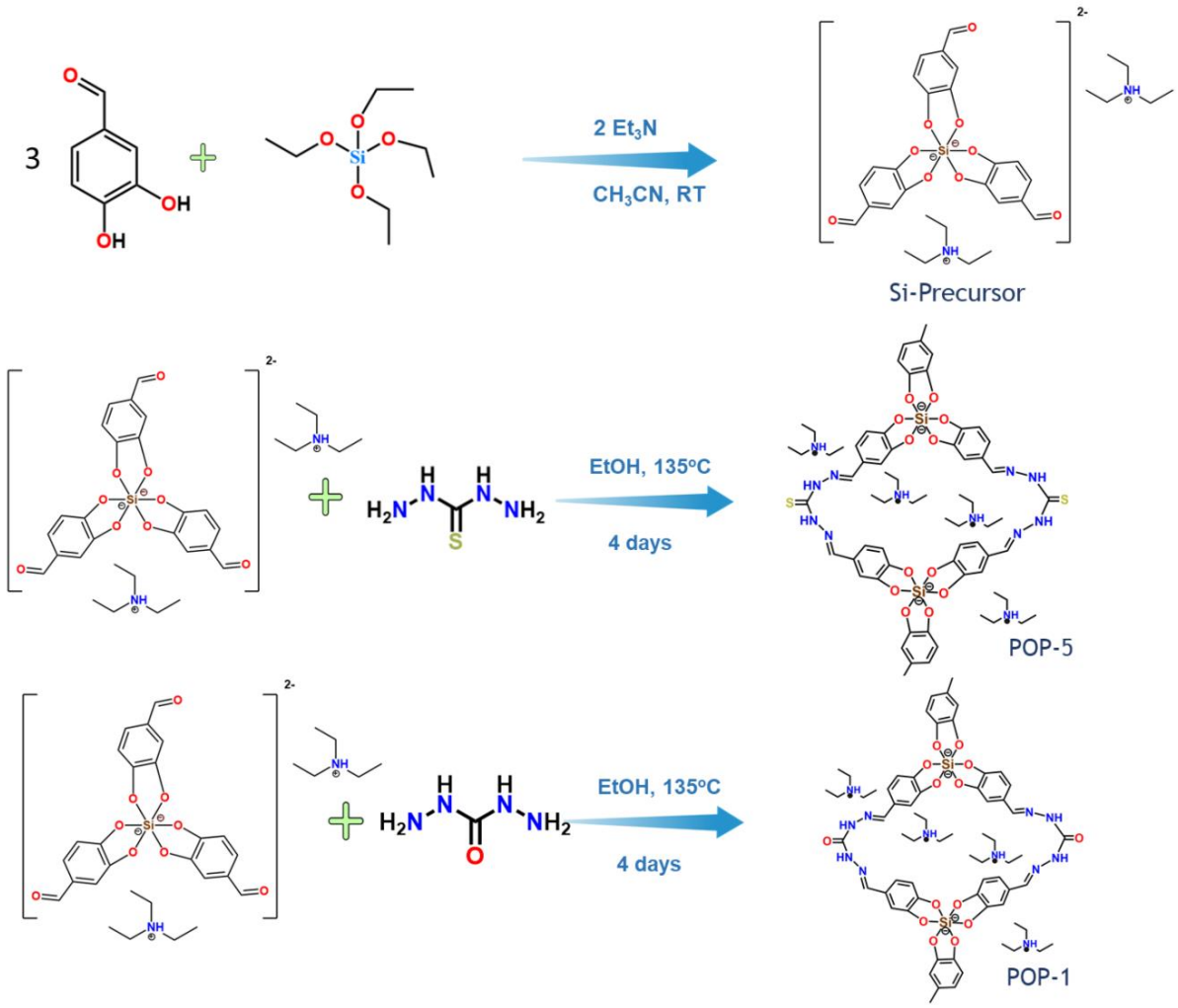

Scheme 3.2: Synthesis of silicon precursor, POP-5 and POP-1

3.2.3 Ion-exchange Studies

Hg^{2+} capture study: Mercury capture experiments were performed with various concentration of aqueous solutions of $HgCl_2$. In a typical experiment, the supernatant solution of each reaction vessel was taken and diluted and further subjected to ICP-AES and ICP-MS analysis.

Capture study: For kinetics measurement for mercury removal time dependent titration was carried out in 10 ppm aqueous solution of $HgCl_2$. 5 mg of each polymer was taken in 10 ml solution (concentration 10 ppm) at different time interval. For adsorption isotherm and capacity measurement various concentration of $HgCl_2$ (50ppm-1200ppm) were used and for each experiment. 5 mg of each polymer is stirred with 10 ml of solution for 24 hours. Further the supernatant solution was analysed by ICP-AES. We have calculated percentage removal and time dependent concentration decrease from the following equation.[11]

$$\boldsymbol{D_t = \frac{C_0 - C_t}{C_0} \text{ x } 100\% = \frac{A_0 - A_t}{A_0} \text{ x } 100\%}$$

$$\boldsymbol{i.e., \quad C_t = C_0 - \frac{A_0 - A_t}{A_0} \text{x } C_0}$$

Here, D_t is represented as exchange capacity, concentration and absorbance of the mercury solution at specific time are C_t and A_t, whereas, initial concentration and absorbance of the mercury solution are denote as C_0 and A_0 respectively. Again, kinetics data for mercury capture were plotted and it well fits in pseudo second-order model calculating from the following equation,[12]

$$\boldsymbol{Q_t = \frac{k_2 Q_e{}^2 t}{1 + k_2 Q_e t}}$$

where, t represents time in minute, Q_t is the amount of adsorbate (mg gm^{-1}) material and Q_e is the adsorbent material.

Competing cations: For selectivity measurement similar concentration of various interfering cations (Zn^{2+}, Cu^{2+}, Ca^{2+}, Ni^{2+}, Fe^{2+} etc.) were mixed with targeted analyte Hg^{2+} in equimolar concentration and mercury removal efficiency in presence of particular cation was analyzed via ICP-AES measurement.

Capacity calculation: 5 mg of each de-solvated compound was put in 10 ml 750 ppm aqueous solution of mercury. The mixture was kept stirring for 24 hours followed by the supernatant put to ICP-AES measurement and we have used the following equation to check the capacity. [11]

$$Q_t = \frac{(C_0 - C_t) * V}{m}$$

Where, V and m are the volume of the solution and mass of the adsorbent respectively whereas, C_0, Q_t, C_t, are initial concentration of mercury solution, capacity of adsorbent and concentration of the mercury solution at specific times respectively.

Recyclability test: The polymer POP-1 was regenerated by taking Hg captured POP-1 (20mg) and 10 equivalent of Na_2S solution was added which suggests the formation of soluble $[HgS_2]^{2-}$ and regenerating POP-1, which is further subjected to mercury capture.[13] The polymer morphology remains intact after recycling. POP-1 shows 5 times recyclable without significant loss of material. (Appendix 3.16)

Adsorption isotherm experiment: 5 mg of the two compounds were dispersed in 10ml of aqueous mercury solution having different concentration (50ppm to 1200ppm). After 24 hours taking the supernatant solution ICP-AES was carried out and the data is further fitted with the following equation.

Langmuir model, $$Q_e = \frac{Q_m C_e}{K_d + C_e}$$

where, the concentration of mercury at equilibrium is denoted as C_e (ppm) and amount of mercury adsorbed at equilibrium is termed as Q_e (mg gm^{-1}). To form a complete monolayer maximum amount of mercury per unit mass of adsorbent is Q_m (mg gm^{-1}). K_d (mg/L) is a constant related to the affinity of the binding sites.

Freundlich Model, $$Q_e = K_F C_e^{1/n}$$

where, K_F and 1/n are the two Freundlich model constants, whereas Q_e indicates capacity and C_e as equilibrium concentration.

3.3 Results and discussion

Herein, we report efficient mercury removal by two anionic polymers synthesized pre synthetically. Scheme 3.2 shows the synthetic procedure for both the polymers POP-1 and POP-5. [10] Thus synthesized two polymers were put into Soxhlet extraction in methanol to remove oligomers and later de-solvated under vacuum at 100 ^oC. Two as-obtained solids were examined by solid-state ^{13}C NMR. Both the polymers show peaks at 100-125 ppm confirming presence of benzene ring whereas peaks above 130 ppm indicates two different carbon atoms present in carbohydrazide and thio-carbohydrazide respectively. The peaks

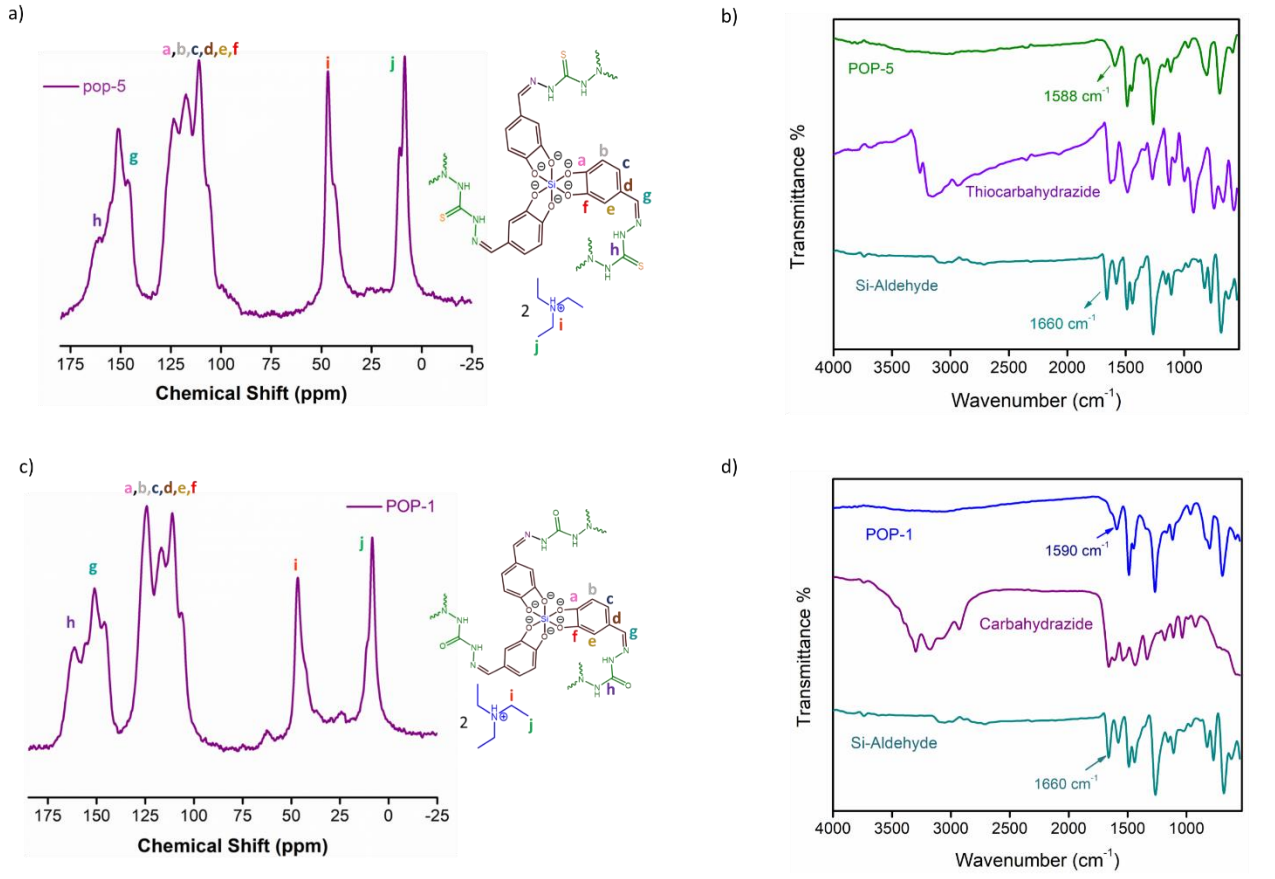

Figure 3.1: a) ^{13}C NMR spectra of POP-5 (corresponding peaks are leveled) b) FT-IR analysis of POP-5 comparing with its starting materials. c) ^{13}C NMR spectra of POP-1 (corresponding peaks are leveled) d) FT-IR analysis of POP-1 comparing with its starting materials.

corresponding to ~10 ppm and ~50 ppm are carbon atoms of extra framework triethyl amine cations. (Fig 3.1). Both the polymers are further subjected to thermogravimetric analysis (TGA). TGA profile of both the de-solvated phase of the polymers revealed that negligible loss up to ~250 ºC (Appendix 3.2, 3.9). Comparative TGA profile of both the polymers with stating materials doesn't show any similar pattern indicating the polymer formation (Appendix 3.1, 3.10). Further FESEM image shows spherical morphology in case of both the polymers. EDX and mapping analysis shows the presence of required elements in both polymers (Appendix 3.4, 3.12). POP-5 shows nitrogen, carbon, sulphur, oxygen and silicon are present whereas nitrogen, carbon, oxygen and silicon are there in POP-1. The N_2 adsorption isotherm at 77 K (Appendix 3.3, 3.11) indicates the presence of potential voids inside both the polymers. In FT-IR spectroscopy peaks at 1660 cm^{-1} in Si-precursor (Si-aldehyde) corresponds to aldehyde group present in

silicon precursor (Figure 3.1). In case of POP-5 peak at 1588 cm^{-1} and in case of POP-1 peak at 1590 cm^{-1} corresponds to C=N imine bond formed after polymerization. Both the polymer shows presence of Silicon-oxygen bond, peak corresponding to ~ 1300 cm^{-1}(Figure 3.1). CHNS analysis of POP-5 shows presence of elements carbon, nitrogen, sulphur and hydrogen whereas POP-1 shows presence of only carbon, nitrogen and hydrogen (Appendix 3.5, 3.13). XPS analysis of POP-5 suggests presence of elements carbon, nitrogen, oxygen, sulphur and silicon (Appendix 3.6). For real time application acid base stability of the both the polymers were checked. FT-IR analysis of POP-5 shows polymers remains intact after treatment with pH-4 and pH-10 solution (Appendix 3.17). Similar result was found in case of POP-1 (Appendix 3.16).

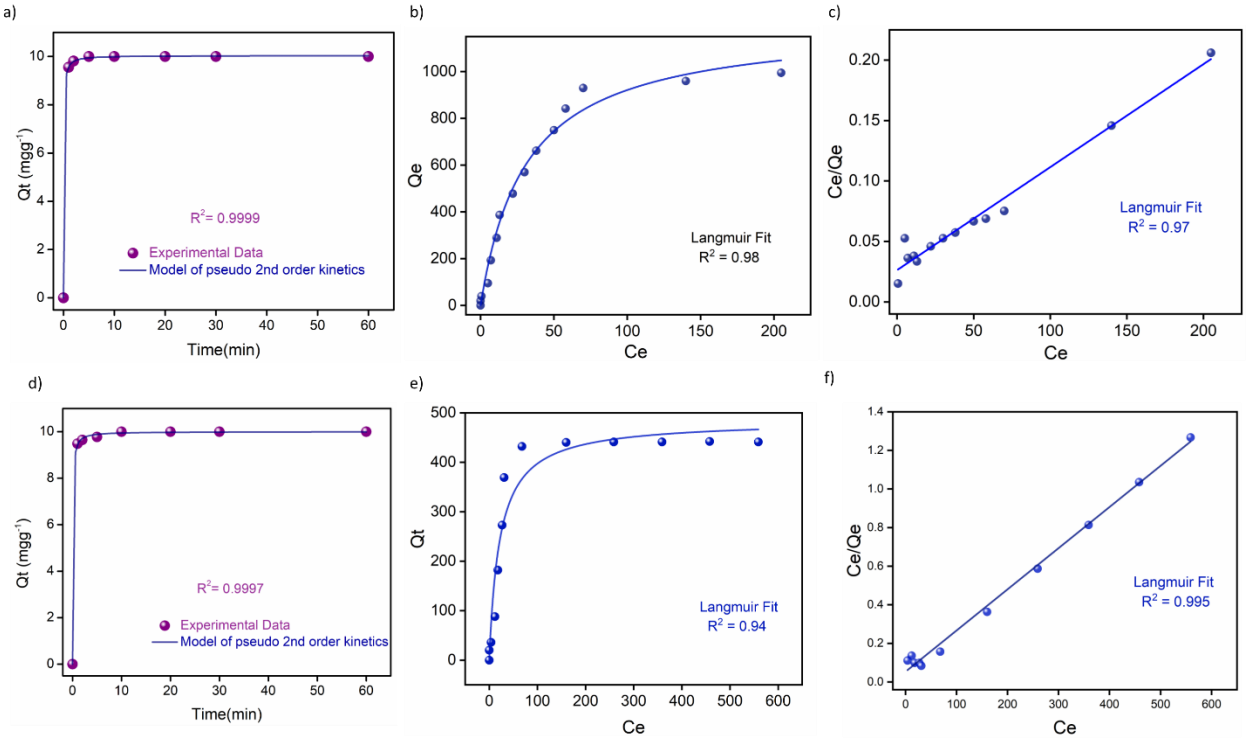

Figure 3.2: a) Adsorption kinetics (Pseudo 2nd order) of POP-5(R^2=0.9999), b) Equilibrium adsorption capacity of POP-5 fitted with non-linear model well fitted in Langmuir model, c) Equilibrium adsorption capacity of POP-5 fitted with linear Langmuir model, d) Adsorption kinetics (Pseudo 2nd order) of POP-1(R^2=0.99997), e) Equilibrium adsorption capacity of POP-1 fitted with non-linear Langmuir model (R^2=0.94). f) Equilibrium adsorption capacity of POP-1 fitted with linear Langmuir model (R^2=0.995).

To check the capture performance of POP-5 we dispersed 1 mg of polymer in 10 ppm mercury solution made using $HgCl_2$. After few minutes the supernatant was subjected to ICP-AES analysis which shows lesser mercury concentration due to ion-exchange. Excited from this result we performed kinetics study of mercury removal by POP-5 taking 10 ppm mercury solution and dipping 5 mg of the de-solvated compound and supernatants of different time interval was collected and analyzed by ICP-AES. The analysis shows complete removal of mercury from the solution in just 1 minute (Appendix 3.7). Similar experiment was carried out with POP-1 which also shows fast kinetics but relatively slower than POP-5. POP-1 shows complete removal of mercury from the solution after 10 minutes (Appendix 3.14). From the kinetics study removal efficiency was also calculated for both the polymers (Appendix 3.8, 3.15). Additionally, adsorption kinetics data were plotted and it fits with pseudo second order model revealing the dependence of capture process upon the quantity of absorbate and absorbent (R^2= 0.9999 for POP-5 and 0.9997 for POP-1) (Figure 3.2a, 3.2d). Enthused by the rapid ion-exchange kinetics we sought to explore the equilibrium adsorption capacity experiment for both the polymers. In a typical experiment different concentration mercury solution was prepared (50-1200 ppm) and 5 mg of both the polymers were dispersed in to the 10 ml of each concentration solution and stirred for 24 hours.

After 1 day the supernatant of each solution was subjected to ICP-AES analysis. The data was plotted in adsorption capacity vs equilibrium concentration and highest uptake capacity was calculated from it (Figure 3.2). POP-5 shows capacity of 992 mg g^{-1} and fits nicely with the Langmuir model having a good correlation co-efficient value (R^2=0.98). Whereas, POP-1 shows relatively less capacity 442 mg g^{-1} and fits well in the Langmuir model with a correlation co-efficient value (R^2=0.94). Further linear curve fit data also well fitted with the Langmuir model in both the polymers (correlation co-efficient of POP-5 0.97, POP-1 0.995) (Figure 3.2). Interfering cations like Zn^{2+}, Cu^{2+}, Ca^{2+}, Ni^{2+}, Fe^{2+}, K^{+} commonly found in industrial waste water along with Hg^{2+}. Selectively of the two polymers towards Hg^{2+} was calculated in the presence of other interfering cations which shows both the polymers are selective towards Hg^{2+} and POP-5 shows more promising result in case of selection, this can be ascribed to the existence of Sulphur in POP-5 and Hg-S soft-soft interaction is well known (Figure 3.3c, 3.3d). [15]

Further the post captured phase was characterized by FT-IR analysis. Shifting of peaks of N-H bending frequency at ~1530 cm^{-1} upon mercury capture in both the polymers indicates incorporation of mercury in the framework (Appendix 3.18, 3.19).[13] FESEM images of both polymers after capture shows morphology remained intact in the capture process (Appendix 3.22).. Further EDX analysis suggests the presence of mercury in both the captured-phase polymers (Appendix 3.23, 3.24). XPS analysis of the Hg captured POP-5 shows presence of Hg 4f orbital compared to the pristine POP-5 (Figure 3.3a). Detailed analysis of sulphur 2p orbital shows shifting of peaks as well as twinning of peaks, this can be attributed to soft-soft

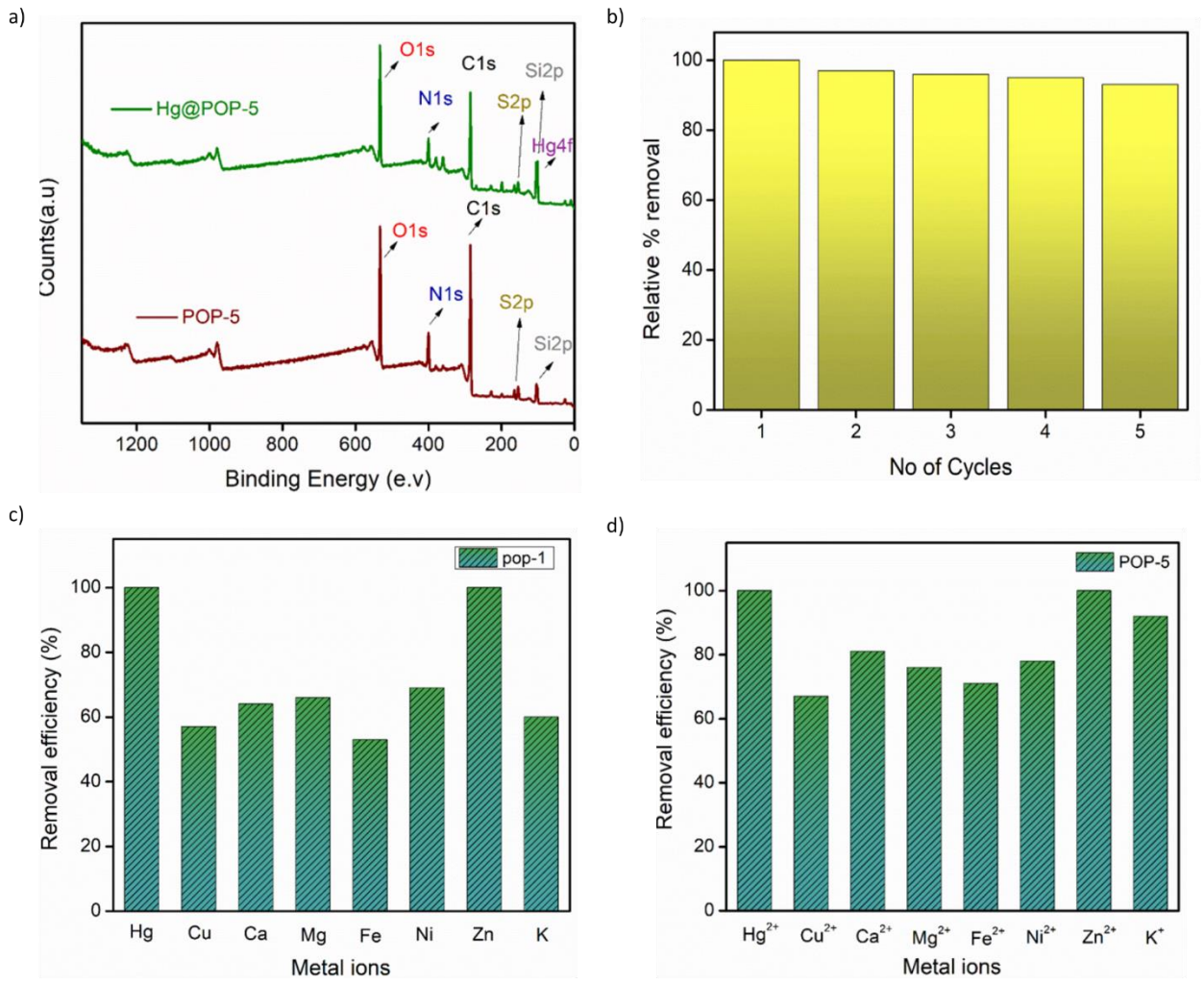

Figure 3.3: a) XPS analysis of pre and post captured POP-5. b) Recyclability study of POP-1. c) Removal efficiency of mercury in attendance of other cations by POP-1. d) Removal efficiency of mercury in attendance of other cations by POP-5.

interaction of mercury and sulphur.[15] As POP-5 is constructed with thio-carbohydrazide unit and due to strong interaction between mercury and sulphur (mercury and sulphur both are softer center), it shows high mercury adsorption capacity but doesn't show recyclable capacity. Whereas POP-1 constituted with carbohydrazide moiety which interacts with mercury relatively weak as a result mercury and oxygen interaction is weak and reversable, because of oxygen is a harder center and mercury is a softer center. In presence of softer center like sulphur, mercury detaches from carbohydrazide and regenerates POP-1. Recyclability experiment was carried out by 10 equivalents of Na_2S solution and mercury incorporated in the POP-1 reacting with excess S^{2-} forms $[HgS_2]^{2-}$ which is soluble in aqueous medium.[14]

3.4 Conclusions

To conclude, we have developed two resilient and cost-effective anionic polymer having exchangeable cations in the framework. The chemistry of ion exchange, and interaction with different functional groups shows effective mercury capture have been performed with two polymers. POP-5 having thio-carbohydrazide have shown a very high capacity of 992mg g^{-1} whereas carbohydrazide moiety articulated POP-1 shows a moderate capacity value 442 mg g^{-1}. Mercury capture performance of POP-5 is not recyclable whereas POP-1 is recyclable up to 5 cycles. Furthermore, both the polymer shows fast removal kinetics as well as good selectivity in presence of other cations. To the best our knowledge, pre-synthetic anionic polymer has not been employed as aqueous phase mercury removal till date. It is our understanding that this will drive the research in the field of mercury sequestration with such durable and affordable materials.

3.5 Appendix Section

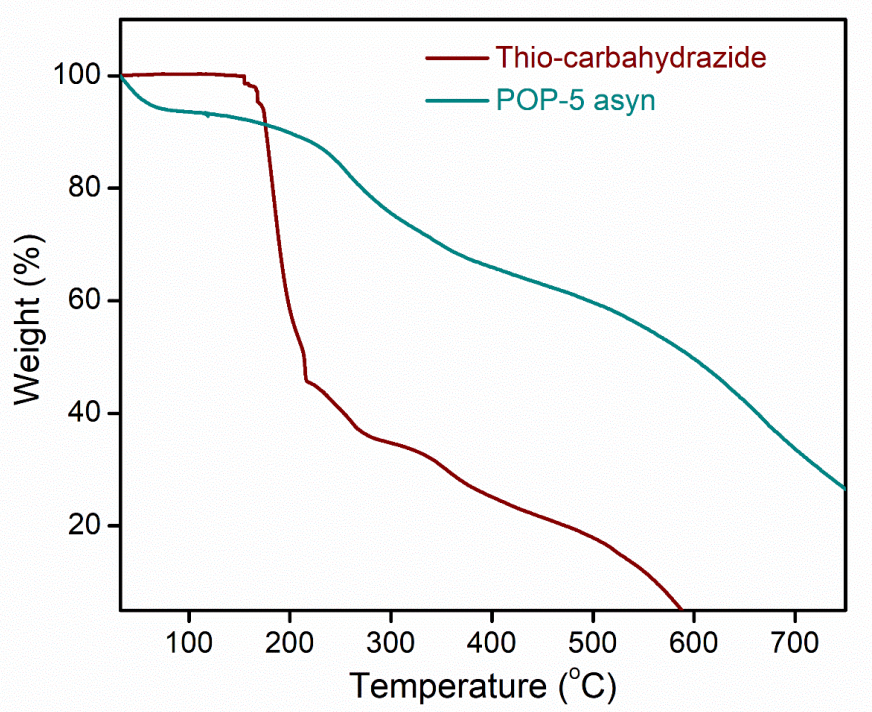

Appendix 3.1: TGA analysis of POP-1 (cyan) and thio-carbohydrazide (brown).

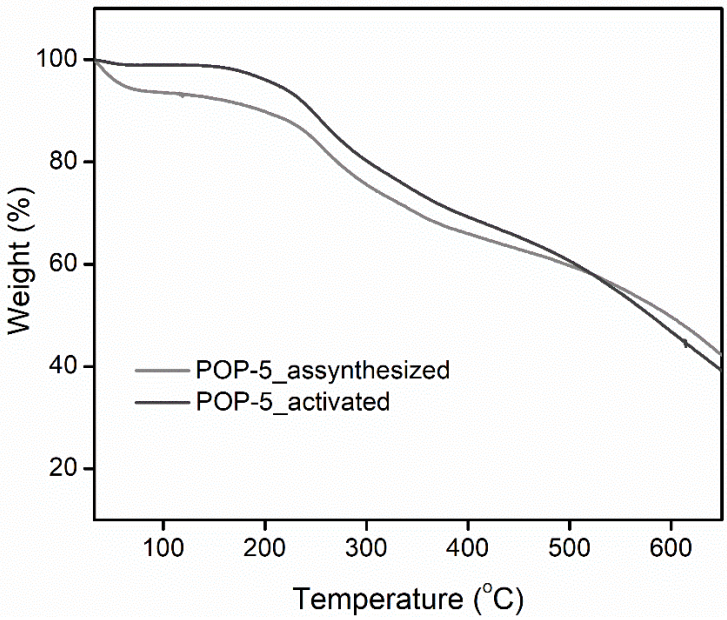

Appendix 3.2: TGA analysis of as-synthesized POP-5 (gray) and de-solvated phase of POP-5 (black).

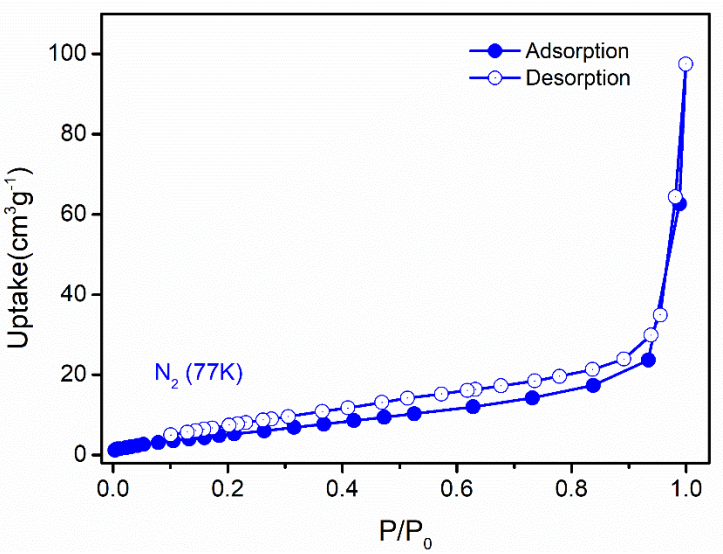

Appendix 3.3: Low temperature (77 K) N_2 adsorption profile of POP-5.(space fill: adsorption, space void: desorption)

a)

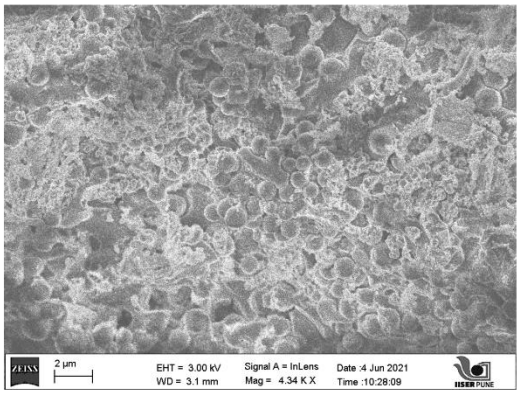

b)

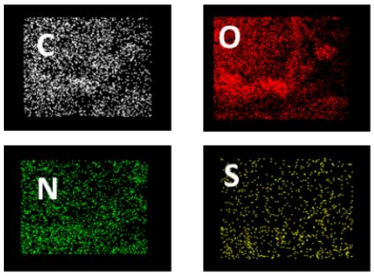

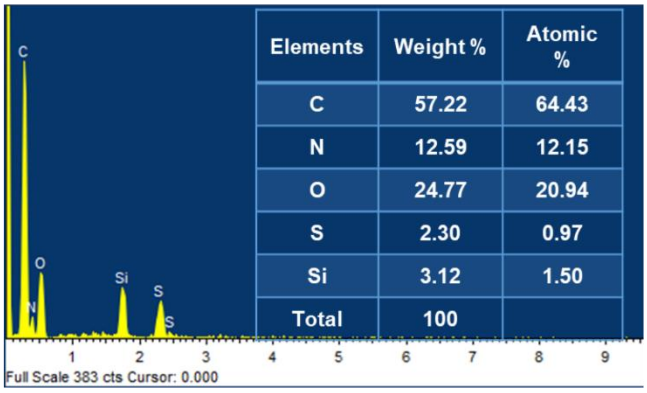

Elements	Weight %	Atomic %
C	57.22	64.43
N	12.59	12.15
O	24.77	20.94
S	2.30	0.97
Si	3.12	1.50
Total	100	

Appendix 3.4: FESEM image, mapping and EDX analysis of POP-5.

Compounds	**% C**	**% H**	**% N**	**% S**
POP-5	49.25	5.46	11.91	3.86

Appendix 3.5: CHNS analysis of POP-5.

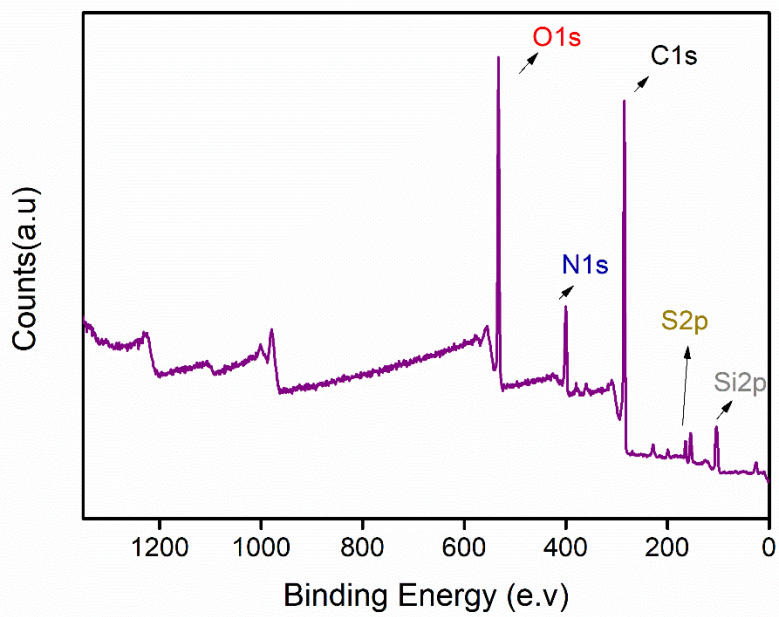

Appendix 3.6: XPS analysis of POP-5.

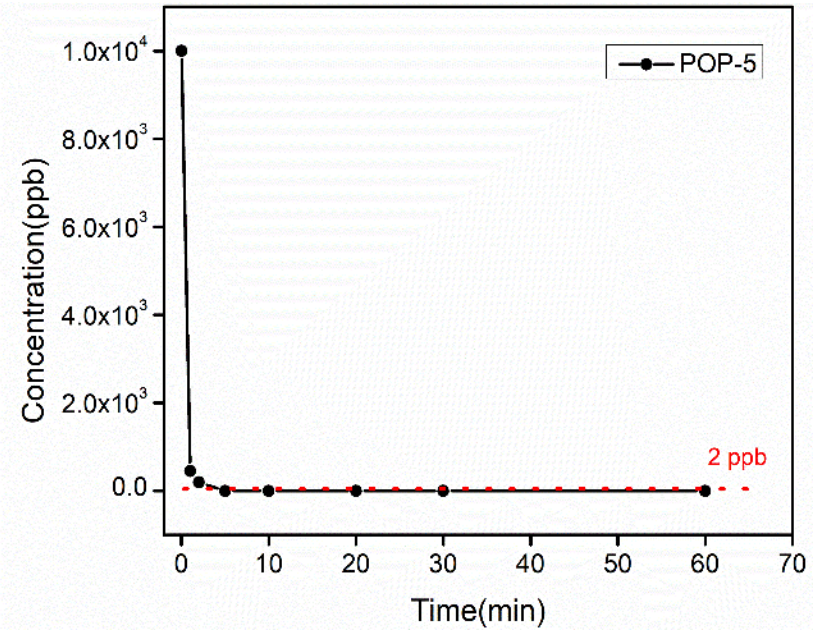

Appendix 3.7: Kinetic measurement of POP-5.

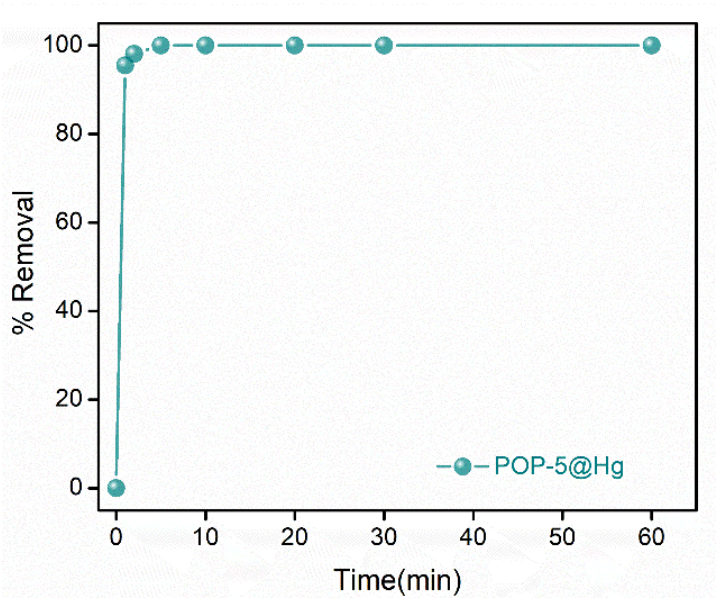

Appendix 3.8: Percentage of removal by POP-5.

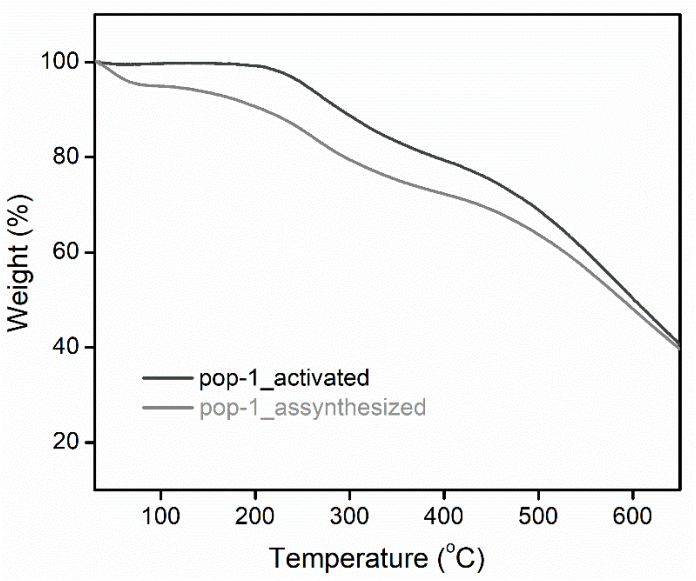

Appendix 3.9: TGA analysis of as-synthesized POP-1 (gray) and de-solvated phase of POP-1 (black).

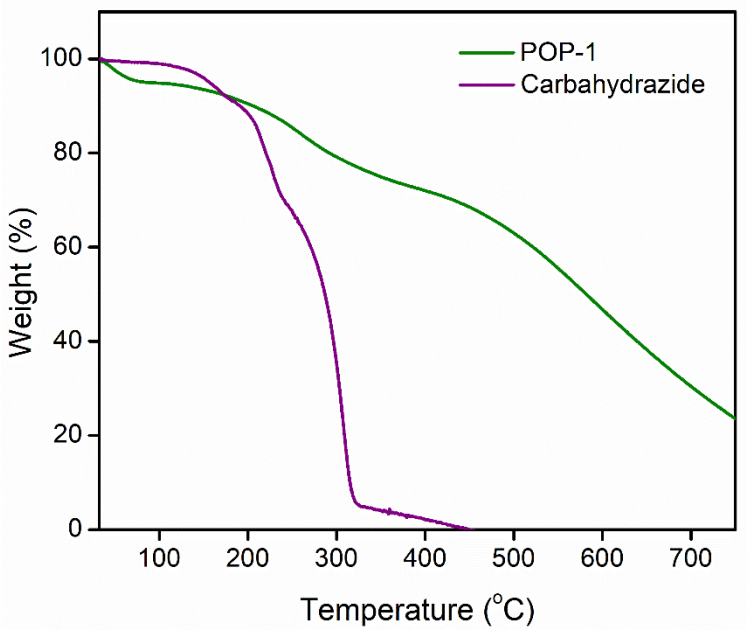

Appendix 3.10: TGA analysis of POP-1 (green) and carbohydrazide (violet).

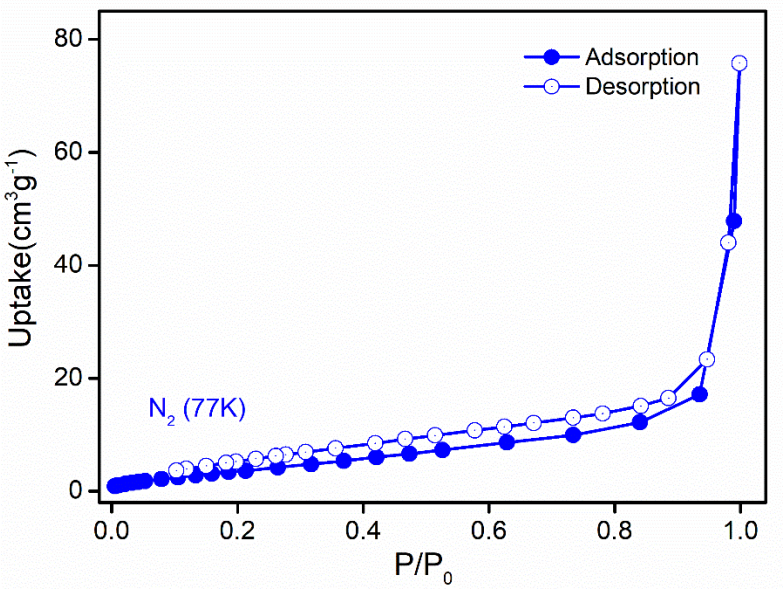

Appendix 3.11: N_2 adsorption profile (77 K) of POP-1.(space fill: adsorption, space void: desorption)

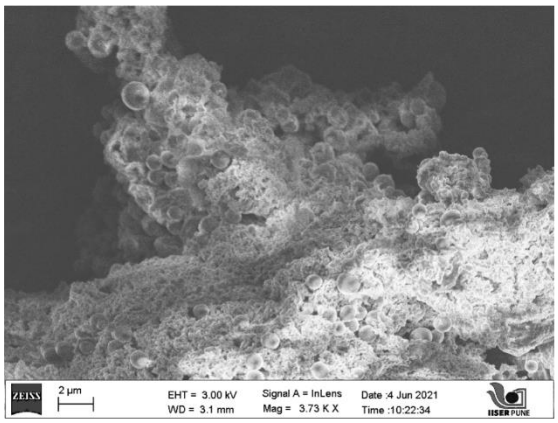

Elements	Weight %	Atomic %
C	59.23	65.86
N	8.45	8.06
O	29.80	24.88
Si	2.52	1.20
Total	100	

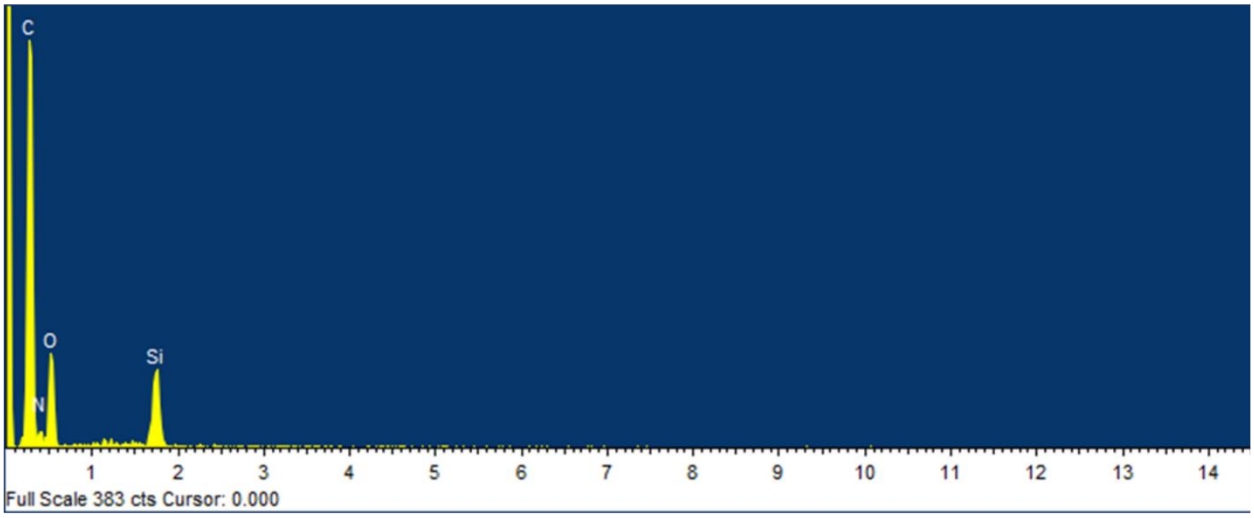

Appendix 3.12: FESEM image, EDX analysis of POP-1.

Compounds	% C	% H	% N	% S
POP-1	49.61	5.59	7.8	0.0

Appendix 3.13: CHNS analysis of POP-1.

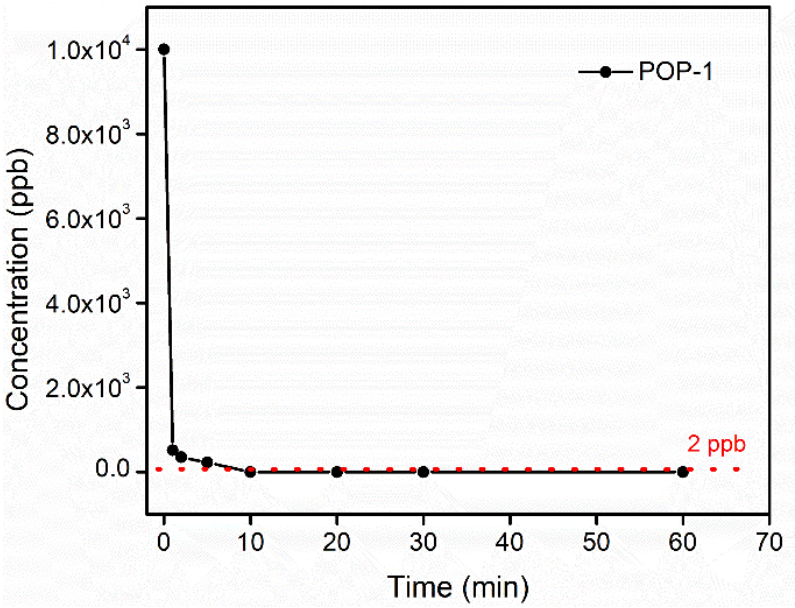

Appendix 3.14: Kinetic measurement of POP-1.

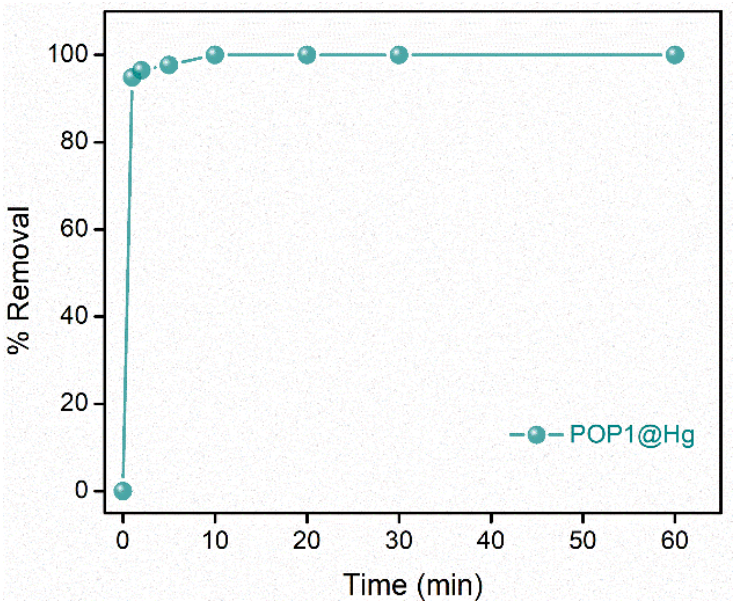

Appendix 3.15: Percentage of removal by POP-1

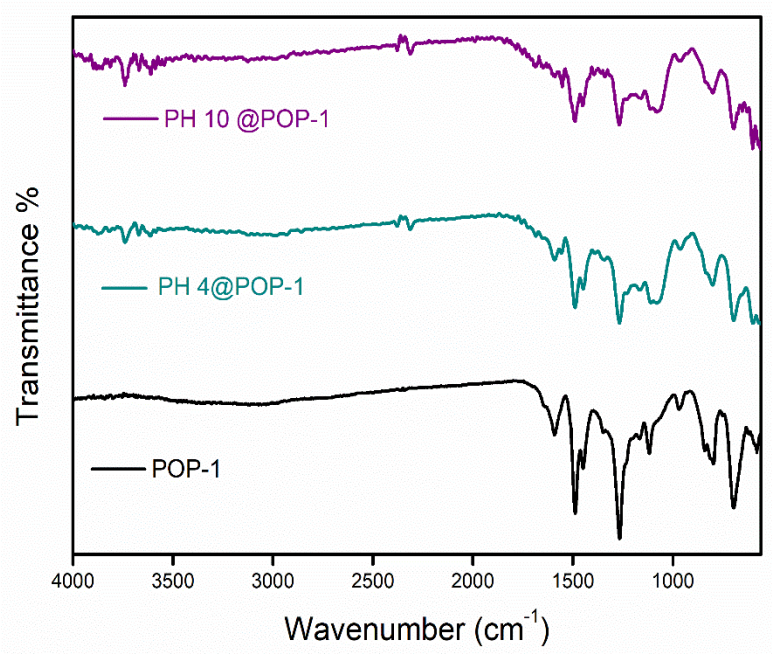

Appendix 3.16: pH stability of POP-1.

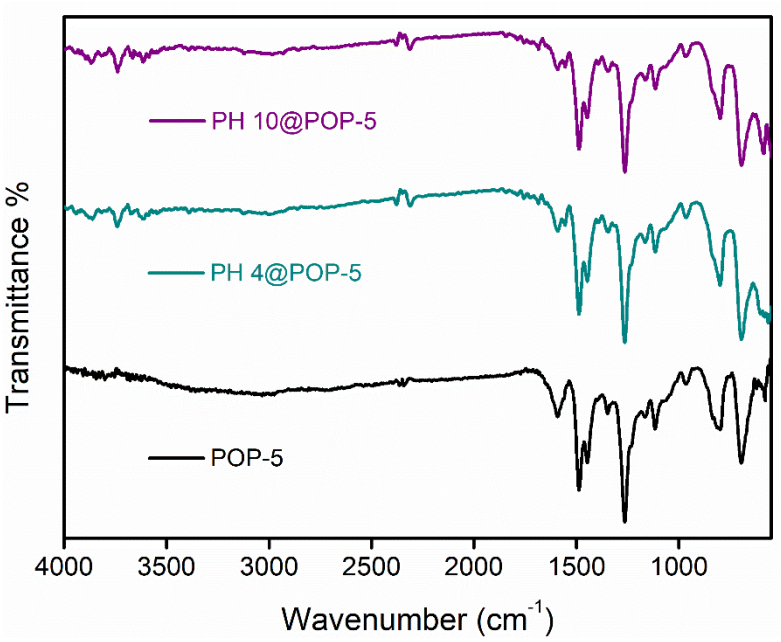

Appendix 3.17: pH stability of POP-5.

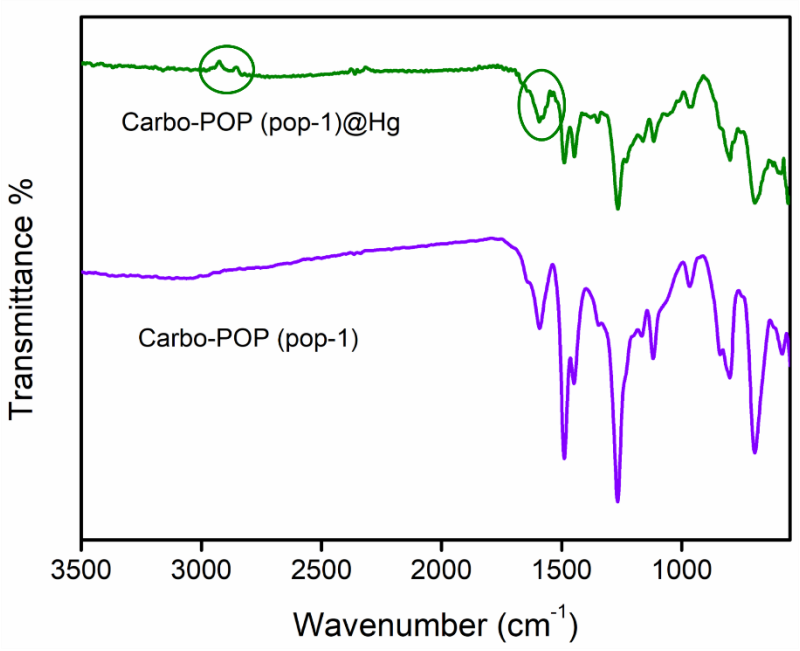

Appendix 3.18: FT-IR analysis of POP-1 before and after capture of mercury.

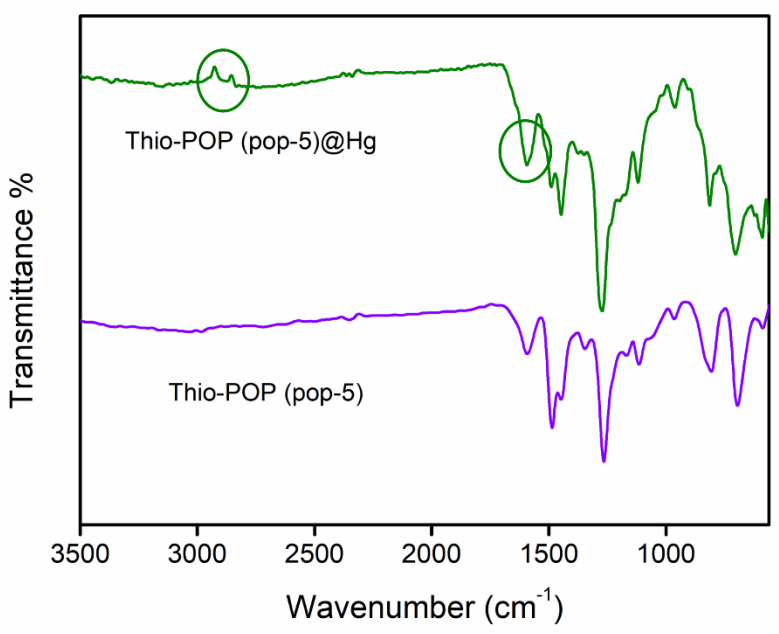

Appendix 3.19: FT-IR analysis of POP-5 before and after capture of mercury.

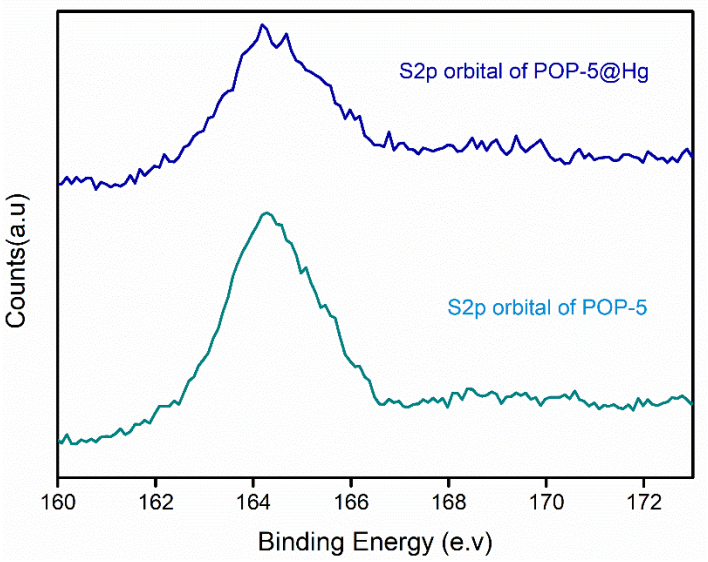

Appendix 3.20: XPS analysis of Sulphur 2p orbital pre and post capture.

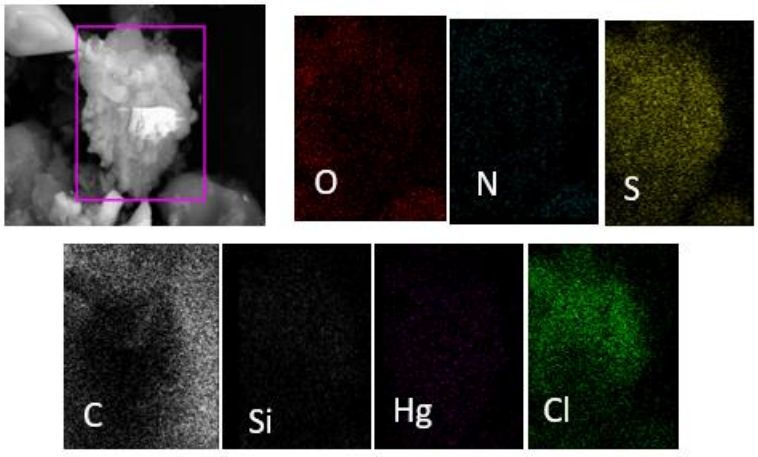

Appendix 3.21: Elemental mapping of Hg@POP-5.

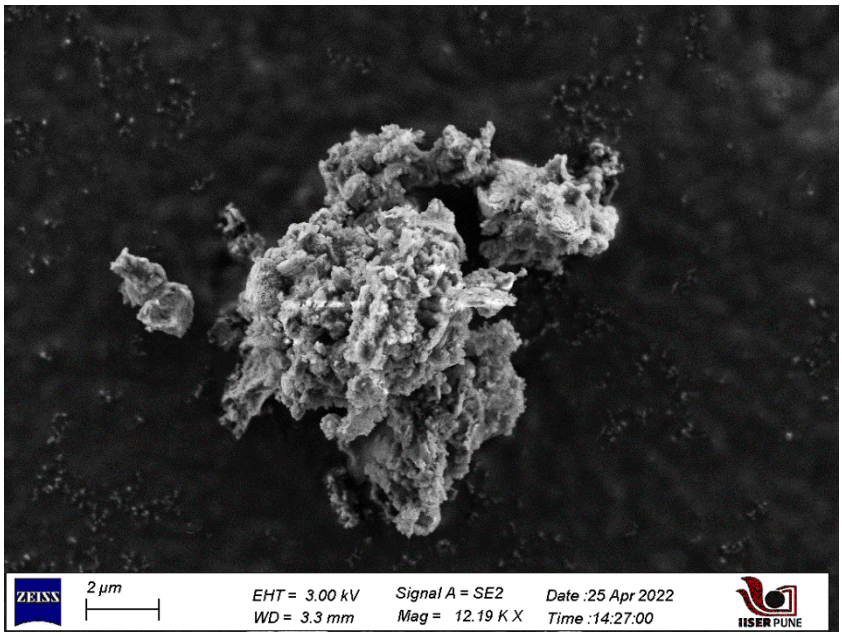

Appendix 3.22: FESEM image of Hg@POP-5.

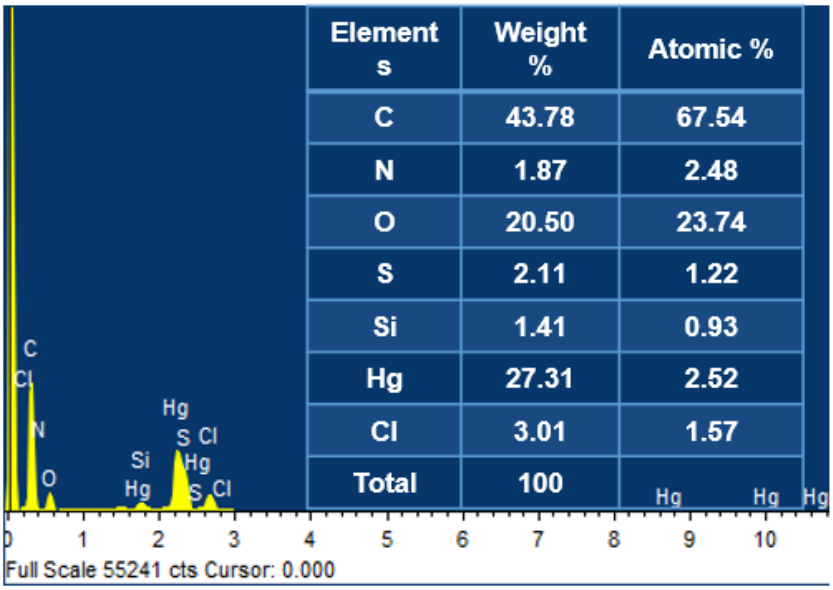

Elements	Weight %	Atomic %
C	43.78	67.54
N	1.87	2.48
O	20.50	23.74
S	2.11	1.22
Si	1.41	0.93
Hg	27.31	2.52
Cl	3.01	1.57
Total	100	

Appendix 3.23: EDX analysis of Hg@POP-5.

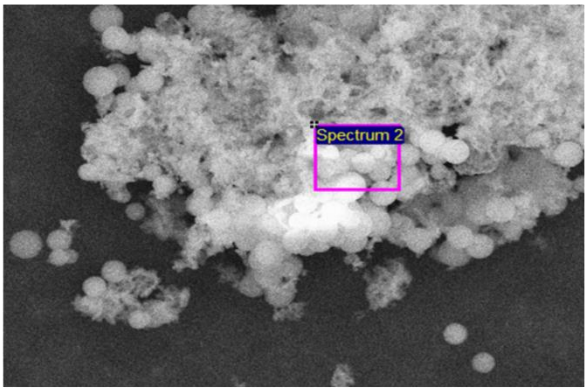

Elements	Weight %	Atomic %
C	52.03	67.55
N	1.89	2.10
O	27.62	26.93
Si	3.28	1.82
Hg	14.03	1.09
Cl	1.16	0.51
Total	100	

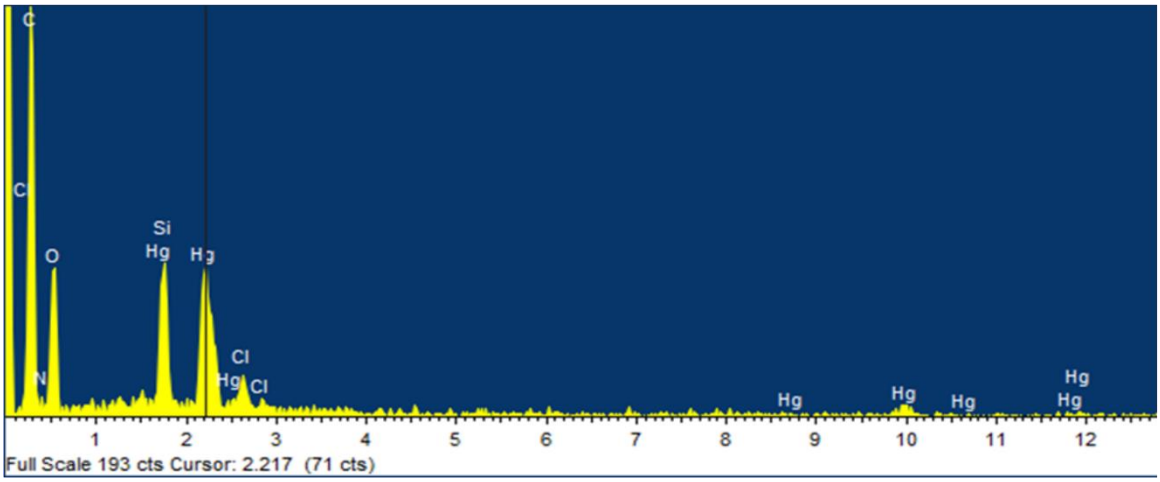

Appendix 3.24: FESEM image and EDX analysis of Hg@POP-1.

3.6 References

1. (a) J. O. Nriagu, J. M. Pacyna, *Nature* ,1988, **333**, 134–139, (b) B. K. Mandal, K. T. Suzuki, *Talanta* 2002, **58**, 201–235, (c) L. Jarup, Br *Med Bull* ,2003, **68**, 167–182.

2. (a) Y.-E. Huang, N. Zhang, Y.-X. Jiang, W. Guo and C.-P. Li, Chinese journal of schistosomiasis control 2015, **27**, 290–294. (b) B.-M. Mahdi, N. Kobra, T. Zoya, K. M. Reza and S. Mahmood, *Frontiers in Pharmacology*, 2021, **12**, 643972.

3. (a) M. K. Hamdy and O. R. Noyes Formation of Methyl Mercury by Bacteria. *Appl Microbiol.* 1975 , **30**(3): 424–432. (b) J. G. Omichinski, *Science*, 2007, **317**, 205–206.

4. (a) T. Pradeep and Anshup, *Thin Solid Films*, 2009, **517**, 6441–6478. (b) U.S. Environmental Protection Agency. Mercury Study Report to Congress: Overview, 2003. http://www.epa.gov/airprogm/oar/ mercover.html. (c) C. Liu, Y. Huang, N. Naismith, J. Economy and J. Talbott, *Environ. Sci. Technol*., 2003, **37**, 4261−4268.

5. (a) F. Z. Cui, R. R. Liang, Q. Y. Qi, G. F. Jiang and X. Zhao, *Advanced Sustainable Systems*, 2019, **3** (4), 1800150, (b) F. Xiong, L. Jiang and Q. Jia, *Anal. Chim. Acta*, 2020, **1099**, 103-110. (c) N. T. T. Hai, N. T. Hue and D. Q. Trung, *Asian J. Chem*., 2013, **25**, 10251-10254.

6. (a) C. P. Huang and D. W. Blankenship, *Water Res*., 1984, **18**, 37-46. (b) J.-G. Yu, L.-Y. Yu, H. Yang, Q. Liu, X.-H, Chen, X.-Y. Jiang, X.-Q. Chen and F.-P. Jiao, *Sci. Total Environ*., 2015, **502**, 70-79. (c) G. Blanchard, M. Maunaye and G. Martin, *Water Res*., 1984, **18**, 1501-1507. (d) G. Yang, H. Han, C. Du, Z. Luo and Y, Wang, *Polymer*, 2010, **51**, 6193-6202. (e) P. Hadi, M. H. To, C. W. Hui, C. S.. Lin and G. Mckay, *Water Res*., 2015, **73**, 37-55.

7. (a) N. Huang, L. Zhai, H. Xu and D. Jiang, *J. Am. Chem. Soc.*, 2017, **139**, 2428-2434. (b) Q. Sun, B. Aguila, J. Perman, L. D. Earl, C. W. Abney, Y. Cheng, H. Wei, N, Nguyen, L. Wojtas and S. Ma, *J. Am. Chem. Soc.*, 2017, **139**, 2786-2793. (c) K.-K. Yee, N. Reimer, J. Liu, S.-Y. Cheng, S.-M. Yiu, J. Weber. N. Stock and Z. Xu, *J. Am. Chem. Soc*., 2013, **135**, 7795-7798.

8. (a) L. Zhou, Y. Wang, Z. Liu and Q. Huang, *J. Hazard. Mater.*, 2009, **161**, 995-1002. (b) X. Yao, H. Wanf, Z. Ma, M. Liu, X. Zhao and D. Jia, *Chinese J. Chem. Eng*., 2016, **24**, 1344-1352. (c) W.-R. Cui,

W. Jiang, C.-R. Zhang, R.-P. Liang, J. Liu and J.-D. Qiu, *ACS Sustainable Chem. Eng.*, 2020, **8**, 445-451.

9. (a) S. Zhang, J. Li, D. Y. Du, J. S. Qin, S. L. Li, W. W. He, Z. M. Su and Y. Q. Lan, *J. Mater. Chem. A*, 2015, **3**, 23426– 23434; (b) J. J. Li, C. C. Wang, H. F. Fu, J. R. Cui, P. Xu, J. Guo and J. R. Li, *Dalton Trans*., 2017, **46**, 10197–10201; (c) Z. Zhu, Y. L. Bai, L. Zhang, D. Sun, J. Fang and S. Zhu, *Chem. Commun*., 2014, **50**, 14674–14677. (d) Z. Li, H. Li, X. Guan, J. Tang, Y. Yusran, Z. Li, M. Xue, Q. Fang, Y. Yan, V. Valtchev and S. Qiu, *J. Am. Chem. Soc*., 2017, **139**, 17771–17774; (e) Y. Liu and K. Landskron, *J. Mater. Chem. A*, 2017, **5**, 23523–23529; (f) Z. Xiang and D. Cao, *J. Mater. Chem. A*, 2013, **1**, 2691–2718. (g) M. Mon, F. Lloret, J. Ferrando-Soria, C. Marti-Gastaldo, D. Armentano and E. Pardo, *Angew. Chem. Int. Ed*., 2016, **55**, 11167-11172.

10. G. Xiong, B.-B. Wang, L.-X. You, B.-Y. Ren, Y.-K. He, F. Ding, I. Dragutan, V. Dragutanb and Y.-G. Sun, *J. Mater. Chem. A*, 2019, **7**, 393–404

11. Y. Su, Y. Wang, X. Li, X. Li and R. Wang, *ACS Appl. Mater. Interfaces*, 2016, **8**, 18904−18911.

12. Q. Zhang, J. Yu, J. Cai, L. Zhang, Y. Cui, Y. Yang, B. Chen and G. Qian, *Chem. Commun.*, 2015, **51**, 14732–14734.

13. W.-R. Cui, W. Jiang, C.-R. Zhang, R.-P. Liang, J. Liu, and J.-D. Qiu, *ACS Sustainable Chem. Eng*., 2020, **8**, 445−451.
14. S.-Y. Ding, M. Dong, Y.-W. Wang, Y.-T. Chen, H.-Z. Wang, C.-Y. Su and W. Wang, *J. Am. Chem. Soc*., 2016, **138**, 3031−3037.
15. O. P. Ajsuvakova, A. A. Tinkov, M. Aschner, J. B.T. Rocha, B. Michalke, M. G. Skalnaya, A. V. Skalny, M. Butnariu, M Dadar, I. Sarac, J. Aaseth and G. Bjørklund *Coordination Chemistry Reviews*, 2020, **417**, 213343.

Chapter 4

Role of Framework Integrated Template Anions in Troger Base Polymer for Selective Ultrafast Removal of Toxic Pollutant from Water

4.1 Introduction

In this 21st century fresh water is imperative for all life forms in our ecosystem to endure, consequently chemical water contamination has become imminent threat to entire system chain. However widespread development in human society and extensive industrialization has resulted in scarcity in fresh drinking water.[1,2] A recent study reveals although total world population has increased 4 fold in the last decade the population under water scarcity has increased 16 fold and of these 1.1 billion people are in high water shortage living in mostly East and South Asia, North Africa and Middle East.[3] Although metals are imperative for the functioning of living creatures, it becomes persistent global environment issue when it exceeds specific limits. In the same line metal-based oxoanions (CrO_4^{2-}, AsO_4^{3-}, TcO_4^-, SeO_3^{2-} etc.) are also contemplated as precedence contaminants by EPA (Environmental Protection Agency, U.S.).[4] Even at a very low concentration hexavalent Cr (VI) in its oxoanion form has severe mutagenic and carcinogenic effects on human life.[5] Due to its high solubility and mobility nature and capability of causing severe impairment U.S. EPA classified it as "Group A" and International Agency for Research on Cancer (IARC) levelled it as "Group I" carcinogen.[6,7] It is extensively used in metallurgy, paper mills, wood preservatives, pigments, metal plating, dying, printing, leather tanning and other industries. For instance, to produce 1 kg of leather, tanning-based companies releases 30 to 35 L of chromium contaminated water. [8,9] Apart from these Cr (VI)-based contaminations, one radio isotope of technetium (^{99}Tc) which primarily resides in the environment in its oxo-anion form pertechnetate (TcO_4^-) emits harmful β-ray. Enduring ($t_{1/2} = 2.13 \times 10^5$ y) radioisotope ^{99}Tc is produced by nuclear fission of ^{239}Pu or ^{235}U which is also has a high fission yield. According to IEPA (International Atomic Energy Agency) accumulation of ^{99}Tc in last 20 years is estimated around 160 metric ton and the number is skyrocketing with increasing number of nuclear powerplants all over the world specially in the developing countries. [10,11] Another isotope ^{99m}Tc is used as radiopharmaceuticals for medical diagnosis and imaging.[12] Segregation of such toxic wastes has attracted a lot of attention recently due to its threat to human health and its emerging medical uses as well as owing to increasing shortage of drinking water. [13,14]

Although several methods have been exploited for the sequestration of oxo-anions, such as adsorption, membrane filtration, ion exchange, precipitation method, electrochemical treatment but amidst ion exchange based methods are adopted owing to its less ability to generate secondary waste, relative simplicity, relative safe and low cost.[15-19] Additionally, the state-of-the-art ion exchangers like silica and zeolites have drawbacks like poor selectivity, delayed kinetics and lack of regeneration abilities, which opens the door to the creation of new, more effective and alternative ion exchange materials.[20,21] Recent reports suggests development of new materials like covalent organic frameworks (COFs), metal−organic frameworks (MOFs) and porous-organic Polymers (POPs) for water purification as they show permanent

porosity and high surface areas.[22,23] However poor physiochemical stability of MOFs and complicated construction of most COFs limits there applications. Contrarily porous-organic polymers prepared from stable covalent bonds have higher physiochemical stabilities even in harsh chemical condition as well as have simple and diversified chemical synthetic route.[24] In this context comes Tröger's base polymer which has a 'V-shaped' bridged bicyclic system which possess two tertiary bridgehead nitrogen atoms gives a strong basicity of (pKHB(N) = 1.15) based on hydrogen bonding acceptor strength.[25] Although the basic site has been previously exploited for organo-catalysis and gas separation but it's never been utilized for post synthetic modification site.[26,27] High stability and presence of different functional group makes Tröger's base polymer for a convenient platform for post synthetic modification or PSM.[28] PSM is a unique strategy to provide an substitute, practical and appropriate tool to modulate the material synthesized, to overcome the pre synthetic condition restrictions.

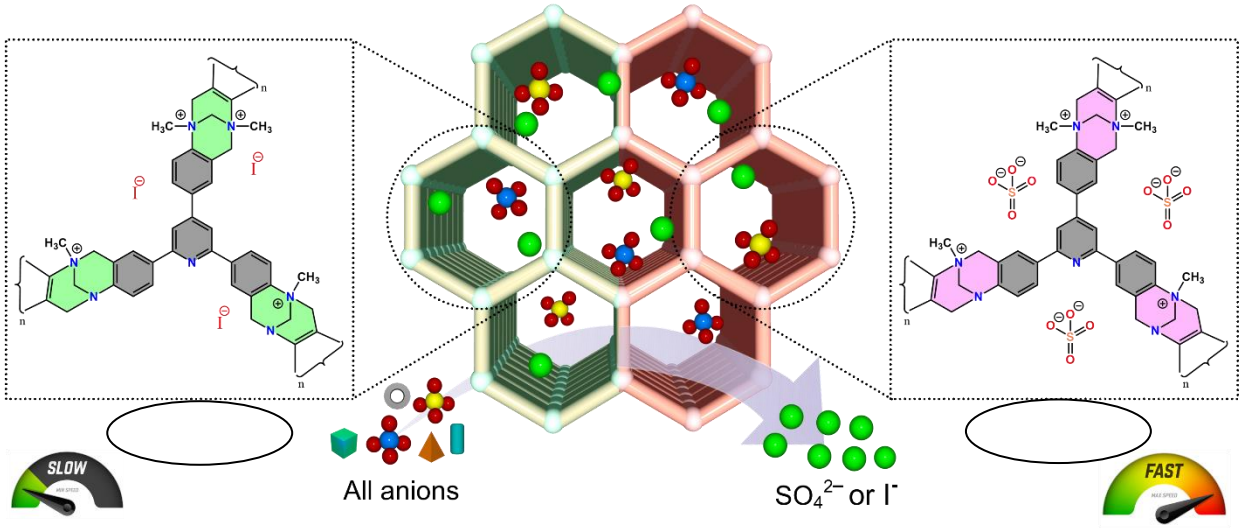

Figure 4.1: Schematic representation of the oxo-anions capture by the two polymers

Here in this work, we have developed two different cationic polymers by post synthetic modification of Tröger's base polymer using two analytes resulting TB-POP@MI and TB-POP@MS having iodide and sulphate as counter anion simultaneously. The role of framework integrated anion for sequestration of harmful oxo-anions has been explored. Besides, exceptional selective oxo-anion capture was further assisted by the density functional theory (DFT) method which is a detailed technique to calculate theoretical binding energy.

4.2 Experimental

4.2.1 Materials:

4-nitrobenzaldehyde, anhydrous ethanol, 4-nitroacetophenone, dimethyl sulfate, methyl iodide, ferric chloride hexahydrate, ammonium acetate, activated carbon, K_2CrO_4, glacial acetic acid, trifluoro acetic acid. ammonium acetate, and hydrazine mono-hydrate (80vol.-%) were obtained locally. Formaldehyde dimethyl acetal (FDA) was obtained from Sigma-Aldrich. Further purchased chemical was utilized without further purification.

4.2.2 Physical Measurements:

Thermogravimetric analysis (TGA) was performed by using a PerkinElmer STA 6000 analyser under a nitrogen atmosphere where temperature was gradually increased from 30°C to 800°C at a heating rate of 10°C/min. All Infra-red (IR) Spectra were measured by using NICOLET 6700 FT-IR spectrophotometer in the range of 400-4000 cm^{-1} using KBr pellet. Low temperature nitrogen adsorption measurements were performed by using Bel Sorp-max instrument from Bel Japan. The SEM images were acquired using FEI Quanta 3D dual beam FESEM at 30KV. Energy dispersive X-ray (EDX) analyses was performed with a Hitachi S3400 N EDX instrument. TEM imaging were obtained on the HRTEM (JEM-2200FS, JEOL) operating at acceleration voltage of 200 kV. UV spectra were acquired on Shimadzu UV 2600 Spectrophotometer. Solid state NMR spectra were performed on Bruker 400 MHz NMR spectrometer. Carbon chemical shifts are expressed in parts per million (δ scale).

4.2.3 Synthesis:

Synthesis of 2,4,6-Tris(4-aminophenyl) pyridine (TAPP): First precursor 2,4,6-Tris(4-nitrophenyl) pyridine was developed via acid catalyzed cyclization of 4-nitrobenzaldehyde, 4-nitroacetophenone and ammonium acetate. After that via complete reduction of 2,4,6-Tris(4-nitrophenyl) pyridine, 2,4,6-Tris(4-aminophenyl) pyridine was developed via following a previously described protocol.[29]

Synthesis of TB-POP: Under N_2 atmosphere 2,4,6-Tris(4-aminophenyl) pyridine (1 mmol) was dissolved in formaldehyde dimethyl acetal (FDA) (1ml, 11.2 mmol) and cooled in ice bath. After that followed by dropwise addition of 15 ml trifluoracetic acid the mixture was stirred for 2 days. After 48 hours the viscous was transferred into a solution of water and aqueous ammonia and stirred vigorously for 2 hours which resulted in a formation of brown solid. After that the brown solid was filtered of and which is followed by washing with methanol and distilled water. Further the brown solid was purified via soxhlet extraction by mixture of water/methanol/acetone for 12 hours and with THF for another 12 hours respectively. The collected brown powder was then heated under vacuum at 110°C (12 hours) for the removal of solvent

guest molecules which resulted in a brown solid TB-POP (yield 81%). Elemental analysis C 74.71%, H 6.1%, N 11.89%.

Synthesis of TB-POP@MS: 4.7ml (50 mmol) dimethyl sulfate was added dropwise to the polymer TB-POP (300mg) dispersed in acetonitrile (150ml). After stirring the mixture for 12 hours in reflux condition the solid was collected via filtration. Which is followed by washing with different solvents like $CHCl_3$, acetonitrile, methanol, THF etc. Further drying under vacuum at 100°C (12 hours) resulted in a brick red powder. Elemental analysis C 46.7%, H 5.78%, N 8.83%, S 11.74%.

Synthesis of TB-POP@MI: 6.2 ml (100 mmol) iodomethane was added dropwise to the TB-POP polymer (300mg) diffused in 150 ml acetonitrile. The reaction mixture then stirred for 12 hours in refluxing condition, and further the resultant solid was collected via filtration. Collected solid was then washed with acetonitrile, methanol, acetone and THF subsequently heated under vacuum at 100°C for 12 hours resulting in a reddish solid.

a)

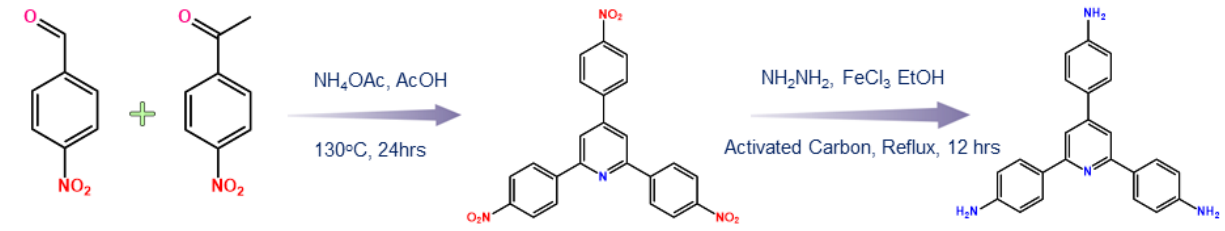

b)

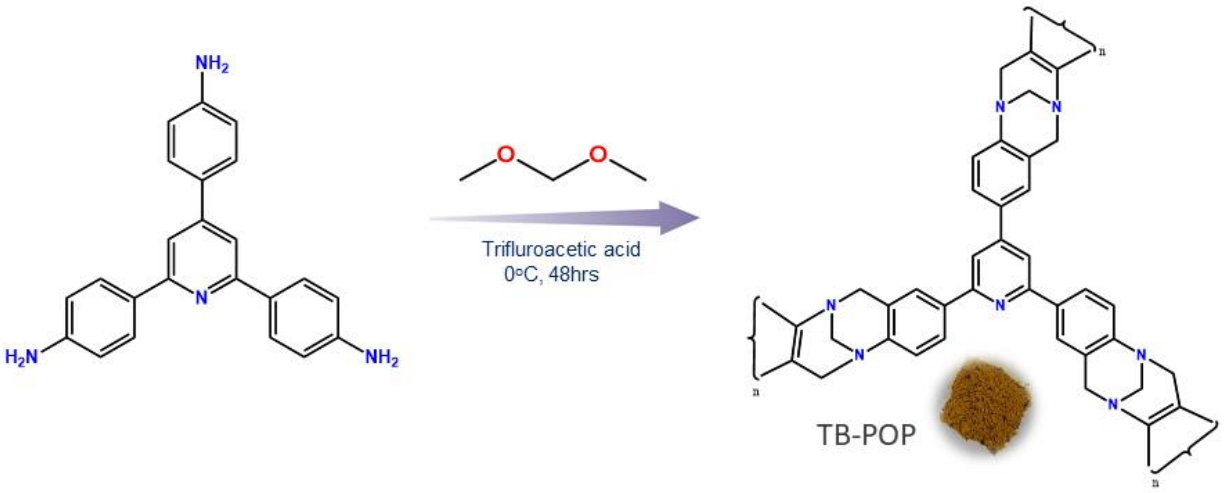

c)

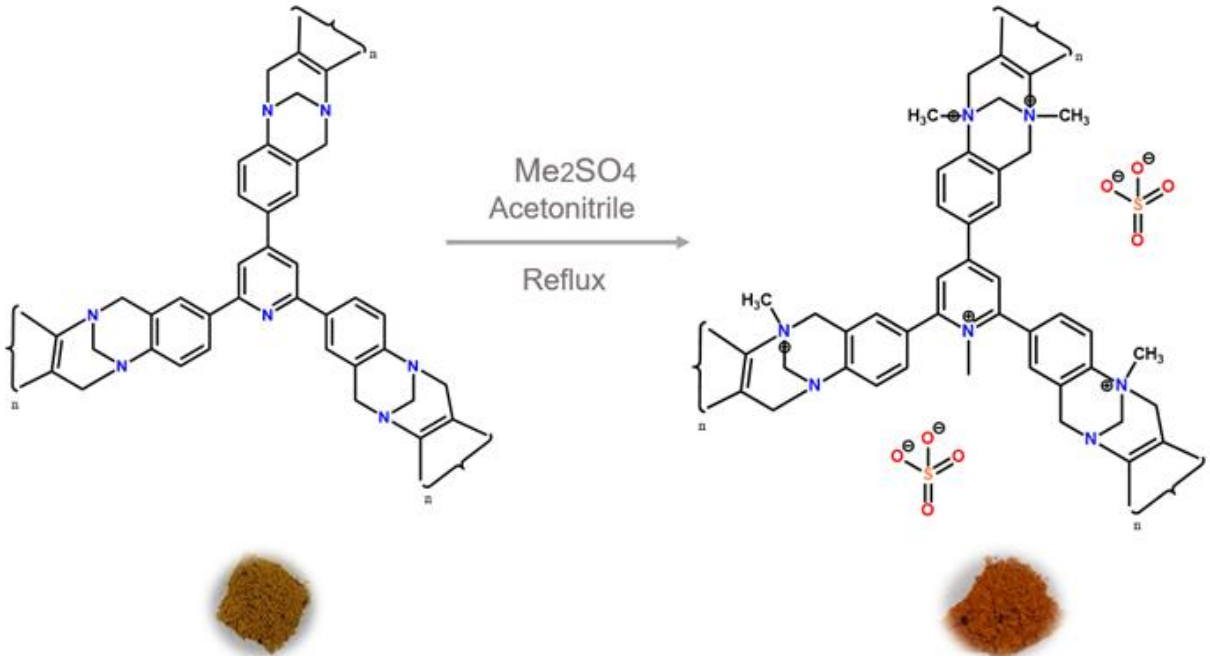

d)

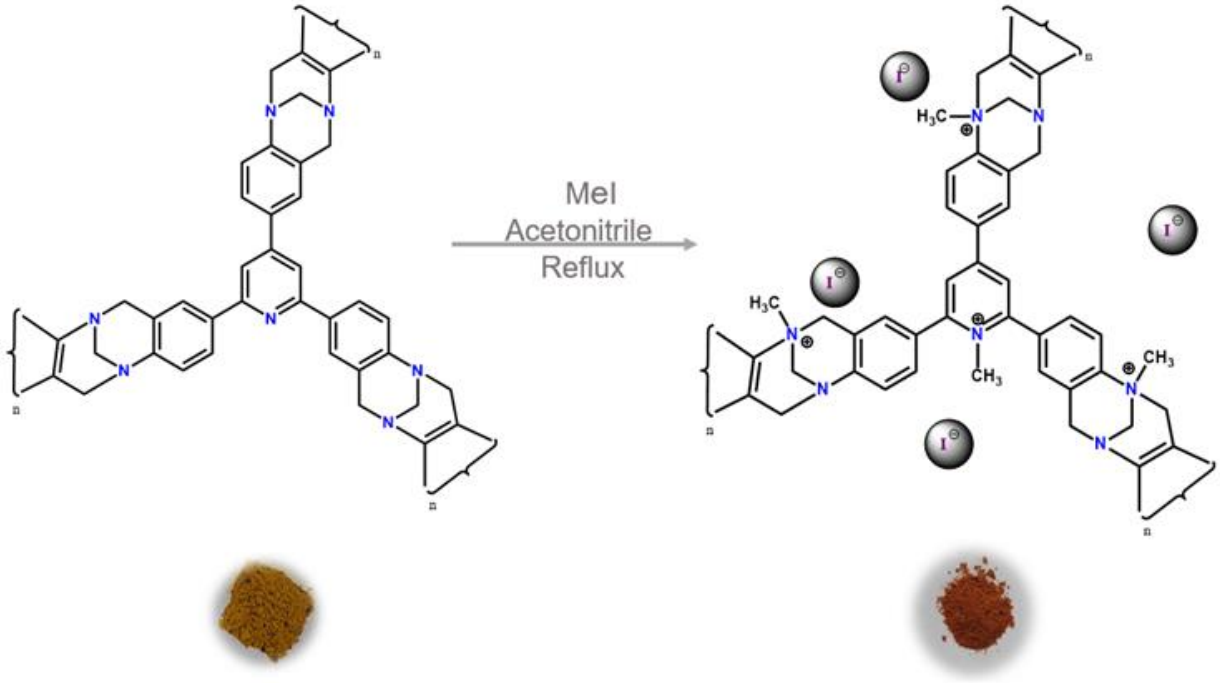

Scheme 4.1: Synthesis scheme of a) 2,4,6-Tris(4-aminophenyl)pyridine, b) TB-POP, c)TB-POP@MS, d) TB-POP@MI

4.2.4 Oxo-anion capture Study:

For the time variable oxo-anion (CrO_4^{2-} and ReO_4^-) sequestration experiment to record the initial absorbance we have taken ml 0.25mM solution of CrO_4^{2-} ion and 3ml 0.5mM solution of ReO_4^- ion in a UV cuvette. 2 mg of each de-solvated compounds have been put to the cuvette and absorbance spectra of corresponding supernatant solution were recorded at different times. Similar process was carried out for both the oxo-anions. Again, we have calculated percentage removal and time dependent concentration decrease from the following equation.[30]

$$D_t = \frac{C_0 - C_t}{C_0} \text{ x } 100\% = \frac{A_0 - A_t}{A_0} \text{ x } 100\%$$

$$i.e., \qquad C_t = C_0 - \frac{A_0 - A_t}{A_0} \text{x } C_0$$

Here, D_t is represented as exchange capacity, concentration and absorbance of the oxo-anion solution at specific time are C_t and A_t, whereas, initial concentration and absorbance of the oxo-anion solution are denoted as C_0 and A_0 respectively. Again, kinetics data for oxoanions capture were plotted and it well fits in pseudo second-order model calculating from the following equation,[31]

$$Q_t = \frac{k_2 Q_e^{\,2} t}{1 + k_2 Q_e t}$$

where, t represents time in minute, Q_t is the amount of adsorbate (mg gm^{-1}) material and Q_e is the adsorbent material.

4.2.5 Oxo-anion capture study in presence of competing anions:

Commonly encountered interfering anions like NO_3^-, SO_4^{2-}, ClO_4^-, Cl^- and Br^- are present in industrial waste water together with the targeted oxoanions. We have conducted the competing anion capture study taking two different concentration ratio. One is equimolar (2.5mM, 1:1) and other one is 100 fold (2.5mM, 1:100). 2mg of the each compounds were used for the measurement and the experiment carried out for 24 hours, following that it was filtered and diluted 10 times for UV-Vis spectroscopic measurement. Further capture efficiency in presence of other anions were calculated comparing with the without analyte measurement data (diluted 2.5mM of oxo-anion).

4.2.6 Calculation of capacity:

5 mg of de-solvated compound was dispersed with 5ml of solution having different concentration (0.5mM to 7.5mM). The supernatant was taken out after 24 hours and subjected to UV-Vis experiment which further fitted with the following equation. The storage capacity of each material has been determined from the initial and final absorbance values of the oxo-anion solution with the help of the following equation, [30]

$$\boldsymbol{Q_t = \frac{(C_0 - C_t) * V}{m}}$$

Where, V and m are the volume of the solution and mass of the adsorbent respectively whereas, C_0, Q_t, C_t, are initial concentration of oxo-anion solution, capacity of adsorbent and concentration of the oxo-anion solution at specific times respectively.

4.2.7 Recyclability test:

The compounds was reconstructed by dipping the compound loaded with oxo-anion (20 mg) for 1 day in 50% aqueous solution of tetrabutylammonium sulfate ($[[CH_3(CH_2)_3]_4N]2SO_4$) (10 mL).[32] The reconstructed material is again dipped into 5 mL of 1 mM oxo-anion solutions tracking the usability of the material. After ~24 hours, with the help of UV-Vis spectroscopy oxo-anion solution concentration was determined. The compound shows recyclability up to 5 cycles.

4.2.8 Adsorption isotherm experiment:

5 mg of the compound was dispersed in 5ml of aqueous oxo anion solution having different concentration (0.5mM to 10mM). After 24 hours taking the supernatant solution UV-Vis spectroscopy was conducted and plotted with the following equation.

Langmuir model, $$Q_e = \frac{Q_m C_e}{K_d + C_e}$$

where, the oxo-anion concentration at equilibrium is denoted as C_e (ppm) and amount of oxo-anion adsorbed at equilibrium is termed as Q_e (mg gm^{-1}) . To form a complete monolayer maximum quantity of oxo-anion per unit mass of adsorbent is Q_m (mg gm^{-1}). K_d (mg/L) is a constant which relates to the affinity of the binding sites.

Freundlich Model, $$Q_e = K_F C_e^{1/n}$$

where, K_F and 1/n are the two Freundlich model constants, whereas Q_e indicates capacity and C_e as equilibrium concentration.

4.2.9 pH-dependent capture study:

2mg of the compound dipped in 2.5 mM oxo-anions were used (pH-1.7, pH-4, pH-9, pH-10 and pH-12.4) and kept in contact for 1 day. Following UV-Vis study was performed and analogized with the data at pH-7 to check the comparative performance,[30]

$$D_t = \frac{C_0 - C_t}{C_0} \text{ x } 100\% = \frac{A_0 - A_t}{A_0} \text{ x } 100\%$$

Here, D_t is represented as exchange capacity, concentration and absorbance of the oxo-anion solution at specific time are C_t and A_t, whereas, initial concentration and absorbance of the oxo-anion solution are denoted as C_0 and A_0 respectively.

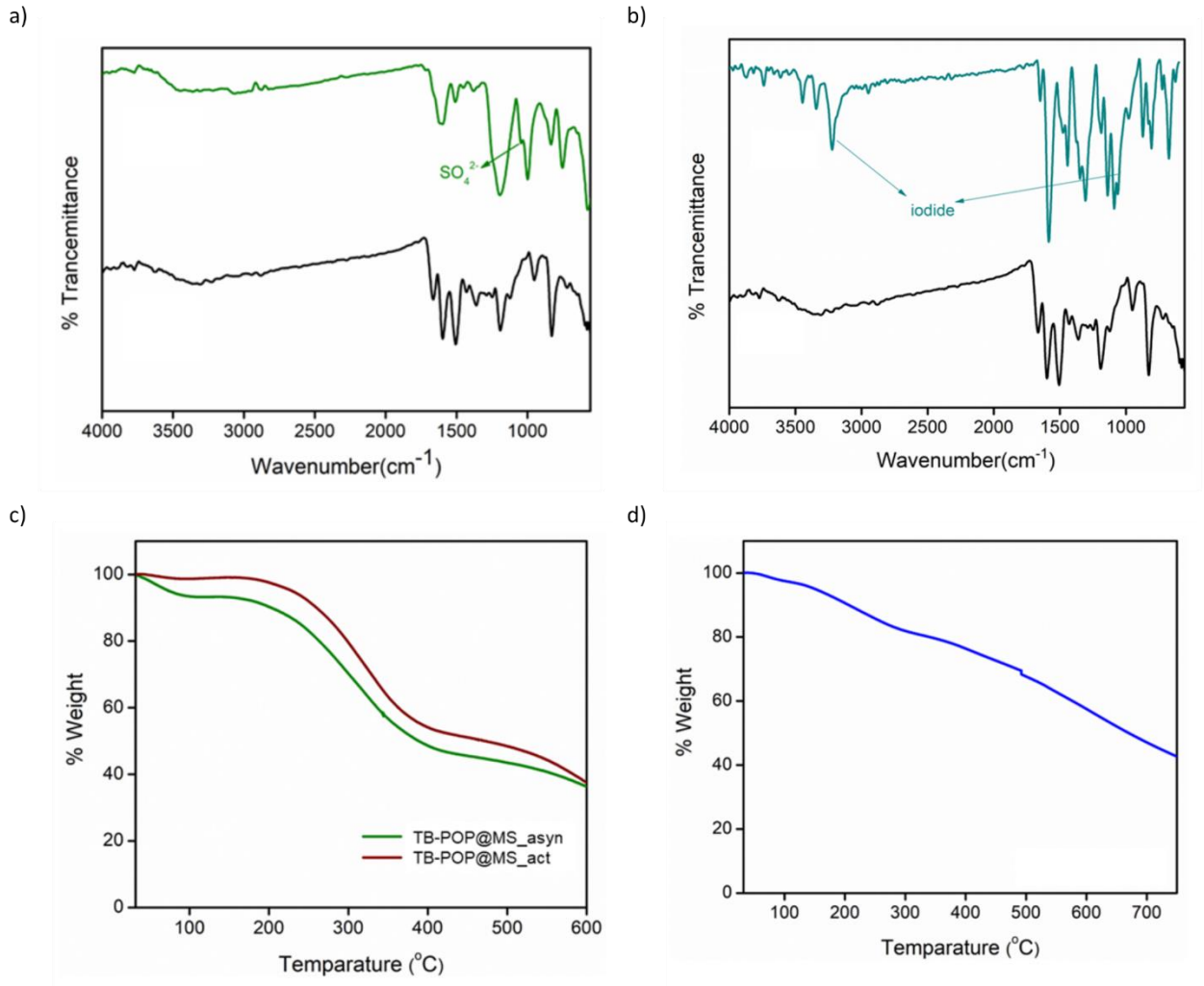

Figure 4.1: FTIR analysis of a) TB-POP@MS and b) TB-POP@MI, TGA analysis of c) TB-POP@MS and d) TB-POP@MI.

4.3 Results and discussion

The Troger's base-derived porous organic polymer (TB-POP) was synthesized with the help of acid-catalyzed polymerization reaction from a pyridine core aromatic triamine shown in (scheme 4.1).[34] Unreacted acid was further neutralized by aqueous ammonia and the compound is found to be highly insoluble, thus washed with various organic solvents (DMF, DMAc, THF, DCM, Acetone and Methanol) followed by further purification using Soxhlet extractions with THF and Methanol. Subsequent quaternization with Methyl Iodide and Dimethyl Sulphate was carried out to generate ion exchangeable sites having different anions (TB-POP@MI and TB-POP@MS). Both the polymers were subsequently washed with various organic solvents. FESEM-EDS mapping shows presence of Iodine and sulphur in the compounds respectively (Appendix 4.8, 4.11). FESEM image shows no morphological change upon methylation (Appendix 4.6, 4.10). CHNS elemental analysis shows the abundance of Sulphur in TB-POP@MS (Appendix 4.12). The structure of the post synthetically modified Troger based polymer (TB-POP@MS) was determined by solid state ^{13}C NMR. The peak assignment of TB-POP@MS resonance is displayed in (Appendix 4.5). Peak at 30 ppm indicates the methylated carbon. The characteristic peaks at 65.1, 55.7 and 50.6 ppm correspond to the methylene carbon which is present in the polymer, comprehensibly recommending the development of Tröger's base linkages. Phenyl carbon atom shows its peak at 112.6, 118.8, 128.7 and 151.7 ppm, and the peak at 150.4 ppm indicating the carbon atoms of the pyridine rings. FTIR spectra of the polymer (TB-POP) shows peaks at 1562 cm^{-1} and 1504 cm^{-1} confirms the presence of pyridine moiety. Vibration band at 1180 cm^{-1} confirms the aliphatic C-N stretching frequency whereas peak at 1360 cm^{-1} confirms the aromatic amine C-N stretching frequency (Appendix 4.2). The formation of TB-POP is established by characteristic vibrations of -CH_2- at 2854 cm^{-1}. Further FTIR analysis was carried out with methylated polymers where TB-POP@MS shows SO_4 peak at 1040 cm^{-1} and TB-POP@MI shows shifting and broadening of peak at 1180 cm^{-1} due to decreasing in conjugation by induction of methyl group (Figure 4.1c, 4.1d). [34] Thermogravimetric analysis (TGA) reveals TB-POP is stable up to 350 ℃ whereas, TB-POP@MS and TB-POP@MI are stable up to 215 ℃ and 180 ℃ (Appendix 4.1, Figure 4.1a, 4.1b). Low temperature N_2(77K) isotherm of the TB-POP shows type IV curve (Appendix 4.3). Nonlocal density functional theory (NLDFT) method was utilized to determine pore size distribution which indicates the mesoporous nature of TB-POP polymer (Appendix 4.4). Further Low temperature N2(77K) isotherm of TB-POP@MS was carried out, which shows non porous in nature (Appendix 4.9). So as for checking the chemical stability of the TB-POP@MS 50mg of the compound was dipped into acid (2N HCl) and base (pH12) solution for 48 hours. Post treated sample shows negligible weight loss and was thoroughly characterize by FESEM, FTIR, TGA analysis. FESEM image study reveals the morphology remains unaltered throughout the acid base treatment. Moreover, FTIR analysis shows

retention of all peaks, indicates no change in functional group (Appendix 4.26). TGA profile shows analogous in nature indicates no change in network structure (Appendix 4.27).

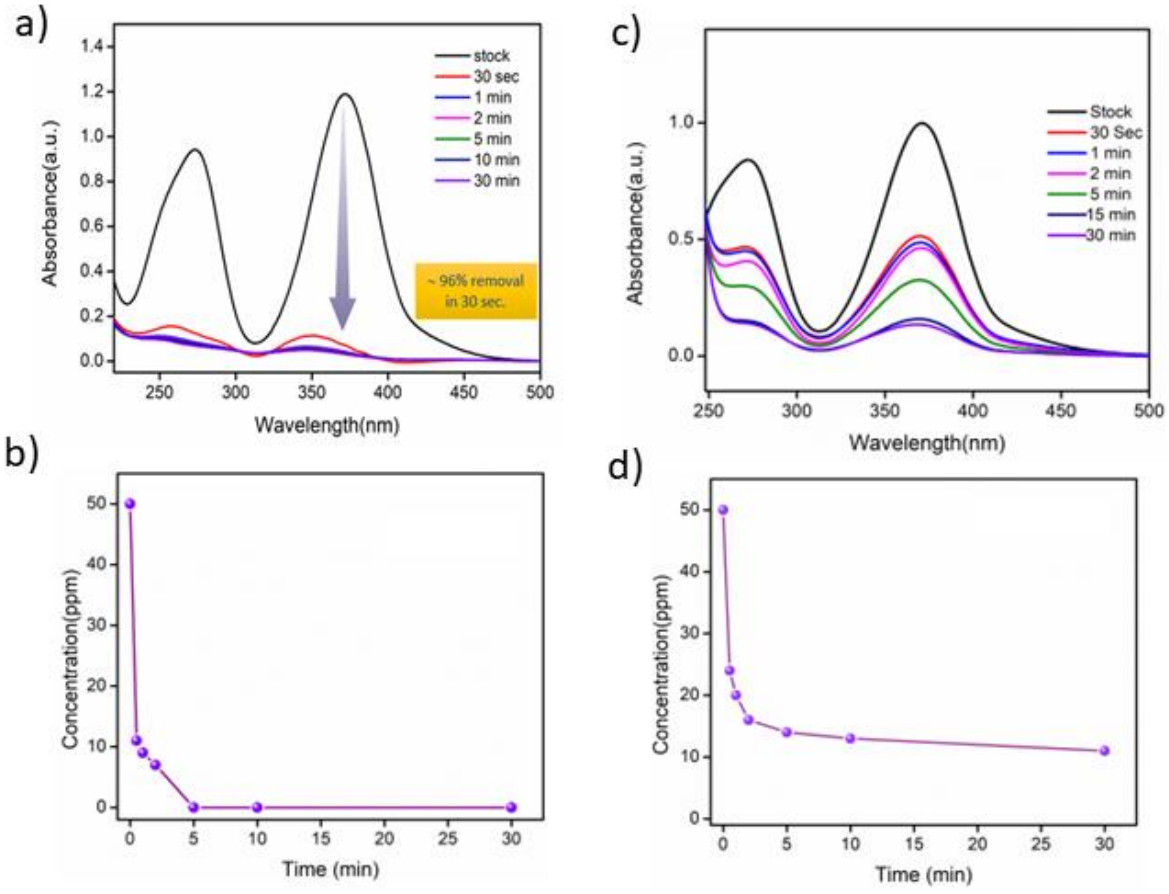

Figure 4.2: UV-Vis spectroscopy in presence of both a) TB-POP@MS and c) TB-POP@MI at various time intervals for the aqueous solution of CrO_4^{2-} ion, decrease in concentration of chromate ion in the medium after addition of b) TB-POP@MS and d) TB-POP@MI.

4.3.1 Capture study:

Encouraged by such physiochemical stability and having different anions inside TB-POP@MS and TB-POP@MI we sought to check their capture performance. For that, we prepared a 2mM chromate solution and dipped 5mg of both the compounds in it. After gentle shaking for few minutes the supernatant of the TB-POP@MS solution becomes colorless, whereas in case of TB-POP@MI no observable color change was observed. This discriminatory in decolorization of chromate solution by TB-POP@MS and TB-POP@MI excited us to perform in situ CrO_4^{2-} removal experiment (fig 4.2). In a typical experiment 2mg

of both TB-POP@MS and TB-POP@MI were taken individually with 3ml of 0.25mM aqueous chromate solution. Capture kinetics was performed via UV-VIS spectroscopy with an absorption maximum at 372 nm. Noticeably TB-POP@MS showed 93% removal of CrO_4^{2-} ions in just 30 secs and reached 99% with saturation in just 1 minute (Fig 4.2). In the contrast TB-POP@MI achieved only 49% removal efficiency in 30 Secs and increased up to 87% in 30 Mins after which it reaches equilibrium (Fig 4.2). The differential performance in capture efficiency highlights the role of anions towards pollutant removal. Sulfate anion being a tetrahedral and smaller anion in size acts as a facilitator for CrO_4^{2-} removal whereas iodide ion is bulkier in size which limits its exchange performance. [35] Additionally, adsorption kinetics data were plotted and it fits with pseudo second order model revealing the dependence of capture process upon the quantity of absorbate and absorbent (Appendix 4.13b). Enthused by rapid ion exchange kinetics of TB-POP@MS equilibrium absorbance capacities were measured in different concentration of aqueous CrO_4^{2-} solution. The result acquired from uptake capacity and equilibrium concentration plot fitted well with the LangmuirEXT1 model having high correlation coefficient value R^2 = 0.99 (Appendix 4.13c). The adsorption capacity of CrO_4^{2-} was measured to be 502 mg g^{-1} which places TB-POP@MS as one of the top contenders in terms of capture capacity in the domain of porous materials.

Alongside β- emitting radioactive element ^{99}Tc which is abundant in the form of TcO_4^- also accounts for significant hazard due to its high-water solubility. As it is not convenient to study such radioactive elements in common laboratory all the experiments have been performed using perrhenate (ReO_4^-), a non-radioactive surrogate of TcO_4^- having similar size-charge distribution.[36] Time dependent removal studies of ReO_4^- ions from aqueous medium was carried out similar to CrO_4^{2-} ion capture. Here also, 2 mg of TB-POP@MS were dipped into 3 ml 0.5mM aqueous solution of ReO_4^-. The capture kinetics process was recorded via UV-VIS spectroscopy with an absorption maximum at 208 nm gradually diminishing with increasing contact time. Almost 70 % removal after 1 min and 92 % after 30 mins shows fast kinetics for removal of ReO_4^- ions from water (Fig 4.3a). Additionally, adsorption kinetics data were plotted and it fits with pseudo second order model revealing the dependence of capture process upon the quantity of absorbate and absorbent (Fig 4.3b). Furthermore, saturation uptake capacities were measured to be 442 mg g^{-1} and capacity vs equilibrium concentration plot fits well with LangmuirEXT1 model having a correlation coefficient value R^2 = 0.99 (Figure 4.3c).

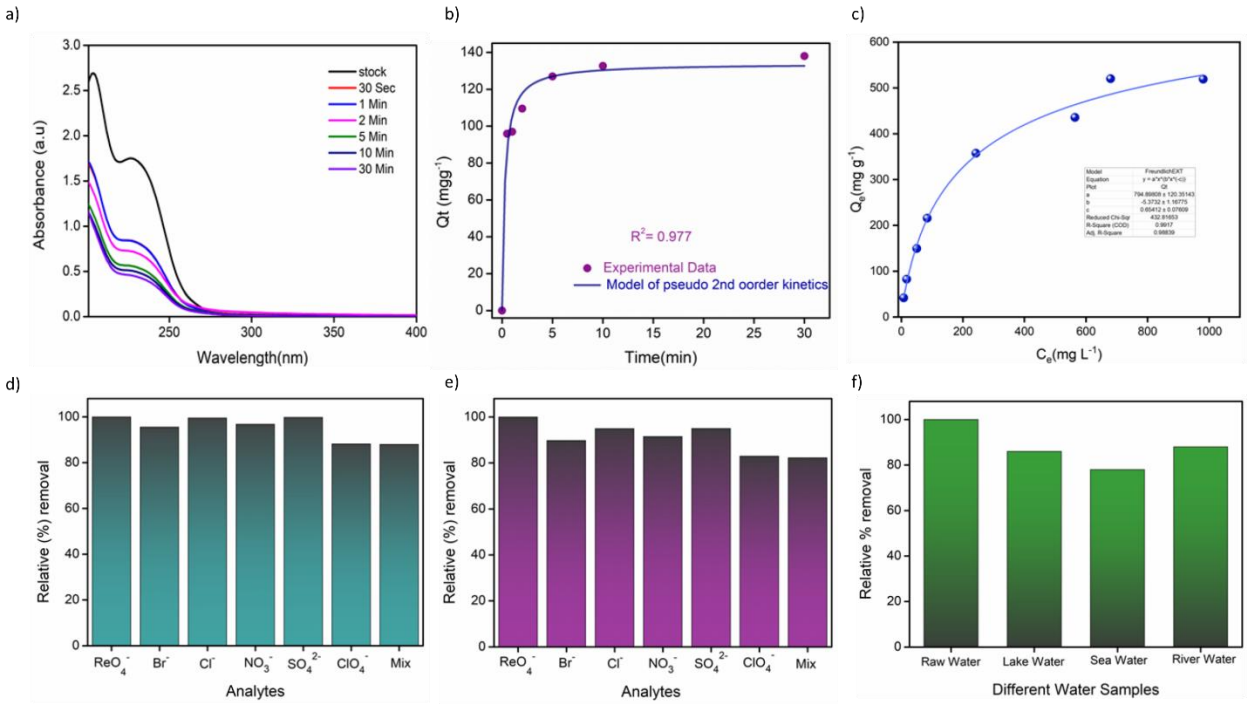

Figure 4.3: Perennate capture Studies TB-POP@MS: a) UV-Vis titration b) kinetics measurement: follows pseudo 2nd order kinetics, c) Adsorption isotherm well fitted with Langmuir model, d) selectivity test in presence of competing anions (1:1), e) Selectivity of chromate in presence of 100 fold competing anions (1:100), f) Perennate Removal efficiency in different water sources.

Commonly encountered interfering anions like NO_3^-, SO_4^{2-}, ClO_4^-, Cl^- and Br^- are present in industrial waste water together with the targeted oxoanions. Motivated from outstanding uptake capacities of TB-POP@MS for CrO_4^{2-} and ReO_4^- ions, we examined oxoanions affinity towards TB-POP@MS with 1:1 mixture of co-existing interfering anions as well as 100-fold excess of competing anions (Appendix 4.13). Excellent selectivity was observed in case of both the oxoanions in binary mixture as well as in 100 fold excess anion mixtures (Figure 4.3). Notably oxoanions removal performance remains very high in presence of four interfering anions (NO_3^-, SO_4^{2-}, Cl^- and Br^-) except for ClO_4^- and all anion mixtures. Further to check the practical applicability of the material TB-POP@MS we treated with different water samples (sea water, river water and lake water) polluted with individual oxoanions and 100-fold excess ion mixtures (Appendix 4.13f, Fig. 4.3f). In addition to this, both CrO_4^{2-} and ReO_4^- capture experiments were performed in wide range of PH and TB-POP@MS shows moderate removal efficiency in both acidic and alkaline condition (Appendix 4.16, 4.20). Additionally for practical utilization, an adsorbent must be able to remove traces of pollutants from low concentration polluted water below the EPA standards. To investigate this,

we carried out low concentration (~ 1000ppb) oxoanion capture studies and recorded via ICP-MS analysis. (Appendix 4.14, 4.18) The study with different time interval reveals very fast removal (~99%) of both the oxoanions below EPA standards.

Among the most important issues for real-time water pollutant sequestration is the sorbent material's reusability. To validate this, we have carried out reversibility experiment in which we put 20 mg of chromate loaded TB-POP@MS_(CrO_4^{2-}) and perrhenate loaded TB-POP@MS_(ReO_4^-) in an 50% weight percentage solution of tetrabutylammonium sulfate in water. A systematic change in color was observed from colorless to yellow in case of TB-POP@MS-(CrO_4^{2-}) upon release of trapped $CrO_4^{2\neg}$ while the compound turns into its initial color. Additionally using UV-vis spectroscopy the concentration of the released oxoanions was also confirmed. It was found that the compound TB-POP@MS demonstrated higher regeneration ability for both the oxoanions up to 5 cycles (Appendix 4.17, 4.21). Owing to rapid and selective oxoanion (Cr and Re) sequestration, we aim to understand the mechanism behind this efficient capture performance using both experimental and theoretical insights. FTIR analysis demonstrated retention of all characteristic peaks in the post captured phase indicating structural robustness of the framework and arrival of new peaks ~950 cm^{-1}(Cr-O stretching frequency) and ~900 cm^{-1} (Re-O stretching frequency) respectively (Appendix 4.26). TGA profile of post captured compounds shows similar nature with the pristine compound. Notably FESEM-EDX mapping revealed the homogeneous distribution of Cr(VI) and Re(VII) in the framework (Appendix 4.24, 4.25). No morphological change was evident from the FESEM image of the captured phase compounds (Appendix 4.23). Again, the efficient selective capture of oxoanions was additionally assisted by theoretical binding energy calculations in detail with the help of density functional theory (DFT) method. (Appendix4.28)

4.4 Conclusions

In conclusion a facile post methylation was carried out by N-quaternization of Tröger's base polymer (TB-POP) giving rise to two cationic POPs; TB-POP@MS having SO_4^{2-} and TB-POP@MI having I^- as counter anions. Upon utilizing both the polymers for sequestration of toxic CrO_4^{2-} from water, compound TB-POP@MS shows ultra-fast kinetics whereas TB-POP@MI shows relatively slow kinetics. This can be attributed to the size of the counter anions. Further oxo-anions capture studies with TB-POP@MS demonstrates high sorption capacities, excellent reusability and outstanding selectivity in presence of 100 fold other countering anions. Moreover, TB-POP@MS shows very good capture efficiency in different water systems as well as different pH mediums. Compound TB-POP@MS shows uptake capacity for chromate 502 mg g-1 which is significantly high in porous materials domain. The rational designing and

development of TB-POP@MS and TB-POP@MI exploits the role of anions in capture kinetics. We believe our work will unplug new approach for the capture of oxo-anions by tuning counter anions.

4.5 Appendix Section:

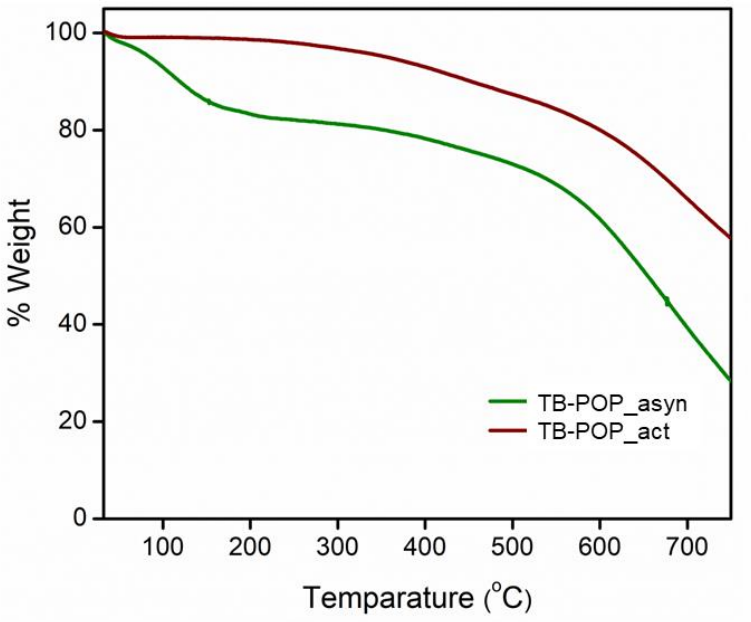

Appendix 4.1: TGA analysis of as-synthesized TB-POP (wine red) and de-solvated phase of TB-POP (green).

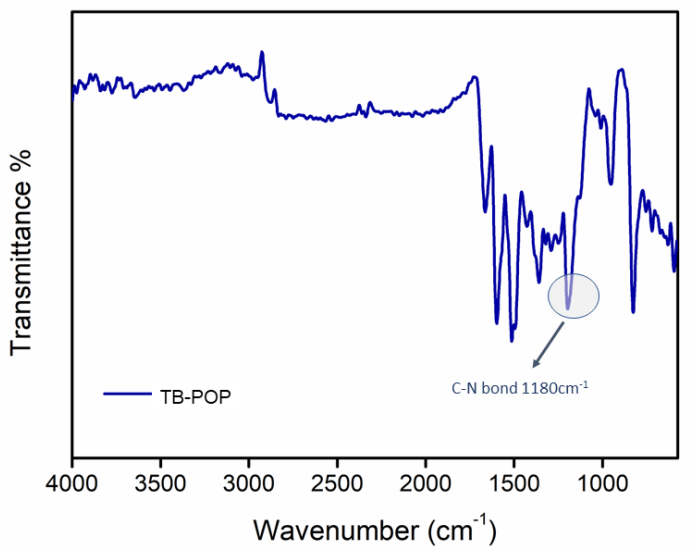

Appendix 4.2: Infra-red (IR) spectroscopy of TB-POP (blue)

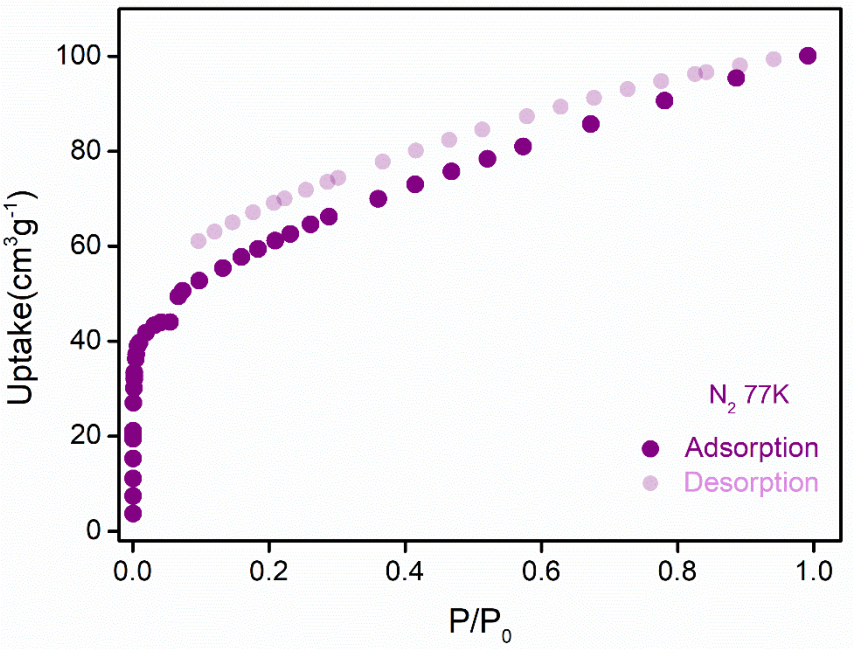

Appendix 4.3: N_2 adsorption profile of TB-POP (77 K).(dark violet: adsorption, light violet: desorption)

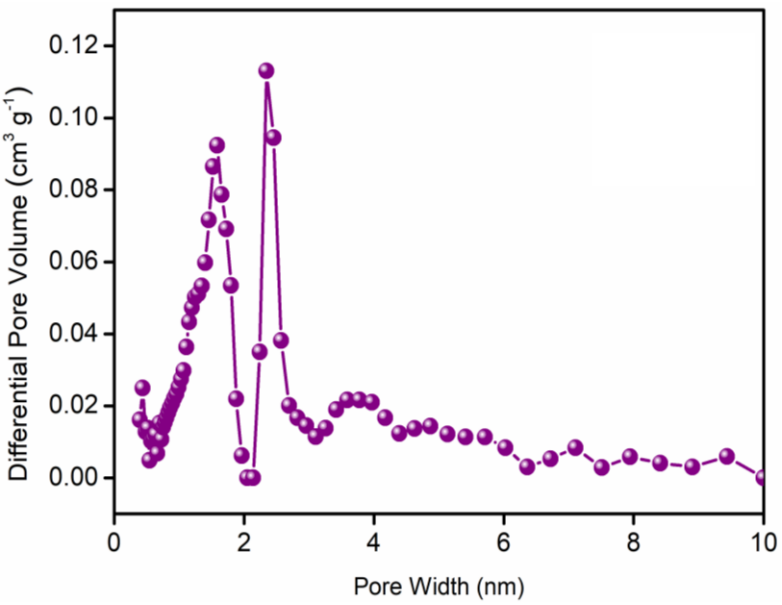

Appendix 4.4: Pore size distribution of TB-POP polymer..

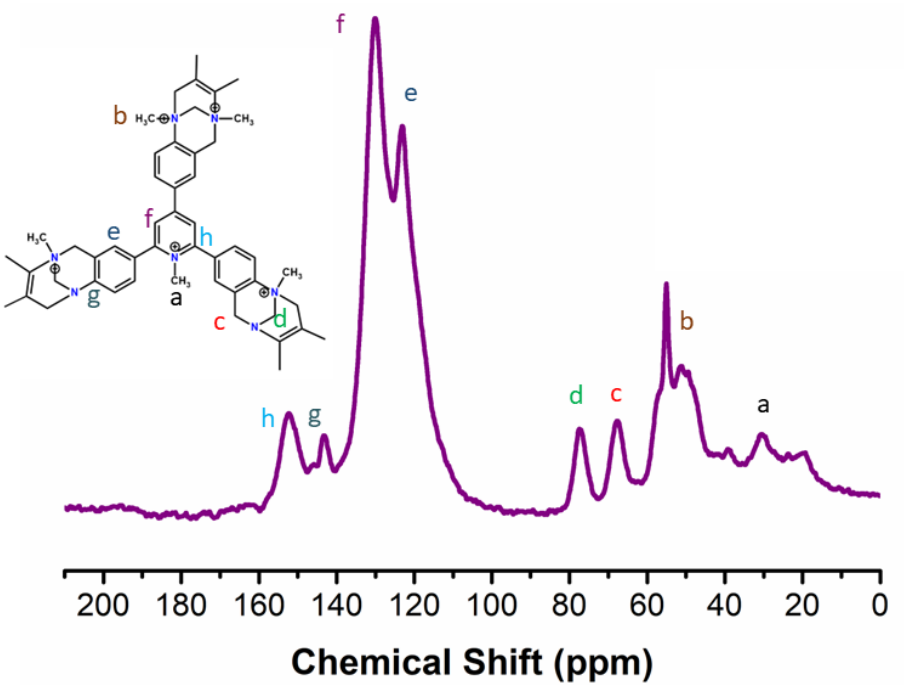

Appendix 4.5: Solid state ^{13}C-NMR of TB-POP@MS.

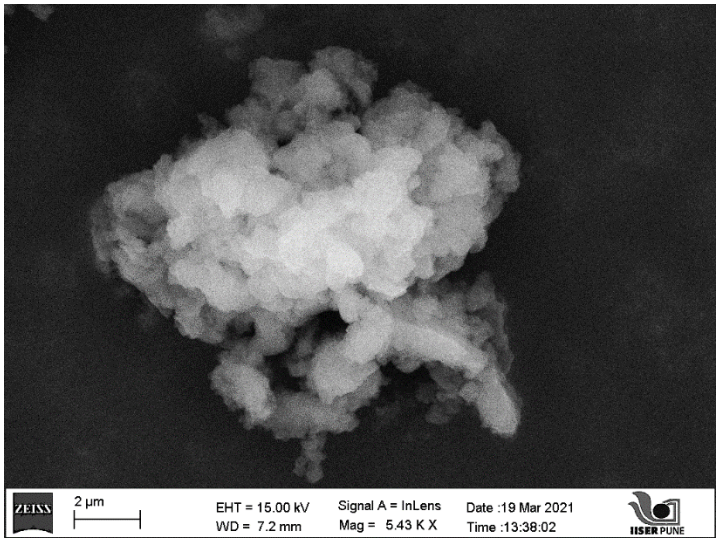

Appendix 4.6: FE-SEM images of TB-POP.

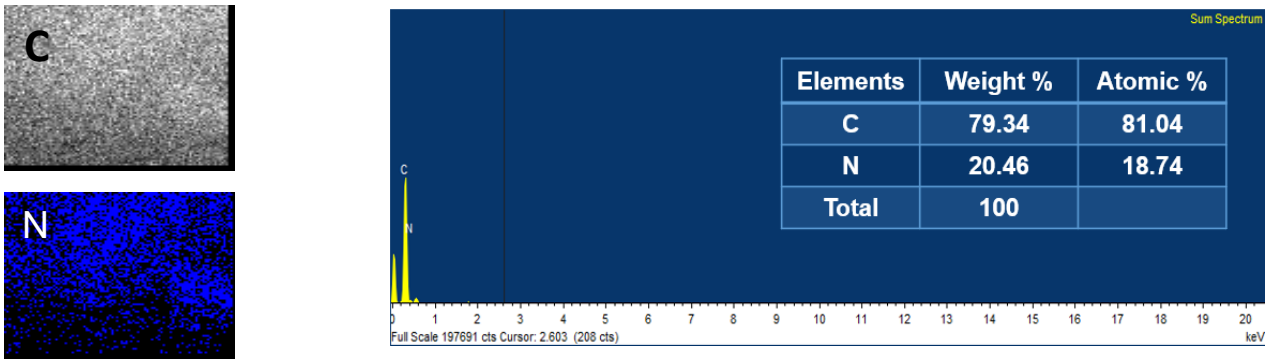

Appendix 4.7: Elemental analysis and mapping of TB-POP

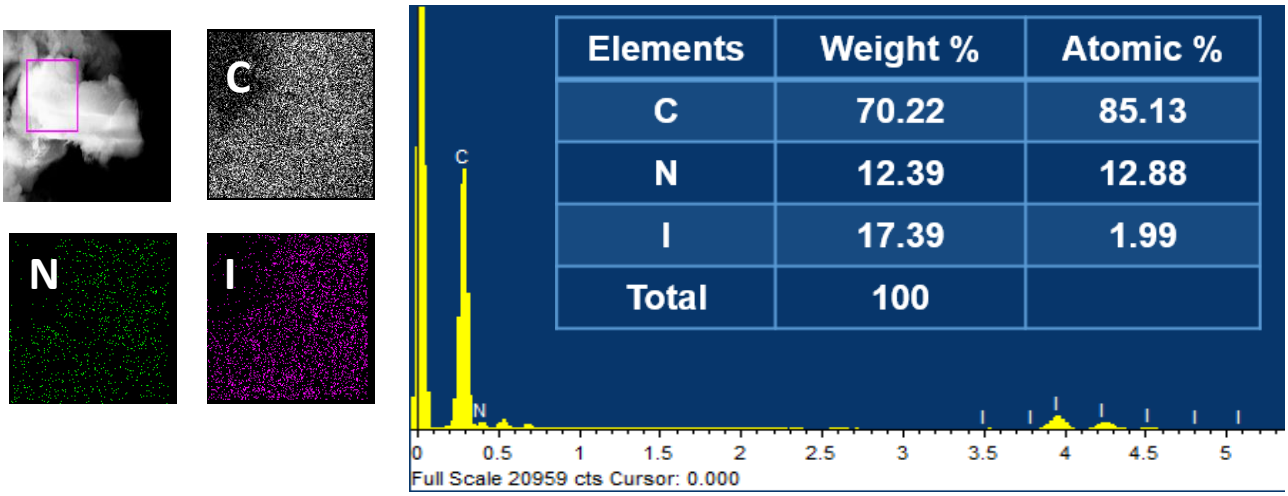

Appendix 4.8: FESEM image, Elemental analysis and mapping of TB-POP@MI

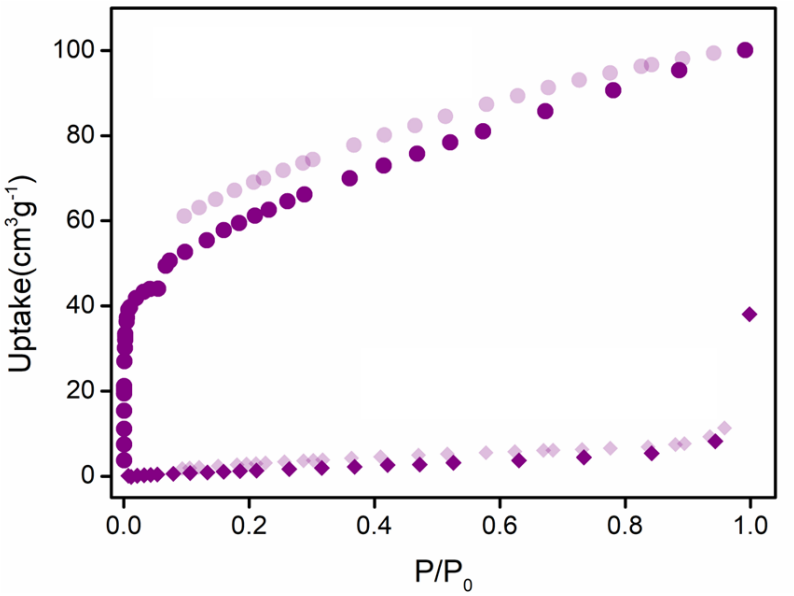

Appendix 4.9: N_2 adsorption profile of TB-POP (77 K) (round shaped) and TB-POP@MS (diamond shaped).

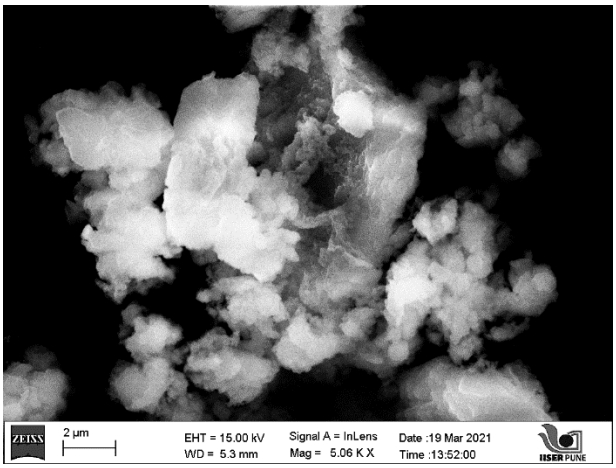

Appendix 4.10: FE-SEM images of TB-POP@MS.

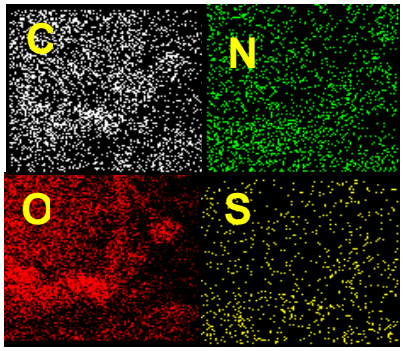

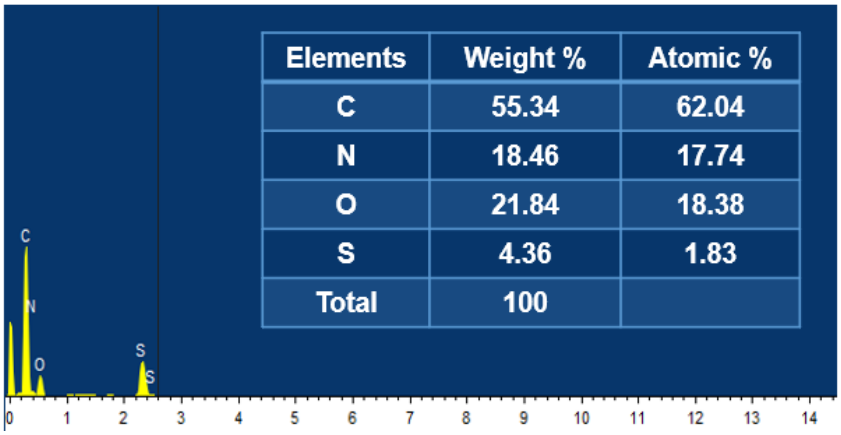

Elements	Weight %	Atomic %
C	55.34	62.04
N	18.46	17.74
O	21.84	18.38
S	4.36	1.83
Total	100	

Appendix 4.11: Elemental analysis and mapping of TB-POP@MS.

Compounds	**% C**	**% H**	**% N**	**% S**
TB-POP	74.71	6.1	11.89	0
TN-POP@MS	46.7	5.78	8.83	11.74

Appendix 4.12: CHNS analysis of TB-POP and TB-POP@MS.

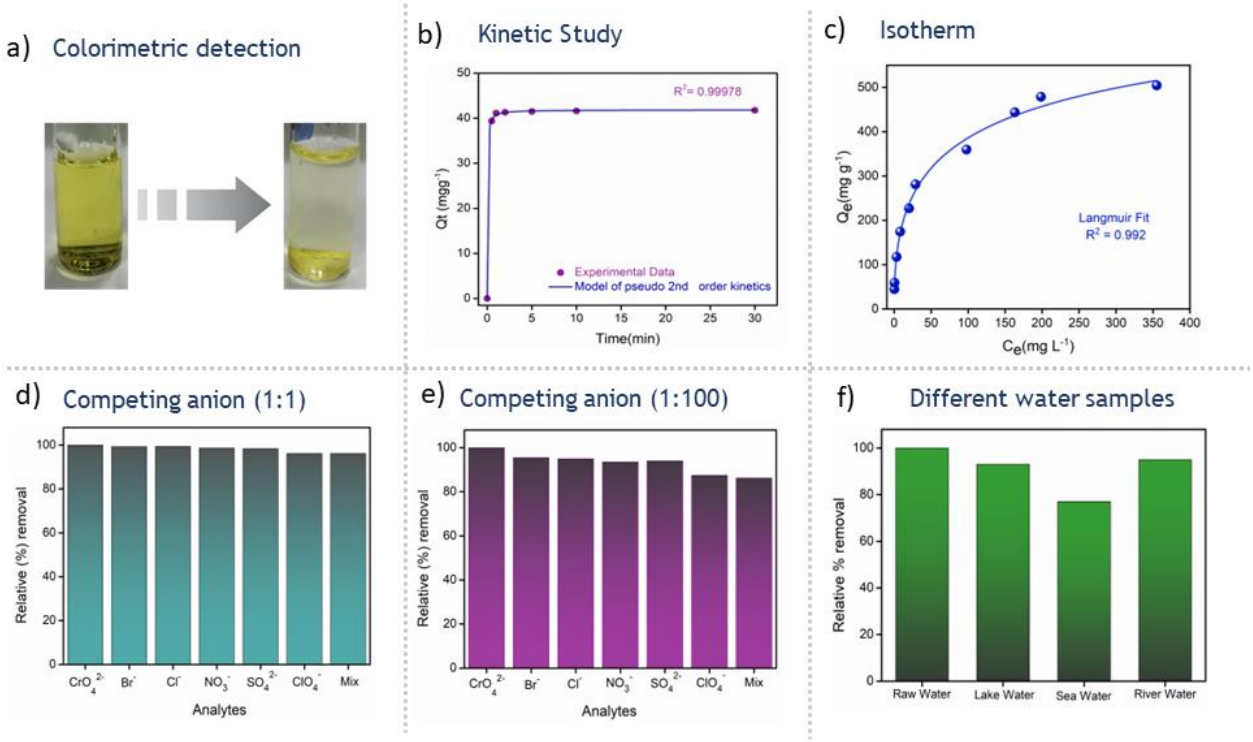

Appendix 4.13: Chromate capture Studies TB-POP@MS: a) naked eye detection of chromate removal, b) ultrafast removal kinetics measurement: follows pseudo 2nd order kinetics, c) Chromate adsorption isotherm well fitted with Langmuir model, d) selectivity test in presence of competing anions (1:1), e) Selectivity of chromate in presence of 100 fold competing anions (1:100), f) Removal efficiency in different water sources.

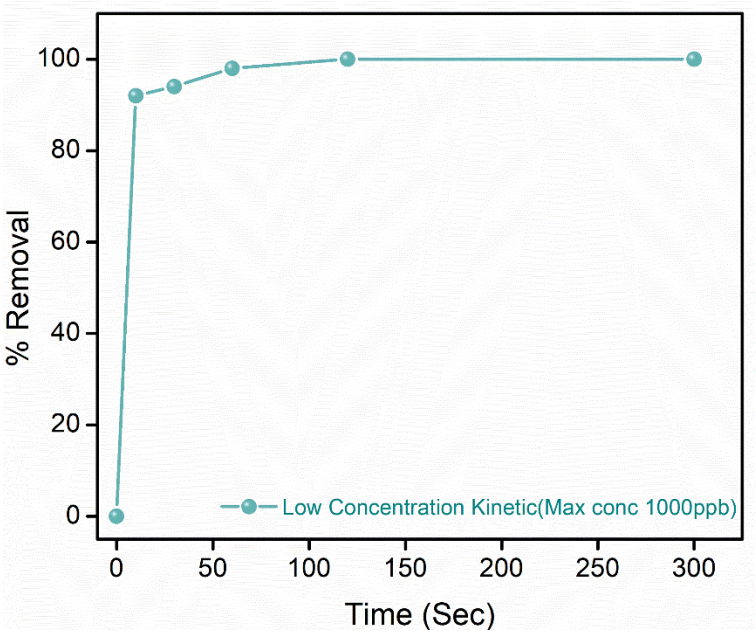

Appendix 4.14: Low concentration chromate removal percentage. (10ppm)

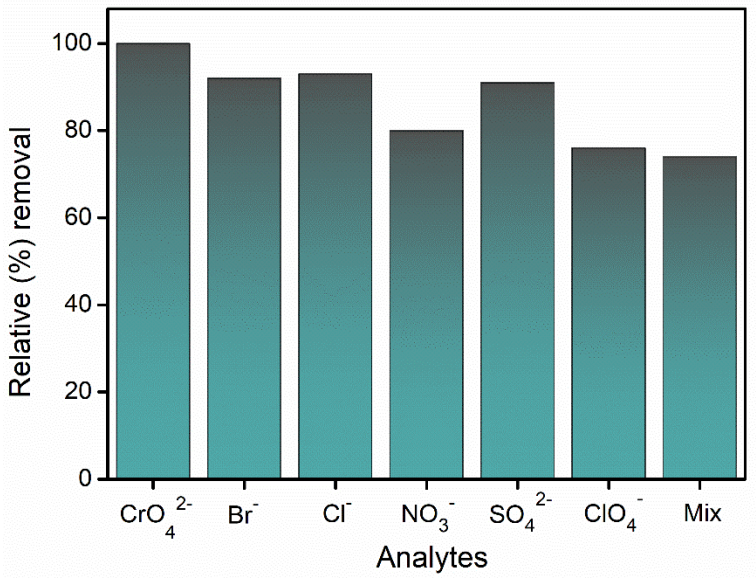

Appendix 4.15: Low concentration relative removal percentage of chromate in presence of competing anions. (10ppm)

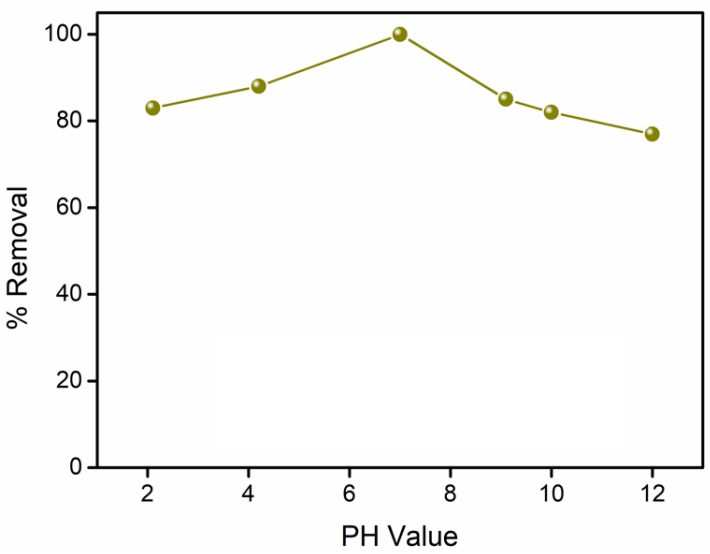

Appendix 4.16: Percentage of chromate removal in various pH condition.

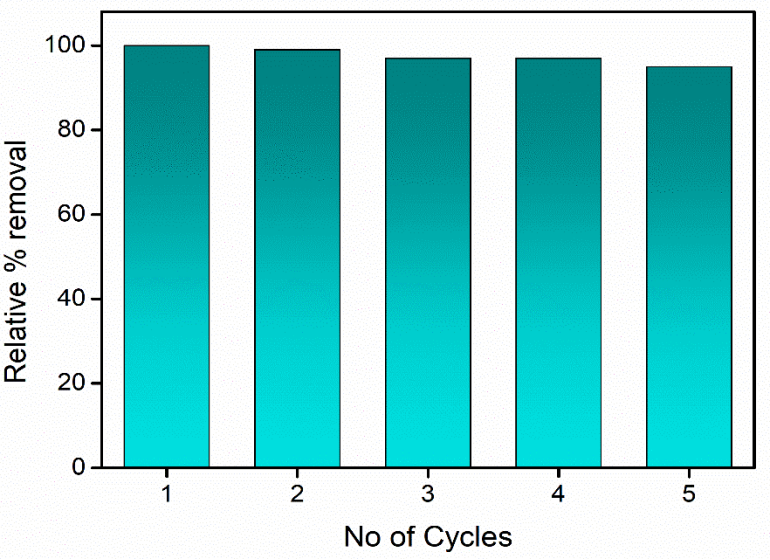

Appendix 4.17: Recyclability study shows compound is recyclable up to 5 cycles after chromate capture.

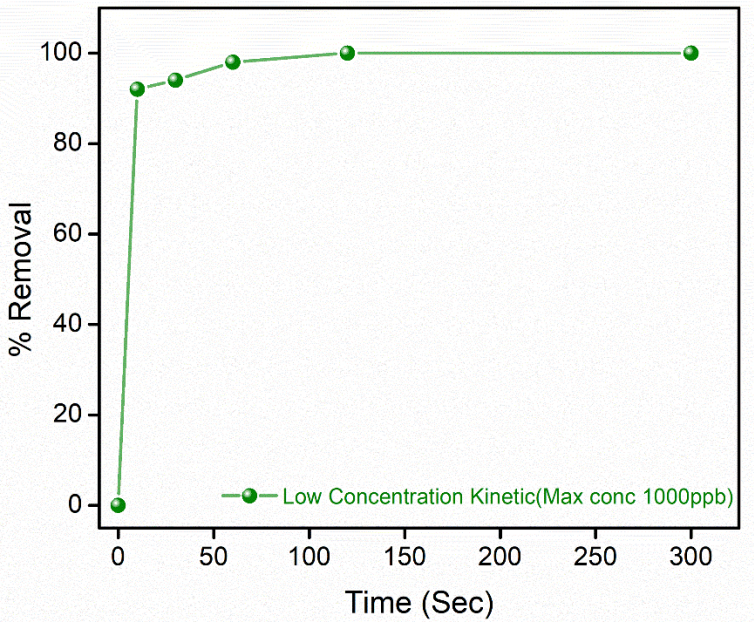

Appendix 4.18: Low concentration perennate removal percentage. (10ppm)

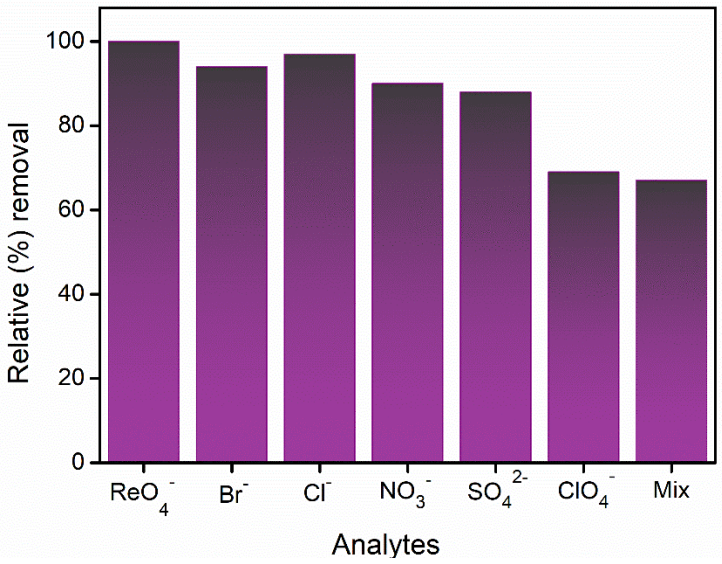

Appendix 4.19: Low concentration relative perennate removal percentage in presence of competing anions. (10ppm)

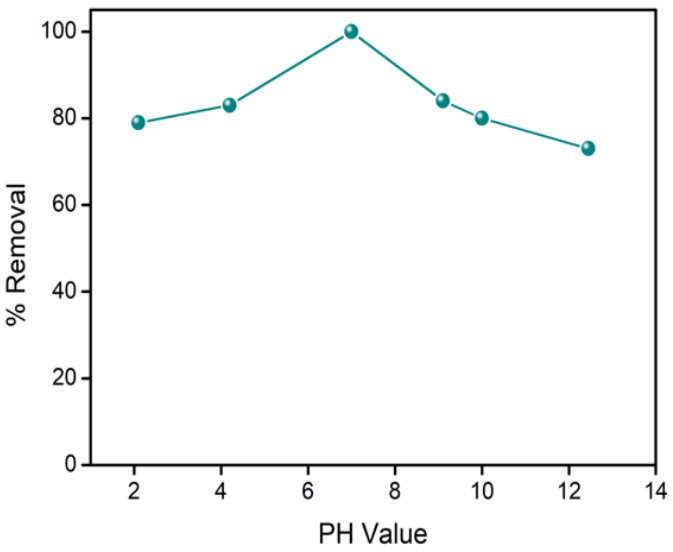

Appendix 4.20: Percentage of perennate removal in various pH condition.

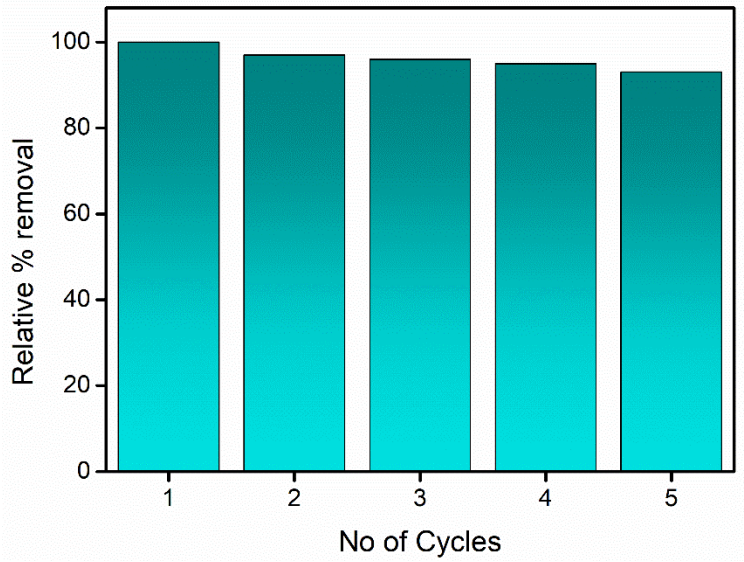

Appendix 4.21: Recyclability study shows compound is recyclable up to 5 cycles after perennate capture.

TB-POP@MS **chromate captured TB-POP@MS**

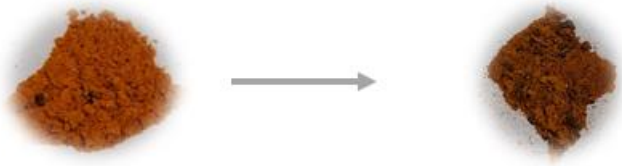

TB-POP@MS **perrhenate captured TB-POP@MS**

Appendix 4.22: darkening of the colour of the polymer after capture.

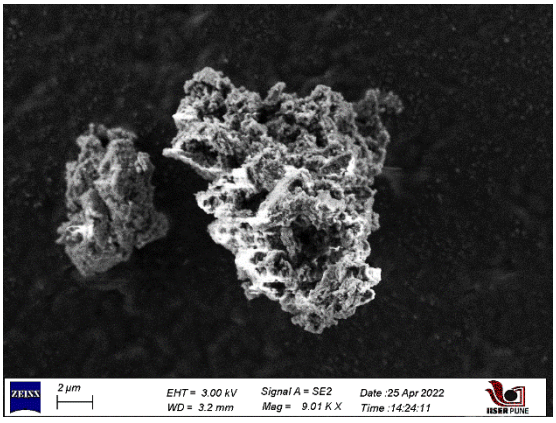

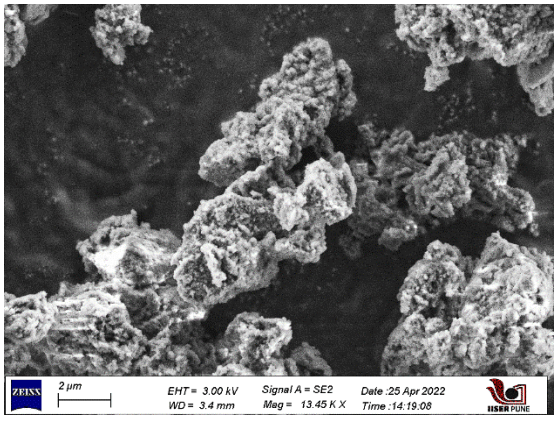

Appendix 4.23: FE-SEM images of TB-POP@MS after capture.

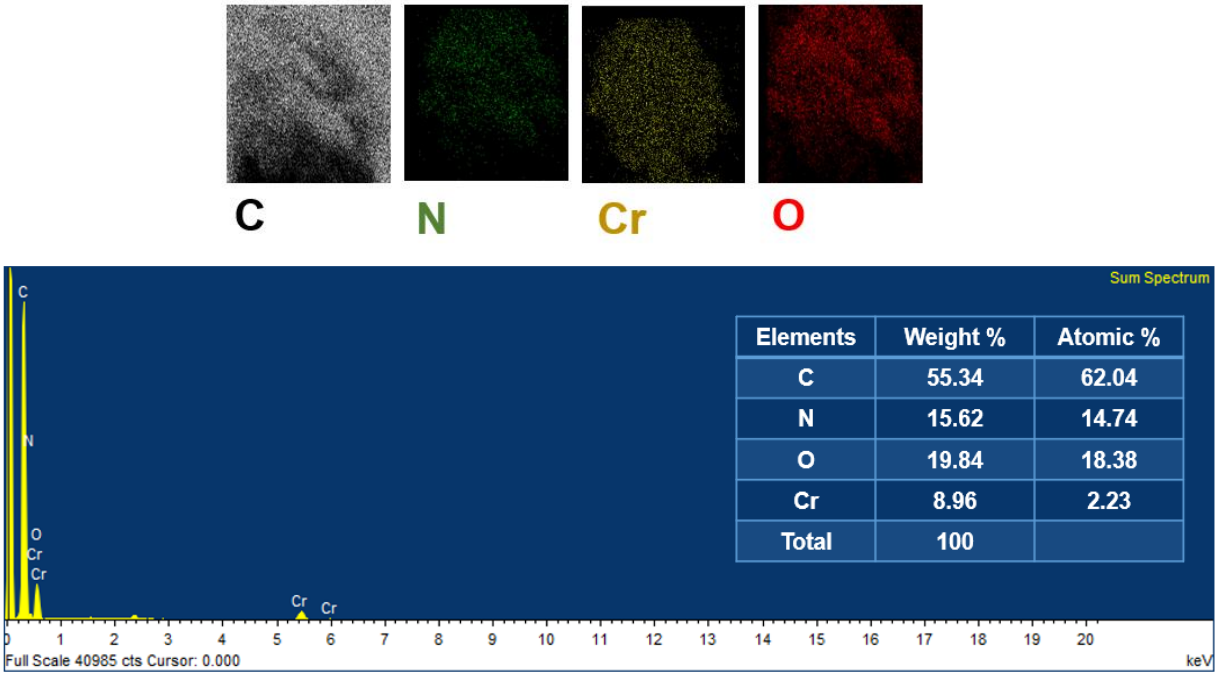

Elements	Weight %	Atomic %
C	55.34	62.04
N	15.62	14.74
O	19.84	18.38
Cr	8.96	2.23
Total	100	

Appendix 4.24: Elemental analysis and mapping of chromate captured TB-POP@MS.

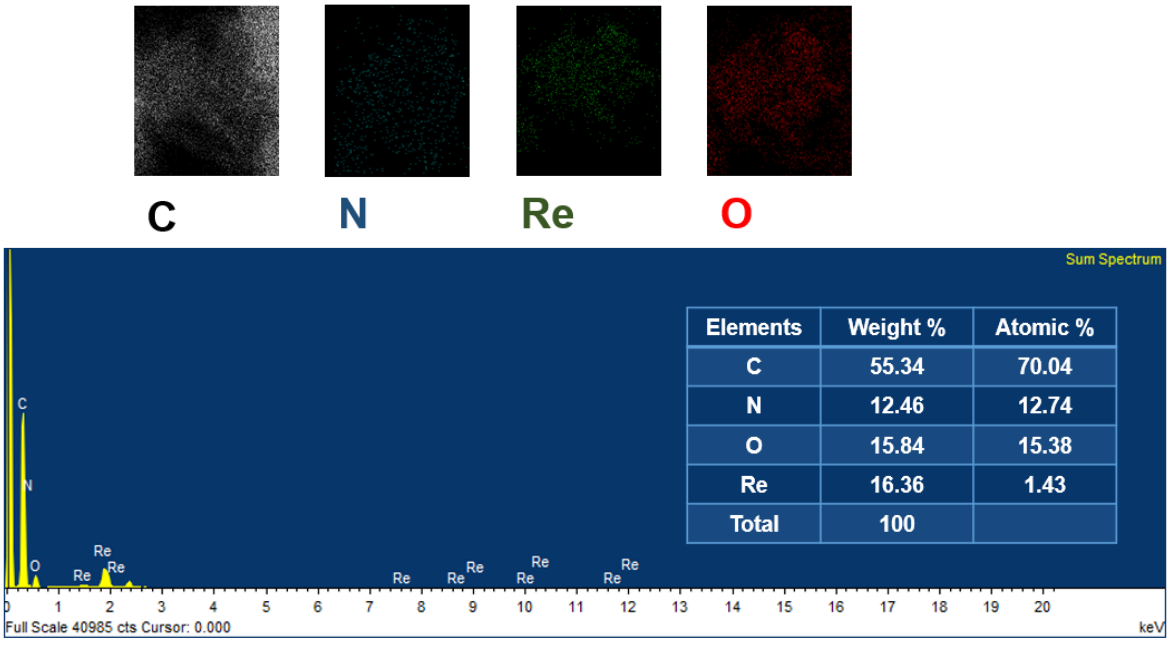

Elements	Weight %	Atomic %
C	55.34	70.04
N	12.46	12.74
O	15.84	15.38
Re	16.36	1.43
Total	100	

Appendix 4.25: Elemental analysis and mapping of perennate captured TB-POP@MS.

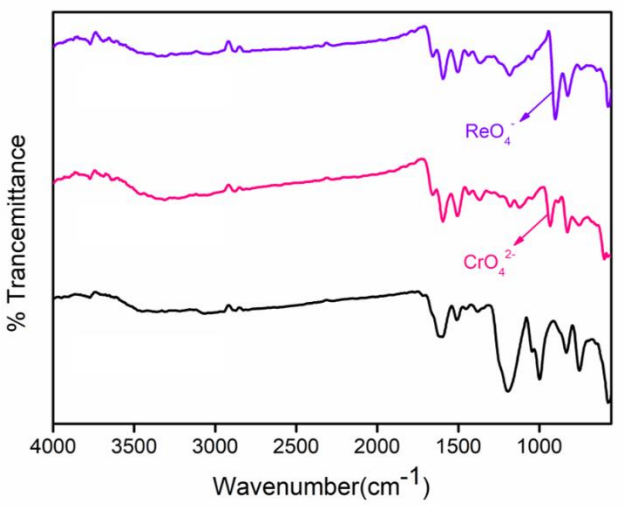

Appendix 4.26: Infra-red (IR) spectroscopy of TB-POP@MS (back), chromate captured TB-POP@MS (pink) and perennate captured TB-POP@MS (violet).

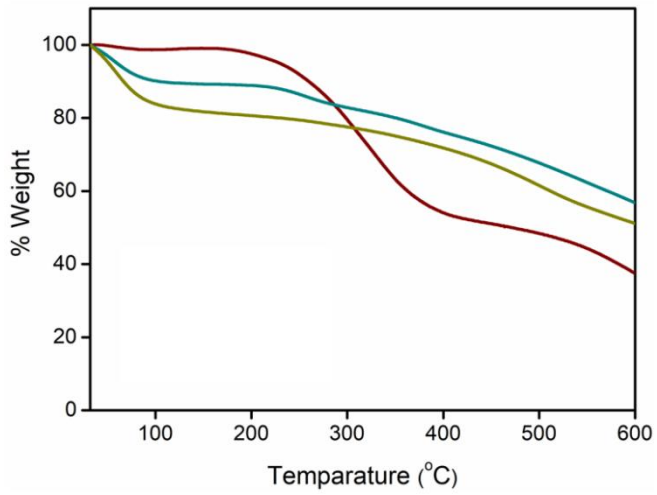

Appendix 4.27: TGA analysis of as-synthesized TB-POP@MS (brown) chromate captured TB-POP@MS (yellow) and perennate captured TB-POP@MS (cyan).

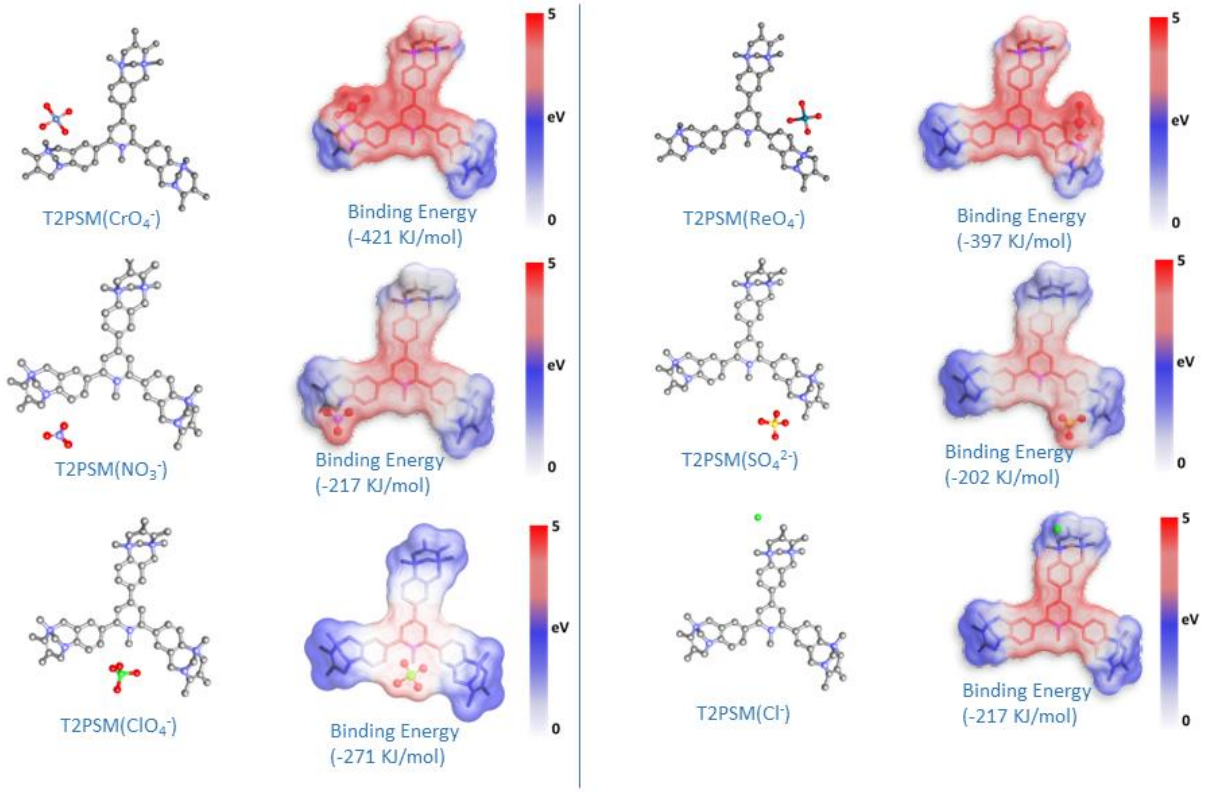

Appendix 4.28: Optimized structures of monomeric unit of TB-POP@MS with various interacting anions and DFT-DMOL3-B3LYP method was used to determine the binding energy,

4.6 References

1. R. P. Schwarzenbach, B. I. Escher, K. Fenner, T. B. Hofstetter, C. A. Johnson, U. Gunten, B. Wehri, *Science*. 2006, **313**, 1072–1077;

2. Q. Sun, B. Aguila, Y. Song and S. Ma, *Acc. Chem. Res*. 2020, **53**, 812−821.

3. M. Kummu, J. H. A. Guillaume, H. de Moel, S. Eisner, M. Flörke, M. Porkka, S. Siebert, T. I. E. Veldkamp and P. J. Ward, *Scientific Reports*. 2016, **6**, 38495.

4. S. R. J. Oliver., *Chem. Soc. Rev*., 2009, **38**, 1868-1881.

5. Toxicological Profile for Chromium, Public Health Service Agency for Toxic Substances and Diseases Registry, U. S. Department of Health and Human Services, Atlanta, GA, 2012.

6. D. Basu, K. Blackburn, B. Harris, M. W. Neal and F. W. Stoss, 1984. Health assessment document for chromium; U.S. Environmental Protection Agency, Office of Research and Development, Research Triangle Park, NC.

7. 1990. IARC monographs on the evaluation of carcinogenic risks to humans: chromium, nickel and welding. Vol 49, IARC, Lyon.

8. R. von Burg and D. Liu, *J. Appl. Toxicol*. 1993, **13**, 225−230.

9. M. B. Luo, Y. Y. Xiong, H. Q. Wu, X. F. Feng, J. Q. Li and F. Luo, *Angew. Chem., Int. Ed.*, 2017, **56**, 16376–16379.

10. Q. Sun, L. Zhu, B. Aguila, P. K. Thallapally, C. Xu, J. Chen, S. Wang, D. Rogers, S. Ma, *Nat. Commun*. 2019, **10**, 1646.

11. International Atomic Energy Agency, Nuclear Power Reactors in the World, Reference Data Series No. **2**, IAEA, Vienna, 2018.

12. M. D. Bartholoma, A. S. Louie, J. F. Valliant and J. Zubieta, *Chem. Rev.*, 2010, **110**, 2903–2920.

13. S. Mollick, S. Fajal, S. Saurabh, D. Mahato, S. K. Ghosh, *ACS Cent. Sci*., 2020, **6**, 1534−1541.

14. L. He, S. Liu, L. Chen, X. Dai, J. Li, M. Zhang, F. Ma, C. Zhang, Z. Yang, R. Zhou, Z. Chai and S. Wang, *Chem. Sci*. 2019, **10**, 4293−4305.

15. W. Jin, Y. Fu, M. Hu, S. Wang and Z. Liu, *J. Electroanal. Chem*., 2020, **856**, 113744.

16. W. Mandal, S. Fajal, S. Mollick, M. M. Shirolkar, Y. D. More, S. Saurabh, D. Mahato, S. K. Ghosh, *ACS Appl. Mater. Interfaces* 2022, **14**, 17, 20042–20052.

17. X. Yang, Y. Wan, Y. Zheng, F. He, Z. Yu, J. Huang, H. Wang, Y. S. Ok, Y. Jiang, B. Gao, *Chem. Eng. J*. 2019, **366**, 608–621.

18. N. Abdullah, N. Yusof, W. Lau, J. Jaafar and A. Ismail, *J. Ind. Eng. Chem*. 2019, **76**, 17–38.

19. J.-H. Park, G.-J. Choi and S.-H. Kim, *J. Korea Org. Resour. Recycl. Assoc.* 2014, **22**, 50–56.

20. S. Hao, A. Verlotta, P. Aprea, F. Pepe, D. Caputo and W. Zhu, *Microporous Mesoporous Mater.*, 2016, **236**, 250–259.

21. Li, Y., Li, L., Yu, J., *Chem*, 2017, **3**, 928–949.

22. F. Yang, M. Du, K. Yin, Z. Qiu, J. Zhao, C. Liu, G. Zhang, Y. Gao, H. Pang, *Small*, 2021, 2105715.

23. Z. Xia, Y. Zhao and S. B. Darling, *Adv. Mater. Interfaces*, 2021, **8**, 2001507.

24. D. Taylor, S. J. Dalgarno, Z. Xu and F. Vilela., *Chem. Soc. Rev*. 2020, **49**, 3981−4042.

25. E. Marquis, J. Graton, M. Berthelot, A. Planchat and C. Laurence, *Can. J. Chem*., 2004, **82**, 1413–1422.

26. J. R. Cabrero-Antonino, T. Garcia, P. Rubio-Marques, J. A. Vidal-Moya, A. Leyva-Perez, S. S. Al-Deyab, S. I. Al-Resayes, U. Diaz and A. Corma, *ACS Catal.*, 2011, **1**, 147–158.

27. M. Carta, R. Malpass-Evans, M. Croad, Y. Rogan, J. C. Jansen, P. Bernardo, F. Bazzarelli and N. B. McKeown., *Science,* 2013, **339**, 303-307.

28. Seth M. Cohen, *Chem. Rev.* 2012, **112**, 970–1000.

29. W. Chen, W. Yan, S. Wu, Z. Xu, K. W. K. Yeung, C. Yi., *Macromol. Chem. Phys*. 2010, **211**, 1803–1813.

30. Y. Su, Y. Wang, X. Li, X. Li and R. Wang, *ACS Appl. Mater. Interfaces*, 2016, **8**, 18904−18911.

31. Q. Zhang, J. Yu, J. Cai, L. Zhang, Y. Cui, Y. Yang, B. Chen and G. Qian, *Chem. Commun.*, 2015, **51**, 14732–14734.

32. S. Dutta, P. Samanta, B. Joarder, S. Let, D. Mahato, R. Babarao and S. K. Ghosh, *ACS*

Applied Materials & Interfaces., 2020, **12**, 37, 41810-41818.

33. Z.-Z. Yang, H. Zhang, B. Yu, Y. Zhao, G. Ji and Z. Liu, *Chem. Commun*., 2015, **51**, 1271—1274.

34. (a) J. Li, B. Li, N. Shen, L. Chen, Q. Guo, L. Chen, L. He, X. Dai, Z. Chai and S. Wang, *ACS Central Science* 2021, **7**, 8, 1441-1450. (b) A. V. Desai, B. Manna, A. Karmakar, A. Sahu and S. K. Ghosh, *Angew. Chem. Int. Ed*. 2016, **55**, 7811 –7815. (c) C. Xiao, A. Khayambashi and S. Wang, *Chem. Mater*. 2019, **31**, 3863−3877.

Chapter 5

Post Synthetically Modified Porous Polymer for Rapid Anionic Organic Dye Removal from water

5.1 Introduction

World population has touched 8 billion this year. For sustainable life and environment fresh water is one of the most crucial natural resources. The clean water environment is said to make up only about 1 % of the planet's surface.[1] As a result, there will be massive need for freshwater each year as the world population increases.[2] Additionally increasing number of human activities and development of contemporary industry has polluted fresh water as well as ground water with a variety of organic pollutants, which includes phenols, dyes, pesticides, hormones etc. Many industries such as, paper, pharmaceuticals, ceramics, printing, cosmetics and textile are generating large amount of waste water in addition with consuming large amount of water resources.[3] Due to extensive use of organic dyes in emerging industries removal of such polluting dyes from coloured waste water has become a major challenge for the researchers. According to an estimated research data, there are over a million dyes are in the market and has a production rate of 7×10^5 tons annually, out of them 2% of dyes are eluted as waste water.[4] Wastewater from textile printing and dyeing has long been a big challenge when it comes to treatment and reuse. These dye molecules in water influencing aquatic plant photosynthesis hinders bacterial growth which were essential for degradation for water impurities.[5] In addition to this, few dye molecules also shows long-term health effects upon exposure to various organs.[6] Unfortunately these organic dye molecules are extremely stable and resistant to degradation due to its fused aromatic structures, which poses a major threat to water ecosystem as well as environment.[7] Various techniques such as degradation, adsorption and advance oxidation technique have been introduced to eliminate organic dye pollutants from waste water. Out of which adsorption-based technique has gained much recognition because of its cost effectiveness, higher efficiency and simple and room temperature functioning.[8] Although a handful number of adsorbent material have been described in previous literature for dye removal; it is still difficult to find materials with high capacity and selectivity.

In the last decade traditional porous material such as activated carbon, zeolites have shown their disadvantages in adsorption capacity as well as selectivity.[9] Therefore with tuneable porous architecture, large surface area and notable stability of inorganic porous materials have attracted attention of the researchers.[10] Recently a variety of microporous polymers such as porous organic polymer (POPs), porous polymer networks (PPNs) metal-organic framework (MOF), covalent triazine frameworks (CTFs), porous organic frameworks (POFs), covalent organic frameworks (COFs), have been investigated.[11] Among them metal-organic frameworks (MOFs) have been exploited in the domain of removing pollutants from wastewater utilizing ion exchange technique by ionic MOFs (i-MOFs) but it shows a few disadvantages like poor physiochemical stability as well as difficult in large scale synthesis.[12]

To address the abovementioned issue, researchers have proposed to replace coordination bond with covalent bonds. Various ionic polymers have been employed as for tapping pollutants from wastewater.[13] In this report, we have strategically developed a robust Troger based polymer formed via V-shaped' bridged bicyclic system linkage. Further the basic nitrogen sites of troger polymer are utilized to post synthetic modification of the polymer with dimethyl sulphate forming a cationic polymeric network having free sulphate ions inside the porous architecture.[14] Post synthetic modification (PSM) is a distinctive method for offering a different, useful and practical tool to go over the constraints imposed by pre synthetic circumstances.

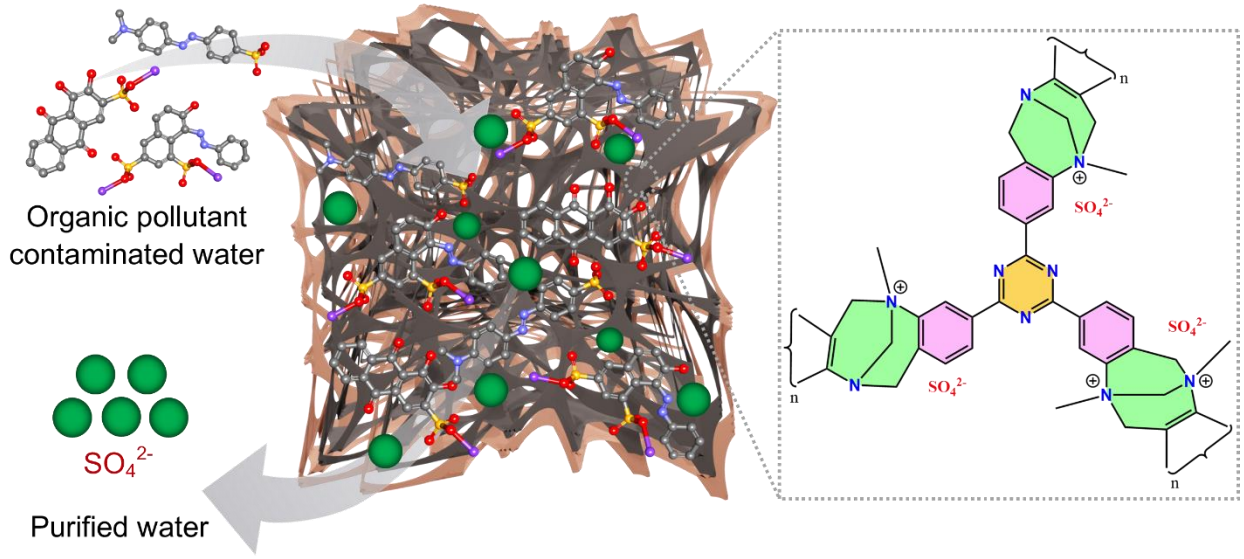

Figure 5.1: Schematic representation of the organic dye capture by T4PSM.

Here in this work, we have employed post synthetic modification technique to develop cationic troger based polymer having sulphate as counter ion. The robust nature of troger polymer gives the physiochemical stability for wastewater treatment application. Further the post synthetically modified polymer has been utilized to capture anionic dyes from aqueous medium.

5.2 Experimental

5.2.1 Materials:

3-amino benzonitrile, dimethyl sulfate, triflic acid, trifluoro acetic acid and organic solvents were obtained locally. Formaldehyde dimethyl acetal (FDA) was acquired from Sigma-Aldrich. Obtained chemical was utilized without purifying.

5.2.2 Physical Measurements:

Thermogravimetric analysis (TGA) was performed by using a PerkinElmer STA 6000 analyser under a nitrogen atmosphere where temperature was gradually increased from 30°C to 800°C at a heating rate of 10°C/min. All Infra-red (IR) Spectra were measured by using NICOLET 6700 FT-IR spectrophotometer in the range of 400-4000 cm^{-1} using KBr pellet. Low temperature nitrogen adsorption measurements were performed by using Bel Sorp-max instrument from Bel Japan. The SEM images were acquired using FEI Quanta 3D dual beam FESEM at 30KV. Energy dispersive X-ray (EDX) analyses was performed with a Hitachi S3400 N EDX instrument. TEM imaging were obtained on the HRTEM (JEM-2200FS, JEOL) operating at acceleration voltage of 200 kV. UV spectra were acquired on Shimadzu UV 2600 Spectrophotometer. Solid state NMR spectra were performed on Bruker 400 MHz NMR spectrometer. Carbon chemical shifts are expressed in parts per million (δ scale).

5.2.3 Synthesis:

Synthesis of 3,3',3''-(1,3,5-triazine-2,4,6-triyl) trainline: The targeted amine has been obtained via acid catalyzed trimerization reaction by following a previously described methodology.[15]

Synthesis of T4_Troger: Under N_2 atmosphere 3,3',3"-(1,3,5-triazine-2,4,6-triyl) trainline (1 mmol) was dissolved in formaldehyde dimethyl acetal (FDA) (1ml, 11.2 mmol) and cooled in ice bath. After that followed by dropwise addition of 15 ml trifluoracetic acid the mixture was stirred for 2 days. After 48 hours the viscous was transferred into a solution of water and aqueous ammonia and stirred vigorously for 2 hours which resulted in a formation of brown solid. After collecting the brown solid it was then washed with methanol and distilled water. Further the brown solid was also purified via Soxhlet extraction by mixture of water/methanol/acetone for 12 hours and with THF for another 12 hours respectively. The product was then heated under vacuum at 110°C (12 hours) for the removal of solvent guest molecules which resulted in a brown solid T4_Troger (yield 79%). Elemental analysis C 64.56%, H 3.4%, N 16.74%.

Synthesis of T4PSM: 4.7ml (50 mmol) dimethyl sulfate was added dropwise to the polymer T4_Troger (300mg) dispersed in acetonitrile (150ml). After stirring the mixture for 12 hours in reflux condition the

solid was collected via filtration. After that the filtrate was washed with different solvents like $CHCl_3$, acetonitrile, methanol, THF etc. Further drying under vacuum at 105°C (12 hours) resulted in a blackish brown powder. Elemental analysis C 45.4%, H 3.93%, N 12.61%, S 11.48%.

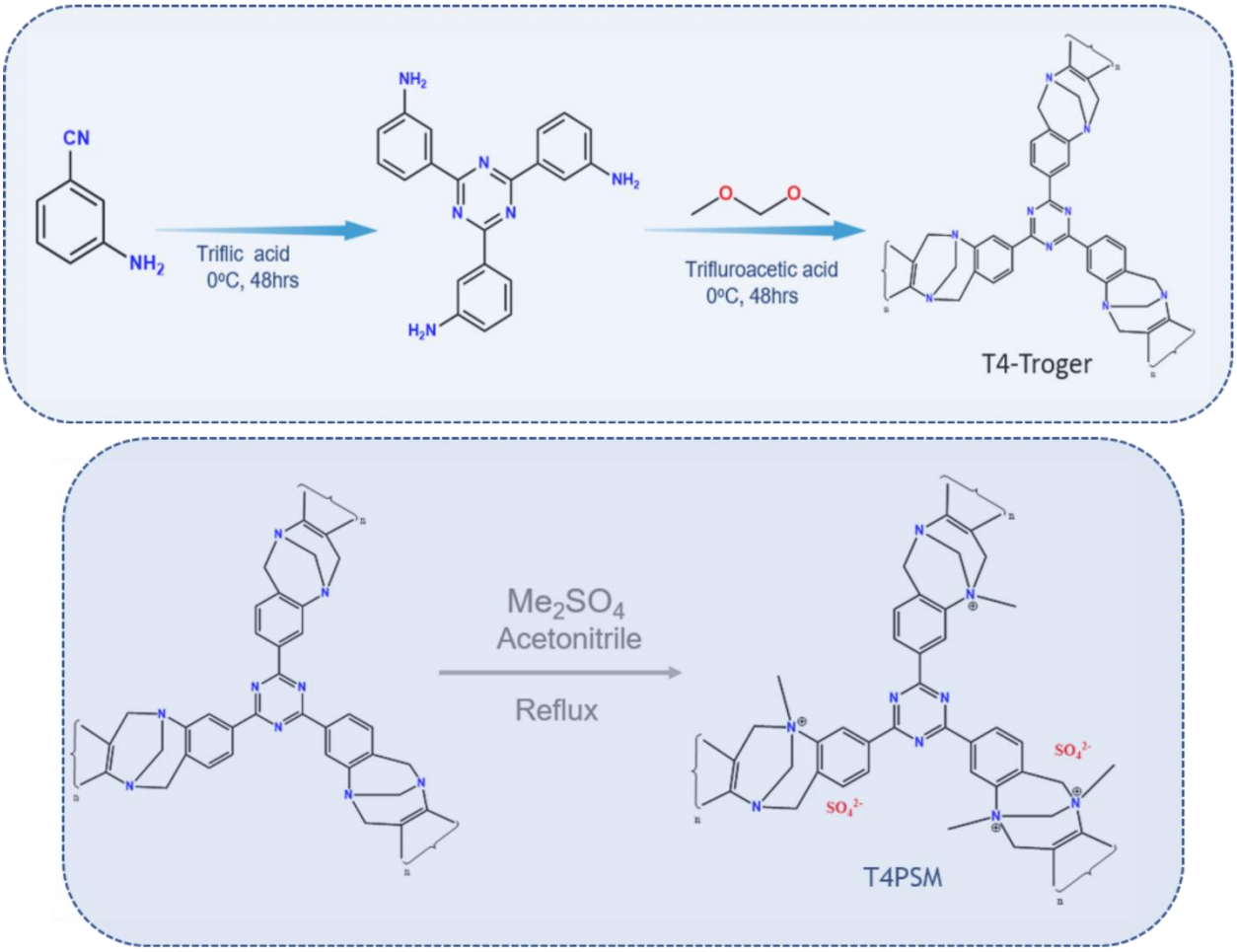

Scheme 5.1: Synthesis scheme of T4_Troger and T4PSM.

5.2.4 Ion-exchange Studies:

Dye capture study: For dye capture experiment 0.1 mM aqueous solution of respective dyes were used. First UV-Vis spectra of 3 ml 0.1mM dye solution was recorded. Further 2 mg of de-solvated compound have been added to the cuvette and we recorded the absorbance spectra in different time interval. We have also calculated decrease in concentration with time and removal percentage from the following equations.[16]

$$D_t = \frac{C_0 - C_t}{C_0} \text{ x } 100\% = \frac{A_0 - A_t}{A_0} \text{ x } 100\%$$

$$i.e., \quad C_t = C_0 - \frac{A_0 - A_t}{A_0} \text{x } C_0$$

Where, D_t is denoted as exchange capacity, initial concentration is C_0 and A_0 is initial absorbance of the anionic dye solution and at specific time interval C_t and A_t are concentration and absorbance of the dye solution.

Kinetics study: From the time dependent titration of the dyes capacity of T4PSM towards each dyes were plotted with time and best fit model was calculated to be pseudo second order kinetics. The equation for the model is as follows.

$$Q_t = \frac{k_2 Q_e^{\,2} t}{1 + k_2 Q_e t}$$

where, t represents time in minute, Q_t is the amount of adsorbate (mg gm^{-1}) material and Q_e is the adsorbent material.

Adsorption isotherm experiment: 5 mg of the de-solvated material was dispersed in 5 ml of aqueous dye solution having different concentration (0.1mM to 2.5mM). The supernatant was taken out after 24 hours and subjected to UV-Vis experiment which further fitted with the following equation.

Langmuir model, $$Q_e = \frac{Q_m C_e}{K_d + C_e}$$

where, the dye concentration at equilibrium is denoted as C_e (ppm) and amount of dye adsorbed at equilibrium is termed as Q_e (mg gm^{-1}) . To form a complete monolayer maximum amount of dye per unit mass of adsorbent is Q_m (mg gm^{-1}). K_d (mg/L) is a constant related to the affinity of the binding sites.

Freundlich Model, $$Q_e = K_F C_e^{1/n}$$

where, K_F and 1/n are the two Freundlich model constants, whereas Q_e indicates capacity and C_e as equilibrium concentration.

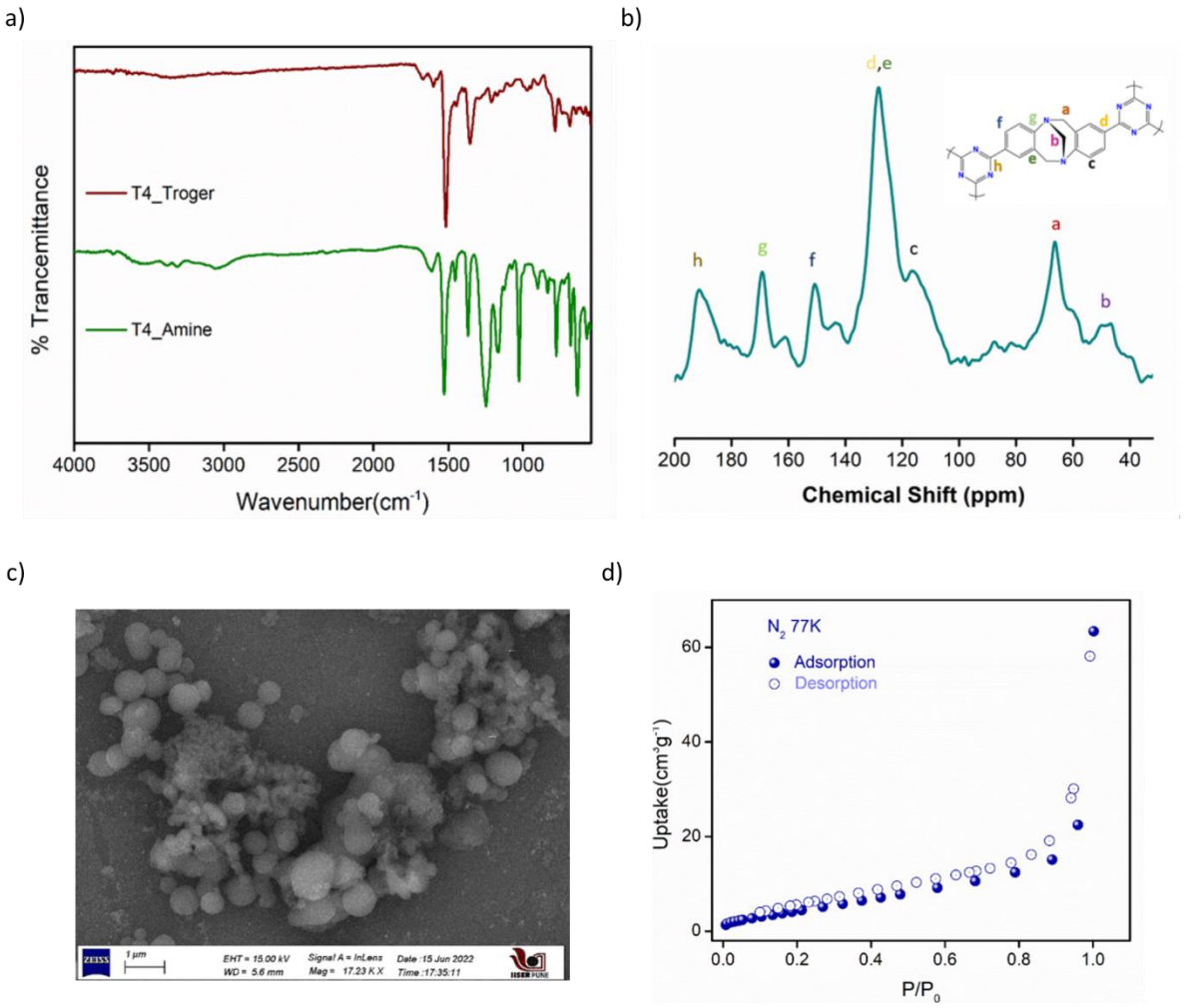

Figure 5.1: (a) Infra-red (IR) spectroscopy of starting materials [T4_amine (green) and T4_Troger (wine red)] (b) Solid state ^{13}C-NMR of T4_Troger. (c) FE-SEM images of T4_Troger. (d) Low temperature (77 K) N_2 adsorption profile of T4_Troger.

5.3 Results and discussion

Acid-catalysed one-pot polymerisation was used to synthesize the Troger based derived porous organic polymer (T4_Troger) from the aromatic triamine shown in (scheme 5.1).[17] Aqueous ammonia was added to reaction mixture to quench the excess acid present in the reaction mixture which resulted in a brown solid which is further washed with various organic solvents (DMAc, THF, DMF DCM, Acetone and Methanol). The monomers and oligomers were further removed by Soxhlet extraction by mixture of THF and methanol. To synthesize the desired polymer T4_Troger is further reacted with dimethyl sulphate, in

presence of acetonitrile as solvent. The resulting blackish brown powder (T4PSM) was collected after washing with various organic solvents. Both T4_Troger and T4PSM have been characterized by ^{13}C solid state NMR, low temperature N_2 adsorption, high-resolution transmission electron microscopy (HR-TEM), (FE-SEM), (TGA) and infra-red (IR) spectroscopy.

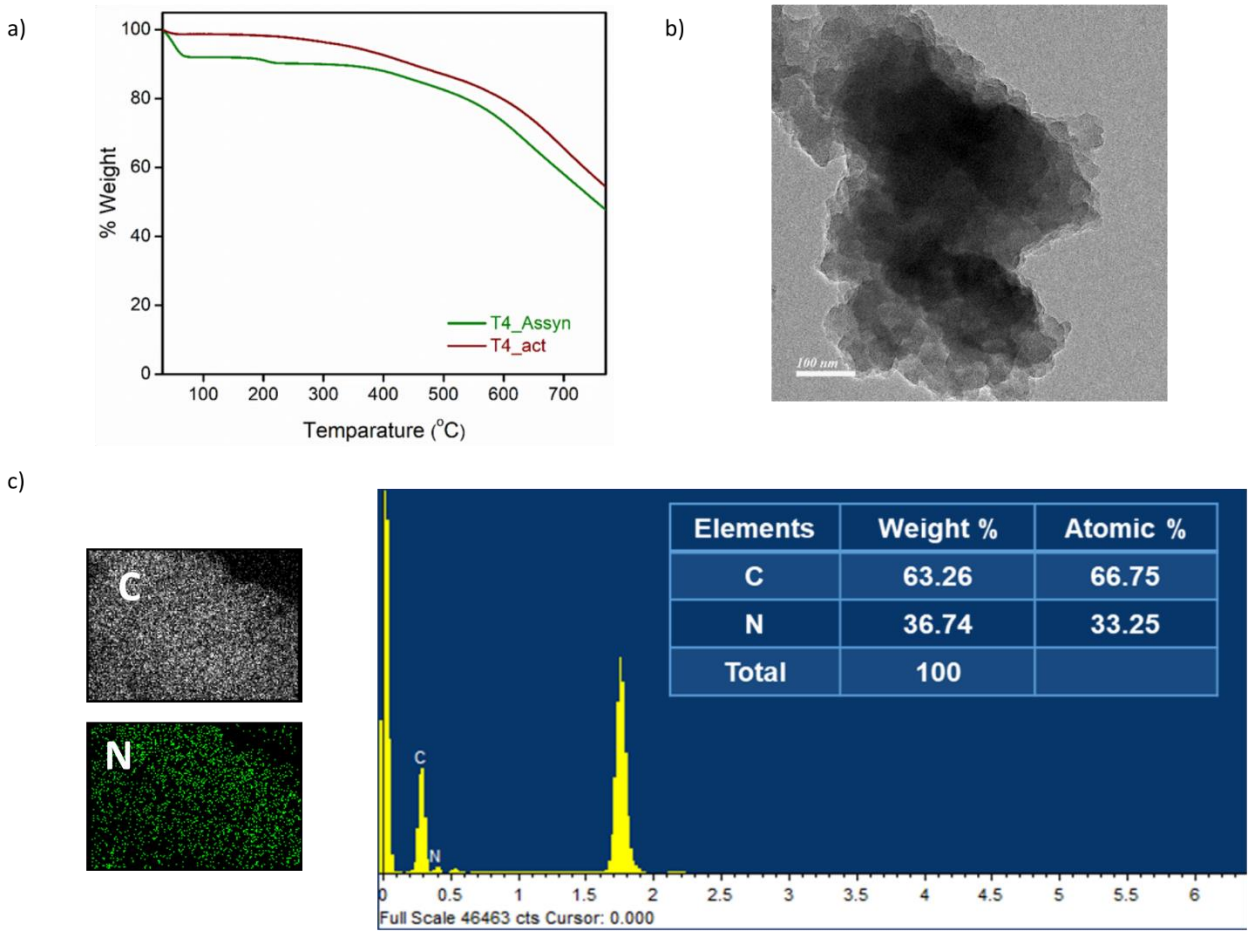

Figure 5.2: (a) Thermo-gravimetric analysis (TGA) profiles of as-synthesized T4_Tröger (green) and de-solvated phase of T4_Troger (wine red). (b) HRTEM Image of T4_Troger. (c) Elemental mapping and EDX analysis of T4_Troger (Carbon- Gray, Nitrogen-Green).

In FT-IR spectroscopy peaks at 1503 and 1362 cm^{-1} confirms the existence of triazine ring. The abolition of peaks around 3300 cm^{-1} indicates the transformation of the amine groups (Fig. 5.1a). Further post methylated polymer T4PSM shows SO_4^{2-} peak around 1020 cm^{-1} and a broader peak at 1100 cm^{-1} (Appendix 5.1). Both the de-solvated phase of the polymers (T4_Troger and T4PSM) shows thermal stability up to

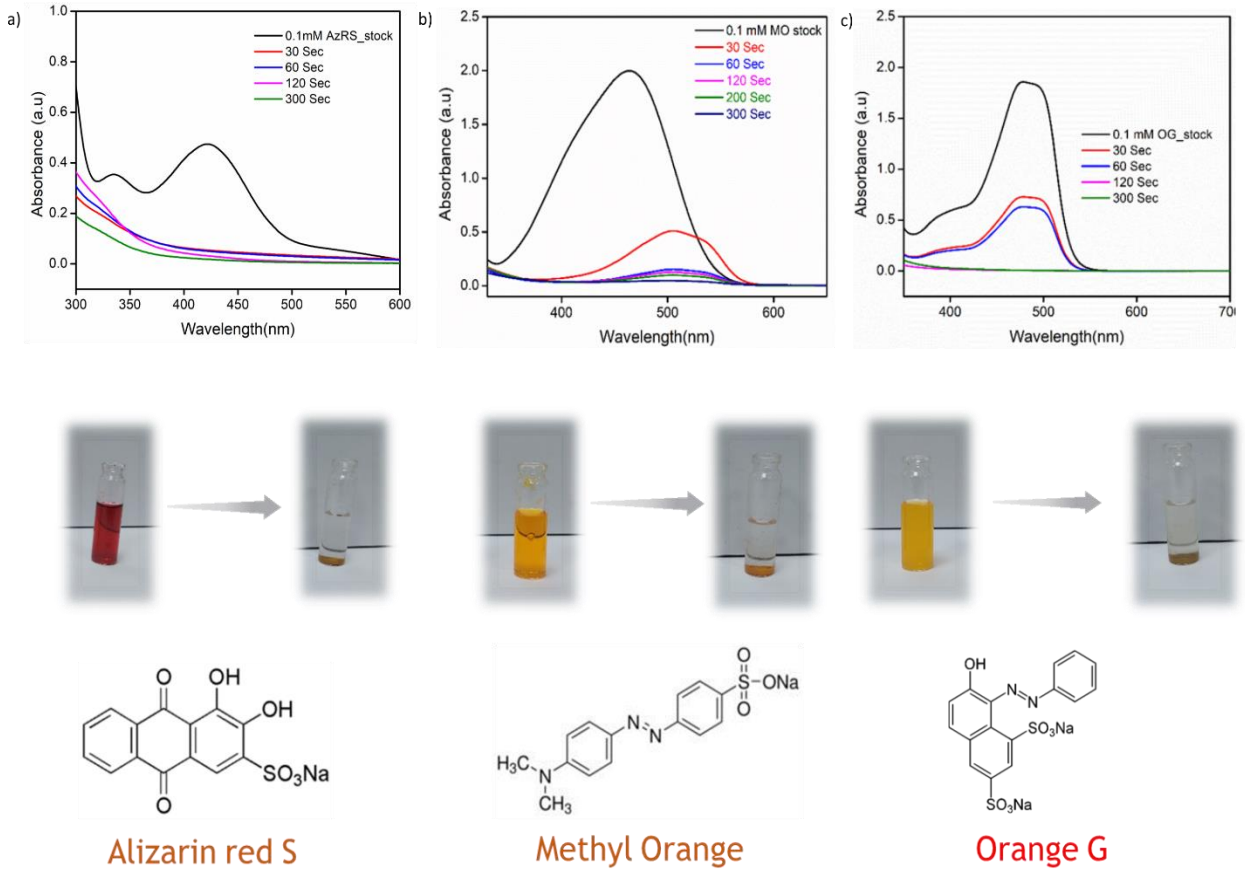

Figure 5.3: UV-Vis spectroscopy of diff dyes at different time intervals for the aqueous solution after T4PSM addition. (a) Alizarin Red S (b) Methyl Orange and (c) Orange G ; below image shows the corresponding dye solution becomes colorless.

~250ºC (Appendix 5.2 and Fig. 5.2a). As a result of incorporation sulphate anion pore size of T4PSM has decreased as compare to T4_Troger and which reflects in low temperature the N_2 adsorption isotherm at 77 K (Fig. 5.1d and Appendix 5.4). The solid state ^{13}C NMR shows peaks at 190 ppm indicating triazine carbon besides that peaks from 110 to 150 ppm are of the attached phenyl ring whereas, peaks at 67.2, and 50.6 ppm represents aliphatic carbons that is methylene carbon atoms of the Tröger's base (Fig. 5.1b). Peak at 30 ppm in T4PSM indicates methylated carbon on the troger center (Appendix 5.3). FESEM images suggests similar globule like morphology in T4_Troger and T4PSM after modification (Fig. 5.1c and Appendix 5.7). Further EDAX analysis shows only carbon and nitrogen are present in the T4_troger whereas T4PSM shows four elements carbon, nitrogen, oxygen, Sulphur (Appendix 5.2c and 5.8). Mapping

of the corresponding elements shows equal distribution of them throughout the material. (Figure 5.2c and 5.9). Further both the polymers were subjected to HR-TEM analysis (Fig. 5.2b and Appendix 5.6). CHNS analysis of the both the polymers were carried out and its shows presence of sulphur as expected in T4PSM (Appendix 5.5)

To check the capture performance of T4PSM towards anionic dyes, we took 1 mg of the polymer and dispersed in 0.1 mM solution of Methyl Orange (MO). The orange-coloured solution became colourless in just a few minutes. Excited from this finding we sought to explore the possibility to study capture performance of four anionic dye molecules. To begin with we have prepared 0.1mM solution of all the four dye molecules. For each measurement 2 ml of 0.1mM of respective dye solution was taken and 2 mg of T4PSM was dispersed in to the medium. The UV-Vis spectrum was recorded in various interval of time and the absorption spectra of the corresponding dye molecules shows gradual decrease with time which indicates adsorption of dye molecules by the material (Fig 5.3 and Appendix 5.10). From the kinetics measurement data, we have further calculated change in concentration of dyes and percentage removal of corresponding dye molecules with time (Appendix 5.11 and 5.12 and 5.15 and 5.23 and 5.18 and 5.22) which shows 99.8% removal of dyes in just 5 minutes and in case of indigo carmine it's just in 30 secs.

Capture kinetics of methyl orange were plotted and it fits further pseudo second order model disclosing the dependence of capture process upon the quantity of absorbate and absorbent (Appendix 5.19). Excited by the rapid kinetics we sought to check equilibrium adsorption capacity of different dye molecules. For this we have taken 5 mg of T4PSM and dispersed in various concentration (0.1mM to 2.5mM) of dye molecules. The uptake capacity and equilibrium concentration were calculated and further plotted and which well fits the Langmuir model with a high correlation coefficient value $R^2 \sim 0.96$ to 0.99 for all four dyes (Appendix 5.13 and 5.14 and 5.16 and 5.17 and 5.20 and 5.21 and 5.24 and 5.25). The maximum adsorption capacity was calculated for all the dyes which shows 364 mgg^{-1} for Indigo carmine, 388 mgg^{-1} for Orange G, 1142 mgg^{-1} for Methyl Orange and 886 mgg^{-1} for Alizarin Red S. After capture study performance, all the dye encapsulated polymers were characterized by thermogravimetric analysis, FESEM image, EDAX, FT-IR analysis. The dye encapsulated polymer shows color change which is clearly visible in the naked eye (Fig. 5.4a). FESEM images shows clearly no morphological change after encapsulation (Appendix 5.26 to Appendix 5.29). Further thermogravimetric analysis (TGA) suggests the polymers reaffirms its stability after dye capture (Appendix 5.30 to Appendix 5.33). FT-IR analysis shows the retention of the polymeric framework as well as corresponding dye encapsulated peaks (Appendix 5.34).

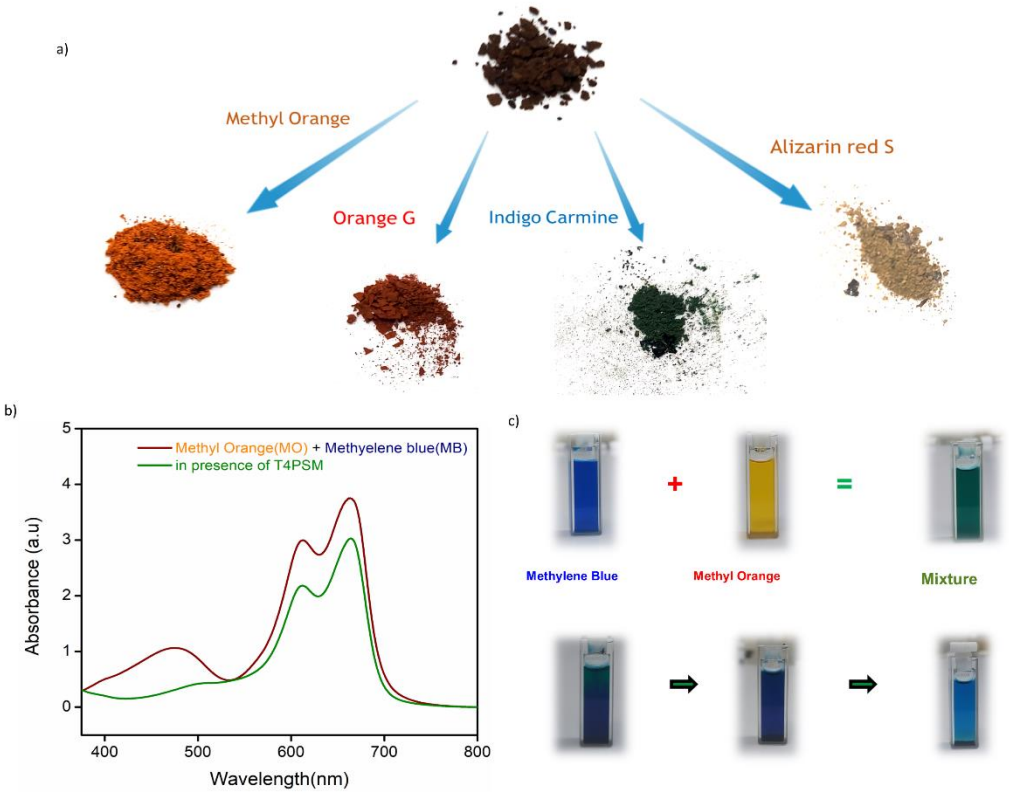

Figure 5.4: (a) Image of corresponding dye encapsulated T4PSM and (b) Adsorption measurement of two different dye (methyl Orange and Methylene Blue) mixtures by T4PSM with UV-Vis spectroscopy. (c) Images of Equimolar mixed solution of methylene blue and methyl orange before and after addition of T4PSM.

In addition of the pore size factor the ionic selectivity also plays a crucial role in removal studies. To check the ionic selectivity, we performed a capture experiment with anionic dye methyl orange (MO) and cationic dye methylene blue (MB). In a typical experiment 0.1mM of both the solutions were prepared and they were mixed together with 1 ml each followed by UV-Vis experiment. After that 2 mg of T4PSM was added to the mixture and shaken for several minutes and followed by absorbance spectra record in UV-Vis spectrometer. We have observed peak corresponding to MO (λ_{max} = 460nm) have drastically decreased whereas peak corresponding to MB (λ_{max} = 670 nm) remain almost unaltered (Fig. 5.4b). The slight decrease is indication for surface adsorption. Along with UV-Vis spectra we also noted visual color alteration after and before the experiment. MB is blue in color and MO is orange so after mixing their color becomes green initially. After adding the polymer gradually, the color of the solution becomes blue (Fig. 5.4c) as only methylene blue is left in the solution. Our material's ability to selectively capture anionic dyes in a combination of cationic and anionic dyes was proven by UV-Vis spectra and visible color change.

5.4 Conclusions

In conclusion, a cationic porous organic polymer was synthesized via post synthetic methylation of bridged nitrogen centre, which resulted in quaternization of nitrogen centre leading to cationic porous architecture with SO_4^{2-} as counter anions. On the basis of ion exchange, efficient anionic dye (Methyl Orange, Orange G, Indigo carmine and Alizarin red S) capture have been performed with T4PSM. Furthermore, selectivity of anionic dye over cationic dye have demonstrated the ionic change selectivity. To our best knowledge, there are not much articles on anionic dye capture via post synthetic modification of a porous polymer. We think that our effort will advance the study of pollutant trapping using such durable and affordable materials.

5.5 Appendix Section

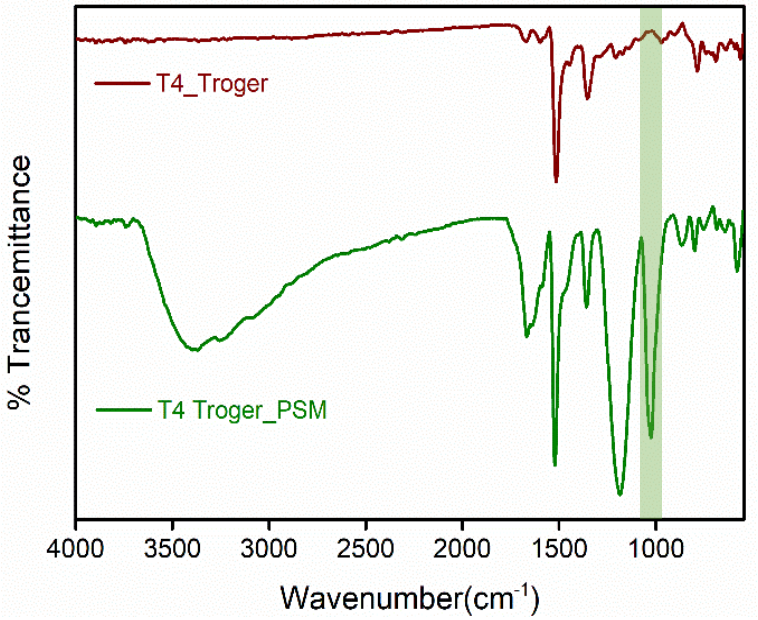

Appendix 5.1: Infra-red (IR) spectroscopy of troger polymer [T4_Troger (wine red) and T4PSM (green)] peak of sulphate ions are highlighted.

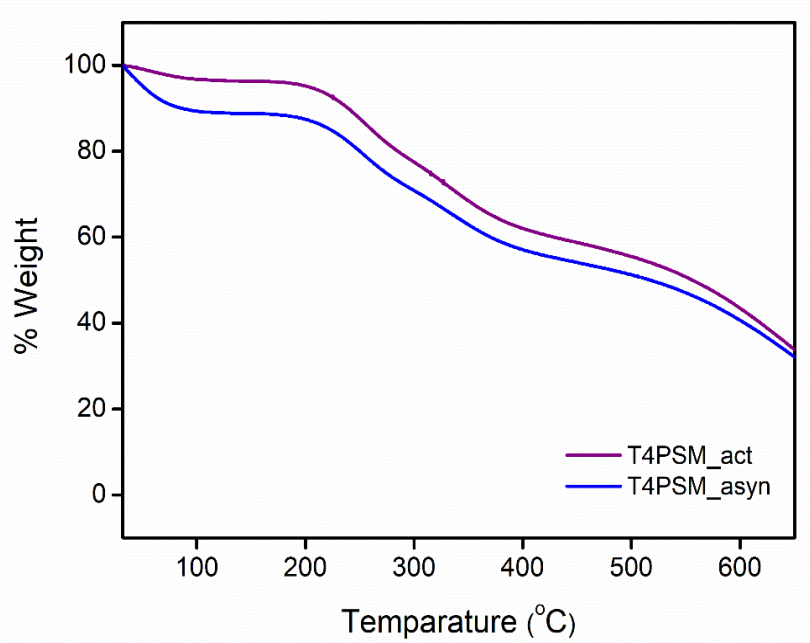

Appendix 5.2: Thermo-gravimetric analysis (TGA) profiles of as-synthesized T4PSM (blue) and de-solvated phase of T4PSM (violet).

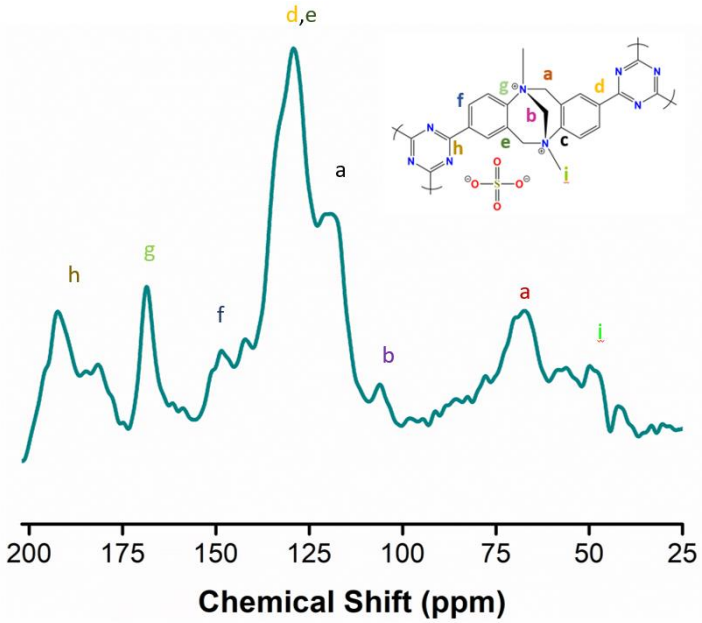

Appendix 5.3: Solid state ^{13}C-NMR of T4PSM.

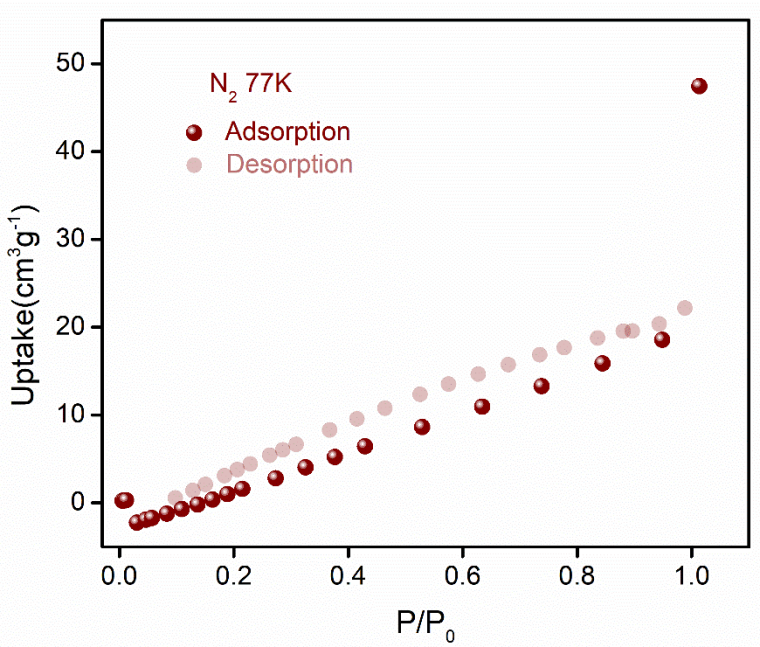

Appendix 5.4: Low temperature (77 K) N_2 adsorption profile of T4PSM.

Compounds	% C	% H	% N	% S
T4	**64.46**	**3.13**	**16.95**	**0.01**
T4PSM	**45.56**	**3.52**	**12.45**	**11.71**

Appendix 5.5: CHNS analysis of T4_Troger and T4PSM.

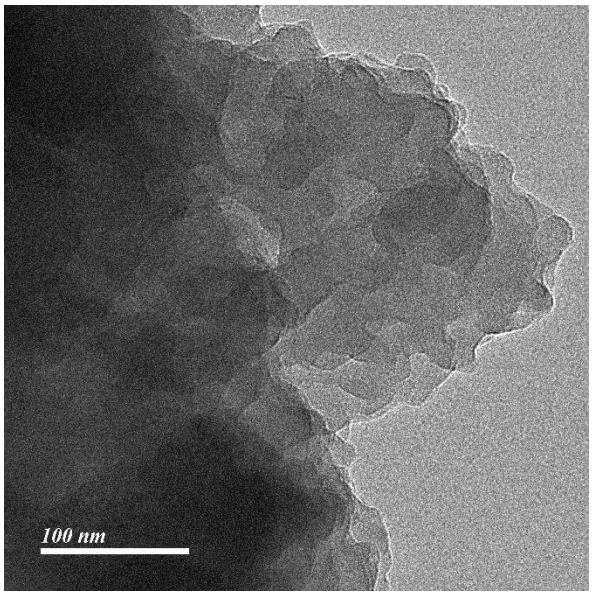

Appendix 5.6: HRTEM image of T4PSM.

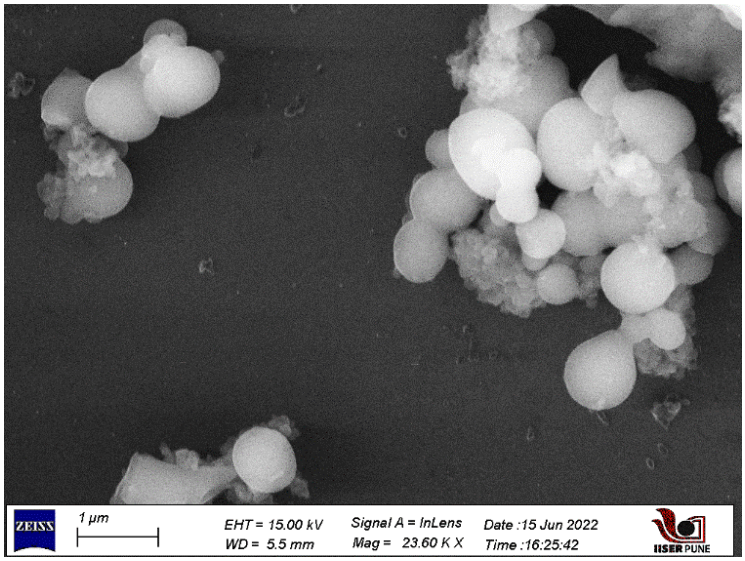

Appendix 5.7: FE-SEM images of T4PSM.

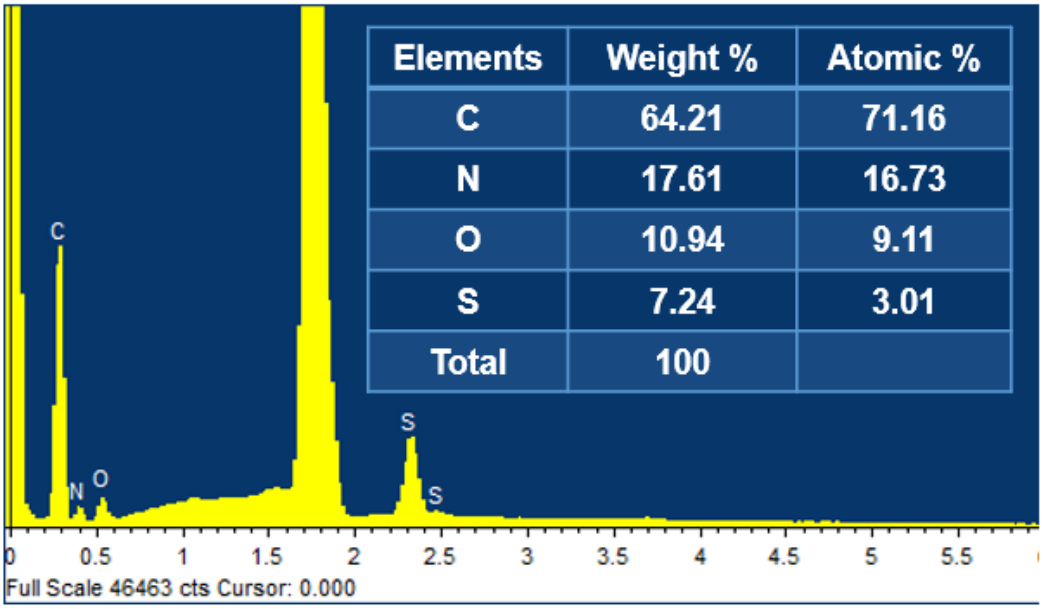

Elements	Weight %	Atomic %
C	64.21	71.16
N	17.61	16.73
O	10.94	9.11
S	7.24	3.01
Total	100	

Appendix 5.8: EDX analysis of T4PSM.

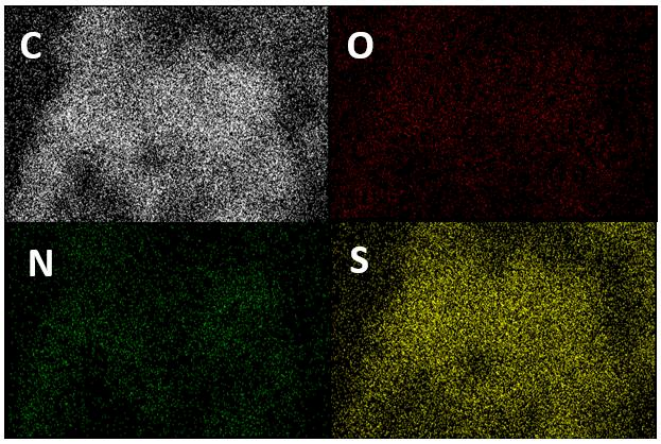

Appendix 5.9: Elemental mapping of T4PSM (Carbon-Grey, Nitrogen-Green, Oxygen-Red, Sulpher-Yellow).

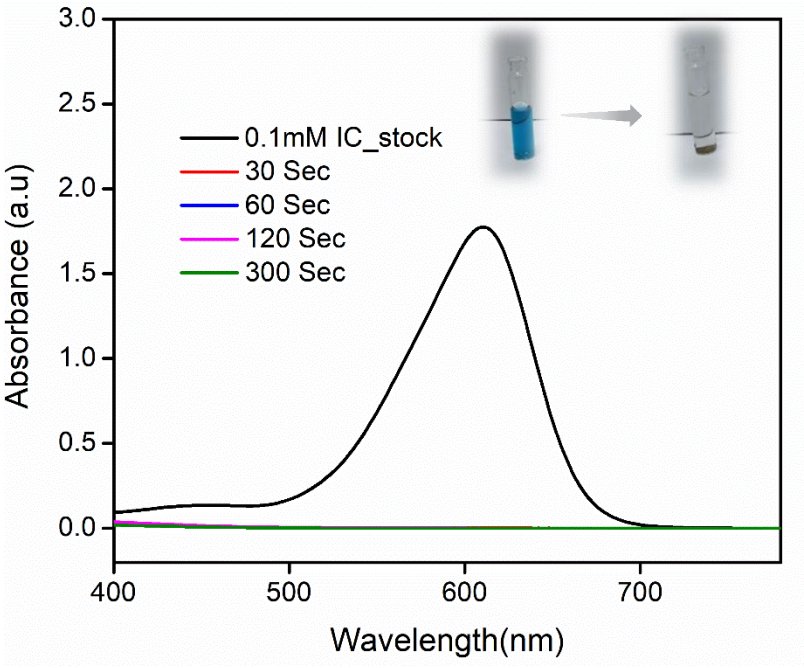

Appendix 5.10: UV-Vis spectroscopy of Indigo carmine solution in water in presence of T4PSM at different time intervals (Inset: images of IC solution before and after of capture study).

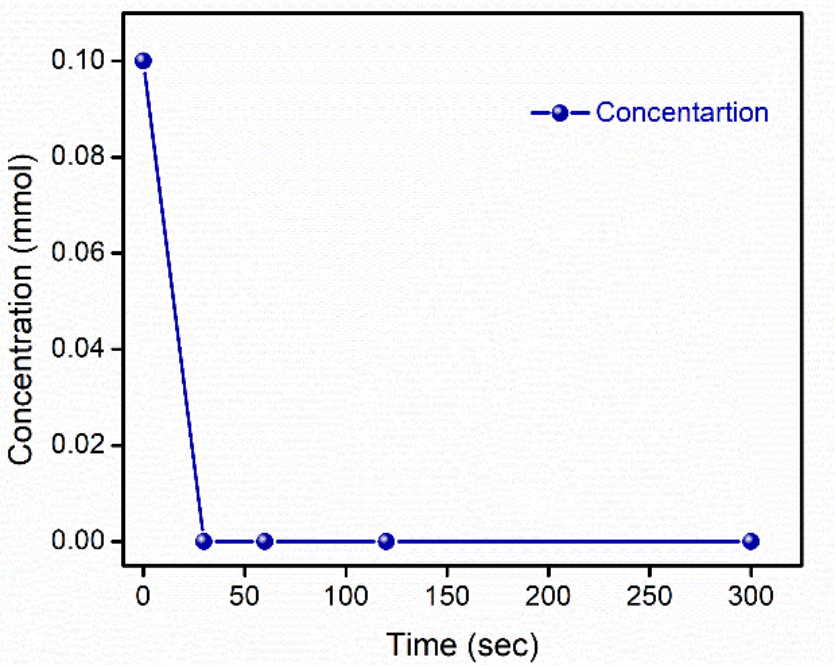

Appendix 5.11: Change in concentration of Indigo carmine with time in presence of T4PSM.

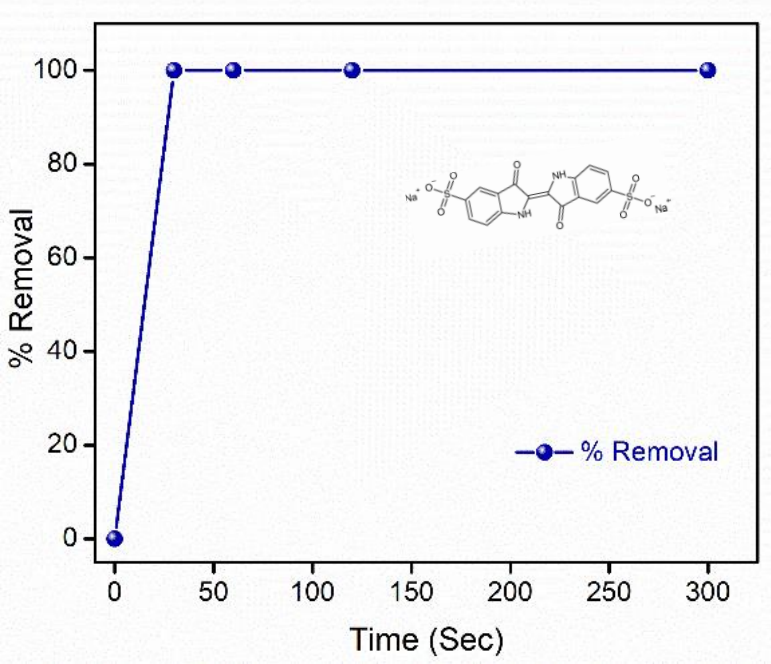

Appendix 5.12: Percentage removal of Indigo carmine with time in presence of T4PSM.

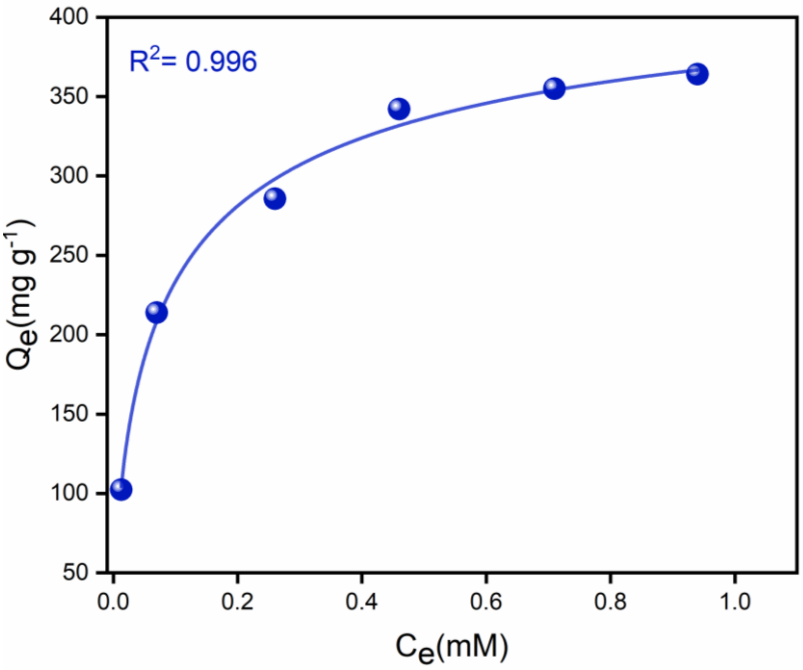

Appendix 5.13: Non-liner isotherm for the capture of Indigo carmine by T4PSM.

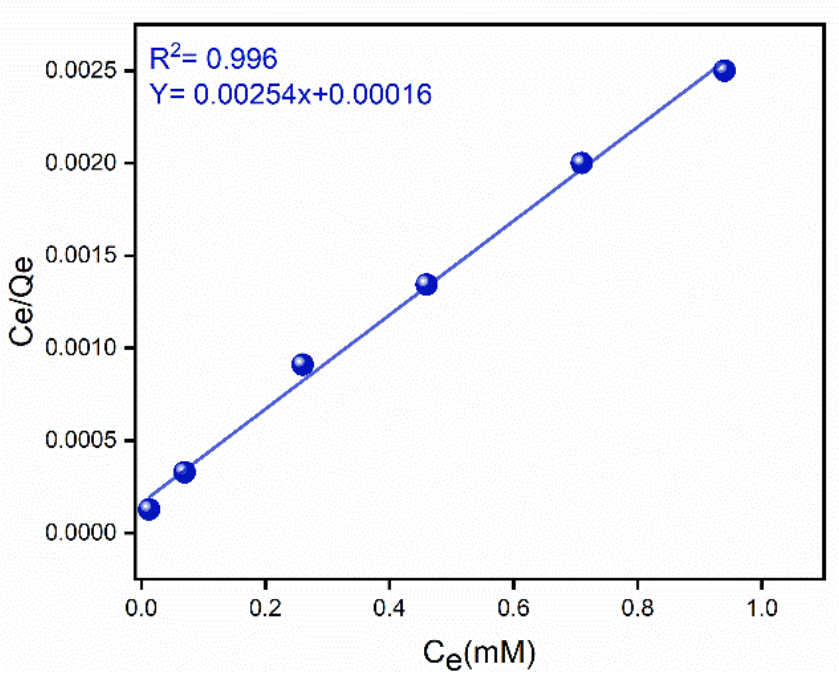

Appendix 5.14: Langmuir fit liner isotherm for the capture of Indigo carmine by T4PSM.

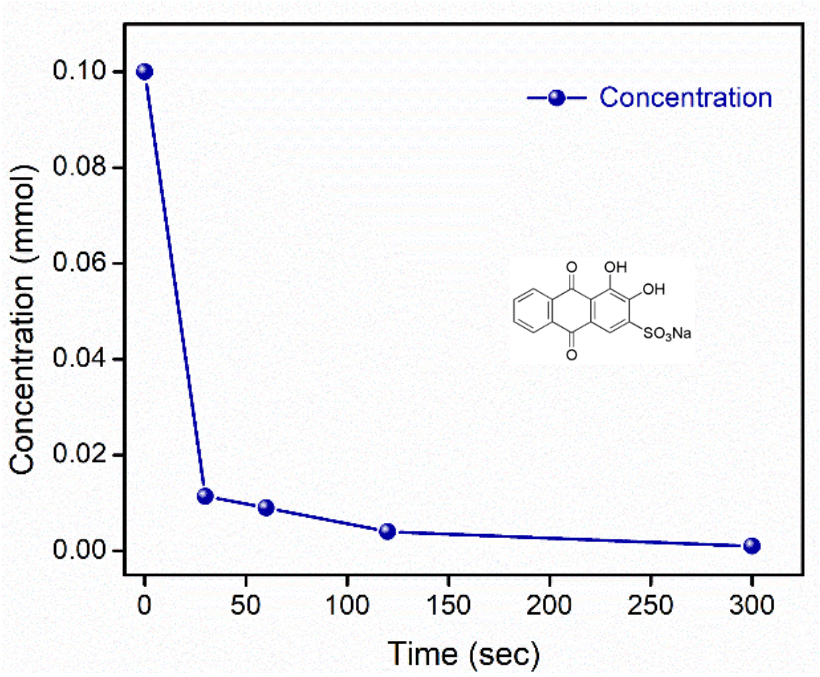

Appendix 5.15: Change in concentration of Alizarin red S with time in presence of T4PSM.

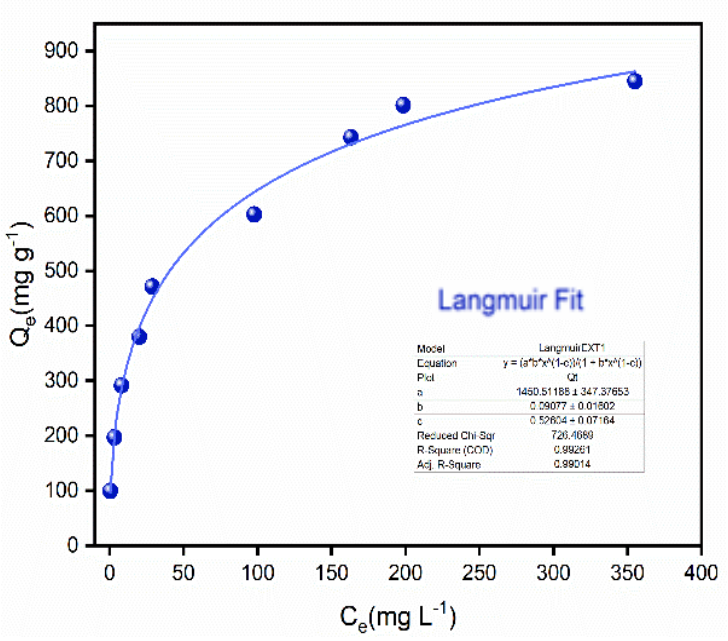

Appendix 5.16: Non-liner and Linear Langmuir isotherm for the capture of Alizarin red S by T4PSM.

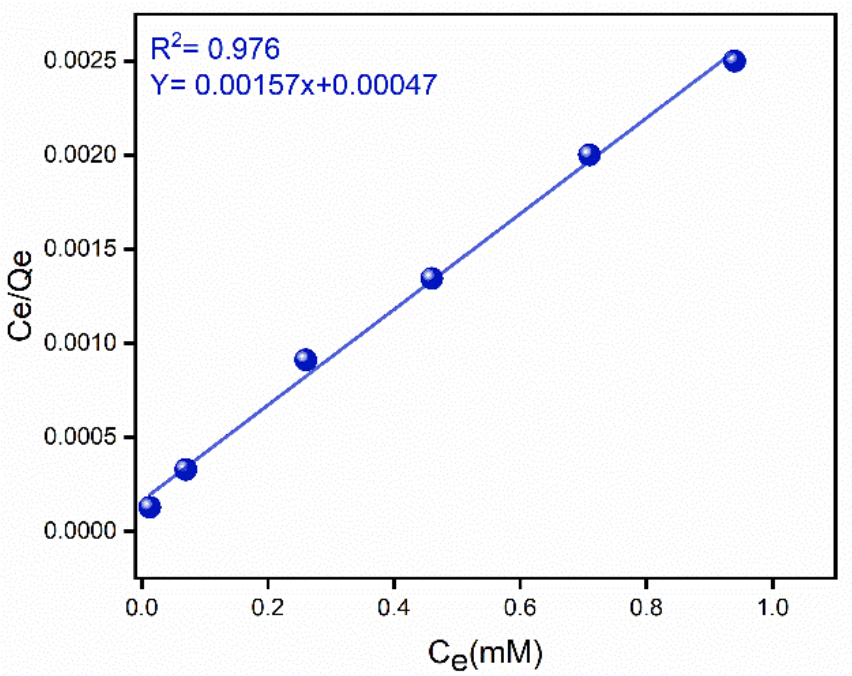

Appendix 5.17: Langmuir fit liner isotherm for the capture of Alizarin red S by T4PSM.

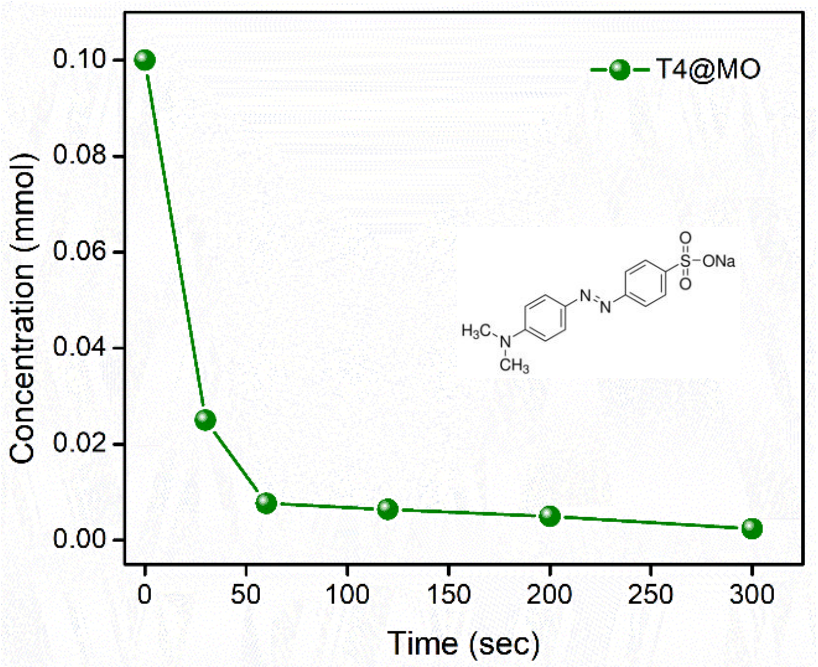

Appendix 5.18: Change in concentration of Methyl Orange with time in presence of T4PSM.

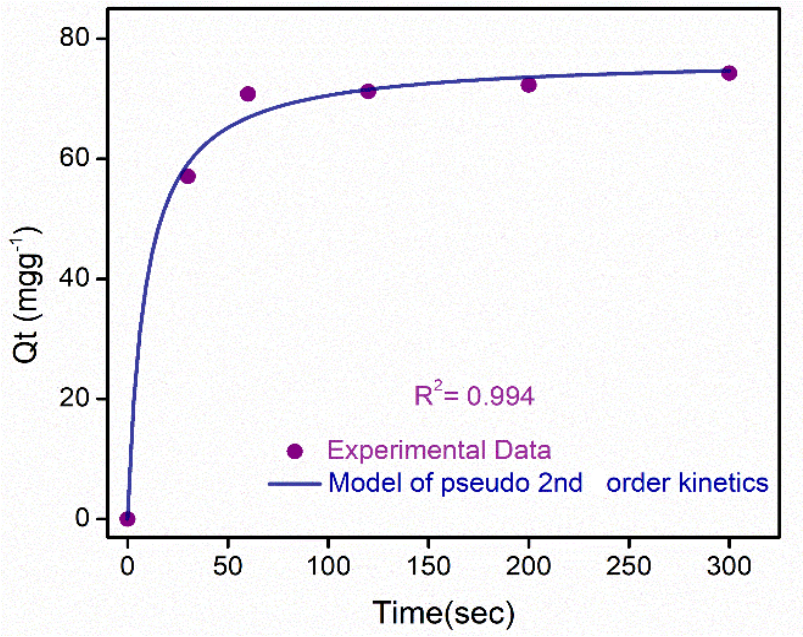

Appendix 5.19: Kinetics for the capture of Methyl Orange with T4PSM.

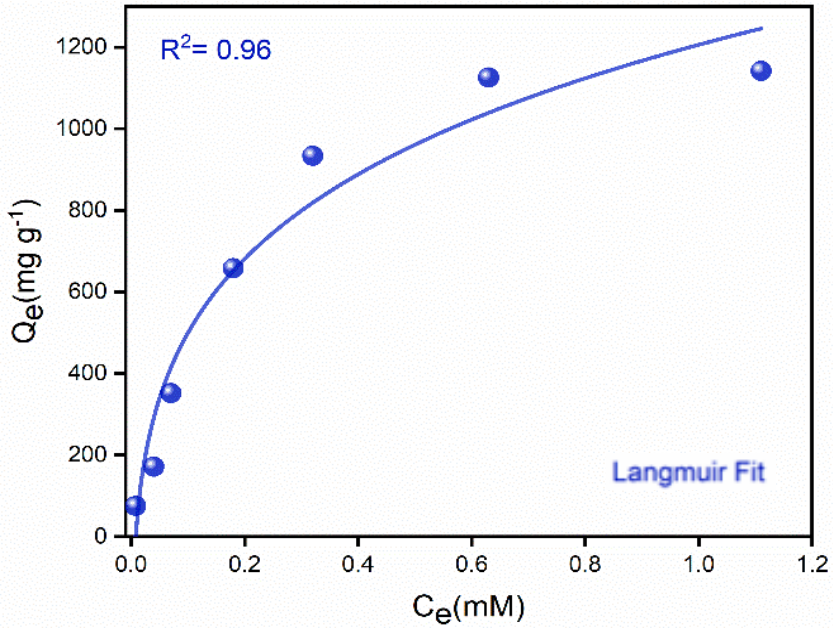

Appendix 5.20: Non-liner and Linear Langmuir isotherm for the capture of Methyl Orange by T4PSM.

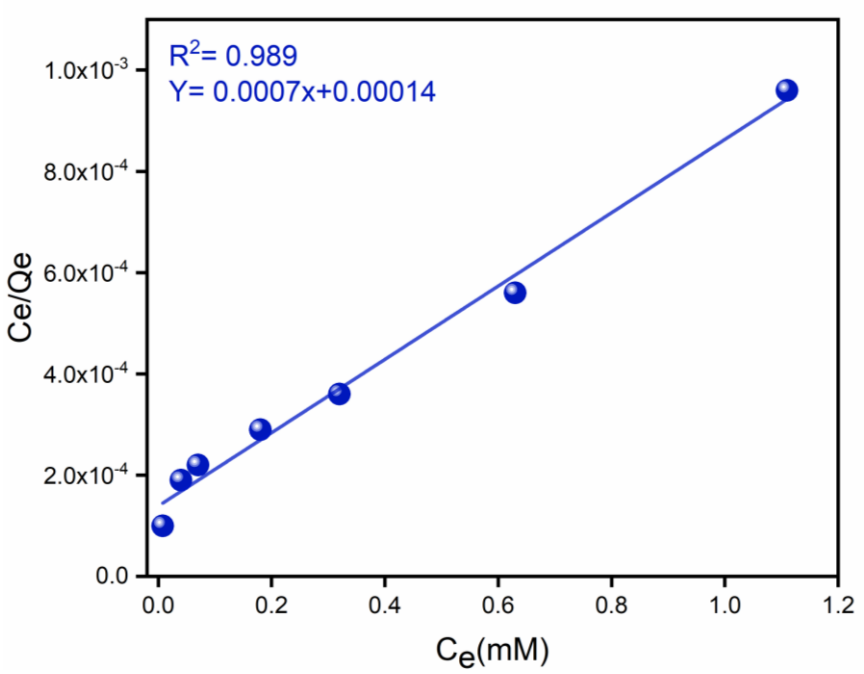

Appendix 5.21: Langmuir fit liner isotherm for the capture of Methyl Orange by T4PSM.

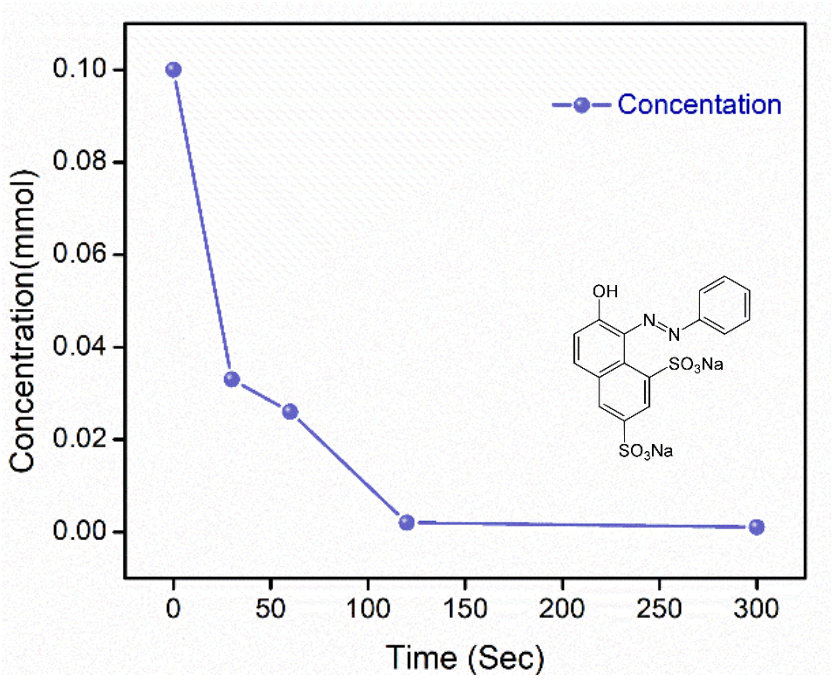

Appendix 5.22: Change in concentration of Orange G with time in presence of T4PSM.

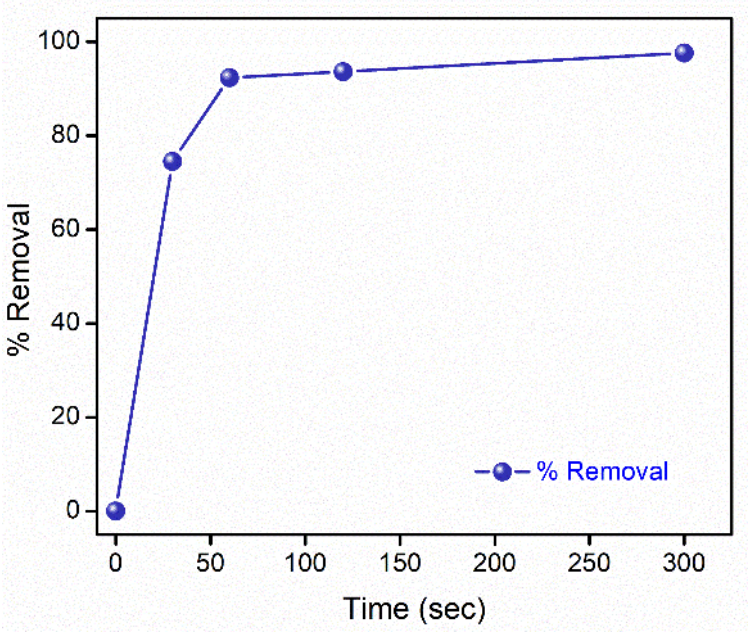

Appendix 5.23: Percentage removal of Orange G with time in presence of T4PSM.

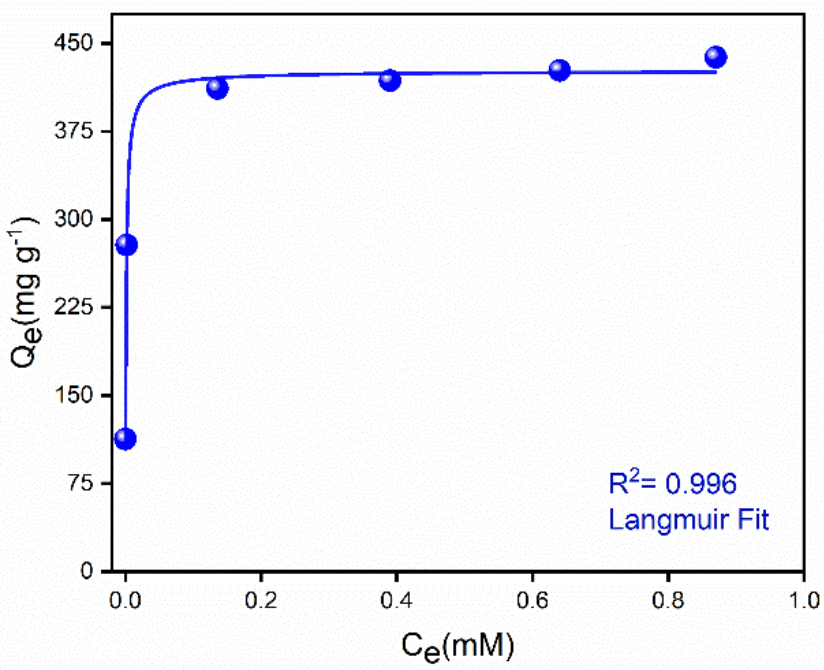

Appendix 5.24: Non-liner Langmuir isotherm for the capture of Orange G by T4PSM

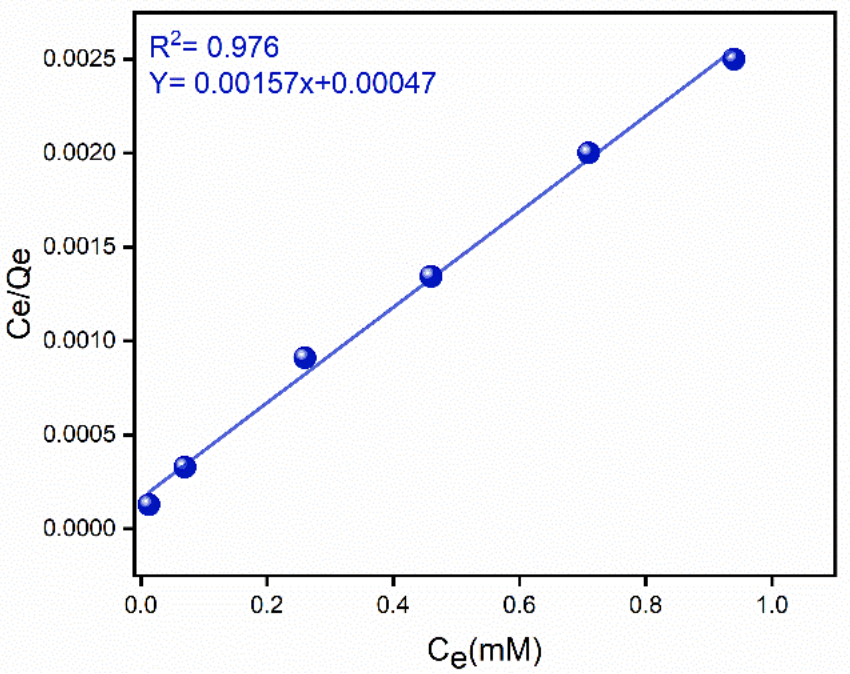

Appendix 5.25: Linear Langmuir isotherm for the capture of Orange G by T4PSM.

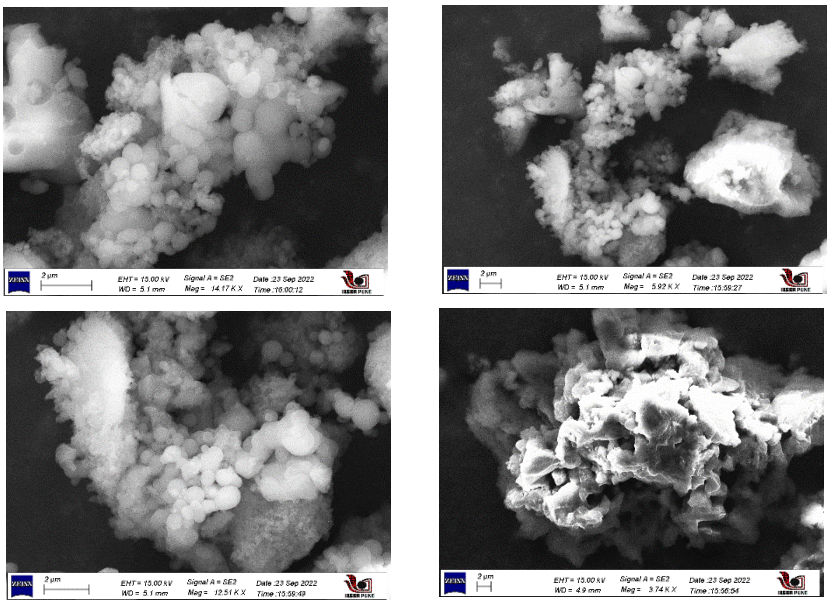

Appendix 5.26: FE-SEM images of Alizarin red S (AzRs) encapsulated T4PSM.

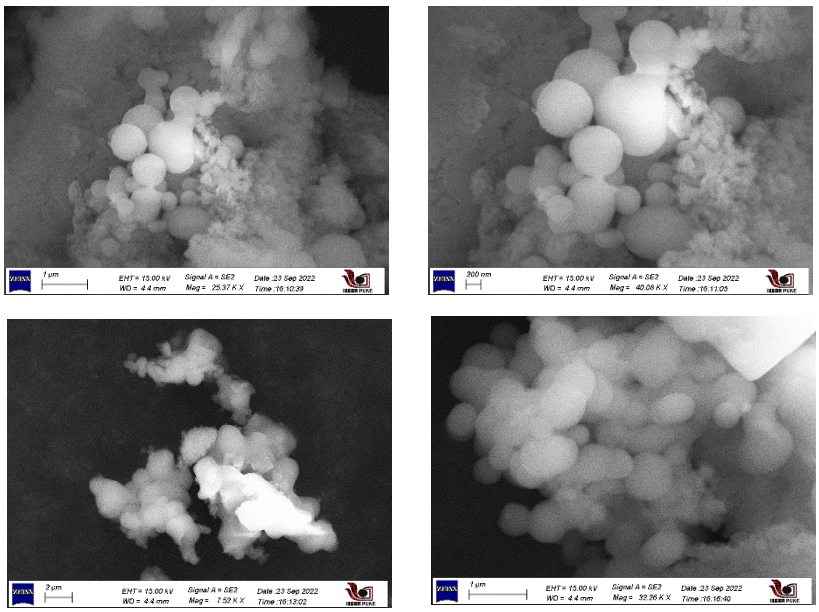

Appendix 5.27: FE-SEM images of Indigo carmine (IC) encapsulated T4PSM

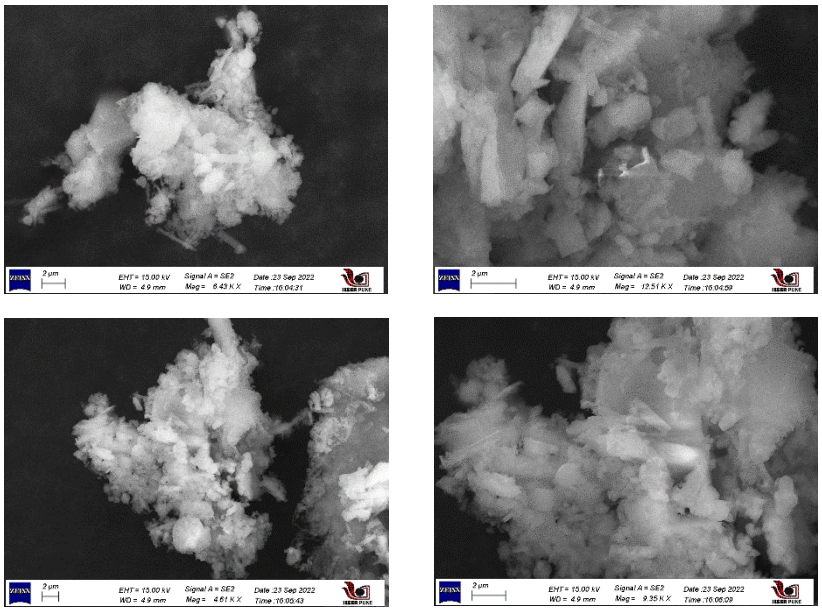

Appendix 5.28: FE-SEM images of Methyl Orange (MO) encapsulated T4PSM

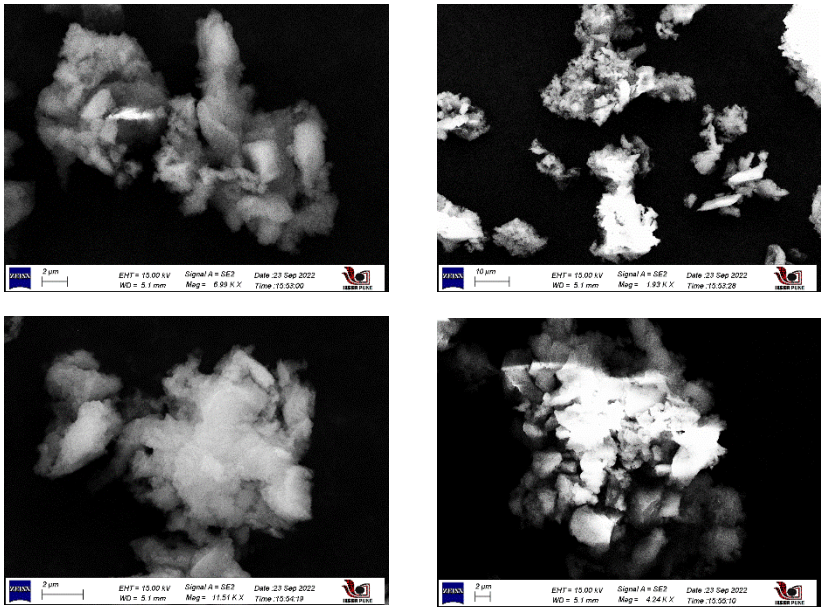

Appendix 5.29: FE-SEM images of Orange G (OG) encapsulated T4PSM.

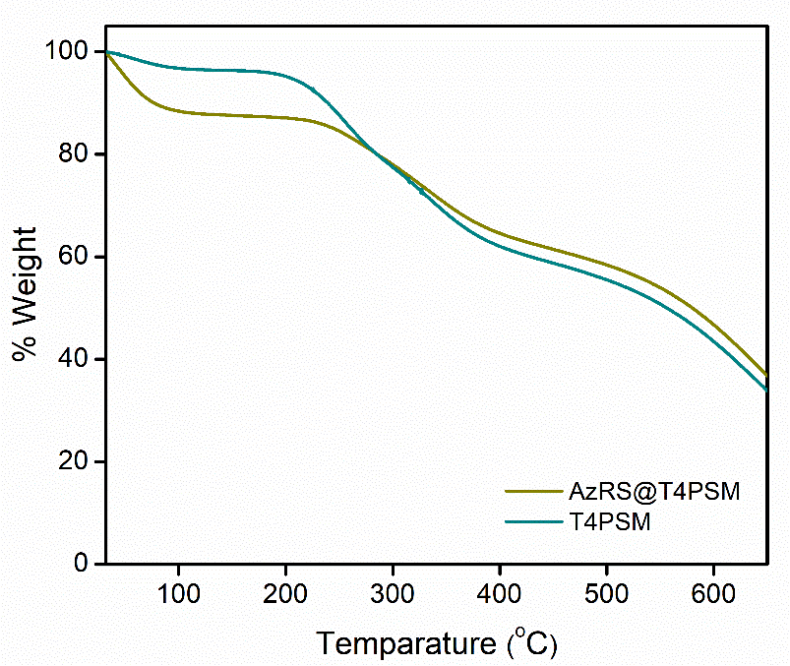

Appendix 5.30: Thermo-gravimetric analysis (TGA) profiles of T4PSM (cyan) and Alizarin red S (AzRs) encapsulated T4PSM (green).

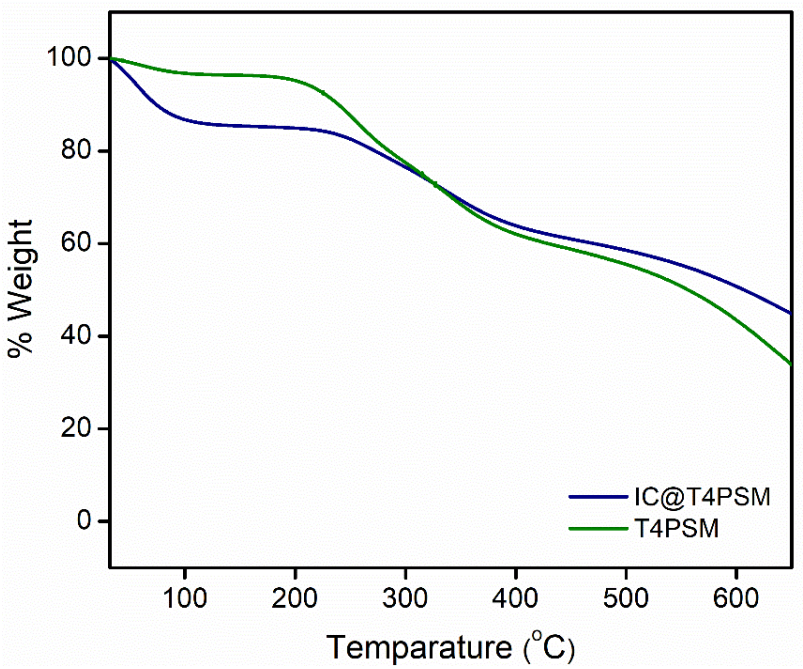

Appendix 5.31: Thermo-gravimetric analysis (TGA) profiles of T4PSM (green) and Indigo Carmine (IC) encapsulated T4PSM (blue).

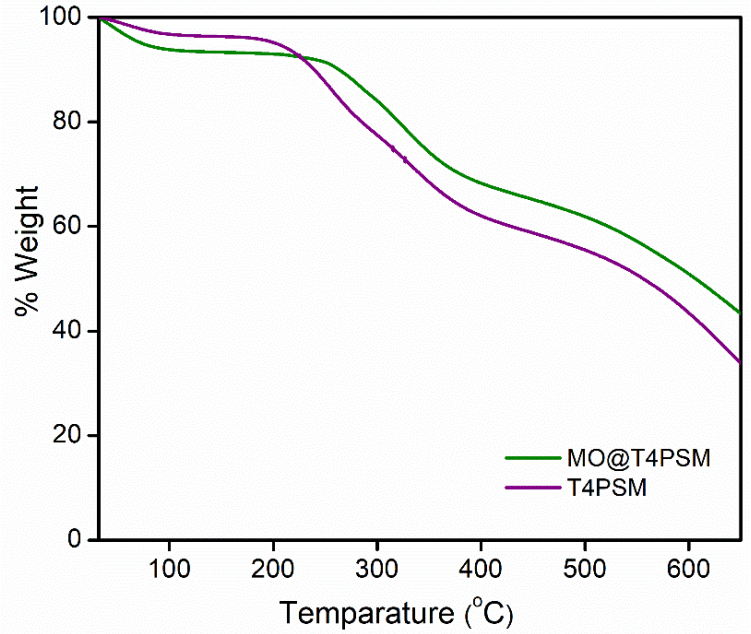

Appendix 5.32: Thermo-gravimetric analysis (TGA) profiles of T4PSM (violet) and Methyl Orange (MO) encapsulated T4PSM (green).

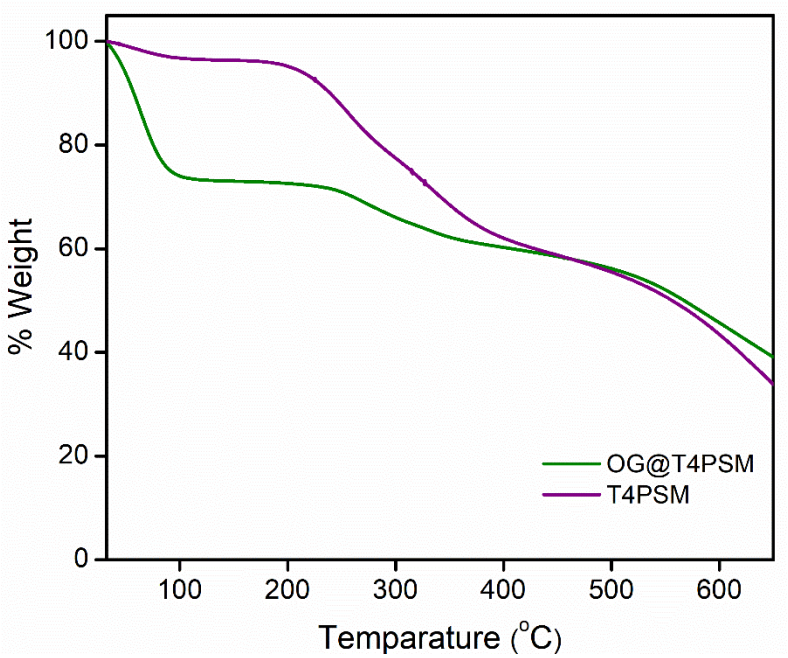

Appendix 5.33: Thermo-gravimetric analysis (TGA) profiles of T4PSM (violet) and Orange G (OG) encapsulated T4PSM (green).

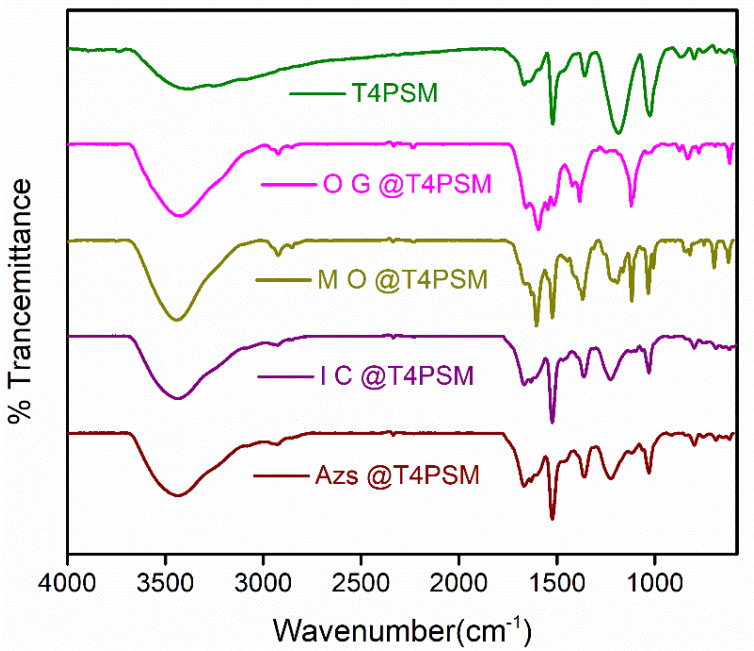

Appendix 5.34: FT-IR spectra of T4PSM and dye encapsulated T4PSM.

5.6 References

1. N. Johnson, C. Revenga and J. Echeverria, *Science*., 2001, **292**, 1071–1072.
2. P. Samanta, A. V. Desai, S Let and S.K. Ghosh, *ACS Sustain. Chem. Eng.*, 2019, 7, 7456–7478.
3. a) M. Hasan, D. A. Gopakumar, V. Arumughan,Y. B. Pottathara, K. S. Sisanth, D. Pasquini, M. Bracic, B. Seantier, A. Nzihou and S. Thomas. *Polymers*, 2019, **11**, 495. b) A. Hasanbeigi and L. Price. *J. Clean. Prod*., 2015, **95**, 30–44. c) J. Rivera-Utrilla, M. S´anchez-Polo, M.´A. Ferro-García, G. Prados-Joya and R. Ocampo- P´erez. *Chemosphere*., 2013, **93**, 1268–1287, d) S. D. Richardson and T. A. Ternes. *Anal. Chem*., 2018, **90**, 398–428.
4. (a) S. J. Allen and B. Koumanova, *J. Univ. Chem. Technol. Metall.*, 2005, **40**, 175 -192; (b) C. –C. Wang, J. –R. Li, X. –L. Lv, Y. –Q. Zhang and G. Guo, *Energy Environ. Sci.*, 2014, **7**, 2831 -2867.
5. X. Liu, W. Gong, J. Luo, C. Zou, Y. Yang and S. Yang, *Appl. Surf. Sci.*, 2016, **362**, 517 -524.
6. (a) A. Ayati, M. N. Shahrak, B. Tanhaei and M. Sillanpää, *Chemosphere*, 2016, **160**, 30 -44; (b) S. –R. Zhang, J. Li, D. –Y. Du, J. –S. Qin, S. –L. Li, W. –W. He, Z. –M. Su and Y. –Q. Lan, *J. Mater. Chem. A*, 2015, 3, 23426 -23434; (c) S. Chen, J. Zhang, C. Zhang, Q. Yue, Y. Li and C. Li, *Desalination*, 2010, **252**, 149 -156; (d) A. Mittal, A. Malviya, D. Kaur, J. Mittal and L. Kurup, *J. Hazard. Mater*., 2007, **148**, 229-240.
7. (a) E. Haque, V. Lo, A. I. Minett, A. T. Harris and T. L. Church, *J. Mater. Chem. A*, 2014, **2**, 193 -203; (b) E. Haque, J. E. Lee, I. T. Jang, Y. K. Hwang, J. –S. Chang, J. Jegal and S. H. Jhung, *J. Hazard. Mater*., 2010, **181**, 535-542.
8. (a) G. Crini, *Bioresour. Technol.*, 2006, **97**, 1061 –1085; (b) K. K. H. Choy, G. McKay and J. F. Porter, *Resour. Conserv. Rec.*, 1999, **27**, 57-71. (c) A. Ajmal, I. Majeed, R.N. Malik, H. Idriss and M. A. Nadeem, *RSC Adv*., 2014, **4**, 37003–37026. (d) S. Chowdhury and R. Balasubramanian, *Appl. Catal. B*

Environ., 2014, 160, 307–324. (e) F. C. Moreira, R. A. R. Boaventura, E. Brillas and V. J. P. Vilar, *Appl. Catal. B Environ*., 2017, **202**, 217–261.

9. (a) S. Hao, A. Verlotta, P. Aprea, F. Pepe, D. Caputo, and W. Zhu, *Microporous Mesoporous Mater.*, 2016, **236**, 250–259. (b) Li, Y., Li, L., Yu, J., *Chem*, 2017, **3**, 928–949.

10. (a) Y. Xu, S. Jin, H. Xu, A. Nagai and D. Jiang, *Chem. Soc. Rev.*, 2013, **42**, 8012-8031 ; (b) A. G. Slater and A. I. Cooper, *Science*,2015**, 348**, DOI: org/10.1126/science.aaa8075; (c) P. J. Waller, F. Gándara and O. M. Yaghi, *Acc. Chem. Res.*, 2015, **48**, 3053 -3063; (d) D. Yuan, W. Lu, D. Zhao and H.-C. Zhou, *Adv. Mater.*, 2011, **23**, 3723 –3725; (e) R. Dawson, E. Stöckel, J. R. Holst, D. J. Adams and A. I. Cooper, *Energy Environ. Sci.*, 2011, **4**, 4239 -4245; (f) C. R. DeBlase, K. E. Silberstein, T. –T. Truong, H. D. Abruña and W. R. Dichtel, *J. Am. Chem. Soc.*, 2013, **135**, 16821 -16824.

11. (a) M. G. Rabbani and H. M. El-Kaderi, *Chem. Mater.*, 2011, **23**, 1650 -1653; (b) B. Li, Y. Zhang, D. Ma, Z. Shi and S. Ma, *Nat. Comm.*, 2014, DOI: 10.1038/ncomms6537; (c) W. Lu, D. Yuan, D. Zhao, C. I. Schilling, O. Plietzsch, T. Muller, S. Bräse, J. Guenther, J. Blümel, R. Krishna, Z. Li, Zhou, H.-C., *Chem. Mater*., 2010, **22**, 5964 -5972; (d) A. Karmakar, A. Kumar, A. K. Chaudhari, P. Samanta, A. V. Desai, R. Krishna and S. K. Ghosh, *Chem. Eur. J.*, 2016, **22**, 4931 –4937; (e) T. Ben, H. Ren, S. Q. Ma, D. P. Cao, J. H. Lan, X. F. Jing, W. C. Wang, J. Xu, F. Deng, J. M. Simmons, S. L. Qiu and G. S. Zhu, *Angew. Chem., Int. Ed.*, 2009, **48**, 9457 –9460; (f) H. A. Patel, S. H. Je, J. Park, D. P. Chen, Y. Jung, C. T. Yavuz and A. Coskun, *Nat. Comm.*, 2013, DOI: 10.1038/ncomms2359; (g) S. Dalapati, E. Jin, M. Addicoat, T. Heine and D. Jiang, *J. Am. Chem. Soc.*, 2016, **138**, 5797-5800; (h) A. Karmakar, R. Illathvalappil, B. Anothumakkool, A. Sen, P. Samanta, A. V. Desai, S. Kurungot and S. K. Ghosh, *Angew.Chem. Int.Ed.*, 2016, **55**, 10667 –10671.

12. (a) C. Zou, Z. Zhang, X. Xu, Q. Gong, J. Li and C. –D. Wu, *J. Am. Chem. Soc.*, 2012, **134**, 87 –90; (b) X. Zhao, X. Bu, T. Wu, S. –T. Zheng, L. Wang and P. Feng, *Nat. Comm.*, 2013, 10.1038/ncomms3344; (c) M. –L. Ma, J. –H. Qin, C. Ji, H. Xu, R. Wang, B. –J. Li, S. –Q. Zang, H. –W. Hou and S. R. Batten, *J. Mater. Chem. C*, 2014, **2**, 1085-1093; (d) Z. Zhu, Y. –L. Bai, L. Zhang, D. Sun, J. Fang and S. Zhu, *Chem. Commun.*,2014, **50**, 14674 -14677; (e) Y. –Q. Lan, H. –L. Jiang, S. –L. Li and Q. Xu, *Adv. Mater.*, 2011, **23**, 5015 –5020; (f) J. –S. Qin, S. –R. Zhang, D. –Y. Du, P. Shen, S. –J. Bao, Y. –Q. Lan and Z. –M. Su, *Chem. Eur. J.*, 2014, **20**, 5625 – 5630; (g) P. Li, N. A. Vermeulen, X. Gong, C. D.

Malliakas, J. F. Stoddart, J. T. Hupp and O. K. Farha, *Angew. Chem., Int. Ed.*, 2016, **128**, 10514 – 10518; (h) S. Kumar, G. Verma, W. –Y. Gao, Z. Niu, L. Wojtas and S. Ma, *Eur. J. Inorg. Chem.*, 2016, 4373 -4377; (i) P. Yu, Q. Li, Y. Hu, N. Liu, L. Zhang, K. Su, J. Qian, S. Huang and M. Hong, *Chem. Commun.*, 2016, **52**, 7978 -7981; (j) X. Liu, Z. Xiao, J. Xu, W. Xu, P. Sang, L. Zhao, H. Zhu, D. Sun and W. Guo, *J. Mater. Chem. A*, 2016, **4**, 13844 -13851; (k) D. Chen, W. Shi and P. Cheng, *Chem. Commun.*, 2015, **51**, 370 -372; (l) Y. Han, S. Sheng, F. Yang, Y. Xie, M. Zhaoa and J. –R. Li, *J. Mater. Chem. A*, 2015, **3**, 12804 -12809; (m) Z. Hasan and S. H. Jhung, *J. Hazard. Mater.*, 2015, **283**, 329 -339; (n) H. Hahm, S. Kim, H. Ha, S. Jung, Y. Kim, M. Yoon and M. Kim, *CrystEngComm*, 2015, **17**, 8418 -8422; (o) Y. Zhu, Y. -M. Wang, S. -Y. Zhao, P. Liu, C. Wei, Y. -L. Wu, C. -K. Xia and J. -M. Xie, Inorg. Chem. 2014, 53, 7692 –7699; (p) A. V. Desai, B. Manna, A. Karmakar, A. Sahu and S. K. Ghosh, *Angew. Chem. Int. Ed.*, 2016, 55, 7811-7815; (q) Y. -Y. Jia, Y. -H. Zhang, J. Xu, R. Feng, M. -S. Zhang and X. -H. Bu, *Chem. Commun.*, 2015, 51, 17439 -17442; (r) A. Karmakar, B. Joarder, A. Mallick, P. Samanta, A. V. Desai, S. Basu and S. K. Ghosh, *Chem. Commun.*, 2017, **53**, 1253 -1256. (s) D. M. D'Alessandro, B. Smit and J. R. Long, *Angew. Chem., Int. Ed.*, 2010, **49**, 6058 -6082; (t) W. Lu, D. Yuan, J. Sculley, D. Zhao, R. Krishna and H. –C. Zhou, *J. Am. Chem. Soc.*, 2011, **133**, 18126 -18129.

13. S. –B. Yu, H. Lyu, J. Tian, H. Wang, D. –W. Zhang, Y. Liu and Z. –T. Li, *Polym. Chem.*, 2016, **7**, 3392 -3397. (b) G. Xiong, B.-B. Wang, L.-X. You, B.-Y. Ren, Y.-K. He, F.u. Ding, I. Dragutan, V. Dragutan and Y.-G. Sun, *J. Mater. Chem. A*, 2019, **7**, 393–404. (c) P. Samanta, P. Chandra, A.V. Desai and S.K. Ghosh, *Mater. Chem. Front*., 2017, **1**, 1384–1388.

14. (a) E. Marquis, J. Graton, M. Berthelot, A. Planchat and C. Laurence, *Can. J. Chem*., 2004, **82**, 1413–1422. (b) J. R. Cabrero-Antonino, T. Garcia, P. Rubio-Marques, J. A. Vidal-Moya, A. Leyva-Perez, S. S. Al-Deyab, S. I. Al-Resayes, U. Diaz and A. Corma, *ACS Catal.*, 2011, **1**, 147–158. (c) M. Carta, R. Malpass-Evans, M. Croad, Y. Rogan, J. C. Jansen, P. Bernardo, F. Bazzarelli, N. B. McKeown *Science*, 2013, **339**, 303-307.

15. (a) R. Gomes, P. Bhanja and A. Bhaumik, *Chem. Commun.*, 2015, **51**, 10050−10053.

16. Y. Su, Y. Wang, X. Li, X. Li and R. Wang, *ACS Appl. Mater. Interfaces*, 2016, **8**, 18904−18911.

17. J. Li, B. Li, N. Shen, L. Chen, Q. Guo, L. Chen, L. He, X. Dai, Z. Chai and S. Wang, *ACS Central Science* 2021, **7**, 1441-1450.

Chapter 6

Summary and Perspectives

6.1 Summary and Perspectives

In last few decades porous materials have gained significant attention due to their applicability in various domains. In summary, this thesis contains design and synthesis of noble porous material (MOFs or POMs) and their application in environmental application. The goal is to develop physiochemically stable porous materials and employed for water remediation application. In this regard a post metalized metal-organic framework (MOF) was synthesized by post metallization of MOF-867 with $CuCl_2$. Further metal loaded MOF $CuCl_2$@MOF-867 was employed for selective sensing of cyanide ion in aqueous medium as cyanide is quite reactive towards Cu^{2+} generating stable $Cu(CN)_2$ species. For complete water remediation sensing of toxic pollutants is not enough so further research was carried out for complete removal of pollutants. Although a handful of MOFs are stable in water, they often found to be unstable in different physiochemical condition. In this context covalently bonded porous organic materials were used to remove a variety of types of water contaminants (mercury, oxo-anions, anionic organic dyes) because of their excellent chemical stability. To remove cationic inorganic pollutant Hg^{2+} two anionic polymer was synthesized with different functionality which plays crucial role in capture performance as well as recyclability guided by hard soft acid base (HSAB) principle. Both the two polymers show selectivity towards mercury in presence of other cations like Pb^{2+}, Cd^{2+}, K^{+} etc. Further metal oxoanions removal from wastewater have drawn huge attention due to their toxic and carcinogenic nature. The role of counter anions in ion exchange-based pollutant removal study has not been well explored. With keeping this mind, we have first synthesized a troger based polymer followed by post synthetic methylation by dimethyl sulphate and methyl iodide which resulted in two cationic polymers having sulphate (TB-POP@MS) and iodide (TB-POP@MI) as counter anions. Further after the kinetic measurement we performed capture studies of chromate (CrO_4^{2-}) and ReO_4^- (surrogate to TcO_4^-) ions with TB-POP@MS as it shows better performance compare to the TB-POP@MI. Further TB-POP@MS shows excellent selectivity in presence of other concurrent anions Cl^-, Br^-, NO_3^- and ClO_4^- ion. Further the material employed for low concentration oxo-anion removal and also capture efficiency in different water systems. Selective removal of anionic dyes over cationic dyes were carried out by post synthetically modified polymer where the cationic polymer has a counter anion i.e., sulfate which is easily exchangeable. This detailed analysis showed functionally tuned porous material with adaptable architecture is suitable for cleaning up environmental contaminates. Although porous organic materials haven't been used much for these kinds of applications up until now, they may soon be ideal for cleaning up water pollution in future.